Modélisation multi-échelle des impacts des feux de végétation sur la dynamique et la chimie de l'atmosphère en région Méditerranéenne

Susanna Strada

Université de Toulouse

THÈSE

En vue de l'obtention du

DOCTORAT DE L'UNIVERSITÉ DE TOULOUSE

Délivré par :
Université Toulouse III Paul Sabatier (UT3 Paul Sabatier)

Discipline ou spécialité :

Physique et chimie de l'atmosphère

Présentée et soutenue par :
Susanna STRADA

le : 26/01/12

Titre :

Modélisation multi-échelle des impacts des feux de végétation sur la dynamique et la chimie de l'atmosphère en région Méditerranéenne

---

Ecole doctorale :
Sciences de l'Univers, de l'Environnement et de l'Espace (SDU2E)

Unité de recherche :
Laboratoire d'Aérologie

Directeur(s) de Thèse :

Céline MARI

Rapporteurs :

Katharine LAW
Matthias BEEKMANN

Membre(s) du jury :

Ana Isabel MIRANDA
Sylvain COQUILLAT
Jean-Baptiste FILIPPI

Contents

Remerciements

Le plus grand remerciement va à Céline, mon encadrante de thèse, pour m'avoir appris à lire le feu dans Meso-NH, pour tous ses enseignements, conseils, corrections, et aussi pour sa présence humaine, son soutien constant et sa patience avec une italienne.

Je remercie beaucoup Jean Baptiste, Frédéric et Xavier de l'Université de Corte d´avoir mis le feu dans Meso-NH, et pour m'avoir accueillie dans leur équipe, toujours avec un grand sourire. Merci aussi à Valérie et Eric pour avoir mis le feu à la végétation corse.

Aux Meso-NH Warriors, Juan & Didier, un grand merci parce qu'ils étaient toujours là, toujours prêts à répondre à mes questions et à éviter que je mette le feu au modèle, ou aux super-calculateurs.

Merci à Soline de m'avoir aidée à bien dessiner les feux avec NCL.

Merci aux informaticiens du Laboratoire d'Aérologie, Laurent, Serge et Jeremy Leclercq, pour m´avoir évité de brûler même mon ordinateur.

Je tiens aussi à faire un remerciement spécial à Jean Pierre Pinty, Jean Pierre Chaboureau, Christine Lac, Valery Masson et toute l'équipe de Meso-NH pour toutes les discussions qui m'ont fait comprendre qu'il n'y a pas que les feux dans Meso-NH.

Merci à Sylvain Coquillat pour avoir accepté de présider ma jury de thèse, et aussi pour m'avoir accompagnée, avec Dominique Lambert, Jean François Georgis et d'autres encadrants, dans l'aventure du monitorat. Un remerciement spécial à deux copains d'aventure, Lola et Romain, parce qu'on a bien rigolé sur le chemin.

Merci à Frank Roux, directeur du LA, à toutes les personnes qui y travaillent et à tous les thésards car chacun a permis que ça brûle bien au sein du LA. En particulier, merci à Alexandre d'avoir pris le rélais de Sarah dans le bureau A105 et avoir voulu commencer une thèse malgré qu'il ait vu à quel point un doctorant peut se reduire pendant sa troisième année de thèse.

Un "super merci" à SarahB pour m'avoir toujours rappelé qu'il n'y a pas que les feux dans la vie et que la grammaire est quand même importante en français. Un "super merci" aussi à Fiona qui m'appris à rester débout dans la vie et meme sur l'océan, au moins à essayer de le faire. Merci à Amandine, France, Fanny, Brice, Héloise, Emilie, Jochem et Pedro pour leurs oreilles toujours disponibles et ouvertes. Merci à Claire, Séverin et leur nouveau monde Maud pour les apéros improvisés qui m'ont toujours laissée avec un grand sourire.

A tous ceux qui ont permis que ma thèse brûle bien ! Quand j'ai imaginé Toulouse j'étais à Paris, c'était en 2006. J'ai continué à travailler sur ce rêve, à Bologne, le soir, après le boulot. Maintenant que je le vis je peux juste me dire que c'est encore mieux que tout ce que j'aurais pu imaginer ! MERCI !

Enfin, merci à l'école publique parce que grâce à toutes les personnes qui y travaillent j'ai pu arrivér jusqu'à ici ! Aujourd'hui, l'education publique est en danger, en Italie comme en France et ailleurs, à cause d'une politique qui favorit les banques, les privés et les armes

et une societé qui décerne l'efficacité, la vitesse, le profit. Pour le futur, j'espere que nous auront le courage de créer des formes alternatives d'education, comme suggeré par Ivan Illich dans son livre "Une societé descolarisée".

Ringraziamenti

Dietro ogni grande piromane, c'è sempre una grande famiglia. Dunque, grazie mille ai miei genitori e a mio fratello per averci creduto fin dal primo viaggio in moto Milano-Tolosa. Grazie ai cugini: dalle cugi-mamme, Ka, Manu e Ele, ad Ali ed Albi. Grazie agli zii e alle zie, ormai dispersi per l'intera penisola, isole comprese: la zia Sbirulino e lo zio Piero, gli zii Lu&Anni, la macrobio-zia Laura, gli zii Ornella&Antonio e lo zio no-limits Mario. Grazie alla Nonna Mat che, seppur mi abbia fatto lo scherzo di partire mentre ero in Brasile, mi ha lasciato la sua macchina da cucire.

Grazie anche agli amici, quelli che restano nonostante i cambi di indirizzi e quelli nuovi che si incontrano girovagando: Yele, Maura, Pio, Ili, Mex, Tia, Giulio, Luca, Ania, Giu, Gio&Gio, Marti, Tita, Mudita, Silvia.

Reconhecimentos

Muito obrigada à Karla Longo e ao Saulo Freitas por me receberem no grupo de pesquisa no INPE em São José dos Campos e por todas sugestões e ajudas para controlar a queimada nos dois modelos: PRM e Meso-NH.

Muito obrigada também a todos os GMAIos: Megan, Madalene, Daniela, Nilton, Rafael, Guilherme... E aos demais do INPE: Hiran, Darcy, Rômulo, André, Etienne, Líliam, Aline, Fernanda, Verônica, Flora, a galera da Capoeira... Agradeço pelos treinos, a carona pela manhã, a travessia da Serra Fina e o surfe.

Muito obrigada as minhas colegas de casa, Yhasmin, Mari, Miriam, Amanda e Ediana, pela alegria, os cursos de samba e de brasileiro, o síndico, as novelas.. na republica da rua Teopompo de Vasconcelos, 81.

Muito obrigada a Ana Isabel Miranda por examinar o meu manuscrito e também pelo clima alegre e convivial na colaboração no projeto PESSOA. Muito obrigada também à Vera e ao Jorge por estarem sempre disponíveis quando chegamos em Aveiro.

Preface

In the present thesis, the scientific work is presented in the form of articles.

Chapter 4 corresponds to the study of the impact of a mediterranean forest fire on the atmospheric dynamics and the chemistry at regional scale. The paper is currently in favourable review at Atmospheric Environment. I wrote this paper as first author.

Chapter 5 is organized around the project that I lead in collaboration with my partners at the *Instituto Nacional de Pesquisas Espaciais* (INPE) in the frame of my scientific visit at São José dos Campos (São Paulo, Brazil), that has been funded by the University of Toulouse, the French Agency of Research (ANR) and the INPE. The cited project deals with the inter-comparison of two different numerical approaches to simulate the height of injection of a fire plume in contrasted meteorological scenarios. This work is intended to be submitted to Geoscientific Model Development.

Finally, Chapter 6 discusses the work that was done with our partners from the University of Corte and Météo-France in the framework of the ANR project IDEA. My contribution to this paper was to provide an expertise on the way the atmospheric model reacts to the fire progression and evolution in terms of both dynamics and chemistry. This study has been the motivation of my scientific staying in Corte.

Introduction[1]

Les feux de végétation dans le système Terre

Il y a 350-400 millions d'années, pendant l'âge paléozoïque sur la Terre, les conditions favorables pour les premiers feux de végétation sont réunies : une accumulation suffisante de combustible (végétation en état de sécheresse critique), du comburant (air ambiant avec présence de dioxygène) et une énergie d'activation (fournie, par exemple, par un éclair) (Pyne et al., 1949, pag. 602). Pendant l'âge tertiaire, la présence des mammifères a ajouté un autre facteur de contrôle au régime naturel de feux (Andreae, 1991), jusqu'à l'arrivée de l'homme préhistorique. Il y a 1.5-2 millions d'années, les premiers hominidés ont appris à se servir du feu (James, 1989; Schule, 1990), d'abord pour cuisiner et chasser, plus tard en l'utilisant dans l'agriculture, le pâturage, la poterie, la métallurgie, etc. (Pyne and Goldammer, 1997). Bien que le feu soit un phénomène naturel, aujourd'hui l'homme est reconnu responsable (directement ou indirectement) d'environ 90% des feux de végétation sur la Terre. Les 10% restant sont des feux naturels déclenchés par des éclairs notamment dans les écosystèmes tropicaux ou boréaux (Andreae, 1991). Si dans les pays en voie de développement les feux de végétation gardent encore un rôle très important dans la culture et l'économie des populations (Andreae, 1991; Pyne and Goldammer, 1997), ailleurs, dans les pays plus développés, les feux de végétation sont souvent accidentels, volontaires ou criminels (Leone et al., 2009).

Distribution et saisonnalité des feux à l'échelle globale

A l'échelle globale les feux de végétation sont présents partout sur la Terre (Andreae, 1991 ; Fig. 1.1) : une estimation récente recense entre 350 et 400 millions d'hectares brûlés chaque année pendant la période 2000-2007 (Tansey et al., 2008).

La saisonnalité des feux de végétation est bien marquée qui est principalement liée à la persistance de conditions de sécheresse. Dans les régions tropicales, les feux brûlent dans l'hémisphère Nord entre décembre et mars et dans l'hémisphère Sud entre juin et septembre (Andreae, 1991; Langmann et al., 2009; Dwyer et al., 2000; Carmona-Moreno et al.,

[1]Ce chapitre est une version condensée des Chapitre 1, 2 et 3 qui sont rédigés en anglais comme le coeur de cette thèse. Une version française de la conclusion est aussi fournie à la fin. This chapter is a condensed version of introductory Chapter 1, 2 and 3. A french translation of the conclusion is presented at the end of this work.

2005). D'autres brûlages présentent un cycle saisonnier prononcé comme par exemple en Indonésie (printemps australe et boréale), en Amérique Centrale (avril-mai), dans les régions boréales et tempérées (mai-septembre), même si la variation inter-annuelle dans ces régions est haute (Langmann et al., 2009 ; Fig. 1.1).

Les feux de végétation dans les écosystèmes terrestres

Les feux de végétation se différencient entre eux par la flore et le climat présents dans la région considérée. Une classification typique sépare les écosystèmes en quatre classes : boréal, tempéré, tropical et méditerranéen (Pyne et al., 1949, pag. 629).

- **Les feux dans les écosystèmes boréaux**

  Aux hautes latitudes, la végétation est confrontée à des hivers longs et rigoureux et à des étés courts. Ces conditions climatiques déterminent une végétation assez complexe qui va de grandes forêts de conifères *taïga*, à une flore plutôt basse composée d'herbacées, principalement de lichen *toundra*, jusqu'à dégénérer dans de la tourbière (Pyne et al., 1949, pag. 632). Dans cet écosystème, où la croissance comme la décomposition de la végétation sont assez lentes, les feux naturels ont un rôle important depuis des millions d'années, en permettant d'enrichir efficacement le sol des nutriments dont il a besoin (Aber and Melillo, 2001) pour stimuler la poussée d'une nouvelle végétation (Stocks, 1991). Les feux boréaux se caractérisent soit par des épisodes rares et intenses avec les feux de forêt, soit par des feux de tourbière qui peuvent se prolonger pendant des mois, sur de très larges surfaces (entre 10000 et 100000 ha, Beverly and Martell 2005). Les hauteurs d'injection des feux se situent majoritairement entre 2 et 4 km (Labonne and Chevallier, 2007; Tosca et al., 2011). Au cours des 20 dernières années, l'intérêt scientifique pour les feux boréaux a augmenté du fait qu'ils représentent des sources très importantes de pollution (Kasischke et al., 2005; Turquety et al., 2007), et sont aussi responsables d'épisodes de pollution transfrontalière (Saarikoski et al., 2007; Goldammer et al., 2009; Chubarova et al., 2009; Pommier et al., 2010; Konovalov et al., 2011).

- **Les feux dans les écosystèmes tempérés**

  Localisé dans une zone intermédiaire (aux moyennes latitudes), l'écosystème tempéré présente une alternance moins marquée entre les différentes saisons. Pour cette raison le régime de feu dans ces régions est gouverné par les conditions météorologiques plutôt que climatiques (Pyne et al., 1949, pag. 633). Si avant les feux tempérés ont été liés à la colonisation des nouveaux territoires par l'homme (Pyne, 1995), aujourd'hui il s'agit pour la plupart de feux volontaires ou accidentels (Chuvieco, 2009) qui brûlent près des zones urbanisées avec des conséquences significatives sur la qualité de l'air urbaine (e.g. Hu et al. 2008). Labonne and Chevallier (2007) estiment

une hauteur d'injection maximale entre 6 km et 7 km en Amérique du Nord par exemple.

- **Les feux dans l'écosystème tropical**

  Dans l'écosystème tropical, les températures restent relativement constantes pendant toute l'année et l'alternance saisonnière est donc réglementée par les précipitations (saison sèche ou humide). Ces conditions climatiques favorisent une croissance extraordinaire de la végétation, qui est extrêmement riche et variée à ces latitudes, en même temps qu'elles définissent le rôle et la fréquence du feu (Pyne et al., 1949, pag. 637). Entre les différents régimes de feux présents dans les régions tropicales, les plus importants sont les feux de forêt et ceux de savane. Les forêts tropicales n'offrent pas un écosystème favorable au feu (forte humidité et combustible très serré) (Hoelzemann, 2006), pourtant des cas exceptionnels ont été enregistrés (e.g. feux du Borneo-Indonésie en 1982-1983 causés par la forte sécheresse due à El Ñino, Molion 1991). Au contraire, la savane brûle assez souvent à cause de l'abondance de combustible et de la fréquence des événements naturels comme la sécheresse et les éclairs (Andreae, 1991). Ici encore, les feux de forêt et de savane sont principalement d'origine humaine pour remplacer la forêt (feux de déforestation) par des terrains dédiés à l'agriculture, au pâturage ou d'autres utilisations (implantations, routes) (Delmas et al., 1991; Goldammer, 1991; Lovejoy, 1991; Wuebbles et al., 2003). Le rôle des feux de biomasse dans les zones tropicales a été très tôt identifié comme primordial pour le climat et la chimie de l'atmosphère à l'échelle globale (e.g. Fishman et al. 1990; Helas et al. 1995). L'analyse de Labonne and Chevallier (2007) sur les panaches d'aérosol produits dans les zones tropicales propose une hauteur d'injection entre 2 et 4.5 km.

- **Les feux dans l'écosystème méditerranéen**

  L'écosystème méditerranéen est caractérisé par un climat bien défini par l'alternance entre des hivers courts, doux et humides, qui favorisent la poussée des plantes, et des étés longs, chauds et secs qui offrent les conditions parfaites pour les incendies (Pyne et al., 1949, pag. 635). Depuis sa création en 1980, le rapport annuel de l'EFFIS (European Forest Fire Information System, `http://effis.jrc.ec.europa.eu/`) montre une nette augmentation de feux de végétation dans les pays du bassin euro-Méditerranéen (principalement Portugal, Espagne, France, Italie and Grèce) puis un tassement de la tendance après les années 90 (San-Miguel-Ayanz et al., 2009). Entre 2000 et 2005, ce sont environ 95000 incendies qui sont comptabilisés pour une surface brûlée totale de 600000 ha principalement pendant l'été boréal (Barbosa et al., 2009). Les hauteurs d'injection dans la zone euro-méditerranéenne sont estimées entre 1.5 entre 5 km (Labonne and Chevallier, 2007). Il s'agit dans la majorité des cas (95%) de feux d'origine humaine (volontaires, criminels ou accidentels) (Alexan-

drian et al., 1999). Les scénarios futurs ne sont pas optimistes quant à l'évolution des feux dans l'écosystème méditerranéen. Le dernier rapport du Groupe d'experts intergouvernemental sur l'évolution du climat (GIEC) (IPCC, 2007) prévoit qu'une augmentation de la température entre 3 et 5 °C pourrait comporter une hausse de risque de feu de végétation. Parmi les régions à risque le GIEC place le bassin méditerranéen en position à fort risque (e.g. Pausas, 2004; Moriondo et al., 2006).

Les impacts du feu sur l'environnement : climat et pollution de l'air

Les feux de végétation ont des impacts dramatiques qui peuvent se produire à des échelles spatiales et temporelles différentes (du court au long terme, de l'échelle locale à l'échelle globale). D'un point de vue sociétal, la force de destruction du feu est bien connue par l'homme : mise en danger des populations et des écosystèmes, effets à court et longue terme sur la santé publique, détérioration des ressources naturelles avec des coûts économiques non négligeables (Chuvieco, 2009). D'un point de vue scientifique, l'intérêt porte sur les impacts environnementaux du feux, en particulier les émissions des feux de végétation (composantes gazeuses, liquides, solides et en phase mixte, les aérosols) et leur influence sur le climat et la pollution de l'air.

- **Les feux de végétation : un paramètre du forçage climatique**

  Les effets des feux de végétation sur le climat sont variés et complexes. Les feux de végétation contribuent à intensifier le naturel "effet de serre" de l'atmosphère terrestre par l'émission directe d'une quantité importante de gaz "à effet de serre" qui absorbent et rediffusent le rayonnement (solaire et terrestre) dans l'infrarouge : il s'agit du dioxyde de carbone CO_2, du méthane CH_4, du protoxyde d'azote N_2O, et de la vapeur d'eau (Crutzen and Andreae, 1990; Andreae, 1991). Les espèces gazeuses et les aérosols émis par les feux déterminent aussi une pollution secondaire qui conduit à la production d'ozone (O_3) troposphérique, un autre gaz "à effet de serre" (Ramanathan et al., 1985). Enfin, les aérosols carbonés sont émis en grande quantités qui contribuent d'une part à l'absorption et rediffusion du rayonnement (*Black Carbon*, Jacobson 2001), et d'autre part peuvent compenser cet effet de réchauffement par un refroidissement (rôle du carbone organique, Schaap and van der Gon Denier 2007). Les aérosols influencent fortement les flux actiniques qui contrôlent la production de l'O_3 troposphériques (Albuquerque et al., 2005) ; ils réduisent ou modifient l'albédo de surface (Stohl et al., 2006, Jin and Roy, 2005). Les aérosols affectent la micro-physique et les processus de formation des nuages en faveur de nuages plus réfléchissants et moins précipitants (Crutzen and Andreae, 1990; Kaufman and Fraser, 1997; Ramanathan et al., 2001) ; ils peuvent éventuellement réduire la formation des cellules convectives, donc inhiber la formation des

nuages (Hoelzemann, 2006; Pace et al., 2005). Les aérosols perturbent les processus microphysiques des nuages (e.g. Rosenfeld 1999; Artaxo et al. 2002, 2005) mais leur impact sur les précipitations reste encore incertain. Dans les tropiques, les forêts vierges alimentent et maintiennent, par leur évapotranspiration et leurs racines, le cycle de l'eau. Le processus de déforestation par le feu accélère la désertification de vastes territoires qui ne sont plus capables de retenir l'eau, en réduisant un cycle naturel et en favorisant la sécheresse (Crutzen and Andreae, 1990).

L'interaction de feux de végétation avec la biosphère a des implications significatives sur le cycle bio-géochimique (Crutzen and Andreae, 1990). En particulier, ils agissent sur le cycle naturel d'émission et d'absorption du CO_2 par la végétation (Conard and Solomon, 2009). L'augmentation de feux de déforestation déséquilibre brusquement le cycle naturel avec une émission rapide et importante du CO_2 qui a été stocké dans le matériel végétal pendant des décennies (Cardoso, 2004) et avec la mort des plantes qui consomment du CO_2 à travers la photosynthèse.

L'étude des impacts de feux de végétation sur le climat ne fait pas partie des objectives de cette thèse, pourtant il est important de poser cette thématique et sa complexité pour mettre en avant la nécessité d'une meilleure compréhension du rôle des feux de végétation sur le climat. Inversement, un changement climatique caractérisé par des températures plus élevées et des précipitations moins intenses favorise une augmentation du risque et de la fréquence des feux (Goldammer, 1991).

- **Pollution de l'air**

  Comme tous les processus de combustion, les feux de végétation émettent des molécules chimiques qui modifient brutalement la composition chimique de l'atmosphère. Parmi les produits émis par les feux de végétation, plusieurs ont des effets dangereux sur la santé humaine avec des effets souvent immédiats (irritation des voies respiratoires, asthme) ou dans le long terme (cancer, mutations génétiques) (Goldammer et al., 2009; Barboni et al., 2010; WHO/UNEP/WMO, 2000). La fumée des feux de végétation peut impacter fortement la visibilité sous le vent du feux (Fox and Riebau, 2009) avec des effets sur les infrastructures (aéroports, autoroutes, hôpitaux) et sur les opérations des pompiers et de la sécurité civile (e.g. Mobley, 1990; Muraleedharan et al., 2000; Dokas et al., 2007; Goldammer et al., 2009). Ces deux impacts illustrent le fort intérêt sociétal qui motive à mieux comprendre le comportement et l'évolution de feux de végétation.

  Il est important de noter que l'impact des feux de végétation sur la chimie de l'atmosphère peut s'étaler sur une région plus ou moins vaste, en fonction des conditions météorologiques (vent, humidité, stabilité) qui interagissent avec le feu et sa puissance qui détermine l'efficacité du transport convectif. Cette interaction dynamique de l'atmosphère/feu se traduit dans la hauteur finale à laquelle les polluants sont

injectés dans l'atmosphère (e.g. Freitas et al. 2007; Kahn et al. 2007; Rio et al. 2010). Cette hauteur dite "d'injection" influence l'efficacité de la dispersion du panache de feux de l'échelle locale (Miranda et al., 2009b; Hu et al., 2008; Strada et al., 2012), dans le cas d'une hauteur d'injection inférieure à la hauteur de couche limite (où les processus de dépôt sont plus efficaces), à l'échelle régionale ou même globale (Damoah et al., 2006; Sofiev et al., 2008; Dirksen et al., 2009; Elguindi et al., 2010), quand le panache atteint la troposphère libre et qu'il est advecté rapidement. Des études récentes ont démontré la détérioration de la qualité de l'air à proximité (Miranda et al., 2005; Alves et al., 2010a) et à des centaines de kilomètres du point d'éclosion des incendies (Phuleria et al., 2005; Miranda et al., 2008; Tressol et al., 2008; Turquety et al., 2009; Dirksen et al., 2009; Alves et al., 2011 ; Fig. 1.2) avec des niveaux de concentrations des principaux polluants urbains (monoxyde de carbone CO, oxydes d'azote NO_x, O_3, particules en suspension PM) en dehors des valeurs fixées par la législation européenne ou américaine. Pendant le transport, le panache de fumées issu d'un incendie évolue chimiquement sous l'effet de transformations chimiques et de dilution avec l'air environnant. Les progrès en modélisation de ces panaches (e.g. Poppe et al. 1998; Mason et al. 2006; Trentmann et al. 2003) et dans le nombre et la précision des espèces chimiques observés dans les panaches (e.g. Hobbs et al. 2003; Jost et al. 2003; Bytnerowicz et al. 2010) ont permis des avancées importantes mais peu sont consacrées aux feux dans les régions méditerranéennes.

Les composantes fondamentales des feux de végétation

Les feux de végétation sont des phénomènes complexes et multi-échelle (Pyne et al., 1949, pag. 3). Ils se différencient par rapport au type de végétation qui brûlent (feux de foret, feux de tourbière, etc.), à la strate végétale dans laquelle ils se propagent (surface, sous-bois ou cimes des arbres), au rôle de l'homme (feux contrôlés, feux accidentels, feux prescrit) (Benson et al., 2009). Ils peuvent être observés, étudiés et reproduits au moyen de la modélisation à différentes échelles. A l'échelle de la flamme (résolution de l'ordre des quelques centimètres) les processus de la combustion gouvernent. Ces processus peuvent être représentés par des modèles qui incluent des centaines de réactions chimiques se produisant au cours de la combustion (Leroy et al., 2007; Auzillon et al., 2011). A l'échelle du feu (entre quelques mètres et des dizaines de mètres) le comportement du feu est lié à l'interaction entre le combustible végétal, le terrain et le vent (Mell et al., 2007; Whitcomb et al., 2008) : des modèles de propagation des feux en surface sont développés (Linn et al., 2002; Clark et al., 2004). Le modèle ForeFire utilisé dans cette étude en fait partie. A plus grande échelle, le feu interagit avec son environnement (résolution comprise entre quelques dizaines de mètres et quelques dizaines de kilomètres) : son interaction avec l'atmosphère devient déterminante pour sa propagation et son évolution (Albini, 1993; Benson et al., 2009). Les modèles couplés atmosphère/feu traitent de cette échelle (Filippi

et al., 2009; Mandel et al., 2011) : c'est le cas du modèle couplé MésoNH-ForeFire utilisé pour ce travail. Enfin, à l'échelle globale (entre quelques dizaines et quelques centaines de kilomètres), il faut considérer l'interaction entre le feu et son régime caractéristique, la végétation et le climat (Crutzen and Andreae, 1990; Chuvieco et al., 2008). Les modèles globaux s'intéressent en particulier à l'étude des émissions des feux et de leur impact sur la chimie de l'atmosphère et le climat (Hoelzemann et al., 2004; Ito and Penner, 2004; van der Werf et al., 2004). Il n'est pas possible à l'heure actuelle de considérer toute la gamme des échelles couvertes par les feux de végétation avec un outil unique. Par contre la connaissance des processus en jeu est essentielle pour le choix ultérieur des paramétrisations et des hypothèses en fonction de l'échelle de travail et du niveau de couplage recherché.

Les processus de la combustion

En littérature, le phénomène du feu est souvent résumé par le fameux triangle du feu : combustible, comburant, chaleur. Il s'agit des ingrédients fondamentaux pour que la combustion ait lieu. La connaissance du combustible est importante pour qualifier les produits qui seront émis (Lobert and Warnatz, 1993; Yokelson et al., 1997; Andreae and Merlet, 2001), comme aussi la connaissance des différentes phases de la combustion et la propagation de la chaleur.

Le matériel végétal sec est constituée en majorité de cellulose et de semi-cellulose (entre 66 et 78 %) qui donnent la structure des plantes et sont responsables des émissions de composantes volatiles, de lignine (de 16 à 33%), dont la présence augmente avec la décomposition biologique de la plante, qui participe à la formation de charbon ; des composantes volatiles (alcools, aldéhydes, terpènes) qui alimentent et maintiennent la flamme ; des minéraux qui contribuent plutôt à la phase finale (extinction) de la combustion. L'eau a un rôle important dans la durée de la combustion et ses émissions. Le comburant est représenté par le dioxigène et son abondance influence le spectre des émissions. La chaleur est l'énergie qui permet l'éclosion du feu et gouverne son évolution. Il peut être transféré d'une partie à l'autre du combustible par conduction, radiation ou convection : les trois processus coexistent effectivement pendant la combustion. Si pour la chaleur d'éclosion du feu il existe une certaine cohérence entre les différentes valeurs mesurées avec des différents combustibles (Pyne et al., 1949; Santoni et al., 2006; Freitas et al., 2007), une très grande variabilité est associée aux flux de chaleur par rapport au type de végétation qui brûle (Butler et al., 2004; Freitas et al., 2006; Santoni et al., 2006; Clements et al., 2007; Silvani and Morandini, 2009).

Le processus de la combustion passe par quatre étapes : pre-éclosion, éclosion, combustion et extinction. Pendant la pré-éclosion, la végétation est réchauffée par des réactions endothermiques qui déterminent l'évaporation de l'eau et des composantes volatiles qui, ensuite, vont alimenter la combustion (*déshydration* ou *distillation*) (Greenberg et al.,

2006). La constante absorption de la chaleur conduit à la dégradation thermique des molécules et à leur rupture (*pyrolyse*) qui produit des composés plus légers et plus facilement inflammables (Yokelson et al., 1996; Leroy et al., 2009). A cette étape, deux chemins sont possibles : le premier conduit à la formation du charbon (solide) et de l'eau, l'autre produit du goudron et des composantes volatiles (Pyne et al., 1949). L'éclosion est la phase de passage à la combustion avec une réaction rapide et exothermique qui déclenche la flamme dans la phase gazeuse du feu (Lobert and Warnatz, 1993). Pendant la combustion, il est possible de distinguer deux phases : gazeuse (feu à flamme vive ou *flaming*) et solide (feu couvant ou *glowing/smouldering*). Le feu à flamme vive (*flaming*) domine dans les étapes initiales du feu, il est caractérisé par la présence des flammes qui convertissent les volatiles émis dans des produits secondaires (oxydés) encore plus légers. Si les conditions du combustible et de l'environnement le permettent, ces émissions peuvent maintenir la combustion dans cette phase. Cette phase est caractérisée par des processus de diffusion et de turbulence, assez complexes à représenter (Auzillon et al., 2011). Le feu courant est une forme de combustion lente, à basses températures, sans flamme ; malgré ça, cette combustion n'est pas facile ni à contrôler ni à prévoir car elle peut déclencher de nouveau un feu désormais éteint, et elle a des effets dramatiques sur la végétation, le sol et la pollution de l'air (e.g. Pyne et al., 1949, pag. 22 ; Rein et al., 2008). Enfin, quand la plupart de composés volatiles ont été émis, le taux de pyrolyse ralenti, moins de composés inflammables sont produits et la chaleur diminue. A ce moment, la flamme cesse et d'autres facteurs peuvent intervenir pour déterminer l'extinction complète (manque de combustible, abondance de cendre, humidité du combustible) (Lobert and Warnatz, 1993), malgré cela la combustion peut continuer plusieurs jours sous forme de feu courant (Yokelson et al., 1997).

Les émissions des feux de végétation

Le spectre des émissions des feux de végétation est assez vaste et dépend des caractéristiques du combustible et des différentes phases de combustion. Les principaux produits sont le CO_2 et l'eau, mais d'autres composés sont émis qui peuvent être de très grand intérêt pour leur impact sur la chimie de l'atmosphère. Il est possible d'associer les émissions aux deux phases principales de la combustion discutée précédemment. Pendant la phase de *smouldering* de grandes quantités d'espèces non oxidées sont émises comme le monoxyde de carbone (CO), CH_4, les composés organiques volatiles (COV), l'ammoniac (NH_3), l'acetonitrile (C_2H_3N), le cyanure d'hydrogène (HCN), le chlorure de méthyle (CH_3Cl), les composés soufrés (Crutzen and Andreae, 1990; Yokelson et al., 1997; Andreae and Merlet, 2001; Urbanski et al., 2009). Ces émissions complètent la production des espèces oxydées provenant de la phase de *flaming* : CO_2, le monoxyde d'azote (NO), l'azote (N_2), le dioxyde d'azote (NO_2), le protoxyde d'azote N_2O, le dioxyde de soufre (SO_2), etc. (Crutzen and Andreae, 1990; Yokelson et al., 1996; Andreae and Merlet, 2001;

Urbanski et al., 2009). La plupart des composés sont émis pendant le *smouldering*, par contre les plus grandes quantités des éléments comme le carbone, l'hydrogène, l'azote et le soufre sont associés au *flaming* (Lobert and Warnatz, 1993). Il est commun d'associer chaque espèce produite par la combustion à une de deux phases en identifiant le CO_2 comme l'espèce majeure du *flaming* et le CO pour le *smouldering*. Pourtant, il existe des exceptions à ce comportement général : l'acétylène (C_2H_2) et le cyanogène (NCCN) sont émis en quantité comparable pendant les deux phases, le cyanure d'hydrogène HCN et l'acétonitrile CH_3CN sont typiquement associés au *smouldering*, mais sont aussi émis pendant le *flaming*. La caractérisation et la quantification des espèces émises en fonction de la végétation brûlée reste donc un enjeu important. Cette connaissance amont conditionne l'estimation de l'impact des feux de végétation sur la composition chimique et le vieillissement des panaches de feu et donc la dangerosité pour les populations exposées.

La composition chimique des panaches de feux

A partir des années 40, des scientifiques se sont intéressés à l'étude des feux de végétation (Sullivan, 2007a). En ce qui concerne les émissions, des premières mesures ont été faites à partir des années 60-70 (Darley et al., 1976; McMahon and Ryan, 1976). Aujourd'hui, différentes méthodes existent pour mesurer les émissions de feux de l'échelle de la flamme à l'échelle globale, en étant même capable, dans certains cas, de séparer les produits du *flaming* de ceux associés au *smouldering*. Entre les différentes techniques, il y a les mesures en laboratoire où le feu est reproduit dans une chambre de combustion, avec la possibilité de contrôler les conditions de brûlage (e.g. Yokelson et al. 1996, 1997; Goode et al. 1999; Holzinger et al. 1999; Greenberg et al. 2006) ; ce type de mesures se révèle très utile pour parcourir le spectre complet des émissions des feux et donner des informations importantes pour la modélisation des réactions chimiques à fine échelle. A plus grande échelle, il y a les mesures en surface qui peuvent être réalisées pendant des feux prescrits à des distance de l'ordre de quelques dizaines de mètres (Miranda et al., 2005; Alves et al., 2010a; Barboni et al., 2010; Alves et al., 2011), ou pendant un feu occasionnel dont le panache a été mesuré par le réseau urbain de contrôle de la qualité de l'air après avoir été transporté sur des dizaines de kilomètres (Cheng et al., 1998; Phuleria et al., 2005; Saarikoski et al., 2007; Hu et al., 2008; Miranda et al., 2009b; Bytnerowicz et al., 2010) ; malgré une limitation intrinsèque pour pouvoir séparer le *flaming* du *smouldering*, ces mesures offrent des informations importantes pour comprendre et représenter l'interaction être la chimie des feux et celle de l'atmosphère, en particulier dans le milieu urbain. Les mesures aéroportés ont permis, entre autres, d'identifier la production photochimique d'O_3 due aux émissions importantes de précurseurs (NO_x, COV) (Helas et al., 1995; Mauzerall et al., 1996; Singh et al., 1996; Sanhueza et al., 1999). Ces mesures aéroportées ont aussi permis de confirmer la destruction de l'O_3 près du point d'éclosion (Hobbs et al., 2003; Jost et al., 2003) anticipée par des modèles. Parmi les études récentes menées

sur des campagnes avions, les travaux de Yokelson et al. (1999, 2003, 2007) sur les feux tropicaux, de Singh et al. (2010) sur les feux boréaux, mais aussi les mesures effectués par des avions de ligne dans le contexte du programme MOZAIC (Tressol et al., 2008; Elguindi et al., 2010) ont permis de progresser sur la caractérisation de la composition chimique des panaches et de leur évolution au cours du transport. La diversité des feux, et des émissions associées, à l'échelle globale ainsi que leur interaction avec le climat et la végétation ont pu être mieux appréhendés par les scientifiques grâce à l'arrivée de satellites. Désormais, les observations satellitaires permettent de mesurer la quantité des gaz et aérosols émis par les feux (e.g. Thomas et al. 1998; Bremer et al. 2004; Barnaba et al. 2011; Mebust et al. 2011), d'identifier les panaches de fumée et la pollution associée aux feux de végétation (e.g. Pace et al. 2005; Mazzoni et al. 2007; Turquety et al. 2009; Rolph et al. 2009), de reconstruire la distribution vertical des aérosols et gaz (e.g. Hoff et al. 2005; Edwards et al. 2006; Gonzi and Palmer 2010), de déterminer la hauteur d'injection de feux de végétation (e.g. Labonne and Chevallier 2007; Martin et al. 2010; Guan et al. 2010), ou de comprendre l'intensité, la durée et la source des panaches de fumée potentiellement associés à des feux de végétation (e.g. Pfister et al. 2005). Des simulations avec des modèles numériques O-D ont permis de qualifier la chimie des panaches de feux, leur interaction avec l'air ambiant et la production de O_3 dans le panache (Poppe et al., 1998; Mason et al., 2001, 2006).

Certaines des études citées ci-dessus portaient sur les incendies dans le bassin méditerranéen (Miranda et al., 2005; Pace et al., 2005; Turquety et al., 2009; Barboni et al., 2010; Alves et al., 2011). Pourtant, à l'heure actuelle, il reste encore un grand écart en terme d'informations disponibles sur les feux de végétations en Méditerranée en ce qui concerne la caractérisation de la végétation, des émissions, de la hauteur d'injection, de l'évolution et propagation.

La modélisation des feux de végétation

En 1996, Liousse et al. conduisent une des premières simulations d'aérosols de combustion à l'échelle globale. Les auteurs concluent sur deux sources d'incertitude majeures : les inventaires d'émissions utilisés et la hauteur d'injection des produits émis par le feu. L'étude présentée ici s'inscrit dans la continuité de ces interrogations en faisant le choix de simulations à plus fine échelle, en intégrant des paramétrisations physiques des soulèvements convectifs associés au feu et en privilégiant finalement un couplage fin entre un modèle atmosphérique et un modèle de propagation de feu. La notion de modèle de propagation de feu n'est pas usuelle dans le domaine des sciences de l'atmosphère. Pourtant la volonté de prévoir le comportement des incendies à l'échelle locale a porté les scientifiques à développer très tôt des modèles numériques qui reproduisent la propagation du feu en surface (Sullivan, 2007a). Trois types de modèles de propagation du feu en surface existent qui se différencient entre eux par leur niveau de complexité dans le traitement de l'interaction du feu avec la végétation, le terrain et le vent. Se distinguent les modèles

empiriques pour lesquels le comportement du feu est défini par rapport à des données expérimentales, des modèles mathématiques qui ont pour but d'améliorer les algorithmes de propagation du feu, et les modèles physiques qui décrivent le feu à partir des lois de la physique, chimie et dynamique de la combustion (Sullivan, 2007a,b,c). Pour l'ensemble de ces modèles, l'interaction avec l'atmosphère n'est pas représentée d'une façon réaliste alors que les échanges atmosphère/feu sont bien identifiés (Santoni et al., 2006; Clements et al., 2007) : un vent constant est généralement prescrit sur tout le domaine d'intégration. Ce verrou est aujourd'hui partiellement levé avec la nouvelle génération de modèle couplé feu-atmosphère : un modèle de propagation de feu en surface est couplé à un modèle atmosphérique pour pouvoir représenter l'impact du feu sur l'atmosphère et l'effet rétroactif de cet impact (Linn et al., 2002; Clark et al., 2004; Mell et al., 2007; Mandel et al., 2011).

Pour représenter la propagation de feu en surface, Balbi et al. (2007) ont développé un modèle physique simplifié qui s'appuie sur les lois fondamentales de la combustion et se sert de certaines approximations pour réduire le niveau de complexité associé à ce processus. Ce modèle a été intégré dans un simulateur qui reproduit l'avancement du feu : le modèle ForeFire. La faisabilité du couplage entre ForeFire et le modèle atmosphérique Méso-NH a été démontré dans Filippi et al. (2009). C'est cet outil qui est utilisé dans le cadre de ce travail avec différent degrés de couplage feu-atmosphère pour l'étude des feux en région méditerranéenne.

Objectifs et plan du manuscrit

Cette thèse a pour but principal d'étudier l'impact des feux de végétation sur la dynamique et la chimie de l'atmosphère en région méditerranéenne. Ce travail s'appuie sur le contexte multidisciplinaire d'un consortium réunissant des atmosphériciens, chimistes, spécialistes de la mécanique des fluides et thermiciens. Les questionnements scientifiques qui ont motivé ce travail sont :

1. déterminer les impacts d'un feu méditerranéen sur la dynamique et la chimie de l'atmosphère près et sous le vent de l'incendie.

2. approfondir la compréhension des processus convectifs induits par le feu et qui contrôlent l'évolution verticale des émissions. Ce point est l'occasion d'évaluer l'influence des conditions météorologiques et des caractéristiques des feux sur la hauteur finale d'injection.

3. étudier l'interaction atmosphère/feu à l'échelle du feu sur de cas réels de feux de végétation en méditerranée.

Le manuscrit est structuré en deux parties. La première partie concerne les fondamentaux du feu (Chapter 2) et les outils et méthodologies utilisés dans cette thèse (Chapter 3). Dans une deuxième partie les objectifs scientifiques listés ci-dessus sont abordés :

modélisation de l'interaction atmosphère/feu du point de vue chimique et dynamique à l'échelle de l'environnement sur le cas du feu de Lançon de Provence 2005 (Chapter 4) ; étude et modélisation de la hauteur d'injection des feux de végétation (Chapter 5) au travers d'un travail d'intercomparaison de deux modèles de thermiques pour des conditions météorologiques contrastées ; modélisation de l'interaction atmosphère/feu à l'échelle du feu (Chapter 6). Enfin, les conclusions et perspectives de ce travail sont données dans le Chapitre 7.

Chapter 1

Introduction: wild-fires in the earth system

Contents

This chapter aims to introduce the reader to the thematic of vegetation fires by giving, firstly, an overview of these events through human history (Section 1.1) and in the actual global perspective (Section 1.2). Secondly, the impact of vegetation fires on climate and air pollution is illustrated in Section 1.3. Finally, the main aims and goals of this thesis are defined (Section 1.4) and the outline of the study is given (Section 1.5).

1.1 From primordial to actual fires

Favourable conditions for the ignition of vegetation fires must have appeared around 350 to 400 million years ago, during the Paleozoic era (Pyne et al., 1949, pag.). At that time, the super continent Pangaea built, this geophysical process favoured the growth of plant matter on dry land and make possible the accumulation of "fire potential" in the form of combustible organic material (Andreae, 1991). Afterwards, climatic and ecological parameters, as drought periods, the lightning or volcanic eruption, started triggering natural vegetation fires. With the advent of herbivorous organisms that consumed vegetation in those layers of wooded savanna where fires would normally propagate, another natural parameter was added to the control of the rate of fire potential accumulation. Until the end of the Tertiary (nearly 2.6 million years ago), the interplay between all these factors (i.e. lightning frequency and dry seasons, plant growth and its removal by mammals) have ruled the natural fire regimes on Earth (Andreae, 1991).

When the prehistoric human overcame the fear of fire, common to all other primates, and learned to use wild-fires, a profound event within the earth system undoubtedly happened (Pyne and Goldammer, 1997). First evidence of the ecological impact of anthropogenic fires can be identified already about 1.5-2 million years ago in African savannas when fire was used by humans for food preparation, hunting and landscape control (James, 1989). Later on, other anthropogenic activities developed and began to make use of fire, as farming, pastoralism and production of ceramics, metallurgy (Pyne and Goldammer, 1997) and the burning of agricultural waste. To put on evidence how profoundly the human use of fire may have affected the earth's ecology, it is interesting to cite the shift from pyrophobic to pyrotolerant and pyrophilic vegetation species observed in pollen records of 40000 million years ago together with an increase of 3 orders of magnitude in charcoal particles in sediment cores (Schule, 1990). Fire has influenced the human development even in terms of culture: in various civilizations, fire is found to be part of ancient philosophies (e.g. in Babylonia, Egypt, Greece, India, China, Japan) as one of those classical elements believed to reflect the simplest essential parts and principles of which anything consists (`http://en.wikipedia.org/wiki/Fire_(classical_element)`). More recently, man-made fire serves a variety of purpose: clearing of forest for agriculture use, pasture-land maintenance, pest-control, nutrient regeneration, control of fuel accumulation in forests, as well as charcoal production for industrial and domestic use and the combustion of biofuels as renewable energy. All these sources have considerably increased human related

fire processes (Andreae, 1991; Pyne and Goldammer, 1997).

1.2 Global and seasonal distributions

Today, fire is a global issue affecting almost all climates and vegetation functional groups. However it is not simple to give accurate statistics on the global burnt area (Chuvieco, 2009). Pessimistic estimates give a value between 500 and 560 million ha burned annually worldwide based on different observations (Levine et al., 1999). Optimistic estimates range between 200 and 350 million ha burned per year based on SPOT-Vegetation data (Tansey et al., 2004). Tansey et al. (2008) recently calculated an updated global amount between 350 and 440 million ha burned every year for the period 2000-2007. Global and seasonal distributions of wild-fires for the period 1997-2006 are shown in Figure 1.1.

Across the world, fire differs in connection with the available fuel. A common typology groups the earth's biomes into four broad bio-climatic zone: boreal, temperate, Mediterranean, and tropical. This division reflects the existence of floral kingdoms whose formation traces back to the breakup of Pangaea into a succession of smaller units (Pyne et al., 1949, pag. 629). North America and Eurasia remained link for a long time, and accordingly share a common boreal biome, mixed with a temperate biome at mid-latitudes. The tropical biotas all lie within the Gondwana supercontinent whose fragmentation led to Central and South America, Africa, South Asia and Australia. The Mediterranean biotas are scattered among the five continents. The boreal, temperate and tropical fire types are discussed in the following sections. Fires in the Mediterranean region are described in a dedicated section (1.2.4).

1.2.1 Fires in the boreal ecosystems

The boreal climate confronts long winters and short, intense summer growing seasons. Under this climatic conditions, the *taiga*, or boreal forest, predominates as a vegetation type and it is mainly composed of coniferous species. Going northern, the tree growth is hindered by low temperatures and the closed-crown boreal forest, with its moist and deeply shaded forest floor, thins into a lichen-floored low-density forest or woodland, which in turn becomes progressively more open and *tundra* dominates with increasing latitudes. In boreal regions, the decomposition of the vegetal fuel is even slower than the growth; hence, woody fuels accumulate, lichens thicken and organic soils build into peat where sites are wet (Pyne et al., 1949).

The normal fire regimes reveal infrequent but large and high intensity crown fires or long-lasting smouldering peat fires. It is recognized that spread rate (and the resulting fire front intensity) for surface fires are much lower than crown fires. The lower intensity creates smoke plumes that are generally weak and diffuse.On the contrary, crown fires are generally associated with strong convective processes. For these fires, the fire plumes

can escape the boundary layer and even reach the stratosphere during strong events of pyroconvection (Fromm et al., 2008). Fires in boreal regions usually burn from May to September, though the inter-annual variations in these regions are high (Langmann et al., 2009). The typical boreal fires cover areas 10000 ha in extent and routinely exceed 100000 ha (Beverly and Martell, 2005). Lavoue et al. (2000) detail contributions from temperate and boreal fires, demonstrating that about 90% of the global boreal fire area is in Russia and Canada. Alaska accounts for only about 4.5% of the global boreal forest, but it accounts for at least 10 percent of the emissions from that source, because of the heavier fuel loads in Alaska.

In the last 20 years, the scientific interest in boreal and peat fires has increased since they are important sources of fire smoke pollution (about 10% of global carbon emissions with high interannual variability (Kasischke et al., 2005; Turquety et al., 2007)), with even some documented episodes of transboundary transport (Saarikoski et al., 2007; Goldammer et al., 2009; Chubarova et al., 2009; Pommier et al., 2010; Konovalov et al., 2011).

1.2.2 Fires in temperate ecosystems

The temperate climatic region is an intermediate zone, a place in which the seasons balance, biomes diversify, and biomass is equitably distributed. The fire season nearly overlays the one of the boreal biota.

Once, during the early colonization of Europe (Roman Empire) and North America (18th and 19th centuries), the deforestation fire trend was more intense in temperate forests (Pyne, 1995). Today, in industrialized societies, deforestation fires are nearly no more used, hence forest fires are principally associated to recreational activities that may cause fires either by carelessness or arson (Chuvieco, 2009). For instance, in central and eastern Europe (CEE), Szczygiełet al. (2009) indicated Poland as the most hazardous situation where over 60% of CEE fire happen. These fires (mainly arson) initiate and spread easily due to the domination of young coniferous stands in temperate forests that are, thus, exposed to medium fire danger. However, fires in temperate ecosystems are minor contributors compared to the boreal and tropical regions. On the other hand, compared to boreal forests and peatlands that are located in remote lands, temperate forests are often found close to urban areas; hence, temperate wild-fires frequently impact the air quality in nearby metropolis (e.g. Hu et al., 2008).

1.2.3 Fires in the tropical region

In the tropics, temperatures remain relatively constant and warm throughout the year, hence seasonal variations are defined with respect to precipitation (dry and wet season). The seasonal trends of wetness and dryness defines a role for fire: the stronger the cycle

from wet to dry, the stronger the presence of fire; the more frequent the oscillation between wet and dry, the more frequent the fire cycle (Pyne et al., 1949, pag. 637).

Closed rainforests burn rarely because of unfavourable microclimate and scarce surface fuel to carry combustion. This means that plants in such a biome are not adapted to survive fire, and thus present a high mortality rate (Hoelzemann, 2006). Some exceptional cases have been reported where short-term natural disturbances (e.g. severe droughts triggered by El Ñino-Southern Oscillation) resulted in devastating fire (rainforest fires of 1982 and 1983 in Indonesian Borneo, Molion, 1991). At present, humans are playing a major role in reducing the natural rainforest cover in the tropics through two methods to forest clearing for agricultural use: the traditional shifting agriculture, which obey a fallow cycle; and the increasing permanent removal of forest, which replaces forest with grazing or crop land. In Brazil alone, from 2000 to 2005, fires were in the conversion of approximately 21800 km^2 per year of primary rain forests into pastures and agricultural lands (Hoelzemann, 2006).

Tropical savanna often burn annually because there is abundant available fuel (mainly grassland with interspersed trees and shrubs) and few competing organisms (other than termites). In savannas, fire regimes maintain an equilibrium between grasses and trees, otherwise trees will potentially expand and convert the grassy savanna into a wooded savanna and further into woodland or even forest. While lightning may start some fires in savanna, the great part of savanna fires are set by humans (slash-and-burn agriculture, pest-control, promotion of the growth of fresh grass for grazing) that caused the increase of the fire frequency with the growing population and more intensive use of rangeland (Andreae, 1991; Menaut et al., 1991).

In the tropics and subtropics most vegetation fire emissions stem from savanna burning in Africa, about 50% of the global total (Barbosa et al., 1999; Justice and Scholes, 2003). Large-scale savanna burning also takes place in Australia (Hurst et al., 1994) and South America (Prins and Menzel, 1992). Deforestation fires occur in Central and South America (in equal proportion with savanna burning, Hao and Lui, 1994), Africa (Delmas et al., 1991) and Southeast Asia (Achard et al., 2002). These emissions are not compensated for by re-growth and provide a net source of CO_2 to the atmosphere (Langmann et al., 2009). Injection heights of tropical fire emissions are still uncertain. Recent studies on equatorial Asia and Africa, based on satellite measurements with CALIPSO or MISR suggest that tropical fires plumes generally remain confined in the boundary layer (Labonne and Chevallier, 2007; Tosca et al., 2011).

As tropical and subtropical fires are typically set to clear fields and pastures in anticipation of the arrival of seasonal rains, the temporal distribution of burning is thus characterized by two main burning periods (Andreae, 1991; Delmas et al., 1991; Langmann et al., 2009): December to March (with maximum fire occurrence in January and February) related to burning in the Northern Hemisphere tropics and subtropics (especially Southeast Asia and Africa); June to November (with maximum peaks in September

and October) mainly caused by burning in South America and Southern Hemisphere Africa. It is worth noting that, due to their abundance and their critical impact on the global climate and atmospheric chemistry (e.g. Fishman et al., 1990; Helas et al., 1995), tropical vegetation fires motivated the first studies on the role of vegetation fires at global scale.

1.2.4 Fires in the Mediterranean region

The Mediterranean region has a clear climatic definition: short, mild and wet winters that are adequate to produce vegetal fuel; long, hot and dry summers that favour an intense and severe fire season. It is an environment designed to burn (Pyne et al., 1949, pag. 635). Mediterranean-type ecosystems are located in mid-latitudes on all continents, often in coastal regions. Vegetation structure is mainly shrub-dominated, but woodlands, forests and even grasslands occur in limited regions. Heavily utilised landscapes are dominated by grasses, herbs and annual plant species (Lavorel, 1999). According to the European Forest Fire Information System of the Joint Research Centre (`http://effis.jrc.ec.europa.eu/`), about 60000 fires occur, on average, every year in the largest European Mediterranean countries (Portugal, Spain, France, Italy and Greece), burning approximately half a million ha (Barbosa et al., 2009; San-Miguel-Ayanz et al., 2009) during the Northern Hemisphere's summer. From its creation in 1980, the EFFIS system have observed a clear increase in the number of Mediterranean fires with a noticeable step in the 1990's (probably due to the improved methods of data collection in the fire-prone Mediterranean countries), followed by a less clear trend. No particular trend was observed in the total burnt areas from 1980 to 2009 (San-Miguel-Ayanz et al., 2009).

Unlike other parts of the world where a large percentage of fires are of natural origin, Mediterranean fires are chiefly human-induced, while natural fires represent only a small percentage of the total number (from 1 to 5%, depending on the country), probably because of the absence of climatic phenomena such as dry storms (Alexandrian et al., 1999). Another characteristic common to the entire Mediterranean Basin is the high number of fires of which the cause is unknown. When the cause is known, fires are in the majority involuntary (negligence or accidents). The accidental causes vary between countries and their list is very long: from fixed installations (power lines, rubbish dumps) to human activities (uncontrolled burning, smokers, campfires, fires set by shepherds). However, it seems that these involuntary fires are directly related to agricultural and forestry activities, hence the parties at fault are mainly permanent inhabitants and seldom passing tourists (Alexandrian et al., 1999).

In industrialized societies, socio-economic changes have led to depopulation of rural areas, abandonment of agricultural land, and in a substantial cultural shift in the popular perception of forests that are no more seen as a resource but as a recreational place (Leone et al., 2009). This resulted in the expansion of wooded areas, erosion of the

financial value of the wooded lands, a loss of inhabitants with a sense of responsibility for the forest and, what is important, an increase in the amount of fuel (Alexandrian et al., 1999). Nowadays, even if fire does not belong anymore to the traditional system of life in industrialized societies, vegetation fires continue to occur and their dramatic consequences are always strongly tied to human activity. Paradoxically, the increased standard of living is the fundamental cause of forest fires in some regions of the world as in the Mediterranean Basin.

The last report of the IPCC (2007) highlighted that in Mediterranean Basin region climate change is making weather conditions more severe. Extreme meteorological situations are likely to allow forested areas to become ignited, strengthening fire intensity, fire extent and fire frequency as noted by Pausas (2004) and Moriondo et al. (2006), and as reported every year by the EFFIS report (e.g. EFFIS, 2008). Recently, 2003 and 2005 summers experienced an unprecedented heat wave together with extreme drought conditions which favoured dramatic fires in south-western Europe (Portugal, Hodzic et al., 2007; Miranda et al., 2008; Tressol et al., 2008; Spain, and southern France, Strada et al., 2012). Similarly, severe conditions (strong winds and extremely high temperatures, following prolonged droughts periods) recorded in summer 2007 favoured large wild-fires in Italy and Greece (Turquety et al., 2009).

The increasing occurrence and severity of wild-fires in the Mediterranean Basin has motivated studies on the chemical behaviour of Mediterranean fires and their influence on air pollution at different scales. Satellite observations (e.g. Pace et al., 2005; Cinnirella et al., 2008; Turquety et al., 2009) and airborne measurements (e.g. Tressol et al., 2008) were used to characterize the fire plume aging and dispersion at regional and continental scales. Modelling exercises (e.g. Hodzic et al., 2007; Valente et al., 2007; Miranda et al., 2008) were dedicated to the characterization of fire emission and their injection heights. Experimental prescribed fires (e.g. Miranda et al., 2005; Alves et al., 2010a; Barboni et al., 2010; Alves et al., 2011) helped in the determination of fire emission factors close to the fire.

1.2.5 Human-caused wild-fires: a global impact

At the global scale, climate, vegetation, and fire interact to produce a complex pattern of fire occurrence. While humans have had an understanding of weather and fire occurrence at a local scale for centuries, only recently, thanks to the satellite imagery, scientists have improved the ability to look at the large-scale connections between wild-fire occurrence, vegetation, and climate (Benson et al., 2009).

Although fire is a natural process, nowadays humans are believed to be responsible (directly or indirectly) for at least 90% of biomass burning on Earth; the remaining 10% of natural fires are still ignited by lightning activity in tropical savanna and some temperate and boreal forest ecosystems (Andreae, 1991). Most anthropogenic wildland fires

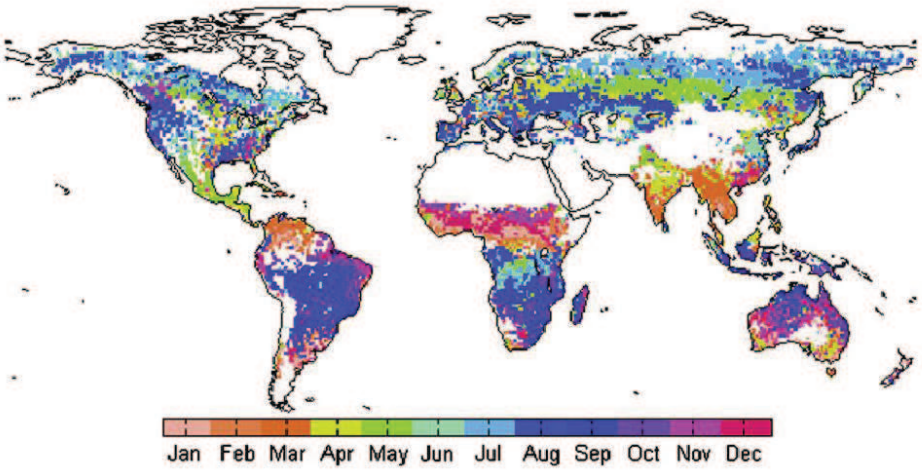

Figure 1.1: Peak fire month based on GFED2 averaged over 1997-2006 (from Langmann et al., 2009).

regularly take place in the tropics, either in tropical savannas for agricultural purposes or as deforestation fires in primary rain forest. It is likely that annual biomass burning has strongly increased (30-50%) over the last century, due to the intense tropical deforestation and enhanced domestic fuel wood combustion (Scholes et al., 2003). Future scenarios seem to be worse. The last report of the Intergovernmental Panel on Climate Change (IPCC, 2007) stated that a temperature increase between 3 and 5 °C may result in an increase of fire hazard for forests; among potential stricken regions, the IPCC drew attention on Australia, New Zealand and Europe (in particular, the Mediterranean Basin region, Section 1.2.4). This scenario put society on the alert because vegetation fires have enormous and devastating impacts, including loss of human and animal lives, short and long-term effects on human health and deterioration of resources (e.g. timber, crops, soils) with related economic costs (Chuvieco, 2009).

1.3 Climate and air pollution impacts

Several studies showed the large spectrum and the huge amount of trace gases and aerosols released by wild-fires during the combustion process (e.g. Crutzen and Andreae, 1990; Yokelson et al., 1996, 1997, 2007; Lobert and Warnatz, 1993; Andreae and Merlet, 2001). Trace gases associated with vegetation fires are carbon dioxide (CO_2, the most abundantly emitted gas), carbon monoxide (CO), methane (CH_4), volatile organic compounds (VOC), nitrogen oxides ($NO_x = NO + NO_2$), nitrous oxide N_2O, ammonia (NH_3), methyl halydes (methyl chloride CH_3Cl, and methyl bromide CH_3Br), etc. (e.g. Pyne et al., 1949; Crutzen and Andreae, 1990; Andreae, 1991; Lobert and Warnatz, 1993; Andreae and Merlet, 2001; Goldammer et al., 2009; Chapter 2). Vegetation fire smoke also con-

tains particulate matter (PM) (Reid et al., 2005) that can be primarily released during combustion or formed through physical and chemical transformations (molecular agglomeration, nucleation) (Goldammer et al., 2009). Particles can be coarse, with diameter up to 10 μm, (PM_{10}), fine with diameter up to 2.5 μm ($PM_{2.5}$), or ultra-fine with diameter smaller than 0.1 μm (Sandstrom et al., 2005).

Global yearly emissions from vegetation fires have been estimated which reveal a high interannual variability, mainly controlled by seasonal distribution, driven by the regional dry seasons (Section 1.2) (Andreae and Merlet, 2001; Ito and Penner, 2004; van der Werf et al., 2006). Globally, the annual contribution of fire emitted species to the total species budget is about 40% for CO, 20% for NO_x and 35% for carbonaceous aerosol particles (IPCC, 2001). A recent estimation of fire CO_2 emissions accounts for 2.5 Pg C $year^{-1}$ over the 1997-2004 period with a large interannual variability (van der Werf et al., 2006). This amount is nearly one third of the total emissions due to fossil fuel combustion, which averages 7.2 Pg C $year^{-1}$ over the 2000-2004 period according to the IPCC (2007). More than 60% of the reported amount of CO_2 is released from savannas and grasslands, and another 25% from tropical forests (`http://www.forestencyclopedia.net/p/p4/p138/p623/p630/p638`). The present annual carbonaceous fire emissions rival or may even exceed those from combustion of fossil fuels (Crutzen and Andreae, 1990).

Vegetation fire products have several environmental impacts on vegetation (e.g. Grulke et al., 2009; Pérez-Cabello et al., 2009), soil (e.g. Bell and Adams, 2009; Pérez-Cabello et al., 2009), water (e.g. Battle and Golladay, 2003; Johnson et al., 2009), and atmosphere. Fire-induced effects may appear in the short and long term, on a local and regional, sometimes even global, scale. Focusing on fire impacts on the atmosphere, all fire released chemical species alter the atmospheric chemistry at diverse spatial and temporal scales, leading to important impacts on the global climate (Section 1.3.1) and the air quality (Section 1.3.2).

CO reacts with about 70% of the hydroxyl radical (OH) that is present in background air. As a consequence, the oxidative efficiency of the atmosphere (mostly associated with OH concentrations) can substantially decrease due to CO emission and the concentrations of many trace species increase (Crutzen and Andreae, 1990; Jacobson, 2001). Fire emitted methyl halides contribute to stratospheric ozone (O_3) destruction. Owing to the phase-out of the halons (chlorofluorocarbons and bromofluorocarbons) under the Montreal Protocol, the relative importance of methyl halides for stratospheric O_3 loss is expected to increase (Andreae et al., 1996a). Many fire-emitted trace gases, especially CO and NO_x, are precursors of the tropospheric O_3. In the troposphere, O_3 photochemical production occurs by hydroxyl radical oxidation of CO, CH_4 and the VOCs in the presence of NO_x (Penkett et al., 2003). Granier et al. (2000) stated that about 25% of the global net chemical production of O_3 results from biomass burning. High tropospheric O_3 abundances, similar to values recorded in highly polluted regions, has been firstly observed over the Southern Atlantic using satellite instruments, and this signature has been ascribed to African

savanna fires (Fishman et al., 1996). This observation has been further investigated by various field and airborne campaigns (Helas et al., 1995; Thompson et al., 1996; Mauzerall et al., 1996; Singh et al., 1996; Sanhueza et al., 1999). These studies also pointed out the large uncertainties on the quantitative estimate of O_3 precursors from wildland fires (Hoelzemann, 2006).

The vegetation fire emissions were found to significantly affect climate and air quality. In the following sections, a brief overview of these two impacts is given.

1.3.1 Fire vegetation as a climate forcing

The Kyoto protocol reinforced the importance of fires within the climate system and has drawn the public attention to this topic (Hoelzemann, 2006). Diverse studies contributed to identify the potential role of vegetation fires on global climate (e.g. Goldammer and Price, 1998; Stocks et al., 2000; Nepstad et al., 1999).

The dominant fraction of fire emissions contains carbon. Among fire carbon products, CO_2 and CH_4 are probably the most important greenhouse gases (i.e. they efficiently absorb and scatter radiation within the thermal infrared range) responsible of the "enhanced greenhouse effect". CO_2 and CH_4 alter the atmospheric chemistry at global scale and contribute to global climate change (Andreae, 1991). Vegetation fires also emit vast amounts of N_2O, water vapour (other two important greenhouse gases), and carbonaceous aerosols (e.g. Crutzen and Andreae, 1990; Brasseur et al., 1999; Crutzen and Lelieveld, 2001). Moreover, as previously explained, some primary gaseous emissions from fires lead to the formation of O_3 that is recognized by now to efficiently absorb infrared radiation (Ramanathan et al., 1985). Fire carbonaceous aerosols can be distinguished between Black or Elemental Carbon (BC or EC), Organic Carbon (OC), and trace inorganic species such as potassium, chlorine, and calcium (Reid et al., 2005). They not only contribute but also counterbalance the effects of greenhouse gases on a regional and global scale (Pfister et al., 2008). In particular, BC aerosols positively contribute to the radiative heating of the atmosphere (Jacobson, 2001); while OC, which is emitted along with BC, has a cooling effect on climate and may totally balance the warming potential of EC in the case of aerosols from vegetation fires, due to their characteristic high OC/EC ratios (Schaap and van der Gon Denier, 2007). Moreover, fire aerosols reduce radiative actinic fluxes, thus severely reducing the photochemical production of tropospheric O_3 below and within the aerosol haze layer (Albuquerque et al., 2005).

On the Earth, the intensity of the greenhouse effect also relies on the surface albedo, the reflecting power of a surface. Vegetation fires influence this parameter in two ways: (1) by deposition of black carbon aerosols onto bright ice and snow surfaces reduces surface albedo (Stohl et al., 2006) inducing a positive radiative forcing (e.g. Hansen and Nazarenko, 2004) and (2) by the modification of the vegetation cover where the fire burnt also changes the surface albedo (e.g. Govaerts et al., 2002; Jin and Roy, 2005).

Fire aerosols also modify precipitation patterns by micro physical and dynamical alterations in cloud formation (Crutzen and Andreae, 1990; Kaufman, 1995; Kaufman and Fraser, 1997; Ramanathan et al., 2001). Cloud droplets form on aerosol particles that are called cloud condensation nuclei (CCN). The number of available CCN define cloud characteristics: enhanced aerosol concentrations make more CCN available, hence, for a given amount of water, more cloud droplets can form with smaller droplet size (Warner and Twomey, 1967; Hobbs and Radke, 1969; Andreae et al., 2004). Clouds made up of many and smaller droplets produce two effects: first, the higher droplet quantity reflects more sunlight back into space (negative radiative forcing); second, the reduced size is less favourable to provoke precipitation, because small droplets do not tend to coalesce into raindrops as efficiently as larger droplets (Crutzen and Andreae, 1990). On the other hand, fire enhanced aerosol levels provoke changes in the thermodynamic stability. By cooling the lower atmosphere through direct interaction with solar radiation, aerosol particles restrict ascending convective cells that are generated close to the surface, and thereby inhibit cloud formation (Hoelzemann, 2006), as it was observed over the Mediterranean Basin region by Pace et al. (2005).

The illustrated potential changes in cloud formation, and their spatial distribution, and in precipitation efficiency add to the perturbation of the hydrological cycle (e.g. Rosenfeld, 1999; Artaxo et al., 2002, 2005). Through evapotranspiration, forests return precipitations back to the atmosphere in the form of water vapour where it can form clouds and rain again in a cycling way. This cycle is extremely efficient in the tropics where precipitations are highest. The conversion of forests into grassland through deforestation impoverishes the soil that will be more prone to desertification, water will run off more quickly and return through rivers to the ocean, allowing less recycling. Such a modification of the hydrological cycle may itself perturb tropical weather and maybe even climate. Furthermore, less evapotranspiration and precipitation will lengthen dry seasons increasing the risk of fire occurrence (Crutzen and Andreae, 1990).

The interactions of fires with the Earth's biosphere have significant and complex implications on biogeochemical cycling (Crutzen and Andreae, 1990). Forest and grassland systems are carbon sinks and sources since they sequester and emit CO_2. In a stable environment, the natural cycle of disturbance (e.g. fire, insects, severe weather events) and regrowth can be expected to result in a constant level of carbon storage, in vegetation and soils, and loss, through fire emissions, decomposition and other processes (Conard and Solomon, 2009). The increasing rate of vegetation fires due to man and climate change may counterbalance and accelerate the long-term dynamics of cycling and storage of carbon and other elements. In the time scale of a deforestation fire (a few hours to days), the CO_2 abundantly stocked in plant material is promptly released. This CO_2 repository took a long time to build and can not be rapidly restored (forests take decades for regrowth), instead of savanna where burnt vegetation can be restored within a period of weeks to months (Cardoso, 2004). Hence, in a substantially lower time scale, all carbon stored for

a long time within the plant is suddenly released in a sort of explosion of the normal CO_2 release rate reached by conventional plant respiration processes. Moreover, the death of plants induced by fire leads the CO_2 uptake by photosynthesis, and thus its removal from the atmosphere, to cease.

Changes on global climate bear a considerable impact on fire: lower precipitation and higher temperatures modify fuel load growth, soil and fuel moisture, being responsible for changes in fire regimes, which in turn influence ecosystem changes (Goldammer, 1991).

1.3.2 Wildfires and air pollution

Nowadays, society, stakeholders (e.g. firefighters, forest service agents) and scientists share the awareness that the abundant release of aerosols and chemical compounds from vegetation fires largely has a detrimental influence on air quality (Langmann et al., 2009; Chapter 2).

Vegetation fire plumes contain diverse toxic compounds that have deleterious or adverse biological effects on human health in the short or long term (Goldammer et al., 2009; Barboni et al., 2010; WHO/UNEP/WMO, 2000):

- *Respiratory irritants*, as NH_3, NO_2, formaldehyde (HCHO) and PM, that can cause inflammation of mucous membranes and even changes in respiration and lung functions.

- *Asphyxiants*, as CO and CH_4, that prevent or interfere with the uptake and transport of oxygen. High levels of CO can result in immediate collapse and death.

- *Carcinogens*, as (in order of toxicity) benzene, HCHO, acetaldehyde (C_2H_4O), toluene and phenol (C_6H_6O), that are known or believed to cause cancer in humans.

- *Mutagens*, as HCHO and toluene, that change the hereditary genetic material, probably an early step to the development of cancer.

- *Systemic toxins*, as mercury (HG), chemicals that can cause toxic effects as a result of their absorption and distribution to a site distant from their entry point.

Some of these effects are even more dangerous than the fire itself as it is reported by Caballero (2003) concerning the summer 2003 in Spain. Furthermore, some of the cited compounds do not have only a single effect on human health (e.g. benzene causes respiratory tract irritation if inhaled, and it is a human carcinogen in the long term, Barboni et al., 2010). The forest-firefighting community has expressed concerns about the listed health risks due to their frequent and extended exposure to fire smoke (Barboni et al., 2010), thus motivating diverse studies on this subject (Miranda et al., 2005; Alves et al., 2011; Adetona et al., 2011).

Exposure limit values have been imposed by national health and safety commissions in the USA and Europe in order to control concentrations of hazardous species emitted by different sources (cars, industries, houses, etc.) (e.g. European Commission Environment `http://ec.europa.eu/environment/air/quality/standards.htm`). During fire episodes, urban and rural air quality monitoring stations have often measured critical concentrations (i.e. higher or close to fixed exposure values) of PM (Saarikoski et al., 2007; Sofiev et al., 2008; Hu et al., 2008; Miranda et al., 2009b; Strada et al., 2012), NO_x and CO (Cheng et al., 1998; Phuleria et al., 2005), O_3 with the associated photochemical smog (Cheng et al., 1998; Bytnerowicz et al., 2010). Experimental fires have highlighted the critical situation in terms of CO, PM, volatile organic compounds (VOC), NO_x and SO_2 emissions near the ignition point (Miranda et al., 2005, 2009a; Alves et al., 2010a,b; Barboni et al., 2010). While airborne (Helas et al., 1995; Yokelson et al., 1999; Hobbs et al., 2003; Yokelson et al., 2007; Singh et al., 2010) and spaceborne (Fishman et al., 1990; Thomas et al., 1998; Lupu et al., 2009; van der Werf et al., 2006; Turquety et al., 2009; Barnaba et al., 2011; Mebust et al., 2011) measurements have explored the large variability of fire pollutant concentrations from the ignition point to several kilometers away from the fire. Investigations of the chemical evolution (Poppe et al., 1998; Mason et al., 2006), the impact on air quality (Cheng et al., 1998; Miranda, 2004; Miranda et al., 2008; Hodzic et al., 2007), and the transport (Saarikoski et al., 2007; Sofiev et al., 2008) of fire plume through modelling exercises have helped to better understand the interactions between the fire plume and the background air and to assess the spatial and temporal extension of the area critically impacted by the fire plume.

Another effect of regional fire haze is a strongly reduced visibility due to the aerosol load in the air (Fox and Riebau, 2009), which repeatedly leads to impacts (e.g. irregularities in operation, closure, accidents) on strategic infrastructures as airports, highways, hospitals (e.g. Mobley, 1990; Muraleedharan et al., 2000; Dokas et al., 2007). Goldammer et al. (2009) reported the case of fires in Sumatra (Indonesia) that reduced the average daily minimum horizontal visibility over Singapore firstly to less than 2 km, and later to 500 m. The author also cited the 1997 Southeast Asia haze that caused regional pollution and resulted in closing of airports and marine traffic. Chemical transformation may lead to enhanced secondary pollution (e.g. ozone formation: Helas et al., 1995; Takegawa et al., 2003; Bytnerowicz et al., 2010) and acid rains (due to fire emissions of organic acids, Andreae, 1991). Hence, hazardous consequences for human beings (Goldammer et al., 2009; WHO/UNEP/WMO, 2000), plants and soil due to elevated concentrations of pollutants are observed near the burning area (Miranda et al., 2005; Alves et al., 2010a) and even far away (Phuleria et al., 2005; Miranda et al., 2008; Tressol et al., 2008; Turquety et al., 2009; Dirksen et al., 2009; Alves et al., 2011).

The impact of vegetation wild-fires on air quality strongly depends on the injection heights of the fire polluted plume. Vegetation fires are intense heat sources that can trigger strong vertical convective transport, depending on fire characteristics (fire heat, fuel

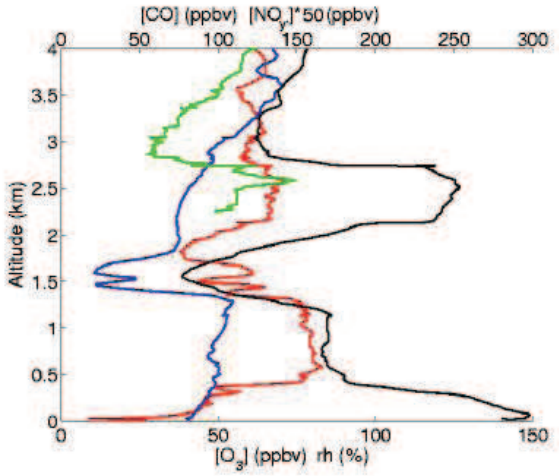

Figure 1.2: Signatures of portuguese wildfires on Nothern Europe during the 2003 European heat wave as seen by the MOZAIC profile at Frankfurt on 6 August 2003, 08:40 UTC. Top axis: CO (black) and 50 NO_y (green) mixing ratio (ppbv). Bottom axis: O_3 mixing ratio (ppbv, red) and relative humidity. The MOZAIC profile shows a CO layer between 2 and 3 km altitude, well correlated with relative maxima of NO_y and O_3 (from Tressol et al., 2008).

moisture) and on atmospheric stability and weather conditions (temperature, humidity and wind) (e.g. Freitas et al., 2007; Kahn et al., 2007; Rio et al., 2010). Hence, atmosphere and fire interact and their interconnection drives the fire propagation and its convective transport (Chapter 5), determining the altitude at which fire products will be finally emitted. Depending on the injection height of the fire plume (Freitas et al., 2007), the induced degradation of the air can extend from local scale, when the smoke plume keeps trapped in the Planet Boundary Layer, PBL (Chapter 4) (Miranda et al., 2009b; Hu et al., 2008; Strada et al., 2012), to regional and, occasionally, inter-continental scale, when fire pollutants are injected above the PBL (Fromm et al., 2005; Damoah et al., 2006) and are efficiently dispersed by stronger wind patterns in higher altitudes (Damoah et al., 2006; Sofiev et al., 2008; Elguindi et al., 2010; see Fig. 1.2). During these transport processes several of the chemical gases or particles are transformed by heterogeneous- and gas-phase chemistry, as modelled by Poppe et al. (1998) and Mason et al. (2001, 2006), as well as by aerosol microphysics and by thermodynamics (e.g. Hobbs et al., 2003; Jost et al., 2003).

1.3.3 Fire-atmosphere coupling: a challenge for models

In 1996, Liousse et al. published one of the first global simulations of fire aerosols. The authors highlighted the two major uncertainties in the fire-atmosphere coupling which are still under investigation today: the accuracy and resolution of biomass burning inventories

and the injection height of fire products. Since then, numerous works have been done with increased resolutions for models and improved physics and chemistry. A substantial effort is being made at the national (ETHER-ECCAD), european and international (GEIA) scales to improve the spatial and temporal resolution of fire inventories. A complete review of these works is out of the scope of this study. However, since the last ten years, an increasing number of publications dealt with the parametrisation of the fire injection height as discussed earlier in this section and on novel approaches of fire-atmosphere coupling at high resolution. In the United States, during the 70's researchers put their efforts into developing numerical models that could describe in (nearly) real time the propagation of a wild-fire (the so-called fire spread models). Operational fire spread models were a first answer to the stakeholders' demand, making it possible to forecast fire behaviour, to reduce fire impacts on the environment and to improve fire prevention (Sullivan, 2007a). Fire spread models have improved in terms of formulation and complexity from purely empirical (i.e. their formulation fits on empirical a-priori data) to physics-based systems (i.e. with a more robust theoretical formulation) to combinations of the two, making each of them appropriate for different applications (Sullivan, 2007a,b,c; Chapter 3). A major drawback of fire dynamic models is the missing atmospheric dimension of the fire propagation: ambient wind is considered as a not-evolving input of fire spread models (i.e. direct interaction between the dynamics of the fire and local winds is not taken into account). However, as previously underlined, fire behaviour is tightly linked to the environmental conditions (weather, terrain and fuel). It is therefore not realistic to treat all these aspects separately. For this reason, in the 90's, researchers began to develop coupled atmosphere/fire models (e.g. Heilman and Fast, 1992; Reisner et al., 1998; Linn et al., 2002; Clark et al., 2004). The main difficulty stems from the fact that the coupled system is an extremely non-linear multi-scale phenomena (Pyne et al., 1949; Mell et al., 2007; Mandel et al., 2011). The wide range of scales at hand in a wild-fire has always limited the development of coupled atmosphere/fire models. A fire front of about ten metres has the potential to release a sufficient amount of energy to impact the local and regional aerology over many kilometres (e.g. Fromm et al., 2005; Damoah et al., 2006), the same concerning air pollution (Section 1.3.2). Coupled atmosphere/fire model studies focus on small scale atmospheric processes, since at these resolutions these models are able to reproduce fire-induced effects on wind and turbulence that are known and feared by firefighters (e.g. Santoni et al., 2006; Clements et al., 2007). Due to their computational cost, coupled atmosphere/fire models at high-resolution are not often designed to consider fire impacts on atmospheric dynamics and chemistry at large scales. In the present work, the impact of fire at meso-scale and local scales is analysed with two levels of coupling between the fire and the atmosphere: a one-way coupling at meso-scale and a two-way coupling at local scales.

1.4 Objectives and methodology of this study

The primary goal of this work is to investigate the chemical and physical behaviour of vegetation fires in the Mediterranean region by means of modelling. For this purpose, a coupled atmosphere/fire model, which includes a chemical reactive scheme, was used with two levels of coupling: a one-way forcing of the atmosphere on the fire propagation and a full two-way coupling between the atmosphere and the fire.

The initial study focused on a real case study of a typical Mediterranean fire. The Lançon-de-Provence wild-fire occurred during summer 2005 (southern France), and was successfully simulated by the ForeFire model alone in Balbi et al. (2007). In order to investigate the fire impacts on the chemical composition of the air downwind of the burning area, the coupled MesoNH-ForeFire model is utilized at meso-scale in an off-line, or one-way, version. The study concentrates on the gaseous phase, while the aerosol phase is only explored by means of passive tracers released from the ignition point. For the Lançon fire, the validation of simulation results is accomplished through comparison with satellite images (regarding the plume transport) and data recorded by the air quality monitoring network available in the region affected by the smoke plume.

The second analysis is to delve into the physics that govern the injection height of the fire products in the atmosphere. This step is especially important given the high degree of uncertainty still associated with the fire injection height in chemical and aerosol transport modelling (Guan et al., 2010). For this purpose, the MesoNH-ForeFire model is utilized in a 1-D configuration with static fire. The model is applied to Mediterranean and Amazonian fires under contrasted meteorological scenarios and different fire characteristics. The Eddy-Diffusivity/Mass-flux (EDMF) approach, already implemented in Meso-NH (Pergaud et al., 2009), is activated to take into account shallow convective processes in the atmospheric boundary layer generated by surface heating. The simulation results are compared with a 1-D physically-based model specifically designed to provide a diagnostic value for the fire injection height, the 1-D Plume Rise Model (Freitas et al., 2010).

Finally, a third study illustrates the application of the two-way coupled version of the MesoNH-ForeFire model at high LES resolutions on real fires. This methodology aims to explore the capacity of the coupled model to correctly represent fire impacts to the atmosphere, in terms of emissions (i.e. passive tracers) and heat flux, when the fire is a resolved process, hence working at the fire scale. This goal has a practical importance since the major source of uncertainty in the prediction of the wild-fire evolution is the transient behaviour of fires due to changes in flows in the fire's environment (Sun et al., 2009) that can only be explored at high resolutions.

To resume, the main questions discussed in this work are:

1. evaluate the fire impacts on the chemical composition and the dynamics of the atmosphere close and downwind of a typical Mediterranean vegetation fire at meso-

scale;

2. assess the sensitivity of the injection height to the fire characteristics and the weather conditions in models when the fire is a sub-grid process;

3. investigate the impact of a two way interaction between the fire and the atmosphere in the propagation rate of the fire and the development of the smoke plume when the fire and the plume are resolved processes.

1.5 Outline

The manuscript has been developed into two main parts. The first one introduces the fire fundamentals (Chapter 2), and the tools and methodologies used in my work (Chapter 3). The second part gathers three studies that have been realized in order to delve into the understanding and the modelling of the atmosphere/fire interactions in terms of chemical (Chapter 4) and dynamical (Chapter 5) interconnections, down to the fire scale (Chapter 6).

Chapter 2 provides a general overview of the fundamentals of wild-fires giving the basic terminology and principles, illustrating mechanisms and products of the combustion process, and making a summary of the current approaches and limitations in the determination of wild-fire emissions. Chapter 3 describes the numerical models used in this work, the atmospheric model MesoNH and the fire spread model Forefire, as well as the development of a coupled atmosphere/fire model, MesoNH-ForeFire, in the light of the state of the art of coupled atmosphere/fire models. Chapter 4 presents the first effort to simulate a real large Mediterranean wild-fire by applying the one-way coupled atmosphere/fire model, MesoNH-ForeFire, in order to explore the impact of the Lançon-de-Provence fire on the atmospheric dynamics and chemistry downwind of the burning region. The chapter includes the research article "Forest Fire and Atmosphere: the Lançon-de-Provence 2005 case study" (now under favourable review on the journal Atmospheric Environment) (Strada et al., 2012). Chapter 5 presents the intercomparison exercise between the one-dimensional version of Meso-NH and a reference fire plume model to determine the fire injection height in contrasted meteorological environment. In the two previous chapters, the fire is seen as a sub-grid phenomenon. In order to study the interaction atmosphere/fire by means of the resolved physics, the fully coupled atmosphere/fire model MesoNH-ForeFire has been applied at the fire scale on real cases in Chapter 6. The chapter includes the research article "Simulation of Coupled Fire/Atmosphere Interaction with the MesoNHChem-ForeFire Models" recently published in the Journal of Combustion (Filippi et al., 2011). Finally, a summary of the most relevant results as well as perspectives on the investigations carried out completes this work in the final section, Chapter 7.

Chapter 2

A review of wild-fire fundamentals and smoke production

Contents

In this chapter, the fundamentals of fires in the wilderness are revised in terms of terminology, basic principles, mechanisms and products of the combustion process. A special attention is reserved to wild-fires in the Mediterranean Basin region.

The chapter is structured as follows: in Section 2.1 the different types of fires that can be observed and studied in the wilderness are defined; Section 2.2 introduces the fire scales from the flame to the global atmosphere; Section 2.3 synthesizes the principal phases of the combustion process and the associated products, mainly focusing on the gas phase; Section 2.4 presents the current approaches and limitations in the determination of forest fire emissions.

2.1 Classification of fires

The word "wild-fire", or its synonymous "wild-land fire", describes any uncontrolled fire that occurs in the wilderness, set by humans or occurred naturally (e.g. lightning or spontaneous ignition). Other names such as brush fire, bush-fire, forest fire, grass fire and peat fire are specifically referred to the type of combustible vegetation.

The complexity of wild-fire naming relies on the vegetation layer in which the fire is burning. Ground fires affect the sub-surface organic fuels (decomposing material and soil); surface fires spread at or near the surface through grass, shrubs, forest needle and leaf litter; finally, crown fires burn through the tree crowns or the canopies of the shrubs, consuming the live and mature foliage (Benson et al., 2009).

Fires are also categorized according to human management action. In United States terminology, wild-fires are those on which suppression action is taken. Prescribed fires can be ignited in order to meet a land management objective. Prescribed natural fires are those allowed to burn under an approved plan to preserve the natural role of fire in the ecosystem (Pyne et al., 1949, pag. 48).

Finally, the term "biomass burning" was defined for the study of all forms of combustion (i.e. prescribed and wild-fires, agricultural burning, fuel wood consumption, charcoal production, domestic fires) and their interaction with the atmosphere on a global scale,e and generally it refers to the production of atmospheric particulates and tropospheric gases (Pyne et al., 1949, pag. 620; Langmann et al., 2009).

2.2 From fire to global scales

Wild-fires are complex events driven by physical and chemical processes operating on vastly different scales (Pyne et al., 1949, pag. 3). The dominating factors that govern the fire regime and the fire impact change across space and time (Fig. 2.1).

At the fire fundamental scale, a wild-land fire is defined as a combustion process with primary interactions on fuel dynamics and fuel chemistry. Within the flame reaction zone

(millimeter scale), the combustion process involves complex series of chemical kinetics phenomena. Specific softwares, as for example the CHEMKIN® code (Kee et al., 1989) or the detailed chemical mechanism Gri Mech 3.0 (Smith et al., 2000), have been designed to develop a comprehensive understanding of the combustion process by solving thousands of chemical reactions, which might involve multiple chemical species, concentration ranges, and gas temperatures. Starting from such detailed chemical kinetic reaction mechanisms, skeletal and reduced mechanisms have been derived with the aim to provide a satisfactory description of the combustion kinetics in the gas phase that is even more convenient, in terms of computational costs and memory use, rather than full chemical mechanisms (Leroy et al., 2007, 2008).

At short-term and stand scales (micro-scale), the fire is seen as a whole. Primary interactions are among fuel conditions (type, mass, moisture), weather and fire behaviour (intensity, spread rate): the classic fire behaviour triangle (Mell et al., 2007; Whitcomb et al., 2008). Fire spread models work at very fine resolution (fire behaviour: $\sim$ 100 m) trying to capture the driving physical processes that governs the complex interaction between wild-fires and their environment, which includes vegetation cover and land use, terrain slope, and weather conditions (Linn et al., 2002). In Chapter 3, Section 3.2 delves into the development and evolution of fire spread models, it illustrates their possible applications.

At regional scale, the interaction between the fire and the landscape must be considered and the atmospheric motions become another important driving force (Albini, 1993; Benson et al., 2009). At this scale, the interactions between the fire and the atmosphere can trigger convective plumes or thermals processes (see Chapter 5). Atmospheric models resolution can range from the micro-scale (Large Eddy Simulation, metric resolution) to large meso-scales (kilometric resolution), hence, they fit for the purpose of analyzing fire impact on the landscape. The research at this scale is however constrained by the scarce amount of observational data.

At a global scale, the effect of fire emissions on the atmosphere dominates. At these scales, primary interactions are among vegetation, climate, and patterns of fire occurrence (frequency, size distribution, seasonality) (Crutzen and Andreae, 1990; Chuvieco et al., 2008). Atmospheric General Circulation Models (AGCM) have typical synoptic resolutions between 1 and 5 degrees in latitude or longitude (hundreds of kilometres). For AGCM models, vegetation fire emission inventories can be derived from a combined approach using satellite data at daily resolution supported by bio-geochemical modelling of the available fuel load (Hoelzemann et al., 2004; Ito and Penner, 2004; van der Werf et al., 2004) but there is no feedback of the simulated atmosphere on the prescribed emissions.

The distinction of fire processes through scales determines a separation of expertise among diverse specialists. Heat engineers and chemists are interested in fire fundamentals; physicists and experts in fluid dynamics focus on fire behaviour; meteorologists, physicists and chemists of the atmosphere look at fire on the landscape and global fires. This

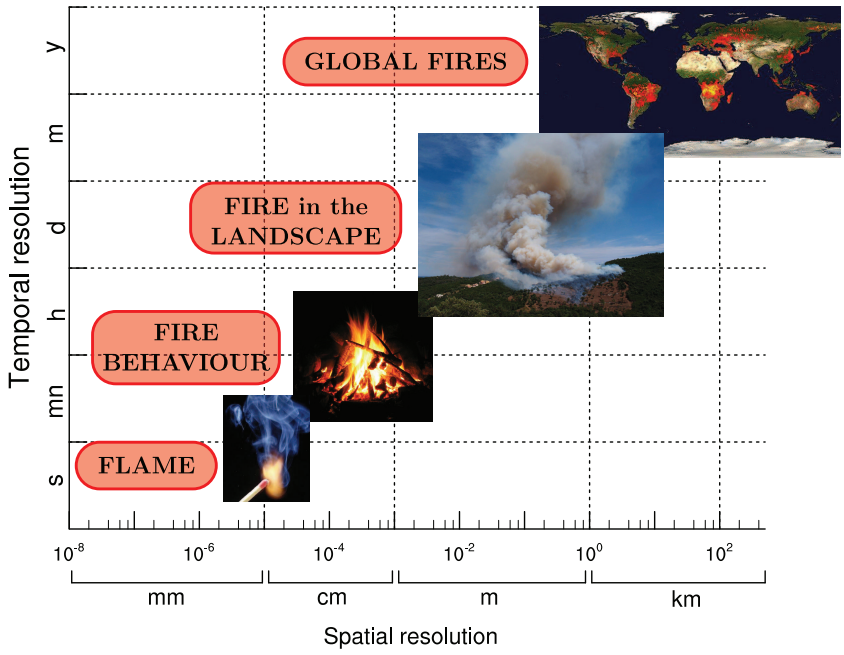

Figure 2.1: Wild-fires are complex events driven by physical and chemical processes operating on vastly different scales. The dominating factors that govern the fire regime and the fire impact change across space and time. The picture illustrates the spatial and temporal scales at which wild-fires can be studied.

separation mirrors the wide variety of models that reproduce a fire episode at different resolutions.

The multiscale processes which defined the fire-atmosphere interactions render a direct numerical simulation intractable: it is computationally not possible to cover all the scales with an unique numerical tool. As a consequence, compromises in the choice of processes to be modeled and in the scales to consider, approximations and parametrisations of sub-grid processes are essential (Mandel et al., 2011). Moreover, once the scales to consider have been chosen, an appropriate coupling between the interacting factors (solid fuels, fire, topography and atmosphere) has to be introduced, paying attention to the dilution problem. The next chapters will present the configurations of the coupled fire-atmosphere model that I used in my thesis for studying fire impact on the atmospheric dynamic and chemistry, focusing on the landscape/fire scale (kilometric resolution) (Chap. 4) and the sub-hectometric scale (Chap. 6).

2.3 Combustion process at the fire fundamental scale

In order to estimate the fire emissions of atmospheric particles or gases at convective, regional and global scales, it is essential to firstly describe the combustion processes that control these emissions at the fire fundamental scale. The fire triangle describes the in-

teracting factors involved in the fire fundamentals. Fire requires all three components: vegetative fuel burns under appropriate conditions reacting with oxygen from the atmosphere, generating combustion products, and releasing heat (Pyne et al., 1949, pag. 6). In the following, the combustion products which directly determine fire emissions are discussed in terms of fuel properties, heat transfer and combustion phases.

Fuel properties

When studying the combustion processes and emissions, it is fundamental to know the physical and chemical properties of the fuel that determine the products of combustion (Lobert and Warnatz, 1993; Yokelson et al., 1997; Andreae and Merlet, 2001). Basically, the composition of most dry plant material is made up of (Pyne et al., 1949, pag. 7):

- *Cellulose* (from 41 to 53%), the principal constituent of all higher plants that provides them the structural strength and rigidity of the cell wall, thanks to the linear structure of this polymer.

- *Hemi-cellulose* (from 15 to 25 %), a carbohydrate polysaccharides that is found in association with cellulose in the cell wall of plants. Cellulose and hemi-cellulose are readily pyrolyzed, and cellulosic materials are a major contributor of combustible volatiles.

- *Lignin* (16 to 33%), an aromatic polymer that gives wood its stiffness. Lignin content arises in decaying wood (up to 65%), since biological degradation removes more easily cellulose than lignin. Being more stable than the cellulosic and extractive components, lignin mainly forms char when heated which is important in carbon cycling (Crutzen and Andreae, 1990). Char is required for glowing combustion.

- *Volatile extractables* are a class of compounds consisting of alcohols, aldehydes and terpenes. Ether extractives constitute a smaller fraction than cellulose and lignin, but they influence the way the fuel burns due to their high heat of combustion, volatility, and lower limits of flammability in air.

- *Minerals* compounds (up to 10%) are involved in the process of fire spread and fire extinction because they can delay flaming combustion by promoting low temperature pyrolysis; they may be important in the formation of tar (gas phase - contains combustible volatiles, the most important of which is believed to be levoglucosan) and char (solid phase).

- Proteins, nucleic acids, aminoacids.

- *Water* (from 1 to 300%, on a dry weight basis) is a crucial component which influences the extent of flaming combustion, hence the production pattern of emissions.

Fire heat release

The heat released in combustion is the driving force of a fire: the higher the heat released is, the faster the fire spreads and the hotter the gases become. The temperature of a substance is a function of the kinetic energy of the motion of its molecules, measured in degrees. The quantification of the temperature of a fire alone does little to characterize the fire. More valuable is the heat flux, a quantification of time-temperature relationships, that indicates the change of fire scale and related hazard (Silvani and Morandini, 2009).

Heat is a form of energy, often referred to as thermal energy. As part of the fire triangle, it is one of the essential ingredients for a wildland fire to start and to continue to burn. *Heat of pre-ignition* is the total heat required to raise the temperature of a unit mass of fuel to the ignition temperature, usually taken to be 320 K (Pyne et al., 1949). *Heat of combustion*, frequently called *heat content*, is the energy that maintains the chain reaction of combustion. Heat content can be measured for any particular fuel, but does not vary widely in forest fuels. A basic value of 19.50 MJ kg^{-1} is used by Santoni et al. (2006) for Mediterranean shrub; Freitas et al. (2007) reported values of 19.60 MJ kg^{-1} for savanna and 15.50 MJ kg^{-1} for Amazon forest; Pyne et al. (1949) defined 18.62 MJ kg^{-1} as a common value for the heat of combustion. The knowledge of the heat content, together with the power of the fire (J s^{-1}), permits to compute the rate of consumption of vegetative fuels that is an crucial parameter for fire modelling purpose (Leroy et al., 2009).

Heat transfer is the process by which the energy is moved from one source to another whenever there exists a temperature difference in a medium or between media. An understanding of heat transfer is essential to the study of fire because the way a fire burns and behaves is closely related to the manner and rate of heat transfer. The *heat flux* (i.e. heat produced per unit area of fuel consumed per unit of time) is therefore an important diagnostic for fires. The three basic mechanisms of heat transfer are radiation, convection and conduction. All three contribute to the combustion process, but in different ways. The dominant heat transfer mechanism depends on the fuel arrangement, the speed of the wind acting on the fire, the slope of the terrain, and the direction the fire is spreading with respect to wind direction and slope (pag. 12 Pyne et al., 1949). Wildfires are a mixed radiative-convective environment, hence the heat flux measurements are not trivial and the related literature offers a wide range of variability in terms of recorded heat flux values. Butler et al. (2004) realized a full-scale boreal forest crown fire experiment in Canada and measured maximum radiant energy flux levels and maximum temperatures of 290 kW m^{-2} and 1330 K, respectively, at 12.3 m above the ground surface. The authors cited two related experimental data: radiant flux from an Australian forest fire was approximately 100 kW m^{-2} near the flames, and 57 kW m^{-2} 7.6 m away from the fire; in crown fires, reported peak heat fluxes are of 125 kW m^{-2} (with associated temperatures of 800 K), with 95% of that attributed to radiant energy transfer. Collected data by Butler

et al. (2004) indicated that radiant energy transfer between the flame and fuels can occur over distances as great as 60 m through the forest canopy, while convective energy transfer can be significant in the upper portion of the canopy. The air temperature remained near the ambient value until immediately prior to the arrival of the fire front, as also observed by Silvani and Morandini (2009). These authors conducted four fire spread experiments across various vegetal fuels in the Mediterranean region; their results show heat fluxes and temperature over 100 kW m^{-2} and 800 K, respectively, and the dominance of radiation among heat transfer mechanisms ahead of the fire front. Radiant heat fluxes recorded at 5, 10 and 15 m from a prescribed fire through Mediterranean shrub were 7.5 kW m^{-2}, 3 kW m^{-2} and 1.5 kW m^{-2}, respectively (Santoni et al., 2006). During the FireFlux experiment, Clements et al. (2007) measured maximum heat fluxes of $\sim$ 28.5 kW m^{-2} at 43 m of altitude for a wild-land grass fires. Finally, heat flux values reported by Freitas et al. (2006) for diverse biome types (tropical forest, savanna and grassland) ranges from a minimum of 3.3 to a maximum of 23 kW m^{-2}, showing lower and upper bound for tropical forest and savanna.

Combustion phases

The combustion process proceeds through four main stages: pre-ignition, ignition, combustion (flaming, smouldering or glowing) and extinction. Gaseous organics and inorganics emissions as well as condensable compounds (tars) are produced during these stages. However the composition and the rates of emissions vary significantly among the various combustion stages.

- **Pre-ignition**

  The pre-ignition step includes endothermic reactions by which the temperature of the fuel is raised to the point where the free water evaporates and the volatile extractables, flammable gases that will support combustion, are released (*dehydration* or *distillation*) (Greenberg et al., 2006). Continued pre-heating then operates on any adsorbed water within the fuel particle (the so called fuel moisture) that is removed from the bulk material or diffused into the inner layers of it (Lobert and Warnatz, 1993). The continuous application of heat determines the thermal degradation of fuel molecules and polymers prior to combustion (*pyrolysis*) at about 400 K (Yokelson et al., 1996; Leroy et al., 2009). During the pyrolytic step, high-molecular weight components are decomposed to compounds of lower-molecular weight, first to char and tar products (intermediate molecular weight), which are the primary energy for the flame process and whose production is mainly promoted by low temperatures, and finally, favoured by high temperatures, to compounds of gaseous nature (Lobert and Warnatz, 1993). Two general reaction pathways of cellulose degradation are recognized: one leads to char and water, while the other leads to tar and volatiles (Fig. 2.2, Pyne et al. 1949). The pre-ignition step depends on both fuel characteristics

and environmental factors (fuel moisture and type, temperature, relative humidity and wind).

- **Ignition**

  Ignition is the transition from pre-ignition to combustion. It is the initiation process, essential for the whole fire process: when the gas evolution rate from the potential fuel due to pyrolysis is sufficient to support combustion, the gas is ignited by the flame and the fire advances to a new position. Spreading fire can be considered as a series of ignitions. Initial ignition is a rapid, exothermic, kinetically controlled process that can terminate, under certain circumstances, before a sufficient, self-sustaining combustion process starts (Lobert and Warnatz, 1993).

- **Combustion**

  Flaming (gas phase) and glowing or smouldering (solid phase) combustion involve different processes and are quite different in appearance.

  - **Flaming stage**

    Flaming combustion is a highly exothermic process that dominates during the startup phase. Firstly, primary combustible emissions from the pyrolytic step mix with the surrounding air, producing a flammable mixture (Leroy et al., 2007); subsequently, the flame basically converts the emitted intermediate volatiles to secondary oxidized combustion products of low-molecular weight. Low-molecular weight substances are either emitted as a final product of the burning process or form new molecules in one of the numerous flame reaction paths (Lobert and Warnatz, 1993). It is important to note that, during the flaming stage, pyrolysis continues to act since solid organic materials do not burn in flaming combustion directly, but must be first pyrolyzed by heat and chemical reactions into combustible, or not, gases. As the temperature of the fuel goes on rising, combustible gases are produced more rapidly and the chemical reactions becomes more strongly exothermic. The heat released by the flame can lead to maximum temperatures between 1900 and 2200 K; thus, flames of vegetation fires are expected to reach maximum temperatures several hundred Kelvin below this limiting value.

    Flame propagation is caused by diffusive processes that equalize concentration and temperature gradients, while chemical reactions produce heat and reactive particles resulting in the buildup of concentration and temperature gradients. Turbulence (generated by either wind or shearing effects due to gas velocity differences within the fuel bed) enhances the mixing process of fuel and air, resulting in an increased eddy diffusivity. As a consequence, the flame has a more pre-mixed turbulent character, thus explaining difficulties that are encountered

in direct simulation: 2 or 3-D description and consideration of complex non-stationary flow features are needed to obtain a quantitative understanding of the flame behaviour (Auzillon et al., 2011).

- **Smouldering or glowing stage**

  Smouldering or glowing is the slow, low-temperature, flameless form of combustion. Although not as visually dramatic as flaming combustion, it is an important component of wild-fires. It occurs on the surface of the solid rather than in the gas phase, as flaming. In suppression and prescribed fire control activities, smouldering ground fire is well known because it has the potential for reigniting surface fire long after the main front has passed. Moreover, smouldering can continue for months or even years and the effect of the released heat on roots and organisms can be significant (Pyne et al., 1949, pag. 22; Rein et al., 2008).

  The pure pyrolytic stage would transform into glowing combustion at about 800 K if oxygen is present, resulting in char being oxidized directly in CO; if the temperature becomes higher than 900 to 950 K, CO_2 will also be formed. The ratio of char to tar is important to the overall process, since a high amount of char relative to tar prevents flaming combustion (Lobert and Warnatz, 1993). Anyway, the emitted gases during smouldering are still flammable and could later be ignited in the gas phase, triggering the transition to flaming combustion.

- **Extinction**

  After most volatile extractables have been emitted from the fuel and the rate of pyrolysis slows down, less flammable gases are released and lower heat is produced. As a consequence, the open flame ceases, also due to other factors as the buildup of a charcoal layers on wet material, the increasing content of ash which contains flame-inhibiting substances, or simply the lack of unburned material. The process of extinction can also be influenced by convective cooling due to entraining air and radiative heat losses to the sides and top of the fuel, a low oxygen supply, a too high fuel density or too large fuel elements, or changing fuel properties (Lobert and Warnatz, 1993).

  On the other hand, smouldering combustion can proceed over days under conditions of low oxygen and high moisture (where flaming combustion would be impossible), if heat release and spread rate are balanced (Yokelson et al., 1997).

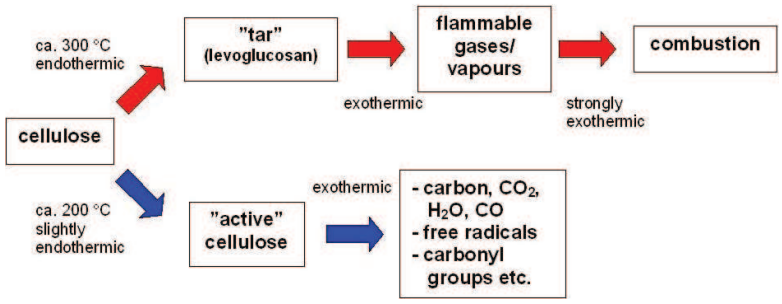

Figure 2.2: Two general reaction pathways of cellulose degradation are recognized: one leads to char and water, while the other leads to tar and volatiles.

2.4 Forest fire emissions relevant for atmospheric chemistry

Smoke production processes are a function of fuel characteristics and combustion stages. The main products of combustion are carbon dioxide and water, but other chemical compounds are released which can be of prime interest for the atmospheric chemistry.

2.4.1 Smoke production during flaming and smouldering phases

During the smouldering stage, large amounts of incompletely oxidized compounds are emitted, such as CO, CH_4, non-methane hydrocarbons (NMHC), NH_3, acetonitrile (CH_3CN), hydrogen cyanide (HCN), methyl chloride (CH_3Cl), sulfur compounds and others (Crutzen and Andreae, 1990; Yokelson et al., 1997; Andreae and Merlet, 2001; Urbanski et al., 2009). These emissions occur along with oxidized products of the flaming stage: CO_2, nitric oxide (NO), nitrogen (N_2), nitrogen dioxide (NO_2), N_2O, sulfur dioxide (SO_2), etc (Crutzen and Andreae, 1990; Yokelson et al., 1996; Andreae and Merlet, 2001; Urbanski et al., 2009). The superior number of compounds from vegetation fires are produced during the smouldering phase, although the largest amount of the fuel elements carbon, hydrogen, nitrogen and sulfur are emitted during the flaming phase (Lobert and Warnatz, 1993).

In general, most compounds can be attributed to one of the two burning stages (flaming or smouldering) and thus their emissions are coupled either to formation of CO_2, if produced mainly during the flaming phase, or to CO if emitted mostly during the smouldering stage of a fire (Table 2.1). There are exceptions to this general behaviour. First, because the pyrolysis process of solid fuel and the compounds consequently produced are similar in both stages. Second, because the larger the molecules are, the more likely a breakdown is to occur due to an attack by a reactive species in the flame. Ethyne (C_2H_2) is produced, on average, in equal amounts during both stages. Cyanogen (NCCN) has a slightly higher relative emission during the flaming stage (58%) than during the smouldering (42%) due to its electronic structure and thermal stability. Hydrogen cyanide (HCN)

is primarily a smouldering stage compound, yet 34% is emitted during the flaming stage. Acetonitrile (CH_3CN), a typical smouldering stage compound, expels only a 15% in the flaming stage. Concerning this classification, Yokelson et al. (1996) invoked one further category of compounds, the "distillation and pyrolysis" category, having observed, during their laboratory fires, fire products that do not correlate linearly with either CO_2 or CO.

In conclusion, the absolute amounts of emissions produced during biomass burning are strongly dependent on the relative ratio of flaming to smouldering combustion. The most important factors affecting the emissions are the moisture of the fuel and its elemental composition. A major task in estimating global biomass burning emissions is to determine the ratio of flaming to smouldering combustion during different fire types (Andreae et al., 1996a).

For completeness, a distinction is also necessary concerning the fire stage during which water vapour is released by biomass combustion: during pyrolysis, the fuel moisture content (the weight of water contained in the fuel expressed as a percentage of its oven dry weight) is dried out, whereas chemical reactions during combustion produce H_2O ("combustion moisture", Parmar et al., 2008).

2.4.2 Measurement methods of fire products in the atmosphere

There exists a wide literature on the identification of biomass burning markers. Different methodologies are used to observe those chemical species whose concentrations are highly elevated (several orders of magnitude) within smoke plumes compared to their background values. A summary of available methods of investigation of biomass burning gaseous markers is given with a focus on the gaseous species and whenever relevant on Mediterranean type fires.

To summarize, a compilation of relevant atmospheric gaseous species observed by laboratory, ground-based, airborne and spaceborne measurements in biomass burning is given in Table 2.2.

Laboratory measurements

The laboratory characterization of the products of wild-fires began during the 70's in the United States with some works to assess the contribution of forest fires to the regional air pollution (McMahon and Ryan, 1976) or to investigate particulate and gaseous emissions from other fire sources (e.g. burning agricultural waste Darley et al., 1976 or wood for heat Dasch, 1982). Studying wild-fires in the laboratory encounters not only the challenge to sample fires representatively but also to identify instrumental techniques that can cope with hot, reactive samples where the potential for chemical interference and the dynamic range of concentration is very high (Yokelson et al., 1996).

In the past ten years, Fourier Transform InfraRed (FTIR) spectrometer has become an important tool for fire hazard assessment. This method provides accurate, continuous,

Table 2.1: List of compounds emitted from biomass fires during different burning stages. Only few compounds cannot clearly be attributed to either flaming or smouldering combustion (Lobert and Warnatz, 1993).

Flaming Stage Compounds	Ambiguous Compounds	Smouldering Stage Compounds
Carbon dioxide (CO_2)	Ethyne (C_2H_2)	Carbon monoxide (CO)
Nitric oxide (NO)	Cyanogen (NCCN)	Methane (CH_4)
Sulfur dioxide (SO_2)		Non-Methane Hydrocarbons (NMHC)
Nitrous oxide (N_2O)		Ammonia (NH_3)
Nitrogen (N_2)		Hydrogen cyanide (HCN)
Nitrogen dioxide (NO_2)		Acetonitrile (CH_3CN)
		Amines, Heterocycles, Amino acids
		Methyl chloride (CH_3Cl)
		Most sulfur compounds (H_2S, COS, DMS, DMDS)
Particles (high elemental carbon content)		Particles (low elemental carbon content)

real-time measurements of a large number of smoke compounds. Yokelson et al. (1996) used FTIR spectroscopy to record mid-infrared spectra of the smoke of 9 large-scale open fires conducted in a controlled-environment combustion facility. Their measurements allowed to distinguish between compounds produced during the flaming stage (CO_2, NO, NO_2, SO_2, and most of the water vapour) and during the smouldering stage (CO, CO_2, CH_4, NH_3, and ethane C_2H_6). The authors registered that a significant fraction of the total emission is composed of unoxidized pyrolysis products: ethanol (C_2H_5OH), formaldehyde (HCHO), acetic (CH_3COOH) and formic acid (HCOOH), ethene (ethylene C_2H_4), ethyne (acetylene C_2H_2) and HCN. They also documented that the fire-production of oxygenated organic compounds was high enough to have significant impacts on local and regional atmospheric chemistry (e.g. acid rain, production of organic acids such as HCOOH). Moreover, the results of Yokelson et al. (1996) suggested that wild-fires may be a more significant source of atmospheric NH_3 that had been generally recognized by non-spectroscopy studies.

Successively, the high temporal resolution and broad sensitivity of the open-path FTIR methodology was used to focus on emissions from smouldering combustion acquired at several heights above burnt biomass samples (Yokelson et al., 1997). The dominant products were CO, CO_2, CH_4, C_2H_4, C_2H_2, propene (C_3H_6), H_2CO, 2-hydroxyethanal ($CHOCH_2OH$), methanol (CH_3OH), phenol (C_6H_6O), organic acids (CH_3COOH and HCOOH), NH_3, HCN and carbonyl sulfide (OCS). The authors related one half of the detected organic emission to fuel pyrolysis, the third combustion phase, with a smoke enriched with oxygenated volatile organic compounds (OVOC); these compounds were well known as secondary photochemical products in fossil fuel combustion, however they turned out to be also important as initial products in the combustion of biomass. Among recorded OVOC, Yokelson et al. (1997) reported, for the first time, significant emissions of 2-hydroxyethanal (hydroxy-acetaldehyde and glicoaldehyde).

The previously cited works quantified the fire emissions from coniferous and brush fuels (Yokelson et al., 1996) and from the smouldering combustion of organic soils, hardwoods, coniferous fuels, grasses and other fuels (Yokelson et al., 1997). Therefore, in order to cover the full range of possible fire emissions in all the important vegetation classes, Goode et al. (1999) used FTIR spectroscopy to accomplish measurements of the emissions from whole grass fires. They identified different trace gases: CO, CO_2, NO, NO_2, N_2O, SO_2, OCS, water vapour, CH_4, C_2H_6, C_2H_4, C_2H_2, C_3H_6, isobutene (C_4H_8), CH_3OH, C_6H_5OH, organic acids (CH_3COOH and CHOOH), HCHO, HCN and hydroxyacetaldehyde ($CHOCH_2OH$). They observed that NO and NH_3 were the major nitrogenous compound emitted during the flaming and smouldering combustion, respectively, but in lower amounts than previous studies.

Holzinger et al. (1999) utilized Proton Transfer Reaction Mass Spectrometry (PTRMS) to estimate emissions from laboratory scale biomass burning experiments. They measured volume emission ratios (i.e. the excess trace species concentrations measured in a fire

plume divided by the excess concentration of a simultaneously measured reference gas, as CO or CO_2) for H_2CO, CH_3OH, HCN, acetaldehyde (CH_3CHO), acetone (C_3H_6O) and (CH_3CN). Holzinger et al. (1999) concluded that biomass burning are important sources of CH_3CHO, CH_3CN and HCN rather than HCHO and C_3H_6O. Together with Yokelson (1996, 1997), the authors showed that OVOC account for most of the non-methane organic carbon (NMOC) in biomass burning. Moreover, their work showed that biomass burning contribute significantly to the atmospheric budget of HCN and CH_3CN.

Alessio et al. (2004) focused on measurements of isoprenoid (isoprene, C_5H_8, and monoterpene) emissions from plants representative of the Mediterranean biome by means of gas chromatography. They exposed vegetation to direct (i.e. exposure to flame) and indirect (i.e. exposure to elevated temperatures) effect of fire. Depending on the plant species, the exposure to fire could lead to a reduction or to a burst of isoprenoid emissions.

Greenberg et al. (2006) identified and quantified VOC emissions during the distillation and the pyrolysis (temperatures between 30 and 300° C) by PTMRS and gas cromatography-mass spectroscopy. Major VOC emissions included CH_3COOH, furylaldehyde, acetol, pyrazine, terpens, 2,3-butadione, C_6H_6O and CH_3OH, as well as smaller emissions of furan (C_4H_4O), C_3H_6O, CH_3CHO, CH_3CN and benzaldehyde (C_7H_6O). Total VOC emissions from distillation and pyrolysis were mostly oxygenated hydrocarbons similar to those from smouldering combustion, as observed by Yokelson et al. (1997). Their conclusion suggested a separate treatment of smouldering emissions to include the effect of these reactive VOCs in regional and global air quality simulations.

Leroy et al. (2007) examined the combustion mechanism of pyrolysis gases through experiments using a Perfectly Stirred Reactor (PSR) accompanied by simulations obtained with the CHEMKIN PSR code (Kee et al., 1989). They recorded two intermediate C_2 species (C_2H_4 and C_2H_6) which can play an important role in soot formation, hence they actively participate to the flame radiation.

To sum up, laboratory measurements are a valid tool for exploring the full spectrum of wild-fire gaseous emissions, even offering the possibility to control fire conditions (e.g. fuel combustible, fuel moisture, fuel load, temperature, etc). They permit to point out the chemical species that govern the fire chemistry at the flame or stand scale; hence, laboratory measurements can guide and steer the development of appropriate chemical mechanisms for modelling the combustion process. However, laboratory measurements do not offer representative information of the fire chemistry at the regional scale.

Ground-based measurements

Ground-based measurements include systematic studies that have been carried out for prescribed or controlled fires (e.g. in North America: Evans et al., 1974; Radke et al., 1991; Woods et al., 1991; in Europe: Miranda et al., 2005; Alves et al., 2010b; Barboni et al., 2010), and other "opportunistic" studies that have taken advantage of existing

pollution monitoring networks (Bravo et al., 2002; Miranda et al., 2009b) or of air pollution studies which happened to be sampling when a wild-fire occurred (Phuleria et al., 2005). These approaches mainly distinguish in the distance of the recording instruments from the burning area (some tens/hundreds of meters for systematic studies against some tens/hundreds of kilometers for "opportunistic" studies). Moreover, "opportunistic" studies are constrained by the range of pollutants that are usually controlled by air quality networks, and they can not separate the flaming from the smouldering combustion phase; whereas systematic studies can set up specific measurements, even if on-field ground-level observations are limited during the flaming phase of a wild-fire due to obvious risks as extreme heat and flames. Furthermore, the flaming stage is more convective than the smouldering stage because of the typical high temperatures, as a consequence fire-emitted particles and gases are directly injected into the atmosphere up to 3-4 km (see Chapter 5). Hence, even observations at ground-level are thus biased toward the smouldering stage (Andreae and Merlet, 2001; Alves et al., 2011).

Starting with some "opportunistic" studies, Cheng et al. (1998) documented the enhancement of the photochemical air pollution in the metropolitan area of Edmonton due to a large forest fire occurred at a distance of about 300 km. Hourly NO_2 and O_3 concentrations measured at the monitoring stations around Edmonton were 50-150% higher than the seasonal median values. Phuleria et al. (2005) measured pollutant gases and PM concentrations in the Los Angeles (LA) basin before, during, and after the October 2003 Southern California wild-fires. They documented a strong degradation of urban LA air quality due to the fires. Downwind of the fires, the greatest impact was observed on coarse-particulate matter (PM) concentrations which exceeded typical background concentrations by factors of three or four: PM_{10} concentrations were near or above 200 μg m^{-3} during the fires. During the same event, CO was increased by nearly 12 ppmv and NO reached 100 ppbv. Interestingly, NO_2 levels remained essentially unchanged and O_3 concentrations decreased by about 25-50 %. The authors proposed the reduction in photochemical activity due to the fire smoke blanketing the LA basin as a possible explanation for the NO_2 and O_3 fire response. Bytnerowicz et al. (2010) analysed the coupled effect of wild-fire emissions and the characteristic Santa Ana winds (dry and warm foehn winds) on ambient O_3 during October 2007. O_3 changes were documented at a remote rural receptor site and at other air quality monitoring stations located in the general area of the fires. At the rural receptor site, diurnal patterns of O_3 were substantially altered over the course of the fires and O_3 fluctuations were strongly influenced by changes in the Santa Ana winds; fire events caused a significant, although short-lasting increase of O_3 concentrations (maximum recorded value: 95 ppbv) and the 8h-average O_3 concentration exceeded the federal air quality standard of 75 ppbv. Elevated O_3 concentrations were measured at the air quality monitoring stations selected for the analysis, and the nightime drop of O_3 concentrations were very pronounced ($[O_3] \sim 0$ ppb) because of enough NO from traffic and fire emissions for O_3 titration. Furthermore, increased concentrations of

PM were reported at various monitoring stations of the San Diego Air Pollution Control District with values that reached a maximum of 450 μg m^{-3}.

Hu et al. (2008) investigated the impact on the air quality of some prescribed fires that burnt in February 2007 about 80 km southeast of the urban area of Atlanta. Looking at the hourly air quality observations collected at some monitoring sites in the Atlanta metropolitan area, in the late afternoon, within a coupled of hours, hourly concentrations of $PM_{2.5}$ soared up to almost 140 μg m^{-3} at several sites; at the same time, hourly O_3 concentrations jumped by up to 30 ppbv, despite the late hour in February when the photochemical activity is less vigorous (Lee et al., 2008).

In Europe, air quality monitoring stations even documented episodes of trans-boundary fire tracer dispersion as reported by Saarikoski et al. (2007) and Sofiev et al. (2008). These works both considered the influence of emissions from Russian and Baltic wild-fires on air quality in northern Europe during spring and summer 2006. Ground-based measurements of $PM_{2.5}$, PM_{10}, common ions and black carbon collected in Helsinki were analysed pointing out that $PM_{2.5}$, concentrations remained at a significantly elevated level ($> 50\mu$g m^{-3}) for almost 12 days, with two peaks of nearly 100 μg m^{-3}.

Concerning systematic studies, in the Mediterranean Basin region prescribed fire experiments are organized regularly in Gestosa (north Portugal) (Miranda et al., 2005). The aim of these field campaigns is to measure fire thermal characteristics and air pollutants such as CO, NOx (NO, NO_2), SO_2, $PM_{2.5}$, PM_{10} and VOC. Extremely high values were registered for CO ($\sim$ 50mg m^{-3} during Gestosa-2002), NO_2 ($\sim 265\mu$g m^{-3} during Gestosa-2003 and 2004) and PM (2350 μg m^{-3} for $PM_{2.5}$ and 1430 μg m^{-3} for PM_{10} during Gestosa-2002) hourly averaged concentrations. Hourly-emissions of PM have exceeded hourly-limited values imposed by the European or USA legislation (Miranda et al., 2005). Also VOC emissions were sampled separating the flaming from the smouldering phase: smaller VOC concentrations characterized the flaming phase. The Gestosa research site was recently used to estimate the human exposure to NO_2 and SO_2. Alves et al. (2010a) conducted seven experimental fires at a shrub-dominated forest in Portugal. The authors found high concentration of aerosols and gaseous species but with large differences according to the burning conditions and wood types. It is worthy noting the maximum $PM_{2.5}$ concentration recorded by the authors: 12500 μg m^{-3}. Using the FTIR instrument, Alves et al. (2010b) were able to sample a wider variety of gaseous species (CO, CO_2, NO, NO_2, N_2O, SO_2, NH_3, CH_4, C_2H_6, C_3H_6, C_2H_2, and CH_3OH) during an experimental fire in a Mediterranean shrubland. The particular conditions of the vegetative fuel contributed to very high-intensity flaming combustion and to the sampling of very fresh plumes. Under these conditions, emissions of CO_2, C_2H_2 and C_3H_6 (flaming compounds) were higher than those reported for savanna and tropical forest fires. Contrarily, emissions of species that are promoted during the smouldering phase (e.g. CO_2 and CH_4) were below the values reported in the literature for biomass burning in other biome types. Barboni et al. (2010) quantified 79 VOC in smoke during five prescribed fires in Corsica. They revealed

high concentrations of benzene (> 40 mg m^{-3}) above the exposure limit values imposed by national health and safety commissions in the USA and Europe, implying that this compound can be considered as a tracer of toxicity for prescribed burning. Alves et al. (2011) documented emissions of CO, CO_2, total hydrocarbons, and coarse (PM_{10}) and fine ($PM_{2.5}$) smoke particles during summer 2009 wild-fires in Portugal.

To conclude, although "opportunistic" studies record fire emissions far away the burning area, they can provide realistic information on fire pollutant emissions. In fact, the reproduced fire conditions during experimental fires are not the same of a real wild-fire in terms of size, temperature, intensity, etc. (Barboni et al., 2010; Alves et al., 2010a). Moreover, "opportunistic" studies offer valuable information about fire impact on air quality levels that can be a useful support in the process validation of atmospheric chemistry modelling of a fire episode whose consequences involved urban areas (see Chapter 4).

Airborne-based measurements

A series of airborne measurements of fire plumes started in the late 80's. Originally, these experiments focused in the tropics as, for example, the campaign DECAFE-88 over the rain-forest areas in central Africa (Helas et al., 1989), or the campaign SAFARI-92/TRACE A over southern Africa and the adjacent Atlantic (Andreae et al., 1996b). Afterwards, field experiments and airborne measurements have moved into the boreal region as the fire research campaign FIRESCAN that put special emphasis on Eurasia (Goldammer, 1996).

At the beginning, the set of available measurements was usually limited (e.g. O_3, CO, CO_2, CH_4, NO_x) but key results were derived from these measurements such as the O_3 formation in smoke plume that has been recorded at different latitudes (over Africa: Helas et al., 1995; Thompson et al., 1996; over the Artic region: Mauzerall et al., 1996; over the South Atlantic: Singh et al., 1996; over South-America: Sanhueza et al., 1999). In general, the higher O_3 levels were observed during the dry season and they were photochemically produced during the oxidation of reactive hydrocarbons in the presence of NO_x, both emitted by vegetation fires, after the dilution of the initial fire plume. Concerning the O_3 chemistry, Andreae et al. (1996a) measured methyl halides (CH_3Cl, CH_3Br and methyl iodide CH_3I) emissions from savanna fires in southern Africa due to their significant contribution to stratospheric O_3 destruction. Their results suggested that vegetation fires contribute significantly to the atmospheric budget of CH_3Cl and CH_3Br, whereas the fire source of CH_3I revealed to be less important, and methyl halides are emitted predominantly during the smouldering combustion.

Yokelson et al. (1999, 2003, 2007) acquired airborne FTIR spectra within a few kilometers of different fires and their measurements yielded excess mixing ratios for CO, CO_2, CH_4, NH_3, C_2H_4, CH_3OH, CH_3COOH, CHOOH, HCHO. In particular, the work of Yokelson et al. (2007) includes data on a number of "new", significant plume constituents

for which information was not previously available (Yokelson et al., 2007, see Table 2).

Hobbs et al. (2003) analysed airbone FTIR spectra showing the aging effects on biomass smoke such as the production of some species (nitrate, O_3 and gaseous CH_3COOH) or the consumption of others (Hobbs et al., 2003, see Table 4-6) by chemical reactions in the plume. In particular, O_3 depletion was documented close to the fire in the young biomass-burning plume.

Singh et al. (2010) explored impacts on the atmospheric composition and chemistry at higher northern latitudes due to boreal and California forest fires during the airborne campaign ARCTAS (`http://cloud1.arc.nasa.gov/arctas`). The authors selected CH_3CN and HCN as tracers to discriminate signatures of biomass combustion in the collected samples. They observed that fresh biomass burning plumes at low altitudes contained very little enhancement in O_3, while, when fire plumes had encountered and mixed with urban emissions, large O_3 formation occurred. The study of the chemical changes in a fire plume by aircraft measurements were also carried out by Jost et al. (2003) during a human-induced biomass fire in Namibia. During the first 2 hours after the emission, highly time-resolved detection of CO, O_3, acetone (propanone, CH_3COCH_3), CH_3CN, NO_x and a variety of NMHC were performed and the O_3 depletion was observed close to the fire, as already highlighted in the work of Hobbs et al. (2003).

Among airborne measurements, it is worth citing measurements of O_3, CO and NO_y realised by commercial airliners within the MOZAIC program (Marenco et al., 1998). During the 2003 European heat wave, the MOZAIC aircrafts crossed atmospheric layers with enhanced O_3, CO and NO_y mixing ratios in the free troposphere over Frankfurt (Tressol et al., 2008), likely due to forest fires burnt in Portugal. Elguindi et al. (2010) documented the quasi-global impact of intense boreal fires during the fall of 2002 by analysing the MOZAIC CO profiles.

Generally, airborne measurements are an efficient method to follow the spatial and temporal evolution of the chemistry of a fire plume; however, airborne instruments sample an integrated mixture of the emissions from both flaming and smouldering combustion (Andreae et al., 1996a; Andreae and Merlet, 2001).

Observations from space

The role of space-based measurements of fire products has increased notably within the past 20 years. A first application of satellite data is the work of Fishman et al. (1990) that, using an O_3 mapping spectrometer (TOMS), showed that O_3 maximizes yearly over the Atlantic Ocean when savanna burning peaks. Afterwards, satellite instruments have evolved and, nowadays, they provide a frequent and global coverage of tropospheric gases and aerosols. Trying to make a roundup of the possible applications of satellite measurements to the study of wild-fires, satellites have contributed to determine:

- Aerosol and gases amount

The Global Ozone Monitoring Experiment (GOME) spectrometer, in addition to its capability as an O_3 instrument, can also retrieve column amounts of a number of minor but chemically important trace constituents, among which there are two key trace species associated with smoke cloud combustion: NO_2 and HCHO. Using GOME to study biomass burning products in Southeast Asia, Thomas et al. (1998) observed a two-fold increase in the vertical NO_2 content over large parts of the smoke clouds, while HCHO was detected only in area closest to combustion sources.

The Measurement Of air Pollution In The Troposphere (MOPITT) instrument has been conceived to measure the mixing ratio of CO on a global scale; CO is a tracer of incomplete combustion, hence it suits to be a wild-fire marker. The Moderate Resolution Imaging Spectro-radiometer (MODIS) provides globally the Aerosol Optical Depth (AOD) that can be used as a proxy of the biomass burning at various places. Studying African and South-American biomass burning, Bremer et al. (2004) found a good correlation between the MOPITT CO seasonal variations and the corresponding variations of AOD climatologies retrieved contemporaneously from MODIS: both variations could be associated to the strong influence of biomass burning. The coupling of the AOD from MODIS and the CO profile from MOPITT has been used by Edwards et al. (2006) to examine 2003 Southern Hemisphere burning season and to estimate the emission ratio of aerosol number density to CO concentration. The information about the AOD is also furnished by the Terra Multi-angle Imaging Spectro-Radiometer MISR (Chen et al., 2008). Barnaba et al. (2011) used long-term AOD data in the attempt to estimate the wild-fires contribution to the European load. From their study, the regions most impacted by wild-fires emissions and/or transport are Eastern and Central Europe as well as Scandinavia. Conversely, a minor impact is found in Western Europe and in the Western Mediterranean.

MODIS provides also a Fire Radiative Power (FRP) estimate that quantifies the thermal radiation emitted by the fire in units of megawatts. FRP is roughly proportional to the chemical energy released by the fires, and thus also to the biomass combustion and pollutant emission rates. Therefore, FRP is considered the most appropriate fire observation product for emission estimation (Kaiser et al., 2009). Mebust et al. (2011) developed a FRP-based parametrisation that succeeded in characterizing the variability in fire NO_x emissions: MODIS FRP are combined with tropospheric NO_2 column measurements from the Ozone Monitoring Instrument (OMI) to derive NO_2 wild-fire emission coefficients. The magnitude of the obtained NO_2 wild-fire emission coefficients was lower than prior studies but similar to several other studies of fire emissions using satellite platforms. Therefore, their results indicated that current emission factors may overestimate the contributions of flaming combustion and underestimate the contributions of smouldering combustion to total fire emissions, and that satellite data can provide an extensive

characterization of the variability in fire NO_x emissions.

Using the space-borne infrared spectrometer ACE-FTS, elevated levels of CH_3OH (Dufour et al., 2006) and of HCN (Lupu et al., 2009) have been identified in the upper troposphere due to biomass burning.

- The occurrence of fire plume and pollution

  Images from MODIS and the Geostastionary Operational Environmental Satellite (GOES) are incorporated in the smoke forecasting system of the National Oceanic and Atmospheric Administration (NOAA) in order to detect smoke plumes (Rolph et al., 2009). Moreover, through specifically developed algorithms, MODIS can deliver in real time the thermal emission during a fire (i.e. "hot spots" or "active fire", Giglio et al., 2003) or it can detect the burnt area after (i.e. "burnt pixel", Roy et al., 2005). These information have been used to build wild-fire emission inventories (Ito and Penner, 2004; Urbanski et al., 2011).

  MISR data make possible unique smoke plume identification and characterization approaches because of the longer optical path through the atmosphere (i.e. use of oblique-angle imagery) and the combination of multiangle and multispectral information that assist in distinguish smoke from clouds or other types of aerosols (Mazzoni et al., 2007; Kahn et al., 2007).

  The Sea-Viewing Wide Field-of-View Sensor (SeaWiFS) permits to visualize smoke events associated with forest fires (Falke et al., 2001) on its true color images aiding in the determination of the aerosol's spatial and temporal properties.

  Coheur et al. (2009) illustrated the ability of the Infrared Atmospheric Sounding Interferometer (IASI) to observe distinctive signatures of NH_3, C_2H_4, CH_3OH and HCOOH in fire plumes; moreover, IASI infrared spectra contain also peroxyacetyl nitrate ($CH_3COOONO_2$, abbreviated as PAN) observed in some smoke plumes.

- The aerosol and gases vertical distribution

  The use of active lidar instruments, such as the Geoscience Laser Altimeter System (GLAS), its predecessor (the Lidar In-Space Technology Experiment, LITE), and its successor CALIPSO (the Cloud and Aerosol Lidar for Pathfinder Spaceborne Observations) allows high resolution profiling of aerosols in the atmosphere. Applying this potential, Hoff et al. (2005) observed long range transport of smoke pollutants from 2003 California forest fires by combining GLAS profiles (to track the aerosol products) and a MODIS images (to detect the fire). The authors underlined the importance of having multiple tools available (e.g. MODIS and GLAS) to observe aerosol in order to reduce intrinsic limitations of each sensor.

  Using CO profiles from MOPITT, Edwards et al. (2006) explored the vertical transport of biomass burning. Low-altitude concentrations were very high close to the

source regions. In regions of significant convection, the CO mixing ratio was greater at higher altitudes, indicating vertical transport of biomass burning emissions to the upper troposphere.

Gonzi and Palmer (2010) utilized the Tropospheric Emission Spectrometer (TES) and the Microwave Limb Sounder (MLS) to infer the vertical distribution of CO surface emissions lofted from boreal and tropical biomass burning. They found that only 10-25 % of emissions are injected above the Planet Boundary Layer.

- The plume height, especially near aerosol sources

  Associating MISR data with MODIS burnt area products, Mazzoni et al. (2007) developed a system to retrieve fire injection height generated by fire buoyancy. A MISR-derived fire plume height is also obtained by Kahn et al. (2007) highlighting the non-negligible influence of the atmospheric stability on the plume elevation. Kahn et al. (2008) suggested to combine lidar observations with stereo imaging to support the modelling of wild-fire smoke injection height. Martin et al. (2010) extended the work of Mazzoni et al. (2007). They correlated the MISR plume climatology with the MODIS FRP and showed that larger summertime heights are the result of higher fire intensity.

  Utilizing data from the space-borne lidar CALIPSO and analyzing the vertical distribution of aerosols, a good marker of fire emissions, Labonne and Chevallier (2007) and Amiridis et al. (2009) assessed the injection height of biomass burning plumes and concluded that, although several plumes are identified above the mixing layer, most of the aerosol load is within the mixing layer.

  Guan et al. (2010) proposed a simple empirical method to identify biomass burning plume heights by coupling the Aerosol Index (AI) measurements, as determined by the OMI instrument, and the top fire height from CALIPSO. The authors derived a best-fit relationship between the AI and the maximum plume height for young plumes that can help to validate the vertical placement of smoke plumes in chemical transport models.

Satellite instruments also provided information on aerosol and gases source location, strength and timing through the combination of inverse transport or back-trajectory models (e.g. MODIS; MISR; MOPITT: Pfister et al., 2005; GOME).

Applications of these observations to the Mediterranean region is currently limited by the small scale of Mediterranean fires compared to the resolution of the satellite pixel. However, during summer 2003, the long-lasting intense fire season was well studied with satellite measurements. Pace et al. (2005) used MODIS observations to derive the spatial and temporal extent of forest fire aerosols over the central Mediterranean region. Cinnirella et al. (2008) estimated mercury (Hg) emissions from forest fires in the Mediterranean region on the basis of burnt area MODIS datasets that allows mapping of fires of

at least 50 ha. IASI performance for the monitoring of pollution during extreme wild-fires in the Mediterranean Basin was evaluated by Turquety et al. (2009). The authors analyzed IASI CO spatial and vertical distributions during summer 2007 Greek fires. They concluded that the fire pollution plumes were trapped below 2 km and transported rapidly across the Mediterranean Basin.

0-D modelling

Detailed analysis of chemical reactions in smoke plume were performed by Poppe et al. (1998) and Mason et al. (2001, 2006) by means of box models.

Poppe et al. (1998) showed the importance of atmospheric mixing of the fire plume with ambient air on the simulated O_3 production in young biomass burning plumes.

In their first study, Mason et al. (2001) focused on the role of 6 oxygenated VOC (HCHO, CH_3COOH, HCOOH, CH_3OH, C_6H_6O, $CHOCH_2OH$) in the photochemistry of the smoke plume. The authors observed that, once oxygenates had been incorporated into photochemical simulations, the primary effects was a decrease in NO_x lifetime. The depletion of NO_x resulted in complex behaviour of O_3 and hydroxyl radical (OH) concentrations (increase or decrease), depending upon the capability of initial NO_x levels to compensate for the increased removal of NO_x. However, oxygenates always increased H_2O_2 and organic hydroperoxide production. In their second work, (Mason et al., 2006) compared two box models with a focus on the photochemical processes in young biomass burning plumes. Both smoke plume models were initiated with emission ratios measured close to the fire; besides previously listed chemical species, measurements used by Mason et al. (2006) also included: $OHCH_2CHO$, C_3H_8, C_3H_6, isoprene, toluene, methyl ethyl, ketone, phenol, acetol. This work led to the conclusion that the primary cause of model differences was the oxidative mechanism of VOC degradation. As only 70% of VOC present within a smoke plume can currently be identified, Mason et al. (2006) put on evidence the need for further investigation and quantification of species released by biomass burning.

2.5 Synthesis

Wild-fires are any uncontrolled fires in the wilderness, human-induced or naturally occurred. Their classification depends on the vegetation layer in which the fire is burning (Benson et al., 2009) and on the role of human management action on fire episodes (Pyne et al., 1949).

Wild-fires are complex events driven by physical and chemical processes operating on vastly different scales (Pyne et al., 1949). The dominating factors that govern the fire regime and the fire impact change across space and time (Fig. 2.1). At each temporal and spatial scale, the comprehension of fire processes implies the understanding of which

factors interact in the fire evolution and the knowledge of fire processes at the relative sub-scale. Such a multi-scale behaviour is a challenge for the numerical modelling of fire episodes, in particular in terms of computational cost. A compromise is to choose the scale to consider, to set up appropriate approximations and parametrisations of sub-grid processes, and to rightly introduce the coupling between the interacting factors, paying attention to the dilution problem (Mandel et al., 2011). The present work focuses on the study of the dynamical and chemical interaction fire/atmosphere at the landscape/fire scale (kilometric resolution, Chap. 4) and the sub-hectometric scale (Chap. 6).

In order to properly describe the impact of wild-fires on the atmosphere, it is important to know the evolution of the combustion process at the fire fundamental scale. The combustion process proceeds through four main stages: pre-ignition, ignition, combustion (flaming, smouldering or glowing) and extinction. During the pre-ignition stage, the degradation of cellulose (i.e. the principal constituent of all higher plants) takes place and two general reaction pathways are recognized: one leads to char and water, while the other leads to tar and volatiles that trigger and maintain the combustion (Fig. 2.2; Pyne et al., 1949; Lobert and Warnatz, 1993). Gaseous organics and inorganics emissions as well as condensable compounds (tars) are produced all along the combustion. However, the composition and the rates of emissions vary significantly among the various combustion stages and depending on fuel properties, as also the amount of released energy. The main products of combustion are CO_2 and H_2O, but other chemical compounds are released which can be of prime interest for the atmospheric chemistry. In general, most compounds can be attributed to one of the two burning stages (flaming or smouldering, see Table 2.1). Thus, their emissions are coupled either to formation of CO_2 if produced mainly during the flaming phase that is dominated by oxidized products (e.g. Yokelson et al., 1996), or to CO if emitted mostly during the smouldering stage of a fire that is characterized by large amounts of incompletely oxidized compounds (e.g. Yokelson et al., 1997). The absolute amounts of emissions produced during biomass burning are strongly dependent on the relative ratio of flaming to smouldering combustion that is, nowadays, an important information to determine in order to better estimate fire emissions associated with different fire types (Andreae et al., 1996a). Concerning water vapour, a distinction exists between "fuel moisture", the water contained in the fuel that is dried out during pyrolysis, and "combustion moisture" that is produced during combustion different chemical reactions (Parmar et al., 2008).

In the last 50 years, scientists developed diverse techniques to observe fire products and to measure their concentrations in the atmosphere near and far away the ignition point. These methodologies vary in a wide range. Laboratory experiments permit to explore the full spectrum of wild-fire gaseous emissions, even by controlling fire conditions (e.g. Yokelson et al., 1996, 1997; Holzinger et al., 1999; Greenberg et al., 2006). Ground-based experiments provide realistic information on fire pollutant emissions and their impact on air quality levels (e.g. Miranda et al., 2005; Alves et al., 2010a,b; Barboni

et al., 2010; Phuleria et al., 2005; Saarikoski et al., 2007; Bytnerowicz et al., 2010); these data can be a useful support in the process validation of the atmospheric chemistry modelling of a fire episode (Chap. 4), even if observations at ground-level are biased toward the smouldering stage (Alves et al., 2011). Airborne-based measurements are an efficient method to follow the spatial and temporal evolution of the chemistry of a fire plume by sampling an integrated mixture of emissions from both flaming and smouldering combustion (e.g. Yokelson et al., 1999, 2003, 2007; Hobbs et al., 2003; Tressol et al., 2008). Observations from space, that increased notably within the past 20 years, contribute to determine aerosol and gases amount (e.g. Barnaba et al., 2011), the vertical distribution of fire emissions (e.g. Turquety et al., 2009), the development of the fire plume and the associated pollution (e.g. Pace et al., 2005), and the plume height (e.g. Martin et al., 2010). Moreover, 0-D modelling supports all these experimental efforts in better understanding chemical reactions that take place in a smoke plume (e.g. Mason et al., 2006). Table 2.2 summarizes the most relevant atmospheric gaseous species that have been observed and measured during wild-fire episodes by the cited techniques. This wish-list represents a reference in the frame of a modelling study that is aimed at reproducing fire impacts on the atmospheric chemistry. To achieve this goal, and in a broader sense, in order to represent the fire/atmosphere interaction, in terms of both dynamics and chemistry, a possible method is to couple models that are capable to describe the evolution of the fire and the atmosphere and their complex and bilateral interconnection, as it is presented in the next chapter.

Table 2.2: List of chemical species observed in biomass burning plumes.

Chemical Family	Chemical Species
Nitrogen	NO (Nitric Oxide) NO_2 (Nitrogen Dioxide) N_2O (Nitrous Oxide) HONO (Nitrous Acid) HNO_3 (Nitric Acid) HCN (Hydrogen Cyanide) NH_3 (Ammonia)
Sulphur	SO_2 (Sulphur Dioxide)
Carbon	CO (Carbon Monoxide) CO_2 (Carbon Dioxide)
Alkenes	C_2H_4 (Ethene/Ethylene) C_3H_6 (Propene) C_4H_8 (Butene) C_5H_{10} (Pentene) C_6H_{12} (Hexene)
Biogenic Alkenes	C_5H_8n $C_{10}H_{16}$ (Limonene) C_1OH_{16} (Alpha-Pinene)
Halogens	CH_3Br (Methyl Bromide) CH_3Cl (Methyl Chloride) CH_3I (Methyl Iodide) HCl (Hydrogen Chloride) HBr (Hydrobromic Acid)
Furans	C_4H_4O (Furan) $C_5H_4O_2$ (Furfural)
Aldehydes	HCHO (Formaldehyde) CH_3CHO, C_2H_5O (Acetaldehyde) CH_3CH_2CHO C_3H_6O (Methylacetaldehyde) C_4H_8O (Butyraldehyde) C_7H_6O (Benzaldehyde) C_4H_6O (Methacroleine)
Ketone	C_3H_6O (Acetone) C_4H_6O (Butenone) C_4H_8O (Butanone) $C_2H_2O_2$ (Glyoxal) $C_3H_4O_2$ (Methylglyoxal) C_3H_4O (Acroleine)
Aromatics	C_6H_6 (Benzene) C_7H_8 (Toluene) C_8H_{10} (Xylene) C_7H_8O (Cresol) C_6H_6O (Phenol) C_8H_8 (Vinyl Benzene)
Alcohols	CH_3OH (Methanol) C_2H_5OH (Ethanol) C_3H_8O (Propanol)
Carboxylic Acids	CHOOH (Formic Acid) CH_3COOH (Acetic Acid)
Alkynes	C_2H_2 (Acetylene/Ethyne) C_5H_8 (Isoprene)

Chapter 3

Towards a coupled fire/atmosphere model

Contents

This chapter describes the numerical models used in this work: the atmospheric model Meso-NH (Sec. 3.1), and the fire spread model Forefire (Sec. 3.2). The last section (Sec. 3.3) focuses on the coupling methodology between the atmosphere and fire models.

3.1 The atmospheric model

3.1.1 General presentation

Meso-NH is an anelastic non-hydrostatic meteorological model jointly developed by the Centre National de Recherche Météorologiques (Météo France) and the Centre National de Recherche Scientifique (Laboratoire d'Aérologie) as a suitable model for research applications (Lafore et al., 1998).

The governing equations are a Euler system of partial differential equations that determine the evolution of the state variables $\Phi = (u, v, w, \theta, r_*, e, s_*)$ through different mechanisms (e.g. advection, Coriolis force, pressure force, turbulence and diabatic sources). The prognostic variables are: the three Cartesian components of the velocity u, v, w, the dry potential temperature θ, the various water mixing ratios r_* for the considered water species, the turbulent kinetic energy (TKE) e, and, if specified, an arbitrary number of scalars s_* available for chemistry computations or other applications.

3.1.1.1 The non-hydrostatic approximation

The non-hydrostatic approximation allows simulating atmospheric motion from the large meso (10 km) down to the micro scale (large eddy, decametres). According to scale analysis, when the aspect ratio (horizontal scale of the motions/vertical scale of the motions) approaches unity the non-hydrostatic equation that describes vertical movements becomes important :

$$\frac{\partial w}{\partial t} + \vec{U} \cdot \nabla w = -\frac{1}{\rho}\frac{\partial \rho}{\partial z} - g\,, \tag{3.1}$$

where w is the vertical velocity, $\vec{U}$ is the atmospheric wind, ρ is the density of the air and g is the acceleration of gravity. Generally, the non-hydrostatic effects are said to be non-negligible at horizontal resolution lower than about 10 km (S. Malardel, personal communication). Because of the non-hydrostatic approximation, w is a prognostic variable in the Meso-NH model.

3.1.1.2 The anelastic approximation

The anelastic approximation filters out vertically propagating acoustic waves which are meteorologically unimportant phenomena but whose presence places a very severe limitation on the time step . The anelastic approximation consists in removing the local

derivative $\frac{\partial \rho}{\partial t}$ from the continuity equation. The continuity equation becomes:

$$\vec{\nabla} \cdot (\rho_{ref} \vec{U}) = 0 \,, \tag{3.2}$$

where ρ_{ref} is the density of the so-called "reference" state of the air (i.e. an atmosphere at rest, in hydrostatic equilibrium, with no condensed water and horizontally uniform profiles of temperature and water vapour). The meaning of the anelastic approach is that the local evolution of ρ_{ref} is neglected as well as the variation of density from the horizontal mean; on the contrary, the density variations along the vertical (variations multiplied by the term g, buoyancy term) can not be ignored. By applying the anelastic constraint to the equation system, the prognostic nature of the continuity equation is eliminated (Xu et al., 1992), hence the pressure problem arises: the equation for the pressure function (same physical dimension as a geopotential) has to be solved, using an appropriate pressure solver, in order to correctly define pressure gradients. The anelastic formulation of Lipps and Hemler (1982) is implemented in the Meso-NH model. The anelastic approximation has well identified detrimental effects : (1) the vertical velocities simulated by the model are slightly inaccurate (because the continuity and vertical momentum equations are approximate) and (2) pressure perturbations linked to the filtered acoustic waves may be transmitted instantaneously in the simulation domain instead of travelling at the speed of sound. The anelastic approximation is valid when relative fluctuation in the thermodynamic variables are negligible. The approximation is therefore adapted to simulations of cumulus clouds or large boundary-layer eddies for which the departure from reference state of thermodynamic variables is small (i.e. 1/300 for temperature). In a fire plume, the relative fluctuations in the thermodynamic variables are still small (i.e. 50/300 for temperature) but larger than those in cumulus clouds. The anelastic approximation is thus expected to induce intrinsic errors on the order of a few percent for most of the atmospheric motions. Clark et al. (1996) and Sun et al. (2009) discussed this potential limitation but concluded that the anelastic equations were adapted for the representation of fire-generated convective flow and the evolution of the convective thermals.

General characteristics

Meso-NH can be used to run idealized as well as real case studies. When the topography is present in the model (i.e. not a flat-terrain configuration), a geometric height is computed based on a terrain-following coordinate transformation. Initial and lateral conditions can be constrained in various ways: by a radiosounding, by operational re-analyses (e.g. fields from the European Center for Meteorological and Weather Forecasting, ECMWF), or by meteorological fields as reproduced by the model itself.

Among other distinctive features of the Meso-NH model there are the so called "interactive grid-nesting technique" that enables simultaneous two-way simulations of several

scales of motion; and the flexibility to switch from the standard three dimensional (3-D) configuration to the two dimensional (2-D), or even one dimensional (1-D), form. Furthermore, an external module, SURFEX, is coupled to Meso-NH in order to include specific parametrisations for the description of surface forcings on the atmospheric motions due to orography, soil characteristics, land use, sea, lakes, etc. (Section 3.1.3). A chemical module is also available for on-line coupling (Section 3.1.4). More information about the model can be found on its web site: `http://mesonh.aero.obs-mip.fr/mesonh/`.

3.1.2 Focus on critical parametrisations for dry convection

Fires induce atmospheric circulations that result predominantly from large temperature anomalies created by the release of energy due to the combustion. The present section focuses on the two fundamental parametrisations needed for a realistic representation of this fire-induced convection: the turbulence (eddy diffusivity) scheme (Sec. 3.1.2.1) and the Mass-Flux scheme for shallow convection (Sec. 3.1.2.2).

The Eddy Diffusivity (ED) method is used to represent vertical turbulent fluxes. ED has important physical limitations related to its locality. On the other hand, the bulk Mass-Flux (MF) approach is commonly used to parametrise shallow and deep convection. Lately, both ED and MF approaches have been combined to address local and non-local turbulent transport in a single eddy diffusivity/mass flux parametrisation (Siebesma and Teixeira, 2000; Hourdin et al., 2002; Soares et al., 2004; Siebesma et al., 2007; Pergaud et al., 2009; Witek et al., 2011), see Fig. 3.1. The EDMF combined approach is particularly adapted for simulations at resolution coarser than 1 km. The prognostic equation for a scalar Φ can be written as

$$\frac{\partial \overline{\Phi}}{\partial t} = -\frac{\partial \overline{w'\Phi'}}{\partial z} + F_\Phi \,, \tag{3.3}$$

where w is the vertical velocity and F_Φ is a source term. The vertical turbulent fluxes are parametrised in terms of the EDMF approach:

$$\overline{w'\phi'} = -K_\phi \frac{\partial \overline{\phi}}{\partial z} + \frac{M_u}{\rho}(\phi_u - \overline{\phi}) \,, \tag{3.4}$$

where ρ is the air density, K is the turbulent eddy diffusivity coefficient for the variable ϕ, M_u is the convective mass flux in the updraft $M_u = \rho a_u w_u$ (a_u is the updraft fractional area and w_u is the vertical velocity in the updraft), $\overline{\phi}$ is the mean value and ϕ_u is the updraft value of the variable ϕ. It is worth noting that for simulations at high resolution (typically sub-kilometrics) the mass-flux term is removed from the equation as the convective boundary layer is fully resolved by the LES equations.

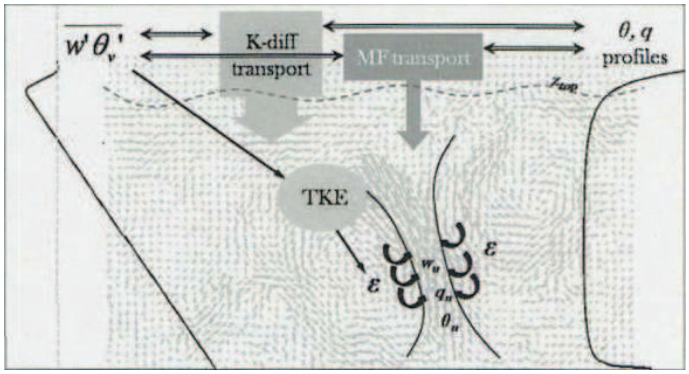

Figure 3.1: Schematic of the approach developed by Witek et al. (2011) showing coupling between the turbulent (TKE) and Eddy-Diffusivity/Mass-Flux (EDMF) parametrisation, embedded in a sample velocity field cross section from a LES simulation of a dry Convective Boundary Layer, on the left. The symbols legend is: θ is the potential temperature; w is the vertical velocity; $\overline{w'\theta_v'}$ is the buoyancy flux; ϵ is the lateral entrainment coefficient; q is the water vapour mixing ratio. The subscript u identifies variables associated with the updraft (from Witek et al. 2011).

3.1.2.1 Parametrisation of the turbulent ED terms

To solve the prognostic equation 3.4, additional parametrisations need to be introduced for the ED coefficients K_ϕ. The ED coefficients are described by

$$K_\phi = C_\phi L \sqrt{e}\,, \tag{3.5}$$

where C_ϕ is a constant coefficient, e is the Turbulent Kinetic Energy and L is the mixing length. The mixing length is a key parameter which is described in more detail in the following.

The turbulence scheme implemented in Meso-NH is a full 3-D scheme that has been developed by Cuxart et al. (2000) with regard to both large-eddy (LES) and mesoscale simulations. The scheme uses a prognostic equation for the TKE whose evolution is governed by various mechanisms: the advection of TKE, the shear production, the buoyancy production, the diffusion, and the dissipation.

The basis of the proposed scheme is an equation system for the second-order turbulent fluxes, variances and covariances for velocities, potential temperature and various water mixing ratios. The closure of this system relies on the choice of the mixing-length expression. This expression defines the size L at which energy is supplied to the turbulence: within the so-called inertial range, the largest energetic eddies L feed the cascade of energy of the turbulence down to scales where the dissipation mechanism starts to dominate. The mixing-length expression is the only parameter that varies between the LES and the mesoscale configuration.

For LES in a 3-D framework, the largest unresolved eddies are by definition of the size

of the grid cell, hence

$$L = (\Delta x\, \Delta y\, \Delta z)^{1/3}\,.$$

This type of closure has been applied in the modelling of the fire/atmosphere interaction at the fire scale (some tens of meters) realized by Filippi et al. (2011) (Chapter 6).

When the scheme is applied at the mesoscale, it can be assumed that the horizontal gradients and turbulent fluxes are much smaller than their vertical counterparts, thus reducing computation of the turbulent mixing only to the vertical (i.e. turbulent fluxes are assumed purely vertical down to a resolution of 1 km). The higher vertical resolution, once compared to characteristic horizontal resolution in the mesoscale framework, imposes that the size of the most energetic eddies is parametrised in a physical way at every level. This can be done through the quasi-1D formulation of the length-scale proposed by Bougeault and Lacarrère (1989). The length-scale L of the largest eddies at a given level is determined as a function of the stability profile of the adjacent levels. The algorithm of Bougeault and Lacarrère (1989) relies on the computation of the maximum vertical displacement allowed for a parcel of air having the mean kinetic energy of the level as initial kinetic energy. The maximum upward displacement, l_{up}, and the maximum downward displacement, l_{down}, are computed by assuming that the parcel will stop when the cumulated buoyancy accelerations equal the initial kinetic energy. Hence, the resulting length-scale is

$$L = \sqrt{l_{up}\, l_{down}}\,.$$

This method allows the length-scale at any level to be affected not only by the stability at this level, but also by non-local effect of remote stable zones.

The quasi-1D scheme of Bougeault and Lacarrère (1989) has been used in the study of fire impact on the atmospheric dynamics and chemistry downwind of a typical Mediterranean wildfire (Chapter 4).

3.1.2.2 The Mass-Flux (MF) scheme

This section describes the diagnostic equations for ϕ_u and M_u which define the mass flux M in equation 3.4. In the following, the subscript u is always used for variables associated with the updraft whereas the subscript e refers to variables associated with the environment.

The basic idea of the EDMF approach is to depict dry thermals as towers of buoyant air rising from the surface and developing in a Convective Boundary Layer (CBL); these strong updraughts are not isolated but they interact with the surrounding environment through turbulent mixing that favours entrainment and detrainment of air masses between the convective parcel and its environment. Therefore, once the EDMF parametrisation is implemented in an atmospheric model, it allows a physical coupling between the updraft and the environmental air: the dynamics and the thermodynamics of both evolve due to

a reciprocal influence.

The Mass Flux approach describes the evolution of updraft structures ensuring the mass balance through a diagnostic mass continuity equation:

$$\frac{1}{M_u}\frac{\partial M_u}{\partial z} = \varepsilon - \delta \,. \tag{3.6}$$

The mass-flux evolves along the vertical at a rate given by the difference between the entrainment ε and the detrainment δ rate (Fig. 3.2).. The definition of entrainment/detrainment rates is the crucial point in EDMF parametrisation: it is at this level that the physical coupling between turbulent mixing and mass flux is done.

The mass-flux profile depends on the vertical velocity of the updraught, whose rate of rise is affected by a buoyancy term (B_u) and a drag term where the entrainment of environmental air, namely lateral mixing, is accounted for:

$$w_u\frac{\partial w_u}{\partial z} = aB_u - b\varepsilon w_u \,. \tag{3.7}$$

The updraft buoyancy acceleration is evaluated related to the difference of virtual potential temperature θ_V between the updraft and its environment, in the absence of phase change in water: $B_u = g(\theta_{u,V} - \overline{\theta_V})/\overline{\theta_V}$; parameters a and b are set to one (Simpson and Wiggert, 1969). The vertical velocity equation (3.7) can be solved to find the top of the updraft imposing $w_u \to 0$ as boundary condition. Moreover, the independent solutions of (3.6) and (3.7) permit to calculate the vertical variation of the updraft fractional area:

$$a_u = \frac{M_u}{\rho w_u} \,, \tag{3.8}$$

that is used to diagnose the cloud fraction, hence to define the sub-grid condensation scheme in the EDMF framework.

In the EDMF approach, a vertical non-local mixing of momentum is also performed in addition to the mixing already activated by the turbulent scheme. Hence, the updraft horizontal wind components evolve as

$$\frac{\partial u_u}{\partial z} = -\varepsilon(u_u - \bar{u}) + C_v\frac{\partial \bar{u}}{\partial z} \,, \tag{3.9}$$

$$\frac{\partial v_u}{\partial z} = -\varepsilon(v_u - \bar{v}) + C_u\frac{\partial \bar{v}}{\partial z} \,, \tag{3.10}$$

where $C_u = C_v = 0.5$; u_u (v_u) is the zonal (meridional) component of wind in the updraft; $\bar{u}$ and $\bar{v}$ are the zonal and meridional mean wind components, respectively.

As pointed out before, the definition of entrainment and detrainment rates characterizes the EDMF parametrisation. Pergaud et al. (2009) chose to draw the definition of lateral mass exchanges from the updraft buoyancy and vertical velocity. Both these parameters are pertinent in shallow convection as they control the mixing rate between the up-

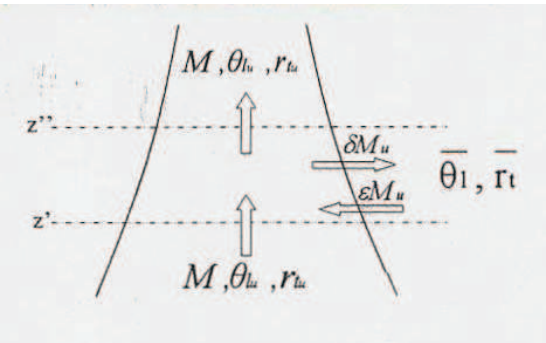

Figure 3.2: Variations of the updraft characteristics M_u (mass flux), θ_{lu} (liquid potential temperature) and r_{tu} (total mixing ratio) dependent on the mixing with the environment dictated by the entrainment $\epsilon\, M_u$ and the detrainment $\delta\, M_u$ (from Pergaud et al. 2009).

draft (dry or moist) and its environment. For the dry case, the entrainment/detrainment rate is locally defined as an equilibrium between w_u and B_u:

$$\varepsilon_{dry}, \delta_{dry} \propto \frac{B_u}{w_u^2}\,. \tag{3.11}$$

For the moist portion of the updraft a different definition of lateral mass exchange is given. In Meso-NH, if the Lifting Condensation Level (LCL) is reached, lateral exchanges are computed using the entraining/detraining plume model of Kain and Fritsch (1990).

Finally, the scheme initialization is given at the surface computing the mass-flux as follows:

$$M_u(z_{grd}) \propto \rho \left(\frac{g}{\overline{\theta_{V,ref}}} \overline{w'\theta'_{V,s}} L_{up} \right)^{1/3}, \tag{3.12}$$

and the vertical velocity of the updraft from the Turbulent Kinetic Energy at the ground, $e(z_{grd})$:

$$w_u^2(z_{grd}) = \frac{2}{3} e(z_{grd})\,. \tag{3.13}$$

Since the EDMF parametrisation has been developed to describe the shallow convection in the boundary layer that is produced by surface heating, such important atmospheric sources of heat and water vapour as wildfires fall within this class of phenomena. In Chapter 5 the potential of the EDMF parametrisation is investigated related to the determination of the fire injection height.

3.1.3 The coupling with the surface: the SURFEX model

The interaction between the atmosphere and surface processes is accounted for in Meso-NH through the coupling with the external model SURFEX (*SURface EXTernalisée*).

In SURFEX, each atmospheric grid-mesh is made of four adjacent surface types: nature, urban areas, sea/ocean, and lake. The coverage fraction of each of these surface

type over an atmospheric grid-mesh is known through the global database ECOCLIMAP (Masson et al., 2003), which combines land cover maps and satellite information to provide to SURFEX the land use information.

The exchanges between each of this surface type and the atmosphere are parametrised according to four different physical models, depending on the cited surface types. During a model time step, each surface grid-mesh receives an atmospheric forcing through variables as the upper air temperature, specific humidity, horizontal wind components, pressure, total precipitation, long-wave radiation, shortwave direct and diffuse radiations, and possibly concentrations of chemical species and scalar. In return, SURFEX computes averaged fluxes for momentum, sensible and latent heat, and possibly chemical species and scalar fluxes; then, SURFEX sends these quantities back to the atmosphere, with the addition of radiative terms like surface temperature, surface direct and diffuse albedo and also surface emissivity. The SURFEX fluxes are the average of the fluxes computed over nature, town, sea/ocean or lake, weighted by their respective coverage fraction. All information from SURFEX is used as lower boundary conditions for the atmospheric radiation and turbulence schemes.

Among the four physical models available in Meso-NH to simulate the exchanges between the atmosphere and each surface type, the Interactions Soil-Biosphere-Atmosphere scheme (ISBA, Noilhan and Planton, 1989) handles land surfaces and parametrises the exchanges of energy and water between the atmosphere and natural or agricultural lands. Since wildfires are events that concern natural lands, the most appropriate way to introduce the fire forcing in the Meso-NH model has been to pass through the ISBA scheme, as it is explained in Sections 3.3.2 and 3.3.3.

The orography is reproduced in Meso-NH using the global database Gtopo30 that has a finest resolution of 1 km (USGS/EROS, 1996) except for the LES simulations presented in Chapter 6 for which high resolution orography was derived from a GIS model and satellite information (`http://eros.usgs.gov/#/Find_Data/Products_and_Data_Available/gtopo30_info`). The vegetative cover is derived from CORINE Land Cover 1990 database at resolution 250 m.

More information about the SURFEX model can be found in the related scientific documentation (Moigne, 2009).

3.1.4 The chemical mechanism

A chemical module is coupled on-line with Meso-NH, which means that the meteorological and chemical fields are simultaneously computed at each time step and each grid point.

The Regional Atmospheric Chemistry Mechanism Stockwell et al. (RACM 1997) served as the reference chemical scheme to develop a reduced (lumped) chemical scheme in order to meet requirements of more efficiency in terms of computational cost and memory use. The Regional Lumped Atmospheric Chemical Scheme (ReLACS Crassier et al.,

2000)reduces the 77 prognostic chemical species and 237 reactions in RACM to 37 prognostic species and 128 reactions . The ReLACS chemical scheme was applied successfully to describe the troposphere gas-phase chemistry from the surface to the upper troposphere in remote to polluted urban conditions. All chemical species contained in the Meso-NH reduced mechanism are listed in Table 3.1 where it is possible to distinguish stable and intermediate organic and inorganic species. Besides all chemical species marked by a P at the end of the name (i.e. excited atoms), peroxy radicals also include: MO_2, PHO, ADD, OLN and XO_2. Moreover, the Meso-NH reduced mechanism includes long-life (e.g. CH_4) or stable (H_2, N_2, O_2) chemical species whose concentrations are fixed to a constant value due to their long chemical lifetime compared to the simulation duration. Except CH_4 and C_2H_6, all other alkanes are aggregated into one model species: ALKA. One model species ALKE is used to represent the anthropogenic emitted alkenes. The ReLACS scheme includes a mechanism for the oxidation of one biogenic organic species (BIO) involving isoprene, α-pinene, and *d*-limonene. Aromatic chemistry is also considered through one model species (ARO) and one aromatic-OH adduct (ADD). The carbonyl species in ReLACS include HCHO, C_2H_4O and higher saturated aldehydes (ALD), C_3H_6O and higher saturated ketones (KET), as well as other carbonyls in the model species CARBO. Concentrations of short-life monoatomic oxygen ($O(^3P)$, $O(^1D)$) are taken at chemical equilibrium and handled as diagnostic variables that are calculated at each chemical time step. In contrast with the Crassier et al. (2000)'s reaction mechanism, the concentration of OH is considered as a prognostic variable, no more as a diagnostic one. This modification increases the stiffness of the chemical reaction scheme but allow to get a more accurate information on the oxydation capacity in the studied air masses.

The temperature dependence of the rate of the chemical reactions k is represented by the Arrhenius expression and is given in cm^3 $molecule^{-1}$ s^{-1}.

$$k = A \exp\left(- \frac{E_{act}}{RT} \right), \tag{3.14}$$

where A is the pre-exponential Arrhenius factor, given in cm^3 $molecule^{-1}$ s^{-1} for second-order rate reactions, E_{act} is the activation energy (J), R is the gas constant (J K^{-1} mol^{-1}) and T is the temperature (K). The value of the rate constant at 298 K is called k_{298}.

In Meso-NH chemical reaction mechanism, rate constants are given for reactions occurring in the background troposphere and stratosphere. The rate constants are valid in a range of temperatures typically between 200 and 400K, which are considerably lower than typical temperatures near a flame (Chap. 2, Sec. 2.3) but still representative of the temperature of air heated by the fire.

The parametrisation for the dry deposition of gaseous species is based on the schemes of Wesely (1989) for vegetated surface and Erisman and Baldocchi (1994) for liquid surfaces. These schemes are included in the previously quoted ISBA surface model (Section 3.1.3)

and coupled with the diverse surface classification types of Meso-NH. ISBA calculates parameters for different vegetation types, so chemical dry deposition velocities evolves at each time step together with surface wind, turbulent conditions and chemical specificity.

The process of photo-dissociation follows the parametrisation of Madronich (1987). The TUV radiative-transfer model was used to calculate tabulated values of photolysis rates for a discrete number of solar zenith angles and for 8 gaseous species (NO_2, O_3, HONO, HNO_3, HNO_4, NO_3, H_2O_2, HCHO) and 6 lumped species (ALD, OP_1, OP_2, KET, CARBO, ONIT). The photolysis rates are interpolated at each grid point and updated every time step.

All chemical species are emitted in the first surface level in the model. Afterwards, they are advected in an Eulerian way by the Piecewise Parabolic Method (PPM, Colella and Woodward, 1984) and mixed in the boundary layer by the appropriate turbulence scheme (see previous Section 3.1.2.1). Moreover, the convection parametrisation of Bechtold et al. (2001), based upon the Kain and Fritsch (1993) mass flux scheme, has been implemented within Meso-NH to calculate the subgrid scale convective transport of chemical species (Mari et al., 2000). The mass flux parametrisation represents the vertical transport in convective drafts (i.e. updrafts bringing boundary layer air upward and downdrafts that represent downward transport of mid-tropospheric air); in addition, the convective drafts horizontally exchange mass with their environment through detrainment of cloudy air and entrainment of environmental air.

3.2 The fire spread model

This section is dedicated to the fire spread models. In Section 3.2.1, a brief introduction is given on different classes of fire spread models that exist nowadays. Section 3.2.2 presents the simplified fully physical model ForeFire used in the present study.

3.2.1 Overview of wild-land fire spread models

Fire spread modelling has a main scope: to predict the progression of a wild-fire in order to support in an operational way stack-holders (e.g. fire-fighters, forest agents, etc.). As a consequence, fire spread models have to respond to some basic requisites:

- CPU time[1] should be lower than the real time scale of the fire propagation.
- The memory use should be kept low making fire spread models sufficiently efficient for being applied on a field scale fire.

[1]CPU time (or CPU usage, process time) is the amount of time for which a Central Processing Unit (CPU) was used for processing instructions of a computer program, as opposed to, for example, waiting for input/output (I/O) operations. The CPU time is often measured in clock ticks or as a percentage of the CPU's capacity. It is used as a point of comparison for CPU workload of a program.

Table 3.1: List of all species included in the chemical reaction mechanism of Meso-NH (Crassier et al., 2000).

Chemical family or compound	Meso-NH acronym
Ozone	1. O_3
Hydrogen Peroxide	2. H_2O_2
Nitrogen Compounds	3. NO
	4. NO_2
	5. NO_3
	6. N_2O_5
	7. HONO
	8. HNO_3
	9. HNO_4
	10. NH_3
Sulfur Dioxide	11. SO_2
Sulfur Compounds	12. SULF
Carbon Monoxide	13. CO
Hydroxyl Radical	14. OH
Hydroperoxyl	15. HO_2
Methane	16. CH_4
Alcohols	17. ETH
Alkanes	18. ALKA
Alkenes	19. ALKE
Biogenic Alkenes	20. BIO
Aromatics	21. ARO
Formaldehyde	22. HCHO
Carbonyls	23. ALD
	24. KET
	25. CARBO
Organic Nitrogen Compounds	26. ONIT
	27. PAN
Organic Peroxides	28. OP_1
	29. OP_2
Organic acids	30. ORA_2
Peroxy Radicals	31. MO_2
	32. ALKAP
	33. ALKEP
	34. BIOP
	35. PHO
	36. ADD
	37. AROP
	38. CARBOP
	39. OLN
	40. XO_2

- Fire spread models should allow the real-time knowledge of the fire front evolution: its kinematic, the heat release, the flame height, the fire front depth, the fire angle, temperatures, the radiant heat flux, etc.

Until nowadays, different methods have been developed, tested and employed for answering to these principal requisites. These methods distinguish in the way they compute the Rate of Spread (RoS) of the fire front: a ratio between the heat flux received by the potential fuel ahead of the fire and the heat required to ignite this fuel (Pyne et al., 1949). The main classes of fire spread models are here summarized (Sullivan, 2007a,b,c).

- *Empirical models*: the formula for the RoS has an algebraic form and it depends on the wind velocity u, the ground slope α, the moisture content m and other parameters called f that are a function of the burning vegetal fuel

$$R = R(U, \alpha, m, f)\,.$$

  Parameters f are not known a priori. They are set up using experimental data in order to fit the modeled Ros on the measured one. This approach is simple and computationally efficient, but it can suit only on the range of experiments parameters have been drawn from.

- *Semi-empirical models*: they are based on a physical conservation law, the energy equation for the vegetal fuel, that is derived and closed by use of empirical values. Therefore, they offer simplicity and computational efficiency but they still need a calibration if the case study does not belong to the operating range defined in the validation framework. The main advantage of semi-empirical models compared to the fully empirical ones is their greater ability to be converted from laboratory to field scale experiments. Among this class of models, a widely used and well-known method is the Rothermel's formulation that can be resumed in the following formula:

$$R = R_0(1 + \phi_w + \phi_s)\,, \tag{3.15}$$

  where R_0 is the spread rate in the absence of wind, ϕ_w and ϕ_s are dimensionless multipliers that accounts for the effect of wind and slope, respectively, in increasing the propagating flux ratio. This formulation of fire RoS is drawn from a strong theoretical base: the energy balance equation within a unit volume of the fuel ahead of the flame. Despite this theoretical definition, Rothermel's model belongs to the group of semi-empirical wildfire spread models (Sullivan, 2007b) since experimental data are integrated to solve the energy equation and to introduce an adjustment for wind and terrain slope influence on fire spread (parameters ϕ_w and ϕ_s). Therefore, the Rothermel's method has a RoS equation depending on empirical coefficients fitted for a mid-flame wind speed. Normally, in the operational setting of the Rothermel's

model, the mid-flame wind speed is the same over the whole domain covered by the fire spread model and throughout the entire simulation; as a result, the Rothermel's model does not allow to take into account non-local heterogeneous change in the wind field and in the fire behaviour caused by the fire/atmosphere interaction. The Rothermel's model is implemented in full-scale simulation codes as BEHAVE which has a simple approach de-coupled from the local meteorology (Burgan and Rothermel, 1984), and FARSITE that adds a level of complexity using time-varying winds (Finney, 2004).

- *Reduced physical models*: in this technique, physical bases are stronger because a partial differential equation for a reaction-diffusion process describes the thermal budget in the solid fuel. As a result, the computational cost increases and the real-time can overlap the CPU time.

- *Fully physical models*: this strategy involves the numerical resolution of the conservation equation for mass, momentum, and energy in a multi-phase medium composed by the vegetal fuel and the surrounding air flow. This means that the range of temporal and spatial scales increases, hence the computational cost in terms of CPU time and memory storage is high. Moreover, the execution time for each simulation overtakes the real time. Some examples are: FIRETEC (Linn, 1997) that is designed to operate over landscape scales ($\sim$ 100 m) and whose governing equations are based on ensemble averaging of the conservation for mass, momentum, energy and chemical species (a full resolving Navier-Stokes simulator); WFDS (Mell et al., 2007) a 3-D, transient (i.e. a transient heat flux is employed in place of a constant flux) model that has been applied to modelling fire spread through surface fuels on flat terrain.

- *Mathematical analogue models*: they utilize mathematical concepts analogous to fire spread but which have no real-word connection to fire. This means that those models are, for the most part, based upon accepted mathematical functions that have been applied to wildland fire spread but are not derived from any understanding of wildland fire behaviour. An example is the study of Mallet et al. (2009) that uses the pure parametric model from Fendell and Wolf (2001) with the level set method to integrate fire front propagation.

In conclusion, empirical models are rapid and simple to use on the field for computing the RoS, on the other hand they cannot provide any information associated with the fire spread (heat flux, fire size, gas or fuel temperatures, etc.). Semi-empiririal models are the best candidates for operational use, but they still need a calibration when it has to do with cases for which they have not been tested for, especially because they do not take directly into account the influence of open areas on fire evolution (ground slope, wind flow, fuel features, etc.). Reduced or fully physical models are reliable for providing

approximations of the 3-D Eulerian fields proceeding from the fire spread as velocity, mass fraction, and temperature. They account for the academic knowledge acquired about natural fires but, up to now, it has not been possible to use them for firefighting due to their high computational cost. However, according to Hanson et al. (2000), physics-based approaches seem to be the better choice for the coupling with meteorological models because they offer a proper framework for linking the physics of combustion and its heat release to the meteorological equations of motion. Moreover, the dramatic increase in the capability of computers and numerical approaches in the last 30 years represent an opportunity for developing more capable physics-based fire models (Mell et al., 2007). Instead, mathematical models constitute a useful tool in the development of theoretical concepts that could be equally applied to the field of research of fire spread or to other field of endeavour.

3.2.2 ForeFire: a simplified physical model

Balbi et al. (2009) propose a new kind of model: a simplified 3-D fully physical model. It is a fully physical model because it obeys the main physical laws of fire propagation, hence, it is a priori usable in every configuration. Moreover, this model provides important global physical quantities related to the fire front. Its simplicity lies in ten theoretical assumptions that reduce the number of budget equations to a single algebraic relation for the RoS. This formula is a function of wind, slope and vegetation, and it depends on a set of four parameters, initially set up using physical data for the vegetal fuel. As a result, the reduced RoS relation implies a quite negligible computational time.

3.2.2.1 Synthesis of the model: theoretical assumptions and equations

This section presents: the major theoretical hypotheses and governing equations, the required parameters and the complete set of geometrical and thermodynamic quantities that the ForeFire gives as outputs. Readers are referred to the work of Balbi et al. (2009) for full derivation of the model.

Theoretical hypothesis

Hyp. 1. *Triangular flame*

The flame profile along the normal direction of propagation has a triangular shape: a simple form that minimizes the number of geometrical parameters. The base size on the ground is given by the depth of the fire front.

Hyp. 2. *Thermal radiation plays the main role on long-range effects that drive the fire progression*

Under the flame the upwind flow can not penetrate to feed convection because of the strong ascending heat flow that the flame produces just above the vegetal stratum. Moreover, typical length scales of convection are shorter than those of radiation and experimental data confirm that the thermal budget ahead of a flame front is essentially radiative (Silvani and Morandini, 2009). As long as the flame is not tilted on the vegetal fuel (e.g. strong winds or steep slopes), this hypothesis is still valid.

Hyp. 3. *Velocity composition*

The velocity in the flame, $\vec{V}$ results from the vectorial sum of the incident wind at the flame location, $\vec{U}$, and the natural convective velocity within the flame, $\vec{u}$:

$$\vec{V} = \vec{U} + \vec{u}\,.$$

Hyp. 4. *State equations*

Ideal gas law, isobaric thermodynamic transformations and an average flame temperature. These assumptions are usual in fire safety science (Balbi et al., 2009).

Hyp. 5. *"Stochiometric" inflow*

The ambient air entrained into the flame by natural convection allows the complete oxidation of reactive gases. The equivalent reaction is

$$\mathrm{C} + \mathrm{O_2} \longrightarrow \mathrm{CO_2}\,,$$

that consists of a strong, but realistic reduction. The chemical analysis of any vegetal fuel shows that it is chiefly composed of carbon and oxygen. The proposed equivalent reaction yields a "stochiometric" coefficient $s = 9$ that stands for: 9 kg of air are needed for the complete burning of 1 kg of pyrolysis gas.

Hyp. 6. *A surface fuel distribution*

Hyp. 7. *Constant mass loss rate*

The mass loss for the vegetal fuel is linear versus time as soon as the gas temperature reaches the temperature of fuel ignition. After, the thermal degradation kinetic is constant over time (i.e. heat release from a flaming fuel is constant over the burning time) and the complexity of the usual exponential Arrhenius model is reduced.

Hyp. 8. *Radiative tangent plane*

For every point close to the flame front, there exists a tangent plane of infinite length and height equal to the flame height.

Hyp. 9. *Pre-heating under the flame*

The radiant plane heats the unburned fuel only under the flame where the air stream can not penetrate (see Hyp. 2).

Hyp. 10. *Radiative factor*

The amount of energy emitted by radiation is a decreasing function of the surface-to-volume ratio of the flame.

To sum up, the main hypothesis of the Balbi's model is that the fire front can come close to a tilted radiant gray panel that is heating the vegetation in front of it, driving water and volatile contents out of the fuel, before starting the pyrolytic step. The terrain slope and the ambient wind impact directly the gas velocity in the flame and the tilting of the flame.

Governing equations

Eq. 1. *Mass balance*

The mass flow rate at the half-height of the model flame equals the sum of the flow rate of the pyrolysis gas and the flow rate of the air entering the flame in the stoichiometric proportion (see Hyp. 5).

Eq. 2. *Composition of velocities and flame tilt angle*

According to Hypothesis 3, the gas velocity in the flame follows $\vec{V} = \vec{U} + \vec{u}$. By geometrical consideration, the normal component of the velocity field can be derived, as also the resulting tilt angle γ. The tilt angle relative to the ground normal is:

$$\tan\gamma = \tan\alpha + \frac{U}{u_0}\,, \tag{3.16}$$

that depends on the terrain slope α, the wind velocity and a vertical gas velocity in the flame for zero wind and no slope conditions (u_0). This equation reproduces the effect of the increase of the flame tilt angle due to high wind velocities or steep slopes (Fig. 3.3).

Eq. 3. *Thermal balance*

The thermal budget in the flame yields a definition for the flame averaged temperature. Afterwards, the knowledge of the flame averaged temperature permits to compute the thermal radiation that a vegetal cell receives from the flame region above the vegetation (Φ_b) and in the flame part inside the vegetation (Φ_b), by using the Stefan-Boltzmann law for a gray body[2]. Finally, the thermal budget inside a vegetal cell can be written by taking into account the positive contribution of radiation (Φ_b and Φ_f) and the reducing contribution of evaporation.

[2]A grey body does not absorb or emit the full amount of radiative flux J^*. Instead, it radiates a portion of it, with its characteristic emissivity ϵ: $J^* = \epsilon\sigma T^4$, where σ is the Stefan–Boltzmann constant ($\sigma = 5.670 \times 10^{-8}\,\mathrm{J\,s^{-1}m^{-2}K^{-4}}$, and T is the thermodynamic temperature.

Eq. 4. *Flame height*

Starting from the equation for the vertical momentum:

$$\rho \frac{du}{dt} = -\rho g + \rho_a g \,,$$

where ρ is the gas flame density and ρ_a is the surrounding air density, the vertical velocity at the mid-height flame u is defined. This buoyancy velocity is defined as the ratio of the vertical velocity u_0 and the terrain slope α; the knowledge of u_0 and α is necessary to compute the flame height.

Eq. 5. *Rate of spread*

Previously stated hypotheses lead to the RoS function (in m s^{-1}):

$$R = R_0 + A \frac{R}{1 + \frac{R}{r_0} \cos\gamma} \left(1 + \sin\gamma - \cos\gamma\right), \tag{3.17}$$

where R_0 is the RoS without wind and slope effects; its value is determined by the actual quantity of water inside the fuel (Balbi et al., 2007). Parameter A is the ratio of radiant to total heat released and it decreases with the surface/volume ratio of the flame. Parameter r_0 is a speed factor due to radiation that depends on the flame thickness. The sign of the flame tilt angle discriminates between a slow backing fire spread ($\gamma \leq 0$) and a fast fire spread ($\gamma > 0$). R is an increasing function of γ. Moreover, for large slope angles R exhibits a linear dependence on U, whereas, for smaller values of γ, the relation between the RoS and wind velocity is strongly non-linear.

In conclusion:

- Assuming some empiricism on how the fuel reacts to radiation, an analytical formulation for the RoS function is obtained (Eq. 3.17) where wind and slope effects are explicitly taken into account, contrary to Rothermel's model. Equation (3.16) and (3.17) are the fundamental equations in the Balbi's formulation.
- Practically, the resolution of Balbi's algorithm depends on a set of four parameters: R_0, u_0, A and r_0.
- Balbi's model gives the radiant flux, the flame temperature, the flame height, the tilt angle, the flame depth, the heat released by time unit and the RoS.

3.2.2.2 Implementation in a fire area simulator: ForeFire

Balbi's model has been integrated in a fire area simulator that performs the numerical integration of the front advance: ForeFire. The fire front is discretised by a set of markers located along the fire perimeter. After a fixed burning duration (the fire Residence Time), front markers are displaced by a vector whose intensity is the RoS parameter and whose

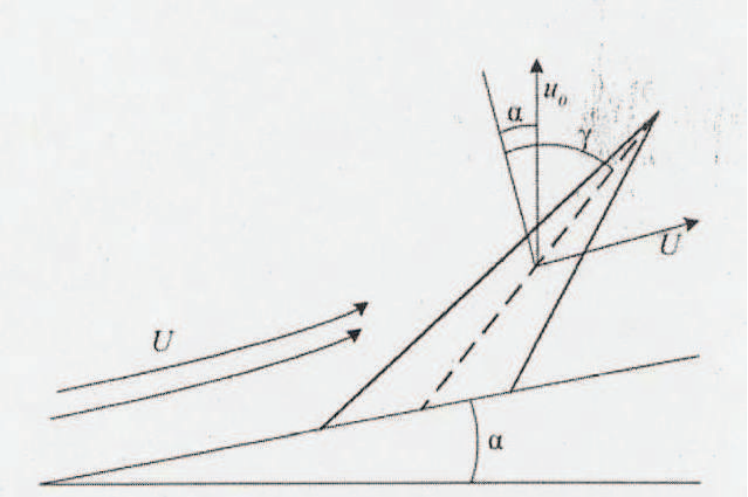

Figure 3.3: Flame profile along the normal direction and simplified schematic of the calculation of the flame tilt angle (Eq. 3.16) (from Filippi et al. 2009).

direction is the normal to the fire-line at this point. Then, front markers are redistributed along the front area to ensure a minimal distance between front agents. This is the way an asynchronous front-tracking method works (Fig. 3.4).

A first benchmark for ForeFire has been the large wild-fire of Lançon-de-Provence 2005. In Balbi et al. (2009) the ForeFire simulation has been cross-validated with the FARSITE simulator (Finney, 2004), a reference in forest fire simulation. Once FARSITE and ForeFire are compared to the observed burned area for the Lançon fire, both simulators achieve good results. Nevertheless, ForeFire has a significantly lower simulation time.

3.3 The coupling method

In this section, firstly the state of the art in coupled fire/atmosphere models is outlined (Sec. 3.3.1). The coupling method between ForeFire and Meso-NH is described in Section 3.3.2 for the high resolution LES applications, and in Section 3.3.3 for applications for which the atmospheric model has a coarser resolution than the fire model. The last section is dedicated to the implementation of the fire emissions in the coupled model.

3.3.1 The state of the art of coupled fire/atmosphere models

The numerical coupling of a fire model with an atmospheric model has already been the subject of numerous studies. The paucity of data and the difficulties to conduct full scale experiments limit the validation of coupled fire/atmosphere models. In the literature, coupled atmosphere-fire models are frequently validated qualitatively to insure that they reproduce the important fire feedback to the atmosphere and viceversa.

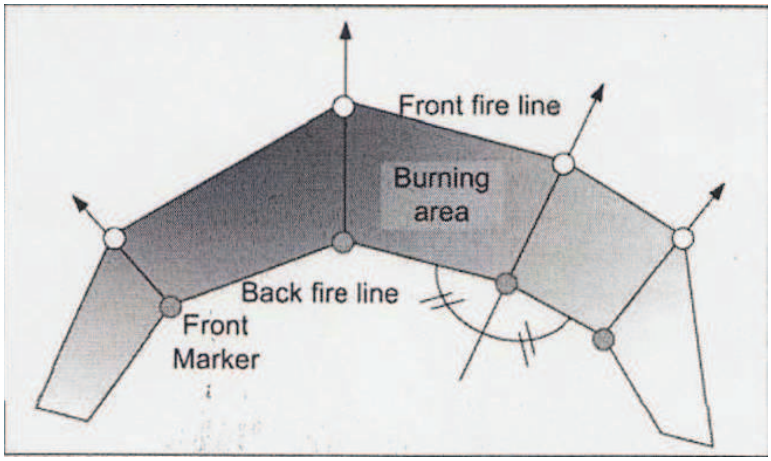

Figure 3.4: Schematic of the front tracking method of markers. Grey circles represent markers along the back fire line. Arrows show the propagation vectors (bisector of the local angle at the marker). White circles along the front fire line show the projected locations of the markers (grey circles) after the local burning duration (from Filippi et al. 2009).

Hanson et al. (2000) made a wish-list of the process representations and model attributes that a prognostic atmospheric model requires in order to simulate the key fire/atmosphere interactions properly. Required features are the following:

- Non-hydrostatic dynamics. The appropriate set of equations to predict the complex airflow near fires needs to be formulated to take into account the strong vertical motions generated by the heat from the fire.

- Sub-grid processes. Since direct numerical simulation of wildland fire is computationally intractable, approximations and parametrisations are essential. Turbulent transport, in particular, is a critical component of this factor.

- A terrain-following coordinate system. The propagation of a fire is strongly affected by terrain features.

- Multiple-level grid nesting. Wild-fire is a complicated multiscale process whose effects spread over different scales (Chap. 2 Sec. 2.2), hence a model structure that allows prediction of the small-scale flow in the fire region as well as the atmospheric processes over the general geographic region of the fire is necessary.

- Temporally and spatially varying fire heat sources. Wild-fires are important sources of heat that is released in the atmosphere in the form of hot gases and water vapour. The atmospheric heating by the fire is the primary coupling from small to larger scales that allows to predict the effect of the fire on the local airflow and weather.

- Transport of embers and firebrands by predicted wind fields. This process, called spotting, has to be parametrised to predict new fires ignited by burning debris.

- Temporally and spatially varying aerosol (smoke) sources. These are required to predict the fate of the fire haze, an important factor in radiation physics and air quality evolution.

A first example of coupled fire/atmosphere modelling is given by the work of Heilman and Fast (1992) that attempted to investigate the impact on the atmospheric turbulence of extreme surface heating, characteristic of fireline. They used a 2-D non-hydrostatic atmospheric model and they represented the fire as a static line source of extreme heating. Even if their results should be viewed qualitatively, in light of the 2-D nature of the model and the lack of a specific parametrisation for the flame dynamics, their simulations demonstrated the ability of a simple coupling fire/atmosphere to reproduce some important tendencies of the atmospheric circulation near a burning region.

The transition to 3-D and dynamic simulations leads to diverse studies of the coupled atmospheric/wildfire behaviour. For an aim of consistency with the classification of fire spread models given in Section 3.2.1, the coupled atmospheric/wildfire models are here presented starting with those that utilize empirical fire modules, then those based on physical fire spread modules.

Coupled models using (semi) empirical fire spread models

Reisner et al. (1998) linked the atmospheric hydrodynamics model HIGRAD to the BEHAVE module with an eye toward operational use. The coupled model was tested on two real fires that burned on complex terrains (canyon configuration). Even with the rather crude empirical functions employed in BEHAVE, the simulations produced results which agree well the observed fire behaviour. In particular, their simulations clearly revealed the intensity of a wildfire on a steep slope.

The work of Clark et al. (2004) proposed the coupling of an empirical fire spread model, based on the Rothermel's formulation, with a non-hydrostatic meso-scale atmospheric model. They developed a tracer method to represent the advancement of the fire perimeter; this method is suited for coupled fire/atmosphere calculations because, even if the computational cost of the tracer approaches is higher, numerical artifacts created by other approaches are less. For the purpose of resolving from meso-scale convective systems to vortices within firelines, the nesting technique is applied. The innermost atmospheric domain is the one that directly interacts with the fire model. The models are fully coupled: at each atmospheric time step of the inner model, atmospheric winds from the lowest vertical atmospheric level are passed into the fire model, where they are used to advance the fireline to a new position. During this time step, the rate at which fuel is consumed, once ignited, is described using a mass loss parametrisation, from the BURNUP

heat release model, that decreases exponentially. Heat and moisture from combustion enter into the atmospheric model as heat and moisture fluxes near the surface.

The evolution of the code of Clark et al. (2004) has led to the coupling between WRF model and the module SFIRE (Mandel et al., 2011). Among novelties in the WRF/SFIRE model, the level set method (Eulerian approach) replaces the tracer method (Lagrangian approach) for the fire propagation: a level set function represents the burning region at time t and it evolves through a first-order partial differential equation. This method seems to be more flexible for the purpose of data assimilation but it has high computational costs because the whole fireline needs to be advanced at each time-step. The methodologies for the computation of the burned fuel fraction and the released fire heat (sensible and latent) are the same than those used by Clark et al. (2004); however, the BURNUP algorithm is anymore used. Since the interaction of the fire and wind is of major importance to predict fire behaviour, especially severe fire behaviour, the Rothermel formula (Eq. 3.15) has been modified to account for the atmospheric wind predicted by the WRF model. However, this coupling is still dependent on a-priori defined wind reduction factors. The WRF/SFIRE model has not yet been tested on real large fires; Mandel et al. (2011) cite preliminary results showing that the WRF/SFIRE model is capable of realistic rendering of the rate of spread. A validation plan is proposed by the authors choosing the FireFlux experiment (Clements et al., 2007) as an appropriate benchmark since it provides data collected during the passage of a real fire.

Coupled models using (semi) physical fire spread models

In their paper, Hanson et al. (2000) supported the potential and promise of physics-based wildfire simulations, stating that the full, or semi, physics approach facilitates the linking between the fire and the atmospheric dynamics.

By running idealized and realistic case studies at high resolution using the HIGRAD/FIRETEC model, Linn et al. (2002) confirmed the potential of a self-determining model developed out of physical laws that drive wild-fires and not from prescribed rules drawn from empirical data. In the HIGRAD/FIRETEC simulations, some important signatures of the fire/atmosphere interaction are visible: irregularities in the fire perimeters, strong inflow of air near the base, change in the fire character due to the change in the ambient wind. The HIGRAD/FIRETEC model mainly focuses on the process of solid fuel pyrolysis, heat transfer and gas phase combustion that are active at very fine scale. Such a highly detailed and computationally intensive model has certainly a strong potential to delve into the physical mechanisms involved in fire spread and it can be a reference for physical and semi-physical coupled model, however it is not properly designed to follow the fire impact up to the large scales of the atmospheric motions.

The WFDS model (Mell et al., 2007) uses computational fluid dynamics methods to solve the governing equations for buoyant flow, heat transfer, combustion, and the thermal

degradation of vegetative fuels. WFDS numerical results have a good correspondence with observational data from Australian grassland fires. In particular, the spread rate of the head fire is well predicted and air entrainment toward the fire from the far-field can be clearly seen. As for the study of Linn et al. (2002), the computational cost limits the application of this kind of model within a certain scale range. They authors plan an improved version of WFDS in a large scale fire/atmosphere model as a longer-term goal, since large scale fire/atmosphere interactions are considered to be of major importance to predicting fire behaviour.

3.3.2 The MesoNH-ForeFire two-way coupled model at high (LES) resolution

In Filippi et al. (2009), the feasibility of the MesoNH-ForeFire on-line coupling has been demonstrated at very fine scale by setting the same resolution for both models to avoid that the fire-released heat is diluted over a large area.

Following the same set up as used by Clark et al. (2004), at every atmospheric time step, the atmospheric model is perturbed by the fire through convective heat and water vapour fluxes and radiant temperature through the surface scheme ISBA (Section 3.1.3). Obviously, these three ways of forcing are obtained through different computations, using characteristic nominal factors; however, they are connected by a common parameter: the burning ratio for each atmospheric grid cell, r_b. This term is given by the ratio of the burning area of the front shape S_b and the ForeFire cell area S_{ff}:

$$r_b = \frac{S_b}{S_{ff}}\,, \tag{3.18}$$

so that the burning portion of the cell ranges from 0 (no fire) to 1 (all burning). In return, the atmospheric model provides updated 3-D wind fields from its lowest vertical level for the prediction of the RoS. The three fire forcings over an atmospheric cell are computed as follows:

- Equivalent radiant temperature in K:

$$T_e = \sqrt[4]{(1 - r_b)\, T_s^4 + r_b T_n}\,,$$

  where T_s is the nominal flame temperature and T_s the soil temperature from the atmospheric model.

- Equivalent convective heat flux in W/m^2:

$$Q_e = r_b\, Q_n\,,$$

  where Q_n is the nominal convective heat flux.

- Equivalent water vapour flux kg/m^2:

$$W_e = r_b W_n$$

  where W_n is the nominal water vapour content.

Different idealized cases were chosen to test the coupled model and results have shown features consistent with observed fire/atmosphere interactions. In particular, the initiation of strong convection, one of the most significant coupled effect of the fire over the atmosphere, has been simulated together with the related area of wind-convergence near the fire-head, just under the fire plume as in Linn et al. (2002). This effect results in the acceleration of the fire front due the acceleration of the ambient wind near the fire front, similar to existing numerical fire/atmosphere experiments from the literature (e.g. Clark et al., 2004); fire-induced surface winds have been also recorded during the experimental wildland grass fire FireFlux (Clements et al., 2007) and an experimental burning through Mediterranean shrub (Santoni et al., 2006). This coupling method is applied to real case simulations in Chapter 6.

3.3.3 The MesoNH-ForeFire one-way coupled model at low resolution

When the atmospheric model is used at a resolution coarser than the fire model, heat fluxes and fire emissions are subgrid-scales processes. In the present work, this configuration was used only in a one-way approach (i.e. without feedback from the atmosphere to the fire propagation). In Chapter 4 this coupling method is applied to study the impact of fire on the atmosphere dynamics and chemistry during the Lançon-de-Provence 2005 case study.

ForeFire provides the burning ratio r_b for each fire cell at a fixed time interval. In order to guarantee the accuracy of the coupling, a total burning ratio (termed R_b) is defined as the sum of all burning ratios r_b produced by ForeFire at the fixed time interval and contained in each Meso-NH grid cell. At each atmospheric time-step (Δt), the surface scheme ISBA accomplishes the fire/atmosphere coupling by computing total wildfire contribution to latent and sensible heat fluxes, taking into account R_b, a nominal flux and the surface ratio between the Meso-NH (S_{mnh}) and the ForeFire (S_{ff}) grid-cells. Finally, calculated fluxes are taken as inputs at the surface level in the atmospheric model.

The sensible heat flux Φ_S is expressed in W m^{-2} and is computed as

$$\Phi_S = R_b \cdot \frac{S_{ff}}{S_{mnh}} \cdot \phi_S \,, \tag{3.19}$$

where ϕ_S is the nominal convective heat flux.

The latent heat flux Φ_L, given in kg m^{-2}, is calculated as

$$\Phi_L = R_b \cdot \frac{S_{ff}}{S_{mnh}} \cdot \frac{\phi_L}{\delta t}\,, \tag{3.20}$$

where ϕ_L is the nominal latent heat flux.

In Equation (3.19) and (3.20), the product between the total burning ratio R_b and the surface ratio $\frac{S_{ff}}{S_{mnh}}$ is the burnt fractional area. The burnt area is calculated as:

$$A = R_b \cdot S_{ff}\,. \tag{3.21}$$

3.3.4 Fire emissions in the coupled model

Burnt area information is also required to calculate chemical emission fluxes due to forest fires. Fire emission fluxes are obtained through a two-step process. Firstly, an estimate of carbon emission, E_{CO} in g, is obtained through the well-known equation of Seiler and Crutzen (1980) that is thoroughly commented in Eq. 3.27. Subsequently, CO emission flux is computed as follows

$$\Phi_{\mathrm{CO}} = \frac{E_{\mathrm{CO}}}{\Delta t \cdot S_{mnh}}\,. \tag{3.22}$$

Secondly, the emission flux for the other gases, Φ_i, is deduced by multiplying Φ_{CO} by the emission ratio with respect to carbon.

Emission information is represented in two basic forms (Andreae and Merlet, 2001):

- *Emission ratio* (ER) that is calculated as the excess trace species concentrations measured in a fire plume divided by the excess concentration of a simultaneously measured reference gas, e.g., CO_2 or CO.

  $$ER_{\text{trace gas}} = \frac{\Delta[\text{trace gas}]}{\Delta[\text{ref gas}]} = \frac{[\text{trace gas}]_{smoke} - [\text{trace gas}]_{ambient}}{[\text{ref gas}]_{smoke} - [\text{ref gas}]_{ambient}}\,. \tag{3.23}$$

  Alternatively, ER can be determined as the regression slope of the species concentrations versus the reference species.

  The selection of CO_2 or CO as reference gas is determined by the ultimate objective of the analysis and on the combustion type (flaming or smouldering) from which the species is preferentially released.

  ER has the advantage that it only requires simultaneous measurements of the species of interest and the reference species in the smoke, and appropriate measurements in the background air.

- *Emission factor* (EF) that corresponds to the amount of a compound released (M_x) per amount of dry fuel consumed ($M_{biomass}$), express in units of g kg^{-1}. Calculation of this parameter requires knowledge of the carbon content of the biomass burned

and the carbon budget of the fire: both parameters are difficult to establish in the field as opposed to laboratory experiments.

$$EF_x = \frac{\mathrm{M}_x}{\mathrm{M}_{biomass}} = \frac{\mathrm{M}_x}{\mathrm{M}_C} \cdot [\mathrm{C}]_{biomass}\,, \tag{3.24}$$

where $[C]_{biomass}$ is the carbon concentration in the biomass burned.

$$EF_x \cong \frac{[x]}{[\mathrm{CO_2}] + [\mathrm{CO}] + [\mathrm{CH_4}] + [\mathrm{VOC}] + [\mathrm{aerosol}] + \ldots} \cdot [\mathrm{C}]_{biomass}\,, \tag{3.25}$$

where $[x]$ is the concentration of the x species, and $[\mathrm{CO_2}]$ etc. are the concentrations of the various carbon species in the smoke.

To convert data given as molar ER to EF, the following equation is useful:

$$EF_x = ER_{x/y} \cdot \frac{MW_x}{MW_y} \cdot EF_y\,, \tag{3.26}$$

where $ER_{x/y}$ is the emission ratios of species X relative to the reference species Y, MW_i is the molecular weights of the i species, and EF_y is the emission factor of the reference species.

Where emission factors were given relative to other fuel mass indicators (i.e. not following the definition specified above, Eq. 3.25), data are multiplied with an appropriate conversion factor , typically, the carbon content of the fuel. Where fuel data at the ground are not available, a fuel carbon content of 45% is usually assumed in order to derive EF from ER (Seiler and Crutzen, 1980).

When modelling fire impacts on atmospheric chemistry, fire emissions are computed utilizing the well-known equation:

$$E_i = A \cdot FL \cdot \beta \cdot EF_i\,, \tag{3.27}$$

firstly defined by Seiler and Crutzen (1980). In Equation 3.27, fire emission E_i (in g) for a specific compound i results from multiplication of:

A ($\mathrm{m^2}$), the burnt area;

FL ($\mathrm{kg\ m^{-2}}$), fuel loading defined as the mass per unit area of fuel material (i.e. biomass, ground litter and dead wood) available for combustion;

β, a dimensionless parameter that is the burning efficiency of the above-ground biomass (given as a per cent). Burning efficiency is usually defined as the fraction of biomass consumed by the fire, or the carbon released to the total carbon present in the fuel;

EF_i ($\mathrm{g\ kg^{-1}}$), the emission factor for the considered species that is calculated as the mass of pollutant produced per mass of dry fuel consumed.

Hence, the estimation of fire emissions requires explicit knowledge of characteristics and condition of the fuels, amount of fuel consumed, combustion phase (e.g. flaming or smouldering), etc.

Different errors and uncertainties are associated to all variables at hand in Equation (3.27); moreover, multiplication of these terms amplifies the final error, according to the theory of error propagation. For this reason, it is important to have in mind weights and sources of error for all cited variables.

$A \rightarrow$ burnt area estimations can be obtained using three sources: wildfire reports, prescribed fire or smoke management reports, and aerial or satellite data. All three methods have problems in providing the actual area burnt because of missing or incorrect data. Simulation of a forest fire by a fire spread model may reduce the uncertainty on temporal and spatial resolution of burnt area, but this procedure depends on the reliability of the fire simulator (i.e. how the physics of the combustion is parametrised).

$FL \rightarrow$ fuel loading can have a large variation even across occidental Europe, where human activities have redesigned the region creating an impressive patchwork of forest, shrublands, grasslands. The large variations in fuel loading across regions can be responsible of 80% of the error associated with estimating emissions (Ottmar et al., 2009).

$\beta \rightarrow$ burning efficiency (BE) is influenced by fire intensity (J m^2), rate of spread (m min^1) and residence time (min) in a certain stage of combustion (e.g. flaming or smoldering). Therefore BE ought to be considered as a dynamical variable rather than a constant parameter, as most regional to global emission estimates assumed. The use of an average value can lead to uncertainties ranging from 23% to 46% (Santis et al., 2010).

$EF_i \rightarrow$ emission factors depend on type of pollutant, type and arrangement of fuel and combustion phase. Average EF for the flaming and smoldering period of a fire can vary in a relatively small range and contribute to nearly 16% of the total error associated with predicting emissions (Ottmar et al., 2009).

On-field campaigns and measurements in laboratory combustion facilities estimated emission factors for primary chemical species (Andreae and Merlet, 2001; Miranda, 2004; Miranda et al., 2008). Tables 3.2, 3.3, 3.4 and 3.5 gather emissions factors available in literature for Mediterranean or European vegetation. It is evident that emission factor list still remains incomplete, in particular regarding Mediterranean vegetation.

3.4 Synthesis

The numerical coupling between an atmospheric model and a fire spread model is a possible technique to reproduce the complex and tight fire/atmosphere interaction. In the litterature, diverse studies showed the potential and promise of coupled fire/atmosphere models. These works mainly differ in the choice of the fire spread model that can be fully or partly based on physical laws (e.g. Linn et al., 2002; Mell et al., 2007), or developed using empirical formula obtained from experimental data (e.g. Clark et al., 2004; Mandel et al., 2011). Furthermore, fire spread models distinguish in the numerical integration of the front advance (e.g. front tracking algorithm, level set method, etc.). The study of Filippi et al. (2009) demonstrated the feasibility of the numerical coupling between the atmospheric model MesoNH (Lafore et al., 1998) and the fire spread model ForeFire (Balbi et al., 2009).

Meso-NH is a non-hydrostatic meteorological model. It is based on a Euler system of partial differential equations that determine the evolution of the state of the atmosphere from the large meso (10 km) down to the micro scales (large eddies, decametres), by taking into account different mechanisms (e.g. advection, Coriolis force, pressure force, turbulence and diabatic sources). Wild-fires induce atmospheric circulations that result predominantly from large temperature anomalies created by the release of energy due to the combustion. As a consequence, wild-fires influence the atmospheric turbulence and the convective process in the planetary boundary layer. Concerning the parametrisation of turbulent motions, Meso-NH includes the turbulent kinetic energy among its prognostic variables. Turbulent fluxes are fully resolved by the 3-D scheme of Cuxart et al. (2000) when the model is run at LES resolutions (i.e. resolutions $< 0.5 - 1$ km); whereas, at the meso-scales, the computation of the turbulent mixing reduces only to the vertical through the quasi-1D formulation proposed by Bougeault and Lacarrère (1989). The recent work of Pergaud et al. (2009) included in Meso-NH the Eddy Diffusivity Mass-Flux (EDMF) parametrisation that combines the local effect of turbulence (Eddy Diffusivity) to the non-local transport that is governed by the Mass Flux. The EDMF approach aims to describe the shallow convection in the CBL that is triggered by surface heating. Hence, the EDMF scheme reproduces the phenomenon of dry thermals whose vertical evolution relies on their interaction with the surrounding environment through entrainment and detrainment of air masses. The surface/atmosphere interaction is described in Meso-NH by the external and coupled module SURFEX that uses the ISBA scheme (Noilhan and Planton, 1989) to handle the exchanges of energy and water between the atmosphere and natural lands. A chemical module is coupled on-line with Meso-NH in order to describe the chemical evolution and the transport of all chemical species listed in Table 3.1.

ForeFire is a semi-physical fire spread model. It is based on the fundamental laws of combustion whose complexity was reduced by applying some simplifying assumptions. These approximations reduce the number of equations that are necessary to follow the

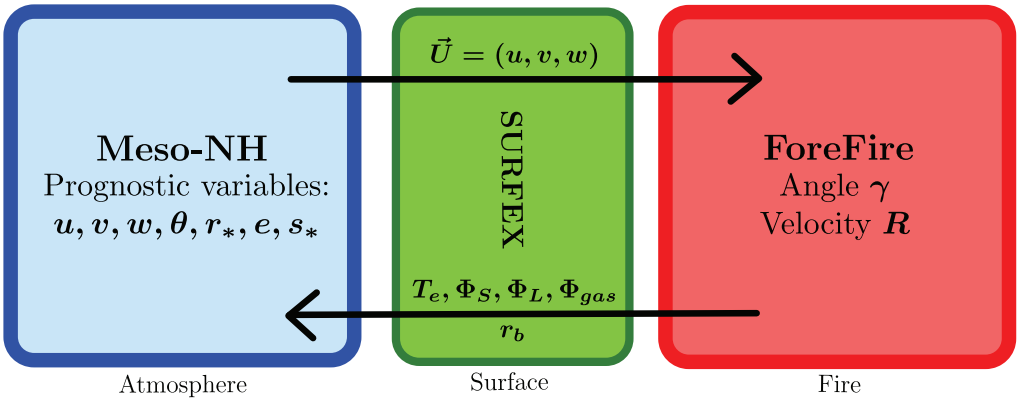

Figure 3.5: Schematic diagram summarizing how the atmosphere/fire coupled model, MesoNH-ForeFire, works. The atmospheric model Meso-NH gives to the fire model ForeFire the information about the atmospheric wind $\vec{U}$. ForeFire determines the advancement of the fire by computing the flame tilt angle γ and the rate of spread R, and it calculates the burning ratio r_b. This term is used to compute the radiant temperature T_e, heat (Φ_S, Φ_L) and emission fluxes Φ_{gas} through the SURFEX model. All these variables influence the dynamical and chemical evolution of the atmosphere in Meso-NH, and a new value for the atmospheric wind is simulated by Meso-NH.

fire advancement to a single algebraic relation for the fire RoS (Eq. (3.17)). In ForeFire, the reduced RoS formula is a function of wind, slope and vegetation, and it depends on a set of parameters initially set up using physical data for the vegetal fuel. The knowledge of the fire RoS permits to perform the numerical integration of the front advance through an asynchronous front-tracking method (Fig. 3.4).

Figure 3.5 summarizes how the coupled MesoNH-ForeFire model works. Practically, Meso-NH gives to ForeFire the information about the atmospheric wind $\vec{U}$. ForeFire determines the fire RoS and it calculates the burning ratio r_b for each fire cell at a fixed time interval. The burning ratio is used in the ISBA scheme to compute, at each atmospheric time-step, the wildfire contribution to the radiant temperature (T_e), latent (Φ_L) and sensible (Φ_S) heat fluxes. Hence, through the SURFEX model, the dynamical evolution of the atmosphere in Meso-NH is influenced by the fire propagation, and a new value for the atmospheric wind is calculated and passed to ForeFire in order to newly integrate the fire advancement. In the present work, the illustrated dynamical coupling was completed with the fire emission fluxes (Φ_{gas}) whose computation relies on the knowledge of the burning ratio and emission information (i.e. fuel loading, combustion efficiency, emission ratio).

In the next chapters, diverse applications of the coupled MesoNH-ForeFire model are illustrated, focusing on the landscape/fire scale (kilometric resolution, Chap. 4 and Chap. 5) and the sub-hectometric scale (Chap. 6).

Table 3.2: Emission factors for Mediterranean forest (Simpson et al., 1999).

Vegetation	Fuel Loading (kg/m^2)	Above-ground Biomass Fraction	Burning Efficiency β	Derived Emission Factors (kg ha)					
				CO	CH_4	NMVOC	NO_x	NH_3	SO_x
Mediterranean Forest	4	0.75	0.25	780	51	71	27	6	6

Table 3.3: Fuel types and emission factors for German grass from a heavily industrialized region (Christian et al., 2003).

Vegetation type	Number of fires	% C	% H	% N	% Ash	Fuel Moisture (%)	Average Fuel Loading (kg/m^2)
German grass	3	45.1	5.73	1.06	5.40	9.2-21.6	1.14

Vegetation type	Emission Factors (g kg^{-1})						
	$PM_{2.5}$	EC	OC	Cl in Fuel	Cl in $PM_{2.5}$	K in $PM_{2.5}$	S in $PM_{2.5}$
German grass - T	3.2			0.218	0.027	0.031	0.01244
German grass - Q		0.38	2.74				

T, teflon filter; Q, quartz filter. EC, elemental carbon ; OC, organic carbon.

Table 3.4: Emission factors (EF) for different types of vegetation typical of Southern Europe (Miranda, 2004).

Vegetation type	Combustion phase/ Fire type	Emission Factors (g kg^{-1})				
		CO_2	CO	PT	CH_4	NMHC
Broad-leaved	F-B		44	13	2	4
	S-H		146	20	8	8
	Global		112	18	6	6
Coniferous	F-B	1615	50	14	0.7	2
	S-H	1416	195	38	4	5
	Global	1497	100	20	5	4
Slash pine needles	F-B	1792	59	7	0.7	
	S-H	1464	164	39	1	
	Global	1757	49		5	
Forest (general)	Global	1304	96	19	5	
Shrub	F-B	1496	59	7	0.7	
	S-H		164	39	1	
	Global		49		5	
Herbaceous	Global	1370	75	10	2	0
Diverse	Global	1178	108	5	5	12

F, flaming; S, smouldering; B, backing; H, heading.

Table 3.5: Emission factors for typical vegetation species of the Mediterranean Basin region (Miranda et al., 2008).

Fuel	Fuel Loading ($kg\ m^{-2}$)	Burning Efficiency	Emission Factors ($g\ kg^{-1}$)						
			CO_2	CO	CH_4	NMHC	$PM_{2.5}$	PM_{10}	NOx
Shrubs	1.00	0.80	1477	82	4	9	9	10	7
Resinous	8.60		1627	75	6	5	10	10	4
Deciduous	1.75	0.25	1393	128	6	6	11	13	3
Eucalyptus	3.90		1414	117	6	7	11	13	4

Chapter 4

Wild-fire impact on gaseous air pollutants

Contents

This chapter presents the first effort to simulate a real large wild-fire by applying the one-way coupled fire/atmosphere model, MesoNH-ForeFire introduced in Chapter 3.

4.1 Resume of the research article

On Friday 1 July 2005, an arson forest fire broke out near Lançon-de-Provence, southeast France. Favoured by extreme weather conditions recorded in south-eastern France the day of the fire (strong northwesterly winds and dry fuel), the Lançon fire spread easily and burned nearly 700 ha, mainly covered by shrub-land. The research article "Forest Fire and Atmosphere: the Lançon-de-Provence 2005 case study" (now under publication in the journal Atmospheric Environment) explores the impact of this Mediterranean fire on the atmospheric dynamics and chemistry downwind of the burning region.

The Lançon fire smoke plume was observed by the MODIS-AQUA instrument several kilometres downwind of the burning area, out of the Mediterranean coast. Signatures of the fire plume on air pollutants were measured at surface stations in southeastern France by the air quality network AtmoPACA. Ground-based measurements revealed unusually high concentrations of PM_{10} and a well marked depletion of O_3 concentrations on the day of the fire. This peculiar behaviour was not observed by the same stations the day before and after. Ground-based stations localised outside of the fire plume did not show changed in pollutant levels, thereby confirming the limited spatial extension of the plume simulated by the model.

The Lançon-de-Provence fire propagation was successfully simulated by ForeFire in the context of a model inter-comparison exercise (Balbi et al., 2009). The burnt areas provided by ForeFire at high temporal and spatial resolutions were scaled to compute the fire heat and water vapour fluxes in the 3-D MesoNH model following the methodology described in Chapter 3 (Sec. 3.3.3). The simulated fire plume was confined in the boundary layer with high values of turbulent kinetic energy. The plume was advected several kilometres downwind of the ignition area by the Mistral winds in accordance with the MODIS and AtmoPACA observations. The vertical plume development was found to be more sensitive to the sensible heat flux than to the fire released moisture. The burnt area information was also used to compute emissions of aerosol and gaseous pollutants, using emission information (fuel loading, combustion efficiency, emission factors) found in the literature for Mediterranean vegetation. A passive tracer (hereafter "fire aerosol-like tracer") was introduced to mimic PM_{10} aerosols. A chemical reaction mechanism presented in the previous chapter (Sec. 3.1.4) was coupled on-line to the Meso-NH model (MesoNH-Chem version) to account for gaseous chemistry evolution in the fire plume. The only source of gaseous species was from the fire, no anthropogenic emissions were considered. The coupled model simulated high concentrations of the fire aerosol-like tracer downwind of the burning zone at the right timing compared to ground-based measurements. High levels of O_3 precursors (NO_x and CO) were simulated in the smoke plume

Figure 4.1: Amateur picture taken during the Lançon-de-Provence 2005 wild-fire that shows clearly well the fire plume keeping in contact with the surface while propagating.

which led to the depletion of O_3 levels above and downwind of the burning zone. This depletion of O_3 was indeed observed at ground-based stations but with a higher impact than simulated. The difference may be explained by the simplified design of the model with no anthropogenic sources and no interaction of the smoke aerosols with the photolysis rates. Ozone production was modelled tens of kilometres downwind of the ignition zone out of the coast.

The study highlighted the strong perturbations of the atmospheric dynamics and chemistry by the fire several kilometers downwind of the ignition area. Among the main results, both the model and the air quality stations proved that the fire plume kept in contact with the surface (see Fig. 4.1 from `http://www.jeune-ailes.org`). This behaviour will be further discussed in the following chapter on the injection height of fire plumes as seen by Meso-NH and a plume rise model.

4.2 The Lançon-de-Provence 2005 case study

Forest Fire and Atmosphere: the Lançon-de-Provence 2005 Case Study

S. Strada[a,*], C. Mari[a], J.-B. Filippi[b], F. Bosseur[b]

[a] *Laboratoire d'Aérologie, University of Toulouse and CNRS, Toulouse, France*
[b] *SPE, University of Corsica and CNRS, Corte, France*

Abstract

Forest fires release significant amounts of trace gases and aerosols into the atmosphere. Depending on meteorological conditions, fire emissions can efficiently reduce air quality and visibility, even far away from emission sources. In 2005, an arson forest fire burned nearly 700 ha near Lançon-de-Provence, southeast France. This paper explores the impact of this Mediterranean fire on the atmospheric dynamics and chemistry downwind of the burning region. The fire smoke plume was observed by the MODIS-AQUA instrument several kilometres downwind of the burning area out of the Mediterranean coast. Signatures of the fire plume on air pollutants were measured at surface stations in southeastern France by the air quality network AtmoPACA. Ground-based measurements revealed unusually high concentrations of aerosols and a well marked depletion of ozone concentrations on the day of the fire. The Lançon-de-Provence fire propagation was successfully simulated by the semi-physical fire spread model ForeFire. ForeFire provided the burnt area at high temporal and spatial resolutions. The burnt areas were scaled to compute the fire heat and water vapour fluxes in the three-dimensional meso-scale non-hydrostatic meteorological model MesoNH. The simulated fire plume kept confined in the boundary layer with high values of turbulent kinetic energy. The plume was advected several kilometres downwind of the ignition area by the Mistral winds in accordance with the MODIS and AtmoPACA observations. The vertical plume development was found to be more sensitive to the sensible heat flux than to the fire released moisture. The burnt area information is also used to compute emissions of a fire aerosol-like tracer and gaseous pollutants, using emission factors for Mediterranean vegetation. The coupled model simulated high concentrations of the fire aerosol-like tracer downwind of the burning zone at the right timing compared to ground-based measurements. A chemical reaction mechanism was coupled on-line to the MesoNH model to account for gaseous chemistry evolution

*Corresponding author
Email address: susanna.strada@aero.obs-mip.fr (S. Strada)

in the fire plume. High levels of ozone precursors (NO_x, CO) were simulated in the smoke plume which led to the depletion of ozone levels above and downwind of the burning zone. This depletion of ozone was indeed observed at ground-based stations but with a higher impact than simulated. The difference may be explained by the simplified design of the model with no anthropogenic sources and no interaction of the smoke aerosols with the photolysis rates. Ozone production was modelled tens of kilometres downwind of the ignition zone out of the coast.

Keywords:

Mediterranean region; off-line coupled model; fire spread; injection height; smoke plume pollutants.

---

1. Introduction

The latest report of the IPCC (2007) highlights that climate change is very likely to impact fire risk in the Mediterranean Basin region. In fact, even if Mediterranean wildfires are mostly human-induced, the study of Moriondo et al. (2006) based on regional modelling indicates that fire frequency, fire severity and the length of the fire season would increase under future climatic conditions (based on the IPCC A2 and B2 scenarios). Furthermore, the analysis of Pausas (2004) for the eastern Iberian Peninsula confirms that a relationship exists between fire events and seasonal meteorological conditions (summer temperatures and mean rainfall), as also shown by annual data reported by the European Forest Fires Information System of the Joint Research Centre (EFFIS, 2008).

Within the context of increasing fire risk, it is necessary to investigate the dynamics and chemistry of forest fires, which are a threat not only to local ecosystems but also to public health. In the vicinity of the fire, biomass burning produces high concentrations of carbon dioxide (CO_2), carbon monoxide (CO), methane (CH_4), nitrogen oxides (NO_x), volatile organic compounds (VOCs) and particulate compounds (Lobert and Warnatz, 1993). CO_2 and CH_4 are the most important greenhouse gases responsible for the "enhanced greenhouse effect". Moreover, CH_4 together with CO, NO_x and VOCs are chemically active gases hazardous to human health both directly and indirectly, since they are precursor gases of tropospheric ozone (O_3); in the troposphere, NO_x from combustion also allow the re-generation of the hydroxyl radical (OH) that, in turn, catalyzes the O_3 production. Lastly, biomass burning particulates can reduce visibility and air quality on a local scale and aerosols can affect the radiation budget of the Earth, impacting global and regional climate. Wildfire emissions can also be transported over considerable distance, spreading their effects from local to regional and occasionally global scales, depending on the efficiency of atmospheric transport (Takegawa et al., 2003; Miranda et al., 2008; Bytnerowicz et al., 2010).

The extent of the degradation of air quality due to forest fires has been quantified at different scales. Fire experimental fields in France (Barboni et al., 2010) and Portugal (Miranda et al., 2005) revealed concentrations of toxic air pollutants well above exposure limit values settled by the European Legislation established in the Council Directive 2008/50/EC. Miranda et al. (2005) analysed concentrations of particulate matter (PM), NO_x, CO and sulfur dioxides (SO_2) during an experimental field fire performed in 2002 at Gestosa. This experiment stresses the critical situation in terms of local air quality that can occur during a fire episode and affect the personnel involved in fire-fighting operations. The maximum hourly averaged values for aerosol particles with an aerodynamic diameter lesser than 2.5 μm (hereafter $PM_{2.5}$) and smaller than 10 μm (hereafter PM_{10}) were, respectively, 2350 μg m^{-3} and 1430 μg m^{-3}. Gestosa PM concentrations are in the range of the hourly averaged data recorded in operational conditions during a wildfire in Greece: 3350 μg m^{-3} and 1300 μg m^{-3}, respectively. Similar PM concentrations were observed near the Quinault fire (Trentmann et al., 2002). During Gestosa-2002, CO concentrations peaked at nearly 60 mg m^{-3}, nitric oxide (NO) at 600 μg m^{-3} and nitrogen dioxide (NO_2) at 500 μg m^{-3}. On a regional scale, Phuleria et al. (2005) measured pollutant gases and PM concentrations in the Los Angeles (LA) basin before, during, and after the October 2003 Southern California wildfires. They documented a strong degradation of urban LA air quality due to the fires. Downwind of the fires, the greatest impact was observed on coarse-PM concentrations which exceeded typical background concentrations by factors of three or four: PM_{10} concentrations were near or above 200 μg m^{-3} during the fires. During the same event, CO was increased by nearly 12 ppmv and NO reached 100 ppbv. Interestingly, NO_2 levels remained essentially unchanged and O_3 concentrations decreased by about 25-50 %. The authors proposed the reduction in photochemical activity due to the fire smoke blanketing the LA basin as a possible explanation for the NO_2 and O_3 fire response. O_3 depletion was also documented by aircraft measurements in young biomass-burning plumes, close to the fire, in South Africa (Hobbs et al., 2003) and Namibia (Jost et al., 2003). In addition, aircraft measurements investigated the change of the mixing ratio of many species in the fire plume moving away from the ignition point. Jost et al. (2003) measured 1703 ppbv of CO over the fire, rapidly decreasing by one-third at a distance of 4 km downwind of the fire. Yokelson et al. (2007) observed average PM_{10} values for vertical profiles that ranged from 70-120 μg m^{-3} at 300-500 m to 30-60 μg m^{-3} near the top ($\sim$ 3000 m) in central Brazil .

In Europe, episodes of trans-boundary fire tracer dispersion have already been observed and modelled. Saarikoski et al. (2007) and Sofiev et al. (2008) consider the influence of emissions from Russian and Baltic wildfires on air quality in northern Europe during spring and summer 2006. They used a Lagrangian dispersion model, SILAM, with fire emissions based on the Moderate Resolution Imaging Spectro-radiometer

(MODIS) hot spots to simulate the observed increase of fire pollutants recorded at ground-base stations. A similar approach was used by Tressol et al. (2008) based on the FLEXPART model to assess the main origin of strong anomalies of O_3, CO and NO_x registered by MOZAIC aircraft above Frankfurt during the 2003 heat wave, when severe wildfire activity hit Portugal. Lagrangian models succeed in reproducing the main characteristics of fire plumes advection. The most important limitation of the current versions is the treatment of fire injection height which is generally kept constant. Lagrangian models are currently not designed to investigate the strong updrafts and convective fluxes associated with wildfires.

Hodzic et al. (2007) investigated the effects of forest fires on air quality in Europe during summer 2003 using the meso-scale chemistry transport model CHIMERE. CHIMERE has been improved to include the MODIS smoke emissions inventory and implements a new parametrisation to simulate the injection of smoke particles. The injection height is calculated as a function of atmospheric conditions and fire characteristics, retrieved from the MODIS inventory. The parametrisation allows for the simulation of the transport of smoke plume at the right altitude. This approach relies on the accuracy of satellite measurements.

Another approach is that of Turquety et al. (2009). The authors used the Infrared Atmospheric Sounding Interferometer (IASI) for the monitoring of CO during the summer 2007 Greek fires. Once a retrieval algorithm of CO vertical profiles is defined, CO mixing ratios are analyzed close to the fires and in the transported plume: this technique allows to study the dispersion of fire tracer and to roughly estimate the general level of injection of the fire plume.

The next level of complexity of fire-atmosphere coupling is the Eulerian high-resolution model ATHAM (Oberhuber et al., 1998). In order to investigate the connection between wildfire and atmosphere, in terms of both dynamics and chemistry, the active tracer atmospheric model ATHAM was forced utilizing wildfires parameters such as heat release and aerosol fluxes, obtained from ground-based observations. A simplified design was chosen with a static fire front and fire fluxes held constant throughout the simulation. Although these simplifications, the ATHAM model successfully simulated the transport of fire emissions, chemical processes leading to the formation of tropospheric O_3 in a young biomass-burning plume and radiative effects in a smoke plume, and pyro-convection (Trentmann et al., 2002, 2003, 2006; Luderer et al., 2006). However, the cited fire-atmosphere coupling does not consider a temporal and spatial evolution of fire characteristics and there is no feedback from the atmosphere to the fire.

The interaction between the atmosphere and the fire can be fully resolved using a fire spread model coupled with an atmospheric model. Fire spread models vary from empirical (Clark et al., 2004) to physics-based systems (Linn et al., 2002, among others). For a complete review of fire spread models the reader

is referred to Sullivan (2007a,b). Semi-physical fire spread models are a good compromise being based on physical laws whose complexity is reduced by imposing realistic assumptions (Sullivan, 2007a; Filippi et al., 2009). Coupled fire-atmosphere model studies normally focus on small scale atmospheric processes, since at these resolutions these models are able to reproduce fire-induced effects on wind and turbulence that have been measured on field campaigns, as, for example, during the Fire-Flux experiment (Clements et al., 2007). At larger scales (meso-scale), an example of one-way coupling between the fire and the atmosphere is illustrated by the work of Miranda (2004). The author coupled the meteorological model MEMO to a semi-empirical fire progression model FARSITE and successfully reproduced the effects of the forest fires on the air quality in Lisbon during summer 2003. However, at resolutions much higher than the fire front resolution, coupled models still have limits and constraints that need to be further explored. The difference between resolution of the meso-scale atmospheric model and the coupled high resolution fire spread model imposes the parametrisation of sub-grid fire processes. Mesoscale models incorporate various parametrisations to include sub-grid vertical transport, but strong vertical updrafts associated with intense heat sources, such as wildfires, are frequently ignored, or, their impact is diluted, at the resolution typical of large-scale models (Freitas et al., 2006). This deficiency implies that the fire injection height may be underestimated. The fire injection height is an important parameter necessary for the study of air quality during fire episodes. If pollutants are released in the Planet Boundary layer (PBL), removal processes are more efficient and can shorten pollutant residence time (Chatfield and Delany, 1990). On the contrary, when emitted into the free troposphere, characterized by faster winds, the pollutants can be transported considerably further and affect air quality from the local through the regional and global scales. Several studies have been carried out to investigate the height to which smoke plumes rise and the variability of this altitude due to atmospheric conditions and fire characteristics (Labonne and Chevallier, 2007; Kahn et al., 2008; Martin et al., 2010; Guan et al., 2010). Current methods to parametrise plume lifting are based on a one-dimensional entrainment plume rise model embedded in a host model (Freitas et al., 2007) or on a mixed eddy diffusivity - mass flux scheme for convective boundary layer plumes (Rio et al., 2010). So far, these approaches have been validated for African and Amazonian fires for which elevated injection heights have been observed.

The objective of this study is to explore fire impact on atmospheric dynamics and chemistry downwind of a burning area located in the Mediterranean region. The atmospheric meso-scale model MesoNH is coupled with the semi-physical fire spread model ForeFire to simulate the Lançon-de-Provence 2005 forest fire. A chemical reaction mechanism is coupled on-line to the MesoNH model to account for gaseous chemistry

evolution in the fire plume. In Section 2, a brief description of the atmospheric and the fire spread model is given, precising model setup and initialization. Section 3 introduces the Lançon-de-Provence 2005 case study, describing the fire history and synoptic meteorological conditions before the wildfire burst out. In Section 4, the fire plume dynamics and chemical composition are compared with MODIS observations and ground-based measurements registered by the air quality survey network available in southeastern France (AtmoPACA). Finally, conclusions are summarized in Section 5.

2. Fire-atmosphere coupling

This section is devoted to the presentation of the models used in the simulation of the Lançon fire. Firstly, Section 2.1 describes the meteorological-chemistry model MesoNH. Section 2.2 briefly presents the fire spread model ForeFire. Finally, Section 2.3 is dedicated to the description of the coupling method adopted for this study.

2.1. The atmospheric model MesoNH

MesoNH is a meteorological model jointly developed by the Centre National de Recherche Météorologiques (Météo France) and the Centre National de Recherche Scientifique (Laboratoire d'Aérologie) (Lafore et al., 1998). This numerical model was designed to simulate atmospheric motion at different scales: from the large meso-alpha down to the micro scale (large eddy). Some of its distinctive features are: the non-hydrostatic assumption, the an-elastic approximation, the so called "interactive grid-nesting technique" and a chemical module available for on-line coupling (MesoNH-C version).

MesoNH incorporates many physical parametrisation options. In the present study all prognostic variables and fire tracers are advected in an Eulerian way, using the Piecewise Parabolic Method (Colella and Woodward, 1984). Cloud micro-physical processes follow a two-moment scheme, considering three water phases with five precipitating and non-precipitating liquid and solid water species (Pinty and Jabouille, 1999). Radiative processes are represented with the radiation scheme developed by the European Center for Medium-Range Weather Forecasts (ECMWF): the Rapid Radiative Transfer Model (RRTM, Mlawer et al., 1997).

In this study MesoNH is run in its standard three dimensional (3-D) configuration, using three two-way grid-nested domains whose horizontal mesh sizes are 25, 5 and 1 km (Fig. 1a). For all three domains, the vertical grid has 72 levels up to an altitude of 23 km, with a level spacing stretching from 40 m near the ground, to 600 m at higher altitude.

The simulation is run from 29 June 2005, 05:00 UTC, to 1 July 2005, 18:00 UTC. The model spin-up is 43 hours before the fire starts. The fire starts at 07:40 UTC on 1 July 2005, and ends on the same day at 16:40 UTC. A different time step is fixed for each domain (25, 5 and 1 s, respectively). Dynamical variables are initialized and constrained at the boundaries using operational reanalysis from the ECMWF (25 km horizontal resolution). Two simulations were conducted with and without perturbations by the fire.

At 25 km and 5 km, the convection parametrisation follows the mass flux scheme of Bechtold et al. (2001). Representation of turbulent motions is based on the quasi-1D scheme of Bougeault and Lacarrère (1989), assuming turbulent fluxes are purely vertical down to a resolution of 1 km.

Surface energy exchanges are parametrised according to four different physical models, depending on the surface type (natural surfaces, urban areas, oceans and lakes). In particular, we use the Interactions Soil-Biosphere-Atmosphere scheme (ISBA, Noilhan and Planton, 1989) that parametrises the exchanges between the atmosphere and natural or agricultural land. Surface schemes need an accurate description of the soil use to define the initial parameters. In MesoNH this land use information is provided by the global database Ecoclimap (Masson et al., 2003). To conclude on surface information, the orography is reproduced in MesoNH using the global database Gtopo30 that has a finest resolution of 1 km (USGS/EROS, 1996).

The model simulates the mixing ratio of 40 chemical species utilising 73 chemical reactions. The ReLACS chemical scheme is described in detail in Crassier et al. (2000). The parametrisation for the dry deposition of gaseous species is based on the schemes of Wesely (1989) and Erisman and Baldocchi (1994) included in the previously quoted ISBA surface model. The process of photo-dissociation follows the parametrisation of Madronich (1987). The TUV radiative-transfer model was used to calculate tabulated values of photolysis rates for a discrete number of solar zenith angles and for 8 gaseous species (NO_2, O_3, HONO, HNO_3, HNO_4, NO_3, H_2O_2, HCHO) and 6 lumped species (ALD, OP_1, OP_2, KET, CARBO, ONIT). The photolysis rates are interpolated at each grid point and updated every time step. In the present version of the coupled fire-atmosphere model, the only source of gaseous species is from the fire. No anthropogenic emissions are considered. All species are emitted in the first surface level in the model and mixed in the boundary layer by the turbulence scheme. There is no a-priori injection height. A simplified chemical initialisation was derived from the simulation of 21 June 2001 at 00:00 UTC done by the MOCAGE model during the ESCOMPTE model inter-comparison exercise (Cros et al., 2004; Dufour et al., 2005). Profiles from the location nearest to Lançon-de-Provence are used for the entire domain (i.e. initial concentrations are homogeneous over the entire domain). A proper vertical profile was derived from MOCAGE simulated values for the following chemical species: O_3 (Fig. 2a), aldehydes (ALD), nitric acid (HNO_3), SO_2 and NO_2

(Fig. 2b). CO, ethane (ETH), formaldehyde (HCHO), OH, hydroperoxyl radical (HO_2), ketone (KET), CH_4 and NO have the same vertical profile (Fig. 2c) that distinguishes from one another through the multiplication factors listed in Table 1. These profiles are assumed to be a fair representation of summer background mixing ratios over the studied area, although it is clear that important geographical and inter-annual variability occurs for the reactive species. The primary role of these initial values is to ensure a realistic ozone chemical regime in the background atmosphere. The impact of mixing between this environmental air and the fire plume on the levels of pollutants in the plume is expected to be limited due to the extremely high concentrations emitted in the fire plume.

There is no aerosol scheme in the present configuration. A passive tracer (hereafter named "fire aerosol-like tracer") has been introduced to mimic fire-produced PM_{10} aerosols. The fire aerosol-like tracer is initialized to zero and has a deposition velocity of 3 cm s^{-1} (Seung-Muk et al., 2006). The fire aerosol-like tracer is only emitted above the fire with the emission rate described in Section 2.3 and its emission equals zero elsewhere. This tracer will be used as an additional proxy for the study of the fire plume dynamics and time evolution.

2.2. The fire model ForeFire

Predicting wildfire behaviour requires a Rate of Spread (RoS) equation: a ratio between the heat flux received by the potential fuel ahead of the fire and the heat required to ignite this fuel (Pyne et al., 1949).

In the field of wild-land fire behaviour modelling, a widely used and well-known method is the Rothermel's formulation. This formulation of fire RoS is drawn from a strong theoretical base: the energy balance equation within a unit volume of the fuel ahead of the flame. Despite this theoretical definition, Rothermel's model belongs to the group of quasi-empirical wildfire spread models (Sullivan, 2007b) since experimental data are integrated to solve the energy equation and to introduce an adjustment for wind and terrain slope influence on fire spread. Therefore, the Rothermel's method has a RoS equation depending on empirical coefficients fitted for a mid-flame wind speed. Normally, in the operational setting of the Rothermel's model, the mid-flame wind speed is the same over the whole domain covered by the fire spread model and throughout the entire simulation; as a result, the Rothermel's model does not allow to take into account non-local heterogeneous change in the wind field and in the fire behaviour caused by the fire/atmosphere interaction.

In this study, the propagation of the Lançon fire is simulated using the quasi-physical fire spread model ForeFire developed by the Laboratoire de Systèmes Physique pour l'Environnement integrating in a fire area simulator the model of Balbi et al. (2009). Readers are referred to this work for full derivation of the model.

For self-consistency, we report here the major theoretical assumptions and the main governing equations. Contrary to Rothermel's model, the ForeFire RoS has an analytical formulation where wind and slope effects are explicitly taken into account. In ForeFire, the main hypothesis is that the fire front can come close to a tilted radiant gray panel that is heating the vegetation in front of it, driving water and volatile contents out of the fuel, before starting the pyrolitic step. Assuming some empiricism on how the fuel reacts to radiation, the RoS function (in m s^{-1}) is given by:

$$R = R_0 + A\,\frac{R\,(1 + \sin\gamma - \cos\gamma)}{1 + \frac{R}{r_0}\cos\gamma}\,, \tag{1}$$

where R_0 is the RoS without wind and slope effects; its value is determined by the actual quantity of water inside the fuel (Balbi et al., 2007). Parameter A is the ratio of radiant to total heat released and it decreases with the surface/volume ratio of the flame. Parameter r_0 is a speed factor due to radiation that depends on the flame thickness. Angle γ is the flame tilt angle relative to the ground normal whose definition relies on the knowledge of terrain slope angle (α), wind velocity (U) and a vertical gas velocity in the flame for zero wind and no slope conditions (u_0) in the following form:

$$\tan\gamma = \tan\alpha + \frac{U}{u_0}\,. \tag{2}$$

This equation reproduces the effect of the increase of the flame tilt angle due to high wind velocities or steep slopes.

The advance of the fire front is simulated using a front-tracking algorithm. To achieve this, the fire front is discretised using a set of markers located along the fire perimeter. After a fixed burning duration (the fire Residence Time) front markers are displaced according to the speed function R along propagation vectors directed normal to the fire-line at this point. Then front markers are redistributed along the front area to ensure a minimal distance between front agents.

2.3. The coupling method

In Filippi et al. (2009) the feasibility of the MesoNH-ForeFire on-line coupling has been demonstrated setting the same resolution for both models. The atmospheric model was perturbed by the fire through latent and sensible fluxes and radiative temperature. In return, the atmospheric model provided updated 3-D wind fields for the prediction of the RoS. Different idealized cases were chosen to test the coupled model and results have shown features consistent with observed fire-atmosphere interactions.

In the present work, the finest horizontal resolution selected for the MesoNH simulation (1 km) is still coarser than the resolution used for simulating the Lançon fire by ForeFire (100 m). For this reason, an off-line coupling is initiated between the fire and the atmospheric model, i.e with no feedback of the atmosphere on the fire.

ForeFire provides the burning ratio r_b (burning area of the front shape / ForeFire cell area) for each fire cell (100 m × 100 m), every 2 minutes. In order to guarantee the accuracy of the coupling, a total burning ratio, termed R_b, is defined as the sum of all burning ratios r_b produced by ForeFire every 2 minutes and contained in each MesoNH grid cell. At each atmospheric time-step (Δt), the surface scheme ISBA accomplishes the fire-atmosphere coupling by computing total wildfire contribution to latent and sensible heat fluxes, taking into account R_b, a nominal flux and the surface ratio between the MesoNH (S_{mnh}) and the ForeFire (S_{ff}) grid-cells. Finally, calculated fluxes are taken as inputs at the surface level in the atmospheric model.

The sensible heat flux Φ_S is expressed in kW m^{-2} and is computed as

$$\Phi_S = R_b \cdot \frac{S_{ff}}{S_{mnh}} \cdot \phi_S \,, \tag{3}$$

where a nominal convective heat flux for Mediterranean fires is used: $\phi_S = 100$ kW m^{-2} (Silvani and Morandini, 2009).

The latent heat flux Φ_L, given in kg m^{-2} s^{-1}, is calculated as

$$\Phi_L = R_b \cdot \frac{S_{ff}}{S_{mnh}} \cdot \frac{\phi_L}{\Delta t} \,, \tag{4}$$

where ϕ_L is 0.1 kg m^{-2} (Filippi et al., 2009).

In Equation (3) and (4), the product between the total burning ratio R_b and the surface ratio $\frac{S_{ff}}{S_{mnh}}$ is the burnt fractional area. The burnt area is calculated as:

$$A = R_b \cdot S_{ff} \,. \tag{5}$$

Burnt area information is also required to calculate chemical emission fluxes due to forest fires. Fire emission fluxes are obtained through a two-step process. Firstly, an estimate of carbon emission, E_{CO} in g, is obtained through the well-known equation of Seiler and Crutzen (1980):

$$E_{\mathrm{CO}} = A \cdot FL \cdot \beta \cdot EF_{\mathrm{CO}} \,, \tag{6}$$

where A is the burnt area (in m^2); FL is the fuel loading (fuel material per unit area, kg m^{-2}); β is the burning efficiency of the above-ground biomass (expressed as a per cent) and EF_{CO} is the emission factor for CO

(produced mass of pollutant per mass of dry consumed fuel, g kg^{-1}). For Mediterranean shrubs, typical values of fuel loading and combustion efficiency are, respectively, 1.00 kg m^{-2} and 80 % (Miranda et al., 2008). Subsequently, CO emission flux is computed as follows

$$\Phi_{\mathrm{CO}} = \frac{E_{\mathrm{CO}}}{\Delta t \cdot S_{mnh}} \,. \tag{7}$$

Secondly, the emission flux for the other gases, Φ_i, is deduced by multiplying Φ_{CO} by the emission ratio with respect to carbon that is defined by the following equation of Andreae and Merlet (2001):

$$ER_{i/\mathrm{CO}} = \frac{EF_i}{EF_{\mathrm{CO}}} \cdot \frac{MW_i}{MW_{\mathrm{CO}}} \,, \tag{8}$$

where MW_i and MW_{CO} are the molecular weights of the species i and of the reference species, in this case CO. $ER_{i/\mathrm{CO}}$ is normally expressed as a per cent. Table 2 lists the emission factor for CO and emission ratios with respect to carbon that have been found in the literature for Mediterranean shrub-lands or similar vegetation (Andreae and Merlet, 2001; Trentmann et al., 2003; Miranda et al., 2008).

3. A case study: Lançon-de-Provence 2005

This section gives a presentation of the chosen case study: the Lançon-de-Provence 2005 wild-fire. The purpose is to offer to the reader a preliminary analysis of the fire in terms of its history (Sec. 3.1), meteorological conditions as simulated by MesoNH and observed by a radiosonde the day of the fire (Sec 3.2), and in terms of air quality conditions recorded by AtmoPACA in southeast France before, during and after the fire (Sec. 3.3).

3.1. Fire history

On 1 July 2005, an arson forest fire broke out southeast of Lançon-de-Provence (southeastern France, 43.59 N, 5.13 E), with two ignition points, threatening downwind inhabited areas and cultivated lands.

The fire started at about 07:40 UTC, 09:40 CEST (Center European Summer Time). Favourable weather conditions, in particular strong and gusty winds, and dry fuel led to the fire spreading easily. At the end of the day, at around 16:40 UTC, Lançon fire was put out, after 9 hours of burning. The Lançon-de-Provence fire spread over 626 ha, in an area characterized by homogeneous fuel density. The burned fuel was *garrigues*, a type of low, soft-leaved shrub-land that can be found around the Mediterranean Basin, generally near the coast.

The Lançon fire has served as a benchmark for fire propagation models. ForeFire successfully simulated the large wild-fire of Lançon-de-Provence 2005 fire (Balbi et al., 2009). For this simulation, the orographic wind map was calculated as a stationary solution at the resolution of the terrain numerical model: 50 × 50 m. Vegetation and soil use were defined using the CORINNE Land Cover database (resolution 250 m over Europe): the main kinds of vegetation were shrub and forest. Weather information were provided by firefighters: a wind speed of about 46 km/h, direction of 330 °; temperature equals 26 ° C and the relative humidity was 20%. In ForeFire, the fire progression was constrained by three fire contours gathered by firefighters (at 12:00, 14:00 and 16:30, local time). ForeFire simulated a total burnt area of 757 ha.

ForeFire simulation indicates that fire intensity maximized between 10:00 and 12:00 UTC. Considering Hodzic et al. (2007), this result is consistent with several studies on satellite and in-situ measurements that put on evidence the pronounced diurnal cycle of biomass burning, characterized by peak emissions during early afternoon (12-14 h local time). Figure 3a shows the temporal evolution of the total burnt area A as simulated by ForeFire every 2 minutes, once ForeFire outputs had been integrated on a grid-cell of 100×100m of resolution. In the ForeFire simulation, the largest area impacted by the fire is 4.92 ha (13:36 UTC). On Figure 1b, the solid line indicates the perimeter within which the burnt area information from ForeFire are localised in the 1-km grid-mesh domain used in the MesoNH-ForeFire simulation.

3.2. Synoptic meteorological situation

On 30 June 2005, MesoNH simulates a synoptic situation over western Europe characterized by a strong pressure gradient with high pressure over the Atlantic Ocean and a cyclonic situation over the Gulf of Genova. This gradient together with a tunnel orographic effect, between the Alps and the Massif Central, favours a strong northwesterly wind, the so-called Mistral. The same meteorological situation persists in the simulation for 1 July 2005. Figure 1b shows simulated winds at an altitude of 40 m above orography on 1 July 2005, 07:00 UTC, reaching maximum speeds of 14 m s^{-1} in the vicinity of Lançon. The same day a wind velocity of 12.8 m s^{-1} was measured by firefighters in the burning area.

On 1 July 2005, at 12:00 UTC, a radiosonde was launched over Nîmes (43.50 N, 4.35 E), a city located 72 km to the northwest of the burning area. In Figure 4, potential temperature (θ, K), water vapour mixing ratio (r_v, g/kg), wind speed (V, m/s) and wind direction (Dir, °) recorded by the radiosonde (empty dots linked by a solid line) are traced up to an height of about 3 km. Vertical profiles from the radiosounding are compared to those simulated by MesoNH over the location of Nîmes, at the same day and hour of the radiosonde (dashed line).

The observed vertical profile of θ (Fig. 4a) reveals instable atmospheric conditions at the surface ($\partial_z\theta < 0$), followed by a first zone where the turbulent mixing is trying to recover the atmospheric stability, then a well marked temperature inversion is registered at about 760 hPa (around 2300 m); above, the atmosphere becomes more stable ($\partial_z\theta > 0$). MesoNH succeeds in simulating the well developed mixed layer ($\theta \sim$ constant): the typical convective boundary layer of a summer early afternoon. The model reproduces a less marked instability at the ground and a temperature inversion, less pronounced than the observed one, at a lower altitude (827 hPa). The temperature inversion is an important atmospheric condition that may control the injection height of the fire plume, preventing it from reaching higher altitudes (Trentmann et al., 2003). Hence, the pointed out discrepancy could influence the simulated fire plume rise, leading to a lower injection height than the real one.

In Figure 4b, simulated r_v overlays fairly well on the radiosounding profile. In the convective boundary layer (CBL) r_v remains constant; above 827 hPa, r_v decreases from $\sim$ 6 g kg^{-1} to 2 – 3 g kg^{-1} at 700 hPa. Values of r_v depict a dry atmosphere.

In Figure 4c, in the first meters of the atmosphere, the simulated wind speed is slightly stronger that the observed one: this is coherent with the difference discussed in Figure 1b between the simulated and the measured wind speed. Above 900 hPa, the situation reverses: the simulated wind speed is 2 m/s weaker than the recorded one. MesoNH reproduces a wind slightly rotated towards the east, when compared to the observed direction (Fig. 4d). It is worth noting that the strong winds blowing on the considered domain may efficiently prevent fire plume to rise in the free troposphere, as pointed out by Trelles et al. (1999) and Freitas et al. (2007).

The model reproduces fairly well the main characteristics of the meteorological conditions observed in Nîmes the day of the fire: a dry atmosphere, a strong temperature inversion (although at lower altitude than observed) and strong northwesterly winds.

3.3. Air quality observations downwind of the fire

Figure 5 presents the observed PM_{10} hourly concentrations registered on 30 June, 1 July and 2 July 2005, respectively, by three air quality stations located near the burning area. The distance between the burning area (43°33′ N, 5°14′ E) and each of the three measurement stations is respectively: 33 km for Marseille Timone, 25 km for Marseille Saint Louis, 55 km for Avignon Mairie. On 1 July 2005 the stations in Marseille measured high levels of PM_{10} hourly concentrations compared to the other two days. The day before and after the fire, PM_{10} concentrations are lower than 70 μg m^{-3} at Marseille Timone and Marseille

Saint Louis. The day of the fire a peak of 151 μg m^{-3} is registered at 12:00 UTC at the Marseille Timone station (Fig. 5a). PM_{10} levels have increased by $\sim$ 80 μg m^{-3} compared to the day before. Air quality stations located out of the smoke plume, such as Avignon Mairie, do not exhibit such a clear increase in PM_{10}, supporting the evidence that PM_{10} peak observed in Marseille on 1 July 2005 can be ascribed to the Lançon fire.

Figure 6 reports the measured O_3 hourly concentrations as recorded on 30 June, 1 July and 2 July 2005, respectively, by three air quality stations located near the burning area. The distance between the burning area and each of the three measurement stations is respectively: 18 km for Bouc Bel Air, 31 km for Marseille Cinque Avenue, 43 km for La Ciotat. The monitoring stations of Bouc Bel Air (Fig. 6a) and Marseille Cinque Avenues (Fig. 6b) recorded a decrease of nearly 40-60 μg m^{-3} (roughly corresponding to 20-30 ppbv) in O_3 hourly concentration on 1 July 2005. Moreover, the amplitude of the diurnal cycle for O_3 on 1 July 2005 is smaller when compared to the day before and after: a fluctuation of 10-15 μg m^{-3} versus 50-60 μg m^{-3} in the time span 8:00-18:00 UTC. These observations indicate that the fire smoke could have counteracted the diurnal cycle of O_3 in a metropolitan area. This behaviour was not observed in La Ciotat (Fig. 6c) where O_3 concentrations show the same diurnal cycle over the three days. 1 July 2005, was a Friday, hence O_3 decrease in Bouc Bel Air and Marseille Cinque Avenues can not be ascribed to traffic reduction during the weekend. Observations of high levels of PM_{10} and depleted O_3 air masses by ground-based stations suggest that the fire plume remained in contact with the surface as it is advected southeastward toward the sea.

Meteorological conditions on 1 July 2005 were comparable to the day before and after: strong north-westerly winds, no clouds and high temperatures. In addition the signatures on O_3 and PM_{10} had limited spatial extension. Ground-based stations near Marseille urban area but out of the fire footprint do not exhibit such peculiar behaviour of O_3 and PM_{10}. Therefore, the Lançon fire seems to be the most probable cause of the changed behaviour in the measured O_3 and PM_{10} concentrations in Marseille.

4. Results and discussion

In this section results are discussed, separating fire impacts on atmospheric dynamics (Sec. 4.1) from those on atmospheric chemistry (Sec. 4.2).

In the following, all graphics referring to MesoNH-ForeFire simulation correspond to results for the inner model at 1 km of resolution on the day of Lançon fire: 1 July 2005; hence, only the hour (in UTC) will be specified.

Figure 7, 8a and 10 illustrate vertical cross sections along the simulated center-line of the fire plume. The direction of the simulated plume slightly differs from the observed one due to the shift in wind direction discussed in the previous section (see Figure 9b).

4.1. Fire impacts on atmospheric dynamics

4.1.1. Fire-induced turbulence

Biomass burning is an intense source of heat in the atmosphere, emitted in the form of hot gases and water vapour (Luderer et al., 2006). Once hot and humid air masses are released into the atmosphere during a fire episode, they interact with the cooler surrounding air and this interaction triggers turbulent eddies. Turbulence associated with the fire can efficiently mix colder air into the smoke plume, diluting the hot plume thus reducing convection (Freitas et al., 2007). For this reason, it is interesting to examine how atmospheric turbulence and turbulent vertical fluxes can be affected by the ignition and spread of a forest fire.

In the MesoNH-ForeFire simulation Turbulent Kinetic Energy (TKE) varies from 3.5 to 5.0 $m^2\ s^{-2}$ over the burning area, once the fire-atmosphere coupling is activated. During the first four hours of fire activity (from 8 to 12 UTC) TKE continues to rise reaching a maximum value of 7 $m^2\ s^{-2}$ above the burning area. Using an instrumented tower during a prescribed grass fire, Clements et al. (2006) measured a change in TKE between 1 and 2 $m^2\ s^{-2}$, with a maximum of $\sim 2.5\ m^2\ s^{-2}$ once the tower was engulfed in the main plume. Fire perturbation on the TKE pattern is highlighted by computing the difference in TKE between the "fire forced" and the "no fire" simulation. Such difference allows to distinguish the impact of fire on turbulence from other contributions like the dynamical instability due to wind shear caused by the topography or the production of positive buoyancy typical of a convective boundary layer. The hatched fill patterns on Figure 7 refer to the TKE perturbation (in $m^2\ s^{-2}$) at 12:00 UTC. The impact of the fire is evident, with a positive difference in TKE of around 1 $m^2\ s^{-2}$ above fire (empty dot). The impact spreads in the vertical up to an altitude of 1.2 km and over nearly 20 km in the horizontal, dimensions which give an idea of the area affected by the fire-induced turbulent mixing. Along the cross-section an area of negative TKE production is located downwind of the fire at a distance of nearly 30 km from the burning area (above the black dot). The analysis of the vertical velocity pattern (not shown) reveals a subsidence zone on the lee-side of the hill visible in the centre of the cross-section. Subsident flows triggered by the orography is a well known process and has been simulated by Jiang et al. (2007) for example. In this particular case, the simulated subsidence is emphasized by the increase of turbulence up hill.

Positive buoyancy production occurs when there is heating at the surface. Field campaigns have measured sensible heat fluxes associated with wildfires that are nearly 3 orders of magnitude higher than natural fluxes (Clements et al., 2006; Silvani and Morandini, 2009). The coloured fill patterns on Figure 7 show the turbulent vertical kinematic sensible heat flux ($w'\theta'$, in K m s^{-1}) as seen at 12:00 UTC by the "fire forced" case. If we multiply $w'\theta'$ by the specific heat capacity of dry air ($C_p \sim 1004$ J K^{-1}kg^{-1}) and the density of dry air ($\rho \sim 1.20$ kg m^{-3}), the maximum of 0.8 K m s^{-1} roughly corresponds to a sensible heat flux of nearly 960 W m^{-2}. This value is significantly above natural fluxes that are estimated among 200-300 W m^{-2}. During a prescribed grass fire, Clements et al. (2006) documented a sensible heat fluxes of 1183.5 W m^{-2}. The turbulent vertical kinematic sensible heat flux is proportional to the buoyancy term in the TKE equation. The maximum of the TKE perturbation overlays fairly well the area of maximal $w'\theta'$, confirming that hot air masses released by the fire clearly feed the buoyancy production and the vertical transport.

A forest fire releases two kind of moisture: the fuel moisture (i.e. the water already contained in the fuel) and the so-called combustion moisture which is chemically produced by the combustion process. Fire-released moisture can potentially be an important driver for the vertical plume development. In their study, Luderer et al. (2009) accounted for both fire moisture terms. Using theoretical considerations and numerical simulations, the authors concluded that the fire sensible heat flux plays a much stronger role than the fire-released moisture flux. Clements et al. (2006) and Potter (2005) stated that large fires can release as much as 1-3 g kg^{-1} in the atmosphere which correspond to an increase of 20-30 % of the background moisture. Their respective works were criticized by Luderer et al. (2009) who pointed out that the experiment conducted by Clements et al. (2006) could not allow to discriminate fire-released moisture from other sources and that the perturbation ratio used in Potter (2005) to account for fire-moisture effect exaggerates the role of latent heat. In the present study, only the fuel moisture is considered. Simulated turbulent vertical kinematic latent heat flux, $w'r_v'$, does not show a prominent fire signature. Simulated values are in the range of or below natural fluxes (~ 120 W m^{-2}) and the moisture increase above the fire is of the order of 0.3 g kg^{-1} only. The simulated increase is clearly below the values reported by Clements et al. (2006) and correspond to 3 % of the background moisture.

4.1.2. Fire injection height

Figure 8a shows the fire aerosol-like tracer concentration (in μg m^{-3}) as simulated at 12:00 UTC along the center-line of the fire plume. Fire aerosol-like particles are released only above the burning area (empty dot). Since they do not react chemically with any other atmospheric gases, once they have been emitted,

they are only subject to atmospheric processes such as turbulent mixing, advection, dispersion and dry deposition (Sec. 2.1). At a distance of nearly 31 km from the ignition point, the fire aerosol-like tracer already reduced to one-sixth of its maximal concentration, decreasing from 240 to 40 μg m^{-3} near the surface. This downwind area is also characterized by the subsidence zone (see also Fig. 7) which maintains the aerosol plume in contact with the surface. Moreover, the fire-aerosol like tracer plume is tilted seaward above the ignition area due to the strong northwesterly winds prevailing the day of the fire. From Figure 8, it can be inferred that the smoke plume spreads over a distance of more than 50 km downwind of the ignition area.

The fire injection height over the burning area is defined as the maximum altitude before which the fire aerosol-like tracer concentration falls below 1 μg m^{-3}. The burning area evolves in time and space within the perimeter shown in Figure 1b. Over this area, from 08:00 to 16:00 UTC, the injection height has been selected by seeking the maximal altitude where the fire aerosol-like tracer concentration reduces to 1 μg m^{-3}. Figure 8b illustrates the time evolution of the injection height which varies between 1.2 and 0.8 km with a maximum altitude of 1.12 km reached at 08:00 and 10:00 UTC. In the morning, from 08:00 to 12:00 UTC, while the burning area is rising (Fig. 3a), the injection height is above 1 km. In the afternoon, the injection height decreases below 1 km following the reduction of the fire burnt area and the consequent diminution of the sensible heat flux.

Figures 8a and b indicate that the Lançon smoke plume remains trapped in the boundary layer rather than being transported in the free troposphere. This behaviour follows the global trend of Mediterranean fires that mostly release emissions into the atmospheric boundary layer, between 1.5 and 5 km (Labonne and Chevallier, 2007; Langmann et al., 2007). In fact, the Lançon fire occurred in a particular meteorological situation characterized by strong horizontal winds and a dry boundary layer. These two conditions constitute strong limitations to the vertical extent of the fire plume, as already pointed out by Bursik (2001) studying volcanic plumes. The interaction between the plume and strong winds favours lateral entrainment of air, increasing horizontal momentum. Particularly for small fires, this phenomenon results in plume bending and may reduce the updraft because of loosing the additional buoyancy that could be gained from condensate water vapour (Freitas et al., 2010). Low values of environmental moisture may strengthen the loosing of buoyancy: strong winds enhance lateral entrainment of dry environmental air in the plume reducing the total condensate water vapour and generating lower positive buoyancy acceleration.

4.2. Atmospheric chemistry downwind of the fire

As already pointed out in the introduction, forest fires release large amounts of aerosols and different trace gases that are hazardous to human health (Miranda et al., 2005) and can influence the regional and global climate (Simmonds et al., 2005). When a wildfire breaks out, fire emissions dispersion depends highly on the height of injection of fire products.

Initial discussions on the synoptic meteorological situation before fire starting (Section 3) and previous analysis on the fire impact on atmospheric dynamics (Section 4.1.1) suggest that Lançon fire plume kept trapped in the PBL. In the following, the evolution of simulated gaseous pollutants downwind of the fire is investigated and discussed in the frame of the MODIS information of plume advection and ground-based measurements from the air quality survey network AtmoPACA.

4.2.1. Direction and horizontal extent of the pollution plume

The MODIS-AQUA instrument captured the Lançon fire plume on 1 July 2005 at 13:00 UTC (Fig. 9a). The MODIS image is compared to the concentration of a fire aerosol-like tracer simulated by MesoNH-ForeFire 40 m above the orography at 13:00 UTC (Fig. 9b). In terms of trajectory the comparison is quite good, with the model reproducing fairly well the overall direction of the fire plume and the narrow structure caused by strong winds blowing over south-eastern France. The simulated plume is narrower and straighter over the continent, then it widens over the Mediterranean Sea. Compared to the real fire plume, the simulated plume is slightly rotated towards the east, differences which appear to be due to the tilted wind field simulated by MesoNH (Fig. 4d).

In the simulation, the rotation of the wind direction seems to happen around 10:00 UTC when the simulated fire plume, that is crossing Marseille before 10 UTC, slightly rotates towards the east. Looking at the air quality measurements in Marseille, a first peak in PM_{10} concentration is observed at 08:00 UTC. MesoNH-ForeFire succeeds in simulating a peak of the fire aerosol-like concentration at the same hour (not shown), then the fire aerosol-like concentrations reduce to zero after 10:00 UTC because of the change in the wind direction. For this reason, the fire impact on the atmospheric chemistry downwind of the fire is discussed in the following over the point indicated on Figure 4d by a white star.

In Figure 9b, near the ignition point a relative increment of about 500 μg m^{-3} is simulated, over the burning area the fire aerosol-like concentration is well above levels of 250 μg m^{-3}. The fire aerosol-like tracer is efficiently transported south-east by strong winds and spreads over more than 100 km after 5 hours and a half since the start of the Lançon-de-Provence fire. At 13:00 UTC the fire aerosol-like concentration

in the proximity of La Ciotat is about 15 μg m^{-3}: a significant reduction over a distance of nearly 40 km that corresponds to a gradient of 11 μg m^{-3} m^{-1} between the ignition point and the considered location

4.2.2. Ozone depletion in the fire plume

To better investigate the evolution of the gaseous pollutants simulated by the MesoNH-ForeFire model, vertical cross sections for different pollutants have been traced along the center-line of the plume. Figure 10 presents the vertical distribution of the fire aerosol-like tracer, O_3, CO and NO_x. Pollutants emitted during the combustion process (CO, NO_x and COV - not shown) show a dramatic rise of concentration in the fire plume compared to background concentrations. In the model, this increase lead to the depletion of ozone with a drop of O_3 concentrations over and downwind of the burning area. The subsequent turbulent mixing of the fire plume with the environmental air, while the plume is advected southeastward, leads to a rapid decrease of ozone precursors concentrations near the surface. Despite of this decrease, the chemical signature of the fire is still simulated more than 20 km downwind of the ignition area. It is worth noting that, southeast of the ignition area (between the empty dot and the black dot in Figure 10) the pollutants reach an altitude of 1.5 km, which is higher than the injection height estimated in Section 4.1.2 above the ignition zone. The polluted plume however remains in contact with the surface.

Figure 10c shows very high mixing ratios of CO (> 3000 ppbv) above the ignition point, which then decrease downwind of the burning area because of mixing of the plume with background air. Inside the plume, 20 km south-east of the fire, CO levels drop back to $\sim 100-200$ ppbv, which are typical background concentration at these latitudes (Fisher et al., 2006). Simulated levels of CO and NO_x close to the source are in the range of observed concentrations during prescribed fires and natural fires. Miranda et al. (2005) observed hourly mean NO_2 of around 100 ppbv at ground level, 200 m from the source, during the Gestosa-2002 experiment in Portugal. During the same experiment, CO mixing ratios higher than 10000 ppbv were also observed. Based on aircraft observations of a biomass burning plume over Namibia, Jost et al. (2003) observed average CO concentrations in the plume of 1703 ppbv (above fire) and 598 ppbv (4 km downwind of the fire). Above the ignition zone (empty dot), CO concentrations decrease from 1000 ppbv to 600 ppbv over a distance of nearly 5 km.

In contrast to the other species, the O_3 mixing ratio is lower than background values near the fire (less than 30 pbbv). Ozone mixing ratios increase with altitude and downwind of the fire. Figure 11 illustrates the perturbations by the fire of NO_x and O_3 mixing ratios. Perturbation is defined as the difference between outputs from a “fire” and a “no-fire” simulation at 12:00 UTC. The perturbation is depicted on a horizontal

plan at an altitude of 40 m above orography. Directly over the burning area, the strong emission of NO_x increases its mixing ratios by 80 ppbv, at the maximum, when compared to background values. Such high NO_x environment limits the formation of peroxy radicals (not shown) which are crucial for O_3 formation. In the current study, low mixing ratios for HO_x were indeed simulated (less than 1 pptv). Another important process to account for is the fast reaction of O_3 with NO which results in a titration of O_3, due to high NO_x levels. Trentmann et al. (2003) and Mason et al. (2001, 2006) demonstrated that during the first hours O_3 production in a biomass burning plume is VOC-sensitive or NO_x-saturated. Close to the fire, simulated VOCs mixing ratios were about 120 ppbv, decreasing with altitude and the distance to the fire (not shown). Despite of these high values and because the chemical regime was dominated by the high NOx content, the photochemical activity remained low. As the plume ages, NO_x mixing ratios decrease due to atmospheric dilution (Poppe et al., 1998) and chemical reactions of OH with NO_2. This leads to an increase of O_3 production (Lin et al., 1988). This O_3 formation is simulated in the model several kilometres downwind of the burning zone, out of the coast, where NO_x mixing ratios fall in the range of several ppbv.

Figure 12 show the difference in O_3 and PM_{10} concentrations as measured by the AtmoPACA air quality monitoring stations Marseille Timone (Fig. 12a) and Marseille Saint Louis (Fig. 12b), located 33 km and 25 km, respectively, downwind of the ignition region. The difference is computed between 1 July and 30 June 2005 (“Fire - Before”) and between 1 July and 2 July 2005 (“Fire - After”). The second row (Fig. 12b and d) refers to the MesoNH-ForeFire simulations. They show perturbations by the fire on O_3 mixing ratios (ppbv) and on the fire aerosol-like concentrations (μg m^{-3}) that are calculated as the difference between a “fire” minus a “no-fire” simulation (“Fire - NO Fire”) for a point located in the fire plume, 31 km from the ignition zone. The qualitative comparison between measured and observed differences is limited by the design of the model exercise. In particular, there is no anthropogenic emissions in the current model version. Hence, NO from traffic emissions does not contribute to O_3 titration. Furthermore, the model does not account for the impact of fire aerosols on the photolysis rates (Trentmann et al., 2003; Phuleria et al., 2005). Nevertheless, a qualitative discussion is still interesting. From Figure 12, it can be stated that both model and observations show a strong decrease in ozone concentration from 09:00 UTC to 11:00-12:00 UTC (resp. increase in PM_{10} and fire aerosol-tracer concentrations). Minimum values of ozone (resp. maximum values of PM_{10} and fire-aerosol like tracer concentrations) are simulated between 12:00 UTC and 14:00 UTC with a good comparison with the observed behaviour of PM_{10} concentrations. Observed ozone concentrations during this time slot exhibits two different behaviour either with an earlier increase than simulated or a continuous decrease of ozone. After 14:00 UTC, observed PM_{10} and simulated fire-aerosol like tracer concentrations

decrease. Simulated ozone increases similarly to the difference between the day before and the day of the fire. Through the time evolution of ozone and aerosols, this qualitative comparison illustrates the correct timing of the fire plume propagation in the model and a similar signature of the fire impact on the atmospheric chemistry in the model and the observations.

5. Conclusions

In the present study the impact of a forest fire on the atmospheric dynamics and chemistry during a Mediterranean fire near Lançon-de-Provence, southeast of France, was investigated utilizing an off-line coupling between an atmospheric meso-scale model (MesoNH) and a fire spread model (ForeFire).

The burnt areas simulated by ForeFire at high temporal and spatial resolutions were used to calculate the latent and sensible heat fluxes and chemical emissions in the host meteorological and chemical model. The coupled atmosphere-wildfire model showed that the sensible heat released by the fire played a more important role in vertical plume development than the fire-released moisture, supporting the hypothesis of Luderer et al. (2009). The smoke plume was highly turbulent with turbulent kinetic energy values as high as 7 m^2 s^{-2}. The turbulent plume extended up to an altitude of $\sim$ 1 km and several tens of kilometres downwind of the fire ignition. Observations from the MODIS-AQUA instrument captured the horizontal extension of the fire plume out of the coast which was well reproduced by the coupled model. The simulated smoke plume was trapped within the boundary layer, a common feature of Mediterranean fires that mostly release emissions into the atmospheric boundary layer (Langmann et al., 2007; Labonne and Chevallier, 2007). The analysis of meteorological conditions before the fire showed strong horizontal winds and a dry atmosphere: two factors that can efficiently limit the altitude to which a plume may rise (Bursik, 2001; Freitas et al., 2010).

The comparison of the fire pollutants simulated by MesoNH-ForeFire and the ground-based measurements of air quality provided by the AtmoPACA network shows that the model reproduced well the advection of the smoke plume within the boundary layer and the right timing of the spread of the Lançon fire haze downwind of the burning area. Air quality ground-based observations supported the evidence that the narrow smoke plume stayed in contact with the surface while advected southeastward. The monitoring stations located along the trajectory of Lançon fire plume measured a dramatic increase of PM_{10} levels on the day of the fire. At Marseille, recorded PM_{10} levels exceeded daily values normally measured in similar metropolitan areas. The same network recorded a highly reduced diurnal cycle for O_3. These peculiar signatures could not be explained by changes in meteorological conditions (strong northwesterly winds, no clouds and

high temperatures remained during several days) or in traffic emissions. Therefore, the Lançon fire seems to be the most probable cause of the unusual behaviour in the measured O_3 and PM_{10} concentrations in Marseille. The coupled model with simplified hypothesis on emissions and initialization simulated an sharp increase of O_3 precursors and a consequent O_3 depletion in the fire plume and a strong increase of a fire aerosol-like tracer at the right timing compared to the observations. Production of O_3 was simulated several kilometres downwind of the fire as already observed in field campaigns (Sanhueza et al., 1999; Jost et al., 2003; Yokelson et al., 2003) and other modelling studies (Lin et al., 1988; Trentmann et al., 2003).

The qualitative comparison between measured and observed values is limited by the current design of the model exercise. In particular, a complete aerosol model and the interaction between the photolysis rates and the smoke plume are not accounted in the present study. Anthropogenic emissions are not considered either. These missing processes could explain part of the bias between the modelled and observed pollutants levels at the surface. Future works on fire emissions of chemical components need to be performed with a focus on the Mediterranean vegetation, including a better characterisation of emissions factors and burning efficiency in this region.

Acknowledgements

This work has been partially supported by the French National Agency (ANR) in the frame of its COSI-NUS program (IDEA, ANR-09-COSI-006). The work was also funded by the french LEFE-INSU program. This work was performed using HPC resources from GENCI-IDRIS (Grant 2010-2011 [rhau]).

Gases	**Mixing Ratio** (ppbv)
Carbon monoxide (CO)	75.0
Nitrogen oxide (NO)	2.5
Ethane (ETH)	
Formaldehyde (HCHO)	0.0012
Ketone (KET)	
Hydroxyl radical (OH)	0.0001
Hydroperoxyl radical (HO_2)	0.01
Methane (CH_4)	1400.0
Hydrogen peroxide (H_2O_2)	0.004

Table 1: Multiplication factors necessary for drawing initial vertical profiles of listed chemical species. These factors are multiplied by the vertical profile seen in Figure 2c.

References	**Gases**	**Emission Factors** (EF_{CO}, g kg^{-1})
Miranda et al. (2008)	Carbon monoxide (CO)	82.0
References	**Gases**	**Emission Ratios** (ER_i/ER_{CO}, %)
Miranda et al. (2008)	Nitrogen monoxide (NO)	8.8
	Nitrogen dioxide (NO_2)	5.2
	Fire aerosol-like tracer	3.4
Andreae and Merlet (2001)	Acetaldehyde (CH_3CHO)	3.4
	Aromatic (Toluene, Xylenes, Phenol)	0.07
	Isoprene	0.05
Trentmann et al. (2003)	Formaldehyde (HCHO)	2.0
	Ethane (C_2H_6)	0.7
	Alkane (HC_3, HC_5, HC_8, CH_3OH)	1.0
	Ethylene (C_2H_4)	1.2
	Propene (C_3H_6)	0.5
	Acetic acid (CH_3COOH)	2.0

Table 2: Emission information used for estimating fire emissions.

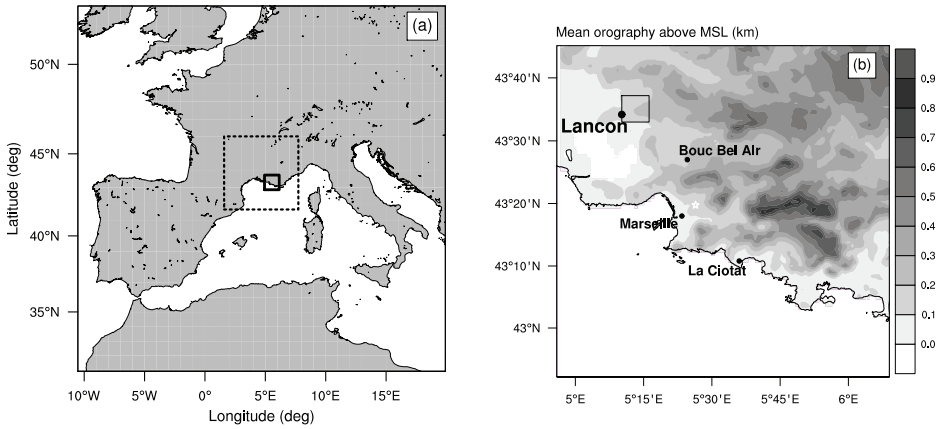

Figure 1: **(a)** Nested domains used in the 3-D MesoNH experiment from the coarse 25-km grid (outermost domain) down to the fine 1-km grid (solid line), passing through the 5-km mesh-grid (dashed line). **(b)** Mean orography (in km) of the 1-km grid-mesh domain used in the 3-D MesoNH model. Cities of Bouc Bel Air, La Ciotat, Lançon-de-Provence and Marseille are indicated. The white star marks the location that has been chosen to discuss fire impact on the atmospheric dynamics and chemistry. The solid line indicates the perimeter within which the burnt area information from ForeFire are localised.

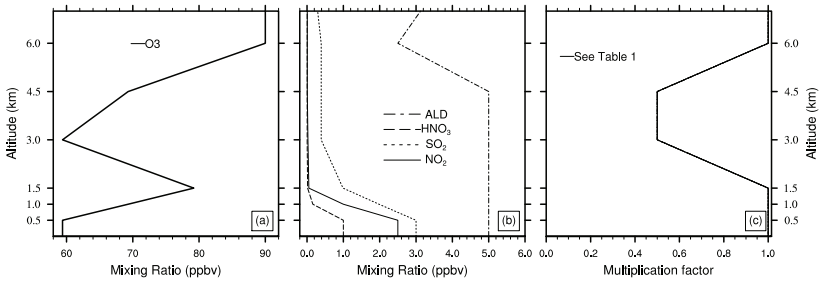

Figure 2: Initial chemical profiles used for the entire domain in the MesoNH simulations shown here as a mixing ratio (ppbv), except for the last graphic (c). Profiles are built utilising MOCAGE simulations from 21 June 2001, 00:00 UTC, at the location nearest to Lançon-de-Provence (MediasFrance, 2001). **(a)** Ozone(O_3); **(b)** aldehydes (ALD), nitric acid (HNO_3), sulfur dioxide (SO_2) and nitrogen dioxide (NO_2). **(c)** Carbon monoxide (CO), ethane (ETH), formaldehyde (HCHO), hydroxyl radical (OH), hydroperoxyl radical (HO_2), ketone (KET), methane (CH_4) and nitrogen monoxide (NO) have the same vertical profile that distinguishes from one another through the multiplication by the respective multiplication factors, reported in Table 1. Hydrogen peroxide (H_2O_2) has a constant vertical profile (not shown).

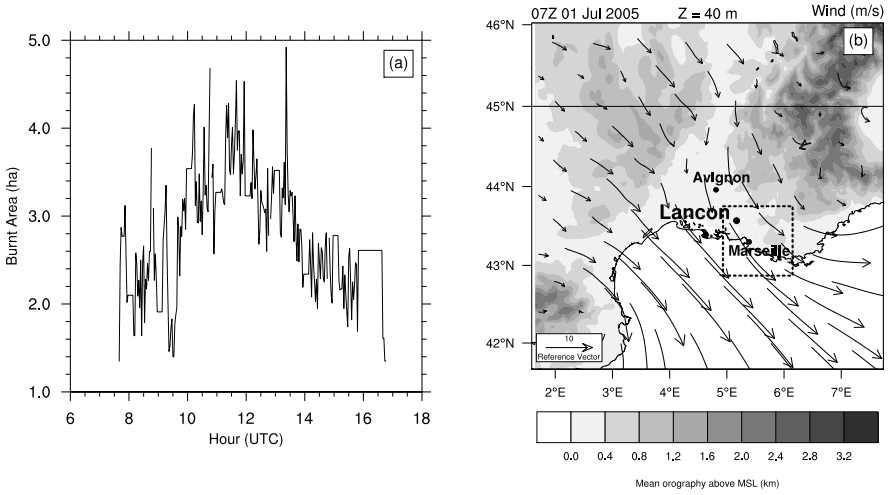

Figure 3: **(a)** Temporal evolution of the burning area (in ha) of the Lançon-de-Provence fire as simulated by ForeFire. The Lançon-de-Provence fire burned on 1 July 2005 from 07:40 to 16:40 UTC. **(b)** Horizontal wind pattern over southeast France at 40 m on 1 July 2005 at 07:00 UTC as simulated by 3-D MesoNH on the 5-km grid-mesh domain. The dashed line indicates boundaries of the finest nested grid (1-km resolution). Wind arrows are expressed in m/s. Mean orography is shown in km. Cities of Avignon, Lançon-de-Provence and Marseille are indicated.

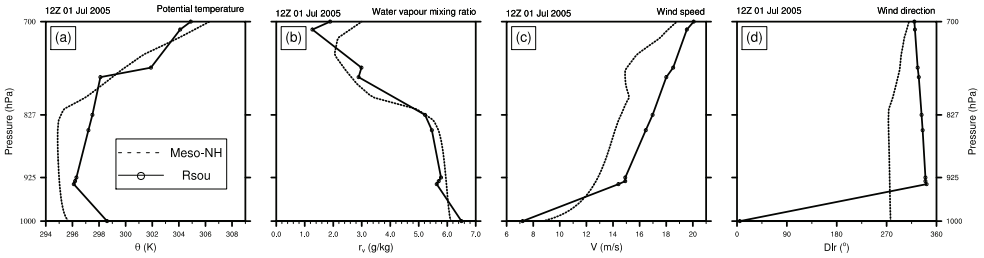

Figure 4: Comparison between the radiosonde data (solid line) and the MesoNH simulation (dashed line) in the first 3 km of the atmosphere. The radiosonde was launched over Nîmes (43.50 N, 4.35 E) at 12:00 UTC on 1 July 2005; radiosonde levels are marked by empty dots. MesoNH profiles are obtained at the same hour, over the location of Nîmes. The four graphics represent the vertical profile of: **(a)** potential temperature (θ, K), **(b)** water vapour mixing ratio (r_v, g/kg), **(c)** wind speed (V, m/s) and **(d)** wind direction (Dir, °).

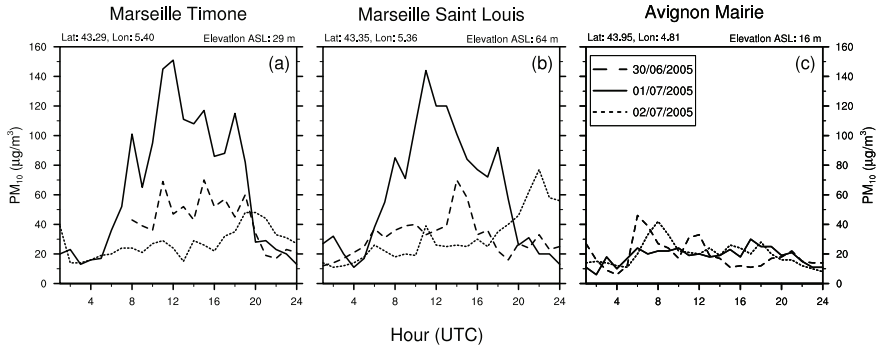

Figure 5: Daily patterns for PM_{10} hourly concentration (in μg m^{-3}) measured on 30 June, 1 July and 2 July 2005, by the AtmoPACA air quality survey network, available in southeastern France, at the air quality monitoring stations of: **(a)** Marseille Timone, **(b)** Marseille Saint Louis and **(c)** Avignon Mairie.

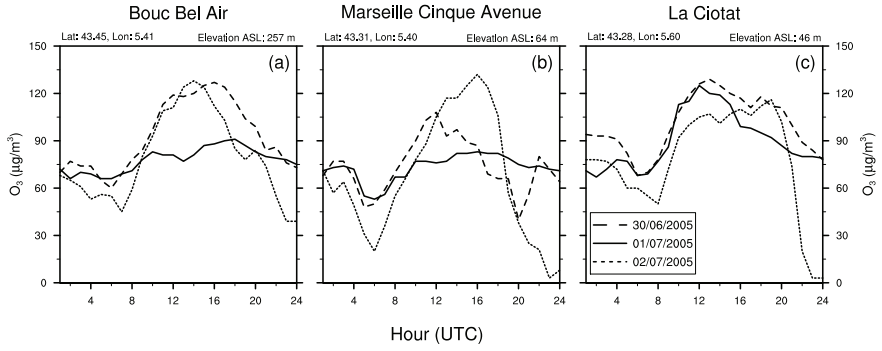

Figure 6: Daily patterns for ozone hourly concentration (μg m^{-3}) measured on 30 June, 1 July and 2 July 2005, by the AtmoPACA air quality survey network, available in southeastern France, at the air quality monitoring stations of: **(a)** Bouc Bel Air, **(b)** Marseille Cinque Avenues and **(c)** La Ciotat.

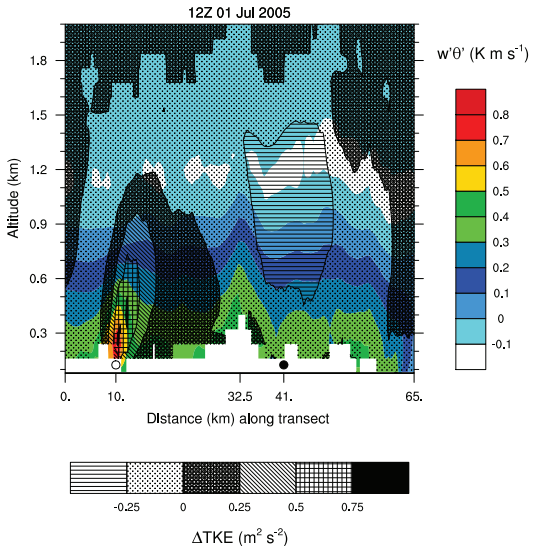

Figure 7: Vertical cross section of the Turbulent Kinetic Energy perturbation by the fire (TKE, in m^2/s^2, gray shaded scale) and turbulent vertical kinematic heat flux ($w'\theta'$, in K m/s, coloured scale) at 12:00 UTC on 1 July 2005, as simulated by the 3-D MesoNH-ForeFire model at a resolution of 1 km. Δ denotes here the difference between a "fire forced" minus a "no fire" simulation. The vertical cross section is taken along the simulated center-line of the fire plume. The black dot is located within the fire plume, 31 km downwind of the ignition area (equivalent to the Lançon-Marseille distance). The white area at the bottom is the orography.

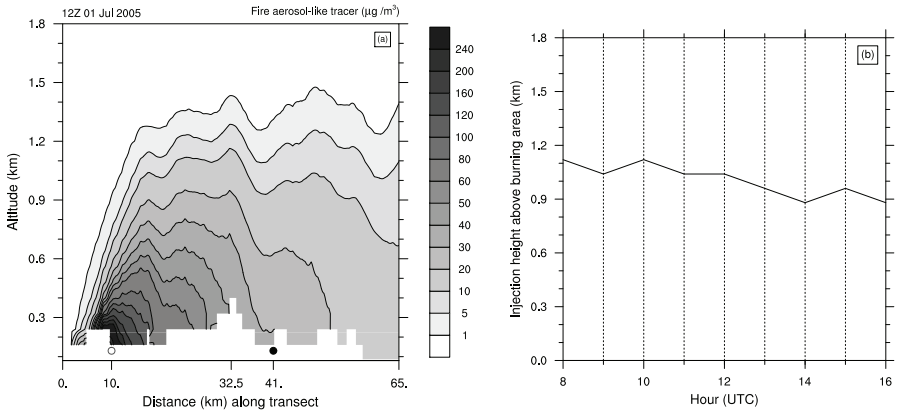

Figure 8: **(a)** Vertical cross section of the fire aerosol-like tracer concentration (in μg m^{-3}) as simulated at a resolution of 1 km by the 3-D MesoNH-ForeFire model on 1 July 2005 at 12:00 UTC. The vertical cross section is obtained along the center-line of the fire plume. The empty dot designates the area where fire emissions maximise. Since the city of Marseille is not placed along the transect, a point (black dot) located within the fire plume and at the same distance between the empty dot and Marseille (31 km) is used to analyze the fire aerosol-like tracer concentration in the vicinity of Marseille. At the bottom of the graphic, the white area represents the orography. **(b)** Temporal evolution of the injection height on 1 July 2005 from 08:00 to 16:00 UTC. The injection height is the maximal altitude where the fire aerosol-like tracer concentration reduces to 1 μg m^{-3} over a 8 km $\times$ 8 km area around the ignition zone, contoured by a solid line in Figure 1.

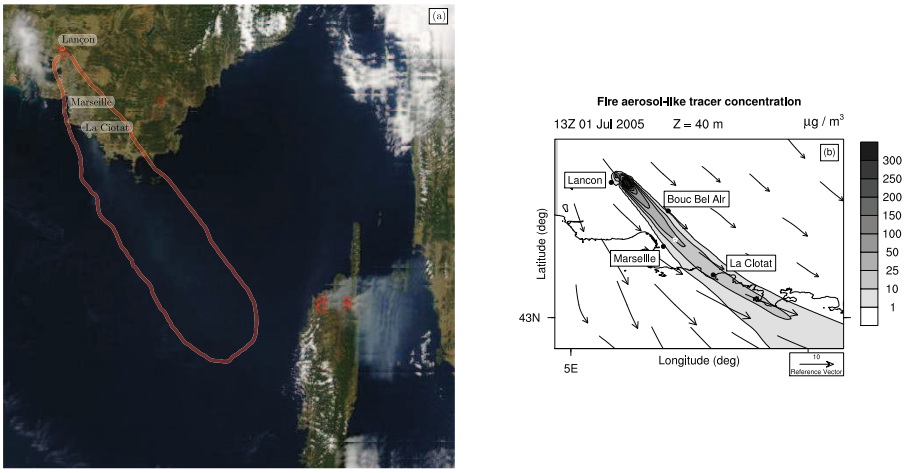

Figure 9: **(a)** MODIS-AQUA image on 1 July 2005, at 13:00 UTC. To help the reader, the Lançon fire plume, as visible to the naked eye on the satellite image, is contoured by a red line. Cities of La Ciotat and Marseille are indicated as also the hot spot concerning the Lançon fire. **(b)** Fire aerosol-like tracer concentration (in μg m^{-3}) as simulated by the 3-D MesoNH-ForeFire model on the finest grid (1-km) on 1 July 2005, 13:00 UTC, 40 m above orography. Some air quality monitoring stations of the AtmoPACA network are here indicated by black dots: Bouc Bel Air, Marseille and La Ciotat. The location of Lançon-de-Provence is also shown as a black dot. The white star within the fire plume is used for discussing fire impact on the atmospheric dynamics and chemistry.

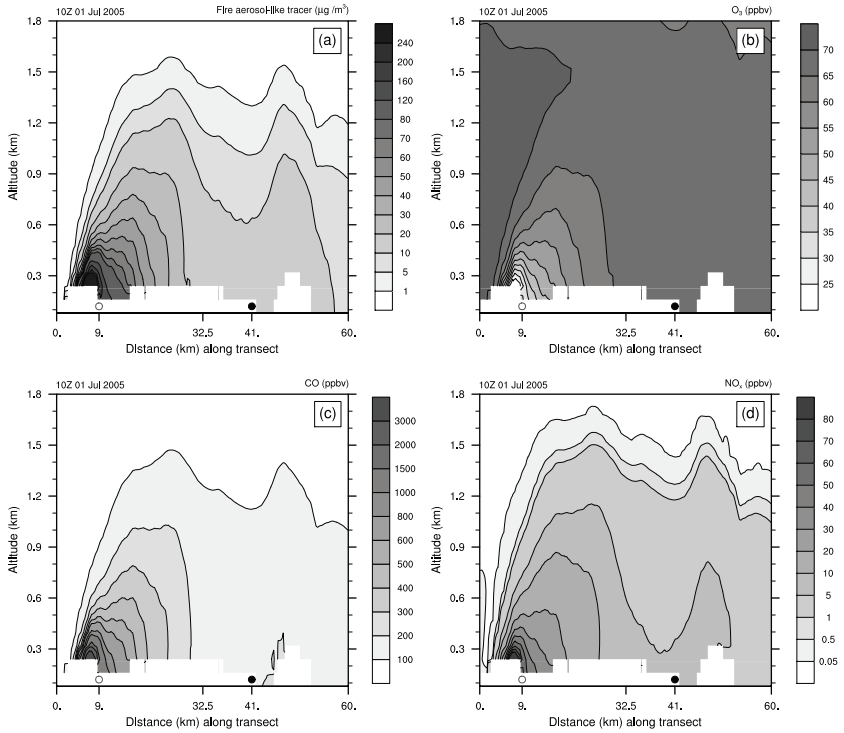

Figure 10: Vertical cross section of: **(a)** fire aerosol-like tracer concentration (in μg m^{-3}); **(b)** ozone mixing ratio (ppbv); **(c)** carbon monoxide mixing ratio (ppbv) and **(d)** nitrogen oxides mixing ratio (ppbv) as simulated at a resolution of 1 km by the MesoNH-ForeFire model on 1 July 2005, 10:00 UTC. The vertical cross section is obtained along the simulated center-line of the fire plume. The empty dot designates the area where the fire aerosol-like tracer emission maximises. See legend Figure 7.

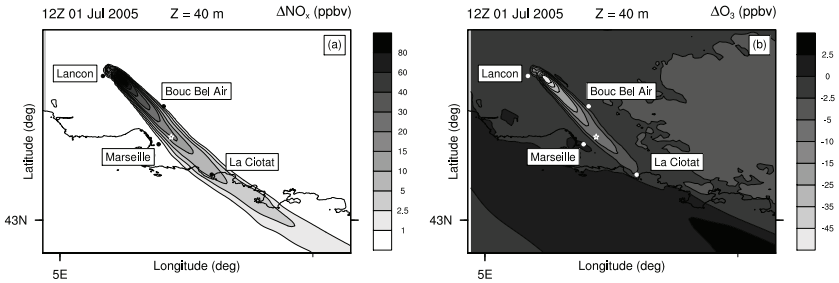

Figure 11: Mixing ratio contour maps, in ppbv, of **(a)** nitrogen oxides and **(b)** ozone at 40 m above orography on 1 July 2005, at 12:00 UTC. Δ denotes here the difference between a "fire forced" minus a "no fire" simulation. Some air quality monitoring stations of the AtmoPACA network are shown: Bouc Bel Air, La Ciotat and Marseille. The location of Lançon-de-Provence is also shown.

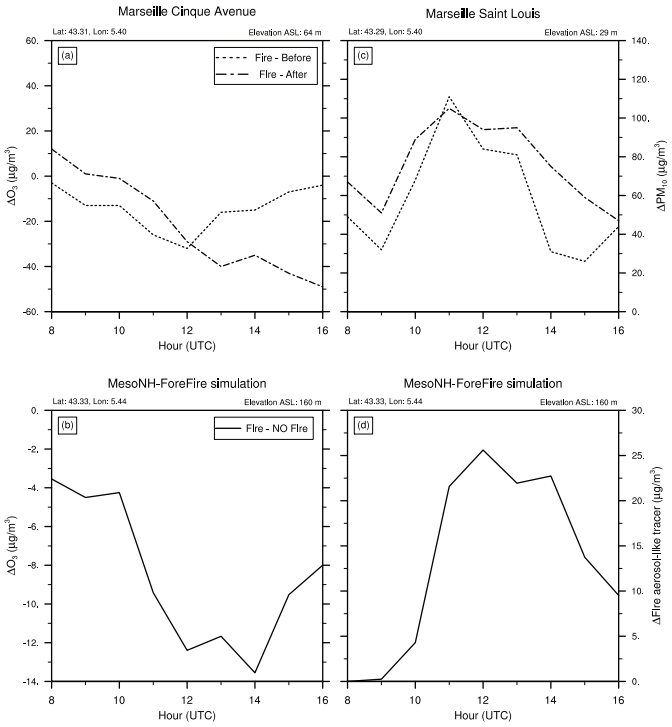

Figure 12: The first two graphics show differences in ozone (on the right) and PM_{10} (on the left) hourly concentrations (μg m^{-3}) in Marseille between 1 July and 30 June 2005 (Fire - Before) and between 1 July and 2 July 2005 (Fire - After). Data were recorded by the following air quality monitoring stations of the AtmoPACA network: **(a)** Marseille Timone and **(c)** Marseille Saint Louis. The last two graphics, **(b)** and **(d)**, show the difference between a "fire forced" minus a "no fire" simulation for the MesoNH-ForeFire model as obtained over a location placed within the fire plume (43.33 N, 5.44 E) for ozone and the fire aerosol-like tracer concentrations (in μg m^{-3}).

References

Andreae, M. O., Merlet, P., 2001. Emission of trace gases and aerosols from biomass burning. Global Biogeochemical Cycles 15, 955–966.

Balbi, J. H., Morandini, F., Silvani, X., Filippi, J. B., Rinieri, F., 2009. A physical model for wildland fires. Combust. Flame 156, 2217–2230.

Balbi, J. H., Rossi, J. L., Marcelli, T., Santoni, P. A., 2007. A 3D physical real time model of surface fires across fuel beds. Combust. Sci. Technol. 179, 2511–2537.

Barboni, T., Cannac, M., Pasqualini, V., Simeoni, A., Leoni, E., Chiaramonti, N., 2010. Volatile and semi-volatile organic compounds in smoke exposure of firefighters during prescribed burning in the Mediterranean region. Int. J. of Wildland Fire 19, 606–612.

Bechtold, P., Bazile, E., Guichard, F., Mascart, P., Richard, E., 2001. A mass flux convection scheme for regional and global models. Quart. J. Roy. Meteor. Soc. 127, 869–886.

Bougeault, P., Lacarrère, P., 1989. Parameterization of orography-induced turbulence in a meso-beta-scale model. Mon. Rea. Rev. 117, 1872–1890.

Bursik, M., 2001. Effect of wind on the rise height of volcanic plumes. Geophys. Res. Lett. 28 (18).

Bytnerowicz, A., Cayan, D., Riggan, P., Schilling, S., Dawson, P., Tyree, M., Wolden, L., Tissell, R., Preisler, H., 2010. Analysis of the effects of combustion emissions and Santa Ana winds on ambient ozone during the October 2007 southern California wildfires. Atm. Env. 44 (5), 678–687.

Chatfield, R., Delany, A., 1990. Convection Links Biomass Burning to Increased Tropical Ozone: However, Models Will Tend to Overpredict O_3. J. Geophys. Res. 95 (D11).

Clark, T. L., Coen, J., Latham, D., 2004. Description of a coupled atmosphere-fire model. Int. J. Wildland Fire 13, 49–63.

Clements, C. B., Potter, B. E., Zhong, S., 2006. In situ measurements of water vapor, heat, and CO_2 fluxes within a prescribed grass fire. Int. J. Wildland Fire 15 (299-306), 1369–1382.

Clements, C. B., Zhong, S., Goodrick, S., Li, J., Potter, B. E., Bian, X., Heilman, W. E., Charney, J. J., Perna, R., Jang, M., Lee, D., Patel, M., Street, S., Aumann, G., 2007. Observing the Dynamics of Wildland Grass Fires: FireFlux - A Field Validation Experiment. Bull. Amer. Meteor. Soc. 88 (9), 1369–1382.

Colella, P., Woodward, P. R., 1984. The piecewise parabolic method (PPM) for gas-dynamical simulations. J. Comput. Phys. 54, 174–201.

Crassier, V., Suhre, K., Tulet, P., Rosset, R., 2000. Development of a reduced chemical scheme for use in mesoscale meteorological models. Atmos. Env. 34, 2633–2644.

Cros, B., Durand, P., Frejafon, E., Kottmeier, C., Perros, P. E., Peuch, V.-H., Ponche, J., Robin, D., Said, F., Toupance, G., Wortham, H., 2004. The ESCOMPTE program: an overview. Atm. Res. 69, 241–279.

Dufour, A., Amodei, M., Ancellet, G., Peuch, V.-H., 2005. Observed and modelled "chemical weather" during ESCOMPTE. Atm. Res. 74 (1-4), 161–189.

EFFIS, 2008. Forest Fires in Europe 2008 report.

Erisman, J. W., Baldocchi, D., 1994. Modelling dry deposition of SO_2. Tellus B 46, 159–171.

Filippi, J. B., Bosseur, F., Mari, C., Lac, C., Lemoigne, P., Cuenot, B., Veynante, D., Cariolle, D., Balbi, J. H., 2009. Coupled atmosphere-wildland fire modelling. J. Advances in Modeling Earth Systems 1 (11).

Fisher, H., Lawrence, M., Gurk, C., Hoor, P., Lelieveld, J., Hegglin, M. I., Brunner, D., Schiller, C., 2006. Model simulations and aircraft measurements of vertical, seasonal and latitudinal O_3 and CO distributions over Europe. Atm. Chem. Phys. 6, 339–348.

Freitas, S. R., Longo, K. M., Chatfield, R., Latham, D., Dias, M. A. F. S., Andreae, M. O., Prins, E., Santos, J. C., Gielow, R., Jr., J. A. C., 2006. Including the sub-grid scale plume rise of vegetation fires in low resolution atmospheric transport models. Geophys. Res. Letters 7.

Freitas, S. R., Longo, K. M., Chatfield, R., Latham, D., Dias, M. A. F. S., Andreae, M. O., Prins, E., Santos, J. C., Gielow, R., Jr., J. A. C., 2007. Including the sub-grid scale plume rise of vegetation fires in low resolution atmospheric transport models. Atm. Chem. Phys. 7, 3385–3398.

Freitas, S. R., Longo, K. M., Trentmann, J., Latham, D., 2010. Technical note: Sensitivity of 1-d smoke plume rise models to the inclusion of environmental wind drag. Atm. Chem. Phys. 10 (2), 585–594.

Guan, H., Esswein, R., Lopez, J., Bergstrom, R., Warnock, A., Follette-Cook, M., Fromm, M., Iraci, L. T., 2010. A multi-decadal history of biomass burning plume heights identified using aerosol index measurements. Atmospheric Chemistry and Physics 10 (14), 6461–6469.
URL http://www.atmos-chem-phys.net/10/6461/2010/

Hobbs, P. V., Sinha, P., Yokelson, R. J., Christian, T. J., Blake, D. R., Gao, S., Kirchstetter, T. W., Novakov, T., Pilewskie, P., 2003. Evolution of gases and particles from a savanna fire in South Africa. J. Geophys. Res. 108, 8485.

Hodzic, A., Madronich, S., Bohn, B., Massie, S., Menut, L., Wiedinmyer, C., 2007. Wildfire particulate matter in Europe during summer 2003: meso-scale modeling of smoke emissions, transport and radiative effects. Atm. Chem. Phys. 7, 4043–4064.

IPCC, 2007. Climate Change 2007: Impacts, Adaptation and Vulnerability. Contribution of Working Group II to the Fourth Assessment Report of the Intergovernmental Panel on Climate Change. Cambridge University Press, Cambridge, UK.

Jiang, Q., Doyle, J. D., Wang, S., Smith, R. B., 2007. On boundary layer separation in the lee of mesoscale topography. J. Atmos. Sci. 64 (2), 401–420.

Jost, C., Trentmann, J., Sprung, D., Andreae, M. O., McQuaid, J. B., Barjat, H., 2003. Trace gas chemistry in a young biomass burning plume over Namibia: Observations and model simulations. J. Geophys. Res. 108 (D13), 3676–3682.

Kahn, R. A., Chen, Y., Nelson, D. L., Leung, F.-Y., Li, Q., Diner, D. J., Logan, J. A., 2008. Wildfire smoke injection heights: Two perspectives from space. Geophys. Res. Lett. 35.

Labonne, M., Chevallier, F.-M. B. F., 2007. Injection height of biomass burning aerosols as seen from a spaceborne. Geophys. Res. Letters 34, 11806–11811.

Lafore, J. P., Stein, J., Ascencio, N., Bougeault, P., Ducrocq, V., Duron, J., Fisher, C., Hereil, P., Mascart, P., Pinty, J. P., Redelsperger, J. L., Richard, E., de Arellano, J. V.-G., 1998. The Meso-NH atmospheric simulation system. Part I: adiabatic formulation and control simulations. Ann. Geophys. 16, 90–109.

Langmann, B., Duncan, B., Textor, C., Trentmann, J., van der Werf, G. R., 2007. Vegetation fire emissions and their impact on air pollution and climate. Atm. Env. 43, 107–116.

Lin, X., Trainer, M., Liu, S., 1988. On the Nonlinearity of the Tropospheric Ozone Production. J. Geophys. Res. 193, 15879–15888.

Linn, R., Reisner, J., Colman, J. J., Winterkamp, J., 2002. Studying wildfire behavior using firetec. Int. J. Wildland Fire 11, 233–246.

Lobert, L. M., Warnatz, J., 1993. Fire in the Environment:The Ecological, Atmospheric, and Climatic Importance of Vegetation Fires. John Wiley & Sons, Inc., Berlin, Ch. 2, pp. 15–37.

Luderer, G., Trentmann, J., Andreae, M. O., 2009. A new look at the role of fire-released moisture on the dynamics of atmospheric pyro-convection. Int. J. Wildland Fire 18, 554–562.

Luderer, G., Trentmann, J., Winterrath, T., Textor, C., Herzog, M., Graf, H. F., Andreae, M. O., 2006. Modeling of biomass smoke injection into the lower stratosphere by a large forest fire (Part II): sensitivity studies. Atm. Chem. Phys. 6 (12), 5261–5277.

Madronich, S., 1987. Photodissociation in the Atmosphere 1. Actinic Flux and the Effects of Ground Reflections and Clouds. J. Geophys. Res. 92, 9740–9752.

Martin, M. V., Logan, J. A., Kahn, R. A., Leung, F.-Y., Nelson, D. L., Diner, D. J., 2010. Smoke injection heights from fires in north america: analysis of 5 years of satellite observations. Atm. Chem. Phys. 10 (4), 1491–1510.

Mason, S., Trentmann, J., Winterrath, T., Yokelson, R., Christian, T., Carlson, L., Warner, T., Wolfe, L., Andreae, M., 2006. Intercomparison of two box models of the chemical evolution in biomass-burning smoke plumes. J. Atm. Chem. 55, 273–297.

Mason, S. A., Field, R. J., Yokelson, R. J., Kochivar, M. A., Tinsley, M. R., Ward, D. E., Hao, W. M., 2001. Complex effects arising in smoke plume simulations due to inclusion of direct emissions of oxygenated organic species from biomass combustion. J. Geophys. Res. 106, 12527–12539.

Masson, V., Champeaux, J. L., Chauvin, F., Meriguet, C., Lacaze, R., 2003. A Global Database of Land Surface Parameters at 1-km Resolution in Meteorological and Climate Models. J. Climate 16 (9), 1261–1282.

MediasFrance, 2001. ESCOMPTE EXERCISE Homepage. `http://escompte.mediasfrance.org/exercice/HTML/exe.html`.

Miranda, A. I., 2004. An integrated numerical system to estimate air quality effects of forest fires. Int. J. of Wildland Fire 13, 217–226.

Miranda, A. I., Ferreira, J., Valente, J., Santos, P., Amorim, J. H., Borrego, C., 2005. Smoke measurements during Gestosa-2002 experimental field fires. Int. J. of Wildland Fire 14, 107–116.

Miranda, A. I., Monteiro, A., Martins, V., Carvalho, A., Schaap, M., Builtjes, P., Borrego, C., 2008. Forest Fire Impact on Air Quality over Portugal. In: Borrego, C., Miranda, A. I. (Eds.), Air Pollution Modeling and Its Application XIX. NATO Science for Peace and Security Series C: Environmental Security. Springer Netherlands, pp. 190–198.

Mlawer, E. J., Taubman, S. J., Brown, P. D., Iacono, M. J., Clough, S. A., 1997. Radiative transfer for inhomogeneous atmospheres: RRTM, a validated correlated-K model for the longwave. J. Geophys. Res. 102, 16663–16682.

Moriondo, M., Good, P., Durao, R., Bindi, M., Giannakopoulos, C., Corte-Real, J., 2006. Potential impact of climate change on fire risk in the Mediterranean area. Clim. Res. 31 (1), 85–95.

Noilhan, J., Planton, S., 1989. A simple parameterization of land surface processes for meteorological models. Mon. Wea. Rev. 117, 536–549.

Oberhuber, J. M., Herzog, M., Graf, H.-F., Schwanke, K., 1998. Volcanic plume simulation on large scales. J. Volcanol. Geoth. Res. 87 (1-4), 29–53.

Pausas, J. G., 2004. Changes in fire and climate in the eastern Iberian peninsula (Mediterranean basin). Climatic Change 63, 337–350.

Phuleria, H. C., Fine, P. M., Zhu, Y., Sioutas, C., 2005. Air quality impacts of the October 2003 Southern California wildfires. J. Geophys. Res. 110 (D7), 148–227.

Pinty, J. P., Jabouille, P., 1999. A mixed-phase cloud parameterization for use in mesoscale non-hydrostatic model: simulations of a squall line and of orographic precipitations. In: Proc. Conf. of Cloud Physics. Amer. Met. Soc., Everett, WA, USA, pp. 217–220.

Poppe, D., Koppmann, R., Rudolph, J., 1998. Ozone formation in biomass burning plumes: Influence of atmospheric dilution. Geophys. Res. Lett. 25, 3823–3826.

Potter, B. E., 2005. The role of released moisture in the atmospheric dynamics associated with wildland fires. Int. J. Wildland Fire 14, 77–84.

Pyne, S. J., Andrews, P. L., Laven, R. D., 1949. Introduction to wildland fire. John Wiley & Sons, Inc.

Rio, C., Hourdin, F., Chédin, A., 2010. Numerical simulation of tropospheric injection of biomass burning products by pyro-thermal plumes. Atm. Chem. Phys. 10 (8), 3463–3478.

Chapter 5

Modelling smoke injection height: an intercomparison study

Contents

In the previous chapter, the simulated fire injection height played a fundamental role in the scale of dispersion of fire products of the Lançon-de-Provence 2005 fire. The height at which fire pollutants are released depends on the dynamics and the thermodynamics of the fire, as well as on the interaction atmosphere/fire. Hence, the fire injection height can be seen as the key parameter that links the dynamics and the chemistry of a fire.

In this chapter, we present a model inter-comparison exercise focused on the determination of the fire injection height. Firstly, we give an overview about the fire injection height: its importance and its estimation (Section 5.1). Thereafter, we introduce three case studies and their meteorological conditions (Section 5.2), and we describe the one-dimensional models and methodology that have been applied in the present study (Section 5.3). Afterwards, we discuss the simulation results (Section 5.4) and we conclude, giving also some perspectives (Section 5.5).

5.1 Introduction

The spatial scale at which fire emissions may impact the chemical composition of the atmosphere depends on their dispersion, a process that is highly influenced by the height of injection of fire products. The smoke plume injection height is defined as the altitude at which the smoke particles are injected into the atmosphere before transport (Kahn et al., 2008). If fire pollutants stay trapped in the the Planetary Boundary Layer (PBL), their residence time can be shortened by removal processes that act more efficiently in the first layer of the atmosphere (Chatfield and Delany, 1990; Stein et al., 2009). On the contrary, if fire emissions reach the free troposphere, they are transported by faster winds that can spread their effect on air quality from a local to a regional and occasionally global scale (Saarikoski et al., 2007; Sofiev et al., 2008; Turquety et al., 2009; Dirksen et al., 2009).

The final height of injection of a smoke plume is a complex parameter to determine. It depends on both the stability of the atmosphere and on fire characteristics that, in turn, lead to atmospheric feedback. Wildfires are intense sources of heat that is released in the atmosphere in the form of hot gases and water vapour. The contribution to sensible heat flux from wildland fires can not be neglected: on-field campaigns measured values of sensible heat flux that are nearly 3 orders of magnitude higher than natural fluxes (e.g. Clements et al., 2007; Silvani and Morandini, 2009; Chap. 2). Under favourable meteorological conditions, fire-induced sensible heat flux has even the potential to enhance deep convection (so-called pyro-convection), leading to direct injection of smoke into the upper troposphere and lower stratosphere, as observed by Fromm et al. (2005) and Damoah et al. (2006). Also the plume-environment interaction plays an important role in the convection process. The hot fire plume interacts with the cooler surrounding air: this phenomenon can trigger turbulent eddies. Hence, fire-induced turbulence can efficiently mix environmental colder air into the fire plume, cooling the hot plume and reducing its upward movement (Freitas et al., 2006). Smoke plumes are also masses of humid air

with an increase of water vapour mixing ratio of nearly 30% over the ambient air within the plume (Clements et al., 2006) due to fuel and "combustion" moisture (Parmar et al., 2008). If the rising haze plume reaches the Lifting Condensation Level (LCL), additional buoyancy may be gained from latent heat of condensation of the water vapour (Freitas et al., 2007), as already investigated for volcanic plume rise (Graf et al., 1999). Studies on volcanic activities also showed the effect of strong horizontal winds on the final height of plumes (Bursik, 2001). The interaction between the plume and strong winds favours lateral entrainment of air, increasing the horizontal momentum. Particularly for small fires, this phenomenon results in plume bending and might reduce the updraft development because of loosing the additional buoyancy from condensate water vapour (Freitas et al., 2010).

When run at very high resolution, atmospheric models can resolve explicitly convective transport and turbulent motions. Instead, at larger resolution (e.g. meso-scale), several types of atmospheric movements are sub-grid processes, and they are incorporated into atmospheric models through appropriate parametrisation schemes. As explained before, wild-fires can induce direct and rapid transport into the atmosphere, this process may have considerable impacts on the dynamics and on pollutants distribution (Luderer et al., 2006; Tressol et al., 2008). Strong updrafts associated with fires are frequently ignored, or their impact is diluted, at the typical resolution of large-scale models. Using three chemistry transport models (CTM) driven by the same meteorology, Elguindi et al. (2010) performed sensitivity tests that underlined the role of low injection heights in the model's poor representation of the CO plumes.

Several studies were carried out using remote sensing data to investigate the height to which smoke plumes rise and the variability of this altitude due to fire characteristics. Labonne and Chevallier (2007) assessed the injection height of biomass burning plumes by analyzing the vertical distribution of aerosols, a good marker of fire emissions. They compared released data from the CALIPSO space-borne lidar and the mixing layer top diagnosed from the ECMWF; they concluded that biomass burning plumes were injected within the mixing layer. The same method was used by Amiridis et al. (2009); their results outlined that, under strong fire activity, the ECMWF diagnostic underestimates the BL height. Kahn et al. (2008) suggested to combine lidar observations with stereo imaging to support the modelling of smoke environmental impacts. Mazzoni et al. (2007) utilized stereo imaging from MISR and MODIS date to locate fires and their smoke plumes, and they retrieved the injection height generated by fire buoyancy over a 4-month period. This work was extended by Martin et al. (2010) that analyzed a 5-year record of MISR smoke plume injection heights over North America. Their analysis of plume heights indicated that 4-12% of plumes from fires are injected above the BL; moreover, the MISR plume climatology exhibited larger summertime heights that, once correlated with MODIS FRP measurements, seemed to be the result of higher fire intensity, likely due to most severe fire intensity during summer. Gonzi and Palmer (2010) used satellite observations of

CO, a tracer of incomplete combustion, in order to estimate the vertical transport of surface fire emissions. Considering boreal and tropical wild-fires, they found that only 10-25% of emissions are injected above the PBL. Guan et al. (2010) proposed a simple empirical method to identify biomass burning plume heights using the Aerosol Index (AI) measurements as determined by satellite instruments. The authors derived a best-fit relationship between AI and maximum plume height for young plumes that could help to validate the vertical placement of smoke plumes in CTM.

Different methods to parametrise plume lifting were developed and implemented in meso-scale models. Hodzic et al. (2007) applied the meso-scale CTM CHIMERE to investigate the effects of wild-fires on air quality in Europe during summer 2003. CHIMERE was improved to include the MODIS smoke emissions inventory and a new parametrisation to simulate the injection of smoke particles. The injection height was calculated as a function of atmospheric conditions and fire characteristics, retrieved from the MODIS inventory. The parametrisation allowed for the simulation of the smoke transport at the right altitude. However, it relied on the accuracy of satellite measurements. A 1-D entrainment Plume Rise Model (1-D PRM) was presented by Freitas et al. (2006, 2007). It could be embedded in a host 3-D meso-scale or global model to simulate explicitly the convective transport mechanism associated with wild-fires and determine the final height where fire products, emitted during the flaming phase, would be released. This plume rise algorithm was implemented and tested with the Coupled Aerosol and Tracer Transport model to the Brazilian developments on the Regional Atmospheric Modeling System Freitas et al. (CATT-BRAMS, 2009) and with the WRF model with Chemistry (WRF-Chem, Grell et al., 2011), showing significant improvements in the emissions transport and dispersion and also in weather forecasting (Sessions et al., 2011). The study of pyro-convection was also addressed by the work of Rio et al. (2010) who proposed a "pyro-thermal plume model" based on a mixed Eddy Diffusivity/Mass Flux (EDMF) scheme for convective boundary layer plumes. In the EDMF parametrisation, the updraft and the surrounding environment directly interact through local and non-local mixing, respectively associated with the turbulent transport and the mass-flux term; while the methodology of the 1-D PRM model relies on the assumption that at rough resolution (grid-scale $\sim$ 30 to 100 km) fires do not have significant effects on the dynamics and the thermodynamics of the host model. The works of Freitas et al. (2010) and Rio et al. (2010) mark the current state of the art in the domain of atmosphere-wildfire interaction and they underline the challenge that remains when it comes to dealing with fire injection height. So far, these approaches have been validated for African and Amazonian fires for which elevated injection heights have been observed.

In the present chapter, the main goal is to delve into the dynamics of strong updrafts associated with wild-fires, focusing on the main actors participating in the smoke plume rise process: heat fluxes (sensible and latent), turbulence and entrainment of ambient air. Moreover, this work aims to investigate the impact of weather conditions on fire evolution,

taking into account different meteorological forcings. For this purpose, sensitivity tests are designed to compare two approaches for predicting the fire injection height, once both numerical models operate with similar environmental and fire conditions. The Meso-NH model is used at a kilo-metric scale in a 1-D configuration to study a typical Mediterranean fire (Lançon-de-Provence 2005) and two deforestation fires burnt in 2002 in the Amazon basin under different meteorological conditions. The capacity of the EDMF scheme in Meso-NH (Pergaud et al. 2009; Chap. 3, Sec. 3.1.2.2) is here investigated related to strong convective processes associated with wild-fires. Results from the 1-D Meso-NH/EDMF model are compared to corresponding simulations generated by the 1-D PRM model of Freitas et al. (2010). For both models, radiosonde data and re-analyses from the ECMWF are used as initial conditions to explore the sensitivity of both models to different meteorological forcing.

5.2 Data-sets selected for the inter-comparison

The data-sets chosen for the comparison exercise are described in this section. Three wild-fire episodes have been selected as case studies: a Mediterranean arson fire and two Amazonian deforestation fires. These cases differ from one another in vegetation characteristics and in meteorological conditions, suggesting a different evolution of the smoke plume rise.

For each of the three scenarios, initial and boundary meteorological conditions are from radiosondes and operational re-analyses from the ECMWF. The difference in the initial atmospheric profile between a radiosonde and re-analysis field has consequences on the atmosphere that is simulated by the numerical model, leading to different behaviours for the same fire plume.

Figure 5.1 shows the atmospheric conditions in the first kilometres for the Mediterranean fire. The vertical profiles of temperature, wind speed, potential temperature and water vapour mixing ratio are traced up to an height of 8 km for the radiosonde data (dashed line) and the ECMWF analysis (solid line). Data for the Amazonian fires are presented in the same way (Fig. 5.2 and 5.3).

5.2.1 Lançon-de-Provence 2005

On 1 July 2005, an arson wild-fire broke out at about 07:40 UTC, 09:40 CEST (Center European Summer Time) to the east of Lançon-de-Provence (south-eastern France, 43.60 N, 5.20 E), threatening downwind inhabited areas and cultivated lands. At 12:00 UTC, on the burning area, firefighters measured a temperature of 26°C, a wind speed of 46 km h^{-1}, a wind direction of 330° and a relative humidity of 20%. Documented favourable weather conditions led to the fire spreading easily. After 8 hours of burning, the Lançon fire was put out and the burnt area estimated: nearly 626 ha, mainly covered by shrub-land and

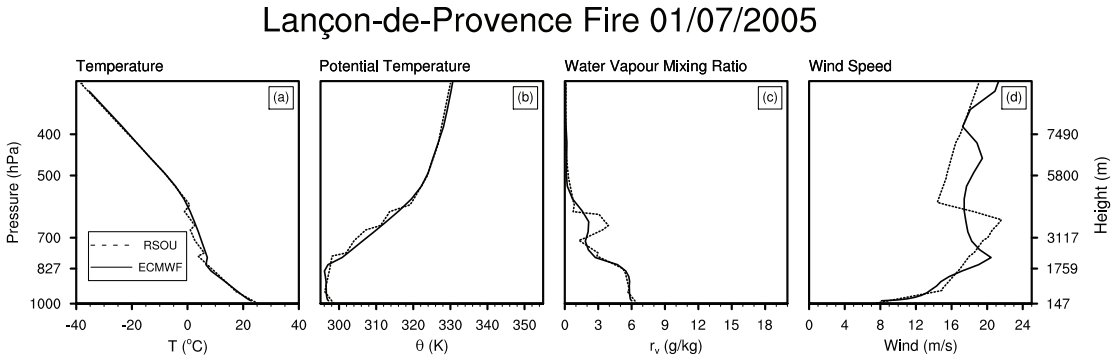

Figure 5.1: Comparison between the radiosonde data (dashed line) and the ECMWF analyses (solid line) for the Lançon-de-Provence 2005. The four graphics represent the vertical profile of: (**a**) temperature T (°C), (**b**) potential temperature θ (K), (**c**) water vapour mixing ratio r_v (g/kg) and (**d**) wind speed (m/s).

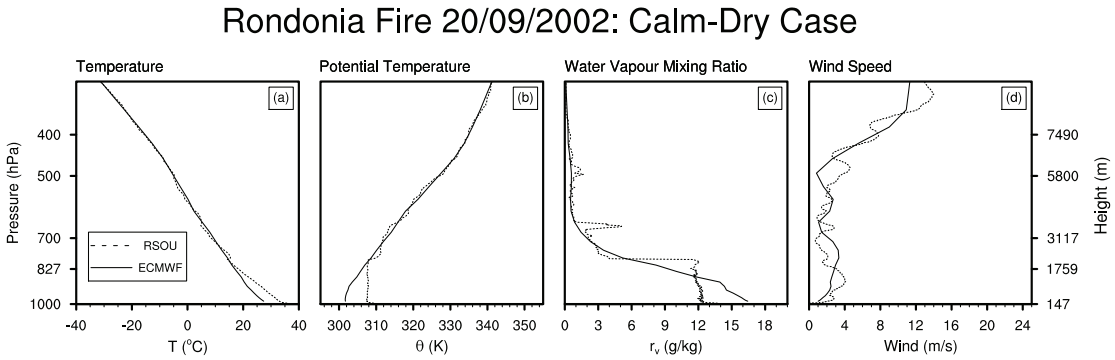

Figure 5.2: The same as Fig. 5.1 but for the calm-dry case of Rondônia 2002.

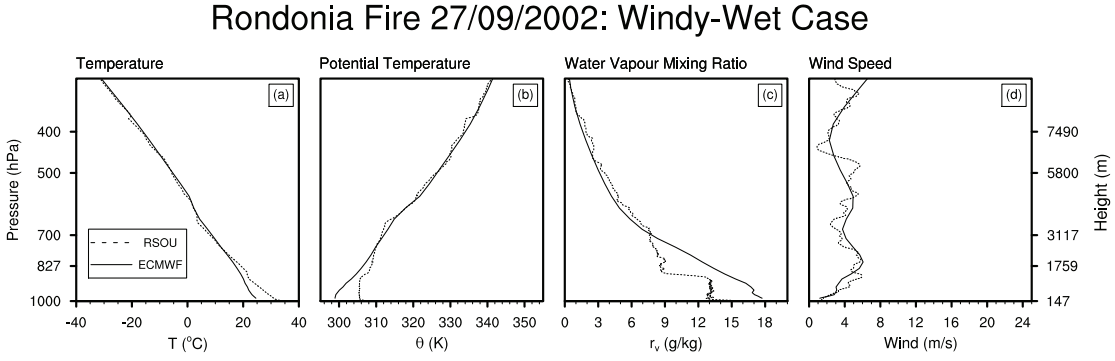

Figure 5.3: The same as Fig. 5.1 but for the windy-wet case of Rondônia 2002.

forest.

Twice a day (at 00:00 and at 12:00 UTC) a radiosonde is launched over Nîmes, a city located 63 km northwest away from Lançon-de-Provence (43 N, 4 E). Looking at radiosonde data measured on 1 July 2005 at 12:00 UTC (14:00 local time), temperatures decrease from 25 to $\sim 0°$ C in the first 5 km of the atmosphere (Fig. 5.1a). A well marked temperature inversion is observed at nearly 760 hPa, around 2.3 km; above this altitude the atmosphere becomes more stable as depicted by the positive slope of the potential temperature trend (Fig. 5.1b). This last graphic highlights unstable conditions at the surface ($\partial_z \theta < 0$), followed by a well developed mixed layer where θ is constant: this is the typical convective boundary layer of a summer early afternoon. Figure 5.1c shows a dry CBL with water vapour mixing ratio that decreases from 6.5 g kg^{-1} at the surface to nearly 1.0 g kg^{-1} at 700 hPa. The layer above is moister, probably as a result of the radiosonde crossing a cloud; normally this "wet" layer would not interact with the fire plume since strong winds, together with a dry BL, may efficiently prevent fire plume rise, as pointed out by Trelles et al. (1999) and Freitas et al. (2007), as well as observed in the previous chapter. Strong northwesterly winds blow over the region with speeds ranging from 8 to 20 m s^{-1} in the first 2 km of the atmosphere (Fig. 5.1d).

The Lançon-de-Provence fire constituted a benchmark for *GDR incendie* and other French fire propagation models (ForeFire, Balbi et al., 2009); moreover, the dynamics and the chemistry downwind of the Lançon fire was investigated by Strada et al. (2012) (Chapter 4).

5.2.2 Rondônia 2002

Rondônia is a state in Brazil located in the north-western part of the country and bordered Bolivia. It covers an area of 243,000 km^2 of the Brazil's "Legal Amazon", an administrative region situated in the Amazon Basin that comprises nine Brazilian states and covers 5,000,000 km^2. In Rondônia, the landscape underwent a rapid conversion between 1984 and 2002. In 1965, the opening of the BR-364 highway (built with World Bank funding, Lovejoy, 1991) provided an overland route between Rondônia and the Atlantic Coast, favouring the arrival of prospectors and settlers in the virgin Amazon forest; afterwards, the introduction of pasture in the '70s determined a significant modification in land use: with one of the fastest rate of tropical deforestation (Lovejoy, 1991), rain-forests have been soon replaced by agricultural and pasture lands by means of fires (de Barros Ferraz et al., 2005). Deforestation fires are arranged as follows: trees are felled, the vegetation is left to dry out in order to obtain better burning efficiency, then the material is set on fire, often after bulldozing it together into large piles (Andreae, 1991).

In 2002, during the burning season, two radiosondes were launched at 18:00 UTC (on 20 and 27 September) near a deforestation area in Rondônia (11.0 S, 60.0 W). Radiosonde time, 18:00 UTC, is 14:00 local time when the diurnal cycle of Amazonian fires reaches its

peak (Freitas et al., 2010) and convective structure are well developed (Chou et al., 2007). The selected days differ in wind intensity and atmospheric humidity, for this reason the considered case studies have been renamed as follows: the calm-dry case corresponds to 20 September 2002; the windy-wet case refers to 27 September 2002.

Considering the radiosoundings:

- **Calm-dry case.** On 20 September 2002 temperatures pass from 35 to $\sim 0°$ C in the first 5 km of the atmosphere; a strong thermal inversion is observed at around 800 hPa, $\sim$ 2 km (Fig. 5.2a). Below 800 hPa the potential temperature and the water vapour mixing ratio are constant in the daytime mixed layer; above the BL is capped by the stably stratified and drier free atmosphere, with r_v decreasing abruptly from 12 to 3 g kg^{-1} (Fig. 5.2b and c). The wind speed accelerates in the first kilometres from 2 to 4 m s^{-1}, then the speed decreases to 1 m s^{-1} at 700 hPa, around 3 km (Fig. 5.2d). Analysing the zonal and the meridional wind, also a directional wind shear is identified in the first 3 km (not shown).

- **Windy-wet case.** On 27 September 2002 the radiosonde registers a weaker temperature inversion at lower levels (around 870 hPa, $\sim$ 1.5 km, Fig. 5.3a). The height of the daytime mixed layer is nearly 1 km ($\partial_z \theta \approx 0$, Fig. 5.3b). Above, in the stable atmosphere, r_v decreases suddenly from 12 to 9 g kg^{-1} (Fig. 5.3c). The wind speed increases with height up to an altitude of 2 km with a strong wind shear from 2 to 6 m s^{-1} (Fig. 5.3d).

These two meteorological situations have already been chosen as case studies for other model comparisons (Freitas et al., 2007, 2010). Significant differences in ambient wind and humidity between the calm-dry and the windy-wet case will permit to better understand the role and the importance of environmental conditions on the smoke rise process, having selected the same fire characteristics for both cases.

5.2.3 Comparison between radiosondes and ECMWF analyses

Considering the Lançon-de-Provence fire, the ECMWF analysis shows a weaker temperature inversion at a slightly lower altitude compared to the radiosounding: 800 hPa, around 1.8 km (Fig. 5.1a). The potential temperature presents a less marked instability at the ground, followed by a mixed layer that stretches up to about 800 hPa (Fig. 5.1b). The trend of the water vapour mixing ratio describes a drier atmosphere at the ground-level and a moister one in the mixed layer, but in general the ECMWF atmosphere is drier compared to the one described by the radiosonde (Fig. 5.1c). In Figure 5.1d the ECMWF wind speeds are quite similar in the first 1.5 km to those of the radiosonde, except for a relative maximum around 2 km of altitude while the radiosonde wind speed increases monotonically.

About the calm-dry case among the Amazonian fires, a rapid inspection of the ECMWF vertical profiles showed a striking difference between the ECMWF and the radiosonde profiles. In the first 2 km the ECMWF atmosphere looks cooler, more stable, with a water vapour mixing ratio monotonically decreasing (Fig. 5.2a, b and c). Moreover, the ECMWF vertical profile is moister in the first kilometer, then it becomes drier. Between the ground surface and an altitude of 2 km, winds are 2 m s^{-1} weaker on the average if compared to the radiosonde atmosphere, in the layer above the magnitude relation inverts. Furthermore, the ECMWF profile shows a weaker wind shear.

As for the calm-dry case, the ECMWF vertical profiles for the windy-wet case look very different compared to those traced using the radiosonde. In the first 2 km the ECMWF atmosphere is 10° C cooler (Fig. 5.2a); moreover, it is more stable with potential temperature increasing with height, Fig. 5.2b. The water vapour mixing ratio monotonically decreases and the ECMWF atmosphere is highly moister than the radiosonde: at the inversion height the difference in water vapour mixing ratio equals 6 g kg^{-1} (Fig. 5.2c). Concerning wind speeds, the comparison is quite good for the windy-wet case (Fig. 5.2d).

Comparing the Lançon-de-Provence case study to the two Amazonian cases, it is worthy to note that the Amazon Basin offers a warmer, moister and less windy atmosphere for the fire starting.

5.3 Description of the one-dimensional models

This section is mainly devoted to the presentation of the numerical models that have been used and compared in the present work: the 1-D PRM and the Meso-NH/EDMF. Because of the computational efficiency of a 1-D model and the ability to isolate a column of atmosphere for study, a single column model (SCM) is an ideal environment in which to develop and test parametrisations (Randall et al., 1996).

5.3.1 The Meso-NH 1-D/EDMF model

The atmospheric model Meso-NH (Lafore et al., 1998) was described in details in Chapter 3. Here, we briefly describe the set-up configuration and the main parametrisations that have been activated for the present study.

Meso-NH is run as a SCM. Cloud micro-physical processes follow a two-moment scheme, using three water phases with five species of precipitating and non-precipitating liquid and solid water (Pinty and Jabouille, 1999). Turbulent motions are represented by the quasi-1D scheme of Bougeault and Lacarrère (1989) (Chap. 3, Section 3.1.2.1). The Eddy-Diffusivity/Kain-Fritsch parametrisation is utilized for representing shallow convection (see Chapter 3, Section 3.1.2.2 for further information).

The used square grid-mesh has an horizontal resolution of 1 km and the vertical grid has 70 levels, with a level spacing stretching from 40 m near the ground to 600 m at

higher altitude. The integration time is one hour with a time-step of one second. Due to the short duration of the simulation (1 hour), radiative processes are neglected (i.e. the downward radiative flux is put to zero) and the Coriolis parameter is set to zero. The orography is not taken into account, depicting a flat domain.

Dynamical variables are initialized and constrained prescribing a stationary vertical profile (i.e. the initial and the final state of the atmosphere are the same). Two different types of vertical profile are used: observational soundings recorded in the vicinity of the burnt area, on the day of the fire; and vertical profiles generated from operational re-analyses of the ECMWF, selecting the same UTC hour of the observational radiosonde and the nearest location to the radiosonde launch station.

The ISBA scheme (Noilhan and Planton, 1989) parametrises exchanges between the atmosphere and natural lands and provides surface energy fluxes to the atmosphere (Chap. 3, Sec. 3.1.3). In order to have the same contribution from the ground in terms of fluxes, the same kind of vegetation cover has been chosen in Meso-NH for all three scenarios, imposing equal conditions for soil humidity and temperature. The selected cover type is cerrado; temperatures of the surface soil layer, the root zone soil layer and the deep soil layer have been set to 303.53 K; and soil water index (SWI) is zero for the surface soil layer and 0.2 for the root zone and the deep soil layer. Through the ISBA scheme, the fire forcing is also activated through heat and scalar fluxes that are prescribed at the surface in the Meso-NH model. Section 5.3.1.2 gives further details on this technique.

5.3.1.1 1-D Meso-NH general equations

A SCM is a stand-alone model that can be pictured as a single vertical array of grid-point cells placed at a specific geographical location. The column model prognostically calculates the evolution of the vertical structure of some variables based on physical parametrisations. In particular, in the 1-D Meso-NH prognostic variables are: latitudinal and longitudinal wind components (u, v), potential temperature θ, water vapour (r_v), cloud (r_c) and rain water (r_r) mixing ratios and turbulent kinetic energy (TKE, $\bar{e}$).

The basic equations implemented in the 1-D Meso-NH are:

$$\frac{\partial \bar{u}}{\partial t} = \frac{\partial}{\partial z}\left(K_m \frac{\partial \overline{w'u'}}{\partial z}\right) - w_{ls}\frac{\partial \bar{u}}{\partial z} \tag{5.1}$$

$$\frac{\partial \bar{v}}{\partial t} = \frac{\partial}{\partial z}\left(K_m \frac{\partial \overline{w'v'}}{\partial z}\right) - w_{ls}\frac{\partial \bar{v}}{\partial z} \tag{5.2}$$

$$\frac{\partial \bar{\theta}}{\partial t} = \frac{\partial}{\partial z}\left(K_h \frac{\partial \overline{w'\theta'}}{\partial z}\right) - w_{ls}\frac{\partial \bar{\theta}}{\partial z} + Q_\theta^{diab} \tag{5.3}$$

$$\frac{\partial \overline{r_j}}{\partial t} = \frac{\partial}{\partial z}\left(K_h \frac{\partial \overline{w'r_j'}}{\partial z}\right) - w_{ls}\frac{\partial \overline{r_j}}{\partial z} + Q_{r_j}^{diab}\,; \quad j \in \{v, c, r\} \tag{5.4}$$

$$\begin{aligned}\frac{\partial \bar{e}}{\partial t} &= \frac{\partial}{\partial z}\left(K_e \frac{\partial \bar{e}}{\partial z}\right) - w_{ls}\frac{\partial \bar{e}}{\partial z} \\ &+ K_m\left[\left(\frac{\partial u}{\partial z}\right)^2 + \left(\frac{\partial v}{\partial z}\right)^2\right] \\ &+ K_h \frac{g}{\overline{\theta_V}}\overline{w'\theta'_V} - D\,. \end{aligned} \tag{5.5}$$

The parameter w_{ls} is the synoptic-scale vertical velocity, K_m, K_h and K_e are the turbulent mixing coefficients for momentum, heat and TKE, respectively. Q_θ^{diab} and $Q_{q_j}^{diab}$ are the diabatic terms in the heat and humidity equations. The parameter g is the gravitational constant. The temporal evolution of $\bar{e}$ depends on different terms that are, on the right side of Equation 5.5, the turbulent transport by eddies, the vertical advection by LS vertical flow, the shear production or loss term, the buoyancy production, and the dissipation rate of TKE, respectively.

To sum up, in the atmosphere of the SCM the active processes are: vertical advection, turbulent mixing and diabatic exchanges. The vertical velocity is handled as a diagnostic variable.

5.3.1.2 Fire forcing in Meso-NH

In Chapter 3 (Sec. 3.3) we illustrated the method for the one-way coupling MesoNH-ForeFire. In the work of Strada et al. (2012) this methodology was applied for modelling the Lançon-de-Provence fire, considering the fire as a sub-grid process in the atmospheric model. The cited coupling method was simple: every 2 minutes ForeFire provided the total burnt area (S_b) contained in each Meso-NH grid cell (S_{mnh}). At each atmospheric time-step, the surface scheme ISBA accomplished the fire-atmosphere coupling by computing total wildfire contribution to latent and sensible heat fluxes, taking into account a nominal flux and the surface ratio between the Meso-NH and the total burnt area. Finally, calculated fluxes were taken as inputs at the surface level in the atmospheric model. The same coupling method is applied in the present study in a 1-D configuration since in a 3-D simulation it is hard to assess the strength of the fire forcing on the atmospheric dynamics, and it is complex to discriminate fire effects from other phenomena (Chap. 4). Here, the wild-fire is stationary and fire forcing is updated every 2 minutes. A step function tunes the starting of the fire during the first five minutes, as done in the 1-D PRM model.

The sensible heat flux Φ_S, kW m^{-2}, is computed as

$$\Phi_S = \phi_s \cdot C \cdot \frac{S_b}{S_{mnh}}\,. \tag{5.6}$$

The nominal value ϕ_S does not separate radiative from convective energy; hence, the multiplication by a reducing factor, C, is necessary to select the percent of total energy

effectively available to plume convection. The C parameter ranges from 0.4 to 0.8 depending on fire characteristics and ambient conditions; in order to compare results from the Meso-NH and the 1-D PRM model, the same value selected by Freitas et al. (2010) has been chosen: $C = 0.55$. S_{mnh} measures 100 ha. A constant value is imposed for the burnt area, $S_b = 3.35$ ha, by taking the mean burnt area simulated by ForeFire from 12:00 to 13:00 UTC for the Lançon fire (Strada et al., 2012). During the chosen time span, ForeFire burnt a total area of nearly 100 ha. In default of similar information for the Amazonian fires, the same value for S_b is utilized.

The latent heat flux Φ_L, kg m^{-2} s^{-1}, is calculated as in the 1-D PRM model:

$$\Phi_L = \frac{\Phi_S}{E_m} \cdot \left[\frac{m}{100} + EF_{H_2O} \right] . \tag{5.7}$$

The computed sensible heat flux multiplies the heat content E_m (MJ kg^{-1}) by the sum of fuel moisture m (%) and H_2O emission factor (combustion moisture, in kg kg^{-1}).

A fire tracer is emitted and its flux (g m^{-2} s^{-1}) is defined as follows:

$$\Phi_{fire} = \frac{E_{fire}}{S_{mnh} \cdot \tau} , \tag{5.8}$$

where the fire emission E_{fire} (in g) are integrated on the Meso-NH grid-mesh, on a period of 2 minutes, τ. The fire emission is obtained through the equation of Seiler and Crutzen (1980) (Chapter 3):

$$E_{fire} = S_b \cdot FL \cdot \beta \cdot EF_{fire} , \tag{5.9}$$

where FL (kg m^{-2}) is the fuel loading, β (%) is the burning efficiency of the above-ground biomass, and EF_{fire} (g kg^{-1}) is the emission factor for the fire tracer. From Miranda et al. (2008), FL and β for shrub-lands are 1.00 kg m^{-2} and 80%, respectively. The fire tracer is handled as a PM_{10} aerosol ($EF_{fire} = 10$ g kg^{-1}) with no mass (i.e. deposition velocity equals 0 m/s).

Table 5.1 summarizes the fire characteristics used for simulating different fire episodes (for references: Freitas et al. 2007; Silvani and Morandini 2009; Miranda et al. 2008).

5.3.2 The 1-D PRM model

Starting from the simple 1-D time-dependent cloud resolving model of Latham (1994), Freitas et al. (2006) proposed a plume rise model for simulating explicitly strong updrafts associated with vegetation fires and for, finally, predicting the fire injection height. The model governing equation for vertical motion includes the entrainment of environmental air in the plume, the difference of temperature between the environment and the plume, the upward drag of condensate water vapour and the effect of horizontal ambient wind (Freitas et al., 2010). The scope of the 1-D PRM model is to make a parametrisation

Table 5.1: Fire and fuel characteristics for the considered case studies.

Fire features	**Lançon 2005**	**Rondônia 2002**	
		Calm-Dry	Windy-wet
Burnt Area (ha)	100	100	100
Sensible Heat Flux, ϕ_{sh} (kW m^{-2})	100.0	80.0	80.0
Heat Content, E_m (MJ kg^{-1})	19.6	15.5	15.5
Fuel Moisture, FM (%)	10	10	10
Water Emission Factor, EF_{H_2O} (kg kg^{-1})	0.5	0.5	0.5
Fire Tracer Flux, Φ_s (10^{-3} g m^{-2} s^{-1})	2.23	2.23	2.23

available to 3-D meso-scale or global models in order to describe the sub-grid convective transport associated with wild-fires, taking into account fire features, and to better forecast dispersion of fire products (aerosols and trace gases).

The 1-D plume rise model can be embedded in each column of a large-scale atmospheric-chemistry transport model. The coupling between the 1-D PRM and the host model relies on the assumption that at rough resolution (grid-scale $\sim$ 30 to 100 km) fires do not have significant effects on the dynamics and the thermodynamics of the host model. In this way, the 3-D model passes the environmental large-scale conditions to the 1-D PRM model for initializing and constraining it at the boundaries, under the hypothesis of a stationary atmosphere. Once the convective energy flux of the fire and the plume radius have been selected, the 1-D PRM model resolves explicitly the vertical extent of the fire plume. For each biome type two values for the fire heat flux are given: a lower and a upper; therefore, the 1-D PRM model computes a lower and a upper injection height. These two results are returned to the host model that homogeneously releases fire tracers emitted during the flaming phase in the vertical range delimited by the lower and the upper height. The 1-D PRM model can be run independently with initial values from a radiosonde.

The fire heat flux is converted into the available convective energy flux E (in kW m^{-2}) multiplying it by the reducing factor $C = 0.55$, already defined for the Meso-NH model (Sec. 5.3.1.2). Hence, the buoyancy flux (m^4/s^3) generated at the surface by the fire source is calculated using the following expression:

$$F = \frac{g\mathcal{R}}{c_p P_e} E R^2 \,, \tag{5.10}$$

where $\mathcal{R}$ is the ideal gas constant (kg^{-1} K^{-1}), c_p is the specific heat capacity at constant pressure (J kg^{-1} K^{-1}), P_e is the ambient surface pressure (hPa) and R is the plume radius (m), computed assuming the total burnt area as a circle. Buoyancy triggers the vertical velocity ($w_{f,0}$) and the temperature excess ($T_{f,0} - T_{e,0}$) of the in-cloud air parcels at the

surface:

$$w_{f,0} = \frac{5}{6\alpha}\left(\frac{0.9\alpha F}{z_v}\right)^{1/3}, \tag{5.11}$$

$$\frac{\Delta\rho_0}{\rho_{e,0}} = \frac{5}{6\alpha}\frac{F}{g}\frac{z_v^{-5/3}}{(0.9\alpha F)^{1/3}}, \tag{5.12}$$

$$T_{f,0} = \frac{T_{e,0}}{1-\frac{\Delta\rho_0}{\rho_{e,0}}}, \tag{5.13}$$

where $\alpha = 0.05$, $z_v = (5/6)\alpha^{-1}R$ is the virtual boundary height, and $\Delta\rho_0$ is the density difference between the in-cloud air parcels and environmental air at the surface. The surface water vapour excess is calculated in the same way that is reported for the Meso-NH model (Eq. 5.7). The heating rate increases following a step function during the first five minutes of the simulation. The time integration is fixed to one hour, as for Meso-NH, even if the steady state is typically reached within 50 min (Freitas et al., 2007). Hereafter, the subscript f is used to identify variables associated with the center of mass of the rising plume.

The 1-D PRM model depicts the evolution of the plume utilizing advection equations for the vertical velocity w_f, the temperature T_f, the water phases parameters $r_{f,v}$, $r_{f,c}$ and $r_{f,ice-rain}$, the horizontal velocity of the center of mass of the plume at level z (U_f) and the plume radius R. The governing prognostic equations are:

$$\frac{\partial w_f}{\partial t} + w_f\frac{\partial w_f}{\partial z} = \frac{1}{1+\gamma}gB_f - (\varepsilon_{f,lat}+\varepsilon_{f,dyn})w_f \tag{5.14}$$

$$\frac{\partial T_f}{\partial t} + w_f\frac{\partial T_f}{\partial z} = -w_f\frac{g}{c_f} - (\varepsilon_{f,lat}+\varepsilon_{f,dyn})(T_f - T_e) + \left(\frac{\partial T_f}{\partial t}\right)_{\mu p} \tag{5.15}$$

$$\frac{\partial r_{v,f}}{\partial t} + w_f\frac{\partial r_{v,f}}{\partial z} = -(\varepsilon_{f,lat}+\varepsilon_{f,dyn})(r_{v,f} - r_{v,e}) + \left(\frac{\partial r_{v,f}}{\partial t}\right)_{\mu p} \tag{5.16}$$

$$\frac{\partial r_{c,f}}{\partial t} + w_f\frac{\partial r_{c,f}}{\partial z} = -(\varepsilon_{f,lat}+\varepsilon_{f,dyn})r_{c,f} + \left(\frac{\partial r_{c,f}}{\partial t}\right)_{\mu p} \tag{5.17}$$

$$\frac{\partial r_{j,f}}{\partial t} + w_f\frac{\partial r_{j,f}}{\partial z} = -(\varepsilon_{f,lat}+\varepsilon_{f,dyn})r_{j,f} + \left(\frac{\partial r_{j,f}}{\partial t}\right)_{\mu p} + sedim_j \quad j \in \{\text{ice, rain}\} \tag{5.18}$$

$$\frac{\partial U_f}{\partial t} + w_f\frac{\partial U_f}{\partial z} = -(\varepsilon_{f,lat}+\varepsilon_{f,dyn})(U_f - U_e) \tag{5.19}$$

$$\frac{\partial R}{\partial t} + w_f \frac{\partial R}{\partial z} = (\frac{3}{5}\varepsilon_{f,lat} + \frac{1}{2}\varepsilon_{f,dyn})R\,, \tag{5.20}$$

where in Eq. (5.14) $\gamma = 0.5$ compensates for the neglect of non-hydrostatic pressure perturbations (Simpson and Wiggert, 1969) and B_f is the buoyancy term. Compared to the EDMF parametrisation (Chap. 3, Sec. 3.1.2.2), in the PRM the buoyancy term includes the downward drag of condensate water and its definition is related to the virtual temperature T_V. Index μp denotes the tendencies from cloud microphysics (Freitas et al., 2007). The plume top is identified by means of the in-cloud vertical velocity: when w_f is less than 1 m s^{-1}, the steady state solution is attained and the top of the plume is given by the model.

In the new version of the 1-D PRM model two terms of entrainment have been defined, the classical lateral entrainment

$$\varepsilon_{f,lat} = \frac{2\alpha}{R}|w_f|\,, \tag{5.21}$$

and the "dynamic entrainment"

$$\varepsilon_{f,lat} = \frac{2}{\pi R}(U_e - U_f)\,. \tag{5.22}$$

This additional entrainment term expresses some physical effects on the plume that are enhanced by strong horizontal winds: the reduction of the in-plume vertical velocity ($-\varepsilon_{f,dyn} w_p$), the decrease of the buoyancy term due to the loss of temperature excess ($-\varepsilon_{f,dyn}[T_{f,0} - T_{e,0}]$) and the gain of horizontal velocity of the plume ($\varepsilon_{f,dyn}[U_f - U_e]^2$) (Freitas et al., 2010).

In the last update of the 1-D PRM model, Freitas et al. (2010) introduced the Vertical Mass Distribution (VMD) to mathematically define an injection layer. The VMD provides a probability vertical mass distribution as a function of the simulated vertical velocity profile (w_f). Premising that the main detrainment mass layer of cumulus convection is situated close to the cloud top, two levels are defined: z_i where w_f starts to decrease, and z_f where w_f is less than 1 m s^{-1}. The area included among is the upper half part of the cumulus (plume). Afterwards, a parabolic function of the height z with roots z_i and z_f is defined. Finally, the function is normalized to 1 in the interval $[z_i, z_f]$.

It is important to highlight that the 1-D PRM model is not a SCM as the 1-D Meso-NH model. The evolution of the vertical structure of the prognostic meteorological variables within the plume does not impact the dynamics and the thermodynamics of the surrounding environment. The 1-D PRM model is the adaptation of a cloud resolving model, a numerical model conceived to resolve cloud-scale circulation; therefore, it integrates over the whole cloud-area. For this reason, in the 1-D PRM model the prescribed burning area corresponds to the whole area that is burnt during the time integration: 100 ha (Sec. 5.3.1.2).

5.4 Results and discussion

In this section, results obtained from the 1-D Meso-NH/EDMF and the 1-D PRM model are presented and discussed, firstly by defining a unifying metrics for the discussion of results (Sec. 5.4.1), then by analysing separately the three wild-fire episodes (Sec. 5.4.2), finally by outlining some general discussions (Sec. 5.4.3).

5.4.1 Definition of the metrics used for the comparison

Table 5.2 gathers all variables that have been selected for the comparison between the different numerical models. Regarding these variables, it is important to define a common metrics. First of all, the Meso-NH model distinguishes between grid and updraft variables when the EDMF scheme is activated, otherwise only grid variables are available in the model; on the contrary, the PRM variables only refer to the updraft system. Figure 5.4 shows several parameters from the 1-D PRM model for the Lançon-de-Provence case. Figure 5.5 presents the time evolution of the vertical profiles of parameters for the 1-D Meso-NH simulation on the same case. These two figures will be used to illustrate the variables chosen for the comparison study.

- **Water vapour mixing ratio.** In both models, r_v is expressed in g kg^{-1}. In the PRM model, the water vapour mixing ratio is representative of the updraft ($r_{v,f}$). For the Meso-NH model, $r_{v,env}$ is the value in the environment. It is worth noting that the net contribution of wild-fires is to increase the humidity of the air near the detrainment levels (Fig. 5.4a and 5.5a). This moist enrichment of the atmosphere determines the elevation of the level where $r_v \sim$ constant (5.4a and Fig. 5.5a) along the total integration time.

- **Updraft vertical velocity.** In both models, vertical velocity is expressed in m s^{-1}, but different trends are identified due to different theoretical definitions. In the PRM model w_f is initialised at the surface (Eq. (5.11)) by the buoyancy flux and decreases along the vertical (Fig. 5.4b); whereas in the Meso-NH model, w_u is a prognostic variable whose trend strongly depends on the updraft fraction a_u and the updraft mass flux M_u behaviour (Chap. 3, Sec. 3.1.2.2):

$$w_u = \frac{M_u}{\rho a_u},$$

  where a_u increases near the surface then diminishes along the vertical, while M_u maximises in the mixing layer (Fig. 5.5b).

- **Buoyancy.** The buoyancy acceleration is given in m s^{-2}, and it shows similar trends and values for both models (Fig. 5.4c and 5.5c). In general, the buoyancy acceleration slightly increases near the surface, where the heat source is active and

feeds the rising of the in-cloud parcels, then it reduces until the sign inversion, when downdraft movements start. At the cloud top, equilibrium is attained (buoyancy equals zero).

- **Turbulent parameters.** Updraft turbulent fluxes ($< w'_u\theta'_u >$ in K m s^{-1}, and $< w'_u r'_{v,u} >$ in kg kg^{-1} m s^{-1}) and turbulent kinetic energy (in m^2 s^{-2}) are only available for the Meso-NH model. The updraft turbulent kinetic sensible heat flux $< w'_u\theta'_u >$ represents the buoyancy source in the equation of the TKE, (Eq. (5.5)), therefore its trend nearly resembles that of buoyancy with a deeper increment near the surface heating (in the first kilometres of the atmosphere), followed by a faster decrease until the equilibrium is reached ($< w'_u\theta'_u >= 0$, Fig. 5.5d). The temporal evolution of the updraft turbulent kinetic latent heat flux $< w'_u r'_{v,u} >$ shows a clear rising of the altitude at which the maximum is placed that finally matches with the location of maximal fluctuations of w_u and $r_{v,env}$ at the top of the updraft (Fig. 5.5e).

- **Entrainment.** In Meso-NH, the entrainment rate ε_u is measured in m^{-1} (Chap. 3, Sec. 3.1.2.2), Eq. (3.11)), whereas in the PRM model the two entrainment rates are both expressed in s^{-1} (Eq. (5.21) and (5.22)). For consistency, the entrainment fluxes of Meso-NH/EDMF ($E_u = \varepsilon\, M_u$, in kg m^{-3} s^{-1}) are multiplied by the density of dry air (ρ, in kg m^{-3}) in order to have a common metrics for the entrainment coefficients: s^{-1}. Although the definitions are slightly differents, the lateral entrainment $\varepsilon_{f,lat}$ of the PRM model (Eq. (5.21)) can be compared to the entrainment rate in the EDMF scheme of Meso-NH, Eq. (3.11): their values and exponential trends are similar (Fig. 5.4f and 5.5f). In the PRM model, $\varepsilon_{f,lat}$ has the same value at the surface through the whole set of simulations (between 0.3 10^{-2} and 0.4 10^{-2} s^{-1}), likely due to the huge burnt area (100 ha) that homogenizes the existing differences in terms of fire forcings between Mediterranean and tropical fires (role of the plume radius in Eq. (5.10) and Eq. (5.21)). In the Meso-NH model, the entrainment coefficient at the surface has a constant value of 0.2 10^{-2}.Concerning the dynamic entrainment $\varepsilon_{f,dyn}$ of the PRM model (Eq. (5.22)) a similar parameter is not available in the Meso-NH model, therefore we decided to show in the following the sum of the two entrainment terms in order to illustrate the total entrainment of ambient air that feed, or slow down, the rising of the fire plume in the PRM model. Changes in the vertical profile of $\varepsilon_{f,dyn}$ are driven by the fluctuations of environmental wind. In Figure 5.4d, $\varepsilon_{f,dyn}$ has a quasi monotonic decrease compatible with the wind profile in Figure 5.1d.

- **Detrainment.** As done for the entrainment rate, the Meso-NH detrainment coefficient δ_u is converted from m^{-1} to s^{-1}. The trend of δ_u points out the coexistence of entrainment/detrainment in the CBL that both feed the vertical evolution of the

Table 5.2: Environmental and updraft variables selected in the Meso-NH model and in the PRM model for discussing the simulation results.

Variables	**Meso-NH**		**PRM**
	Grid	Updraft	
Water vapour mixing ratio (g kg^{-1})	r_v		$r_{v,f}$
Vertical velocity (m s^{-1})		w_u	w_f
Buoyancy (m s^{-2})		B_u	B_f
Turbulent heat flux (K m s^{-1})		$< w'_u \theta'_u >$	
Turbulent moist flux (kg kg^{-1} m s^{-1})		$< w'_u r'_{v,u} >$	
Turbulent kinetic energy (m^2 s^{-2})	TKE		
Lateral entrainment rate (s^{-1})		ε_u	$\varepsilon_{f,lat}$
Dynamic entrainment rate (s^{-1})			$\varepsilon_{f,dyn}$
Detrainment rate (s^{-1})		δ_u	
Injection layer		$[\varepsilon_u]_{max}$	VMD (%)
Normalized scalar mixing ratio	r_s		

mass flux; when ε_u goes to zero, δ_u maximises (Fig. 5.5f). In Meso-NH, we define the detrainement zone (or injection layer) as the vertical range where δ_u maximises. The injection height is the altitude at which the detrainment is maximal. Since the PRM model does not have a detrainment rate or zone among its output variables, the Meso-NH detrainment layer is compared to the vertical range enclosed by the VMD in the 1-D PRM simulations. The injection height is identified as the altitude where VMD maximises in the PRM model (Fig. 5.4f). In the graphics, the injection layers are compared by overlaying the VMD for the steady state solution of the PRM (dot filled area) on the plot of the Meso-NH detrainment rate (Fig. 5.5f). The mathematical definition of the VMD implies that the PRM model vents the fire products away from the surface inducing a depletion of the lower levels of the atmosphere in terms of fire pollutants (Fig. 5.4f) which are no more available for turbulent mixing. In the Meso-NH/EDMF model, a part of the released fire tracer is mixed in the first kilometres of the atmosphere by the turbulence, the rest is vertically transported by the thermal plumes (Fig. 5.5f).

- **Scalar.** As explained before (Sec. 5.3.1.2), a fire tracer is released in the Meso-NH simulations. Its mixing ratio is normalized by its maximal value at each temporal session. In general, once released at the surface, the fire tracer is partly transported high in the atmosphere and released near the top of the updraft (Fig. 5.5d) showing a characteristic "C-shape" profile..

Table 5.3: Summary of the discussed numerical experiments that have been performed with the 1-D models: Meso-NH and PRM.

Fire episode		**Atmospheric forcing**	**Meso-NH**		**PRM** Environmental wind effect
			TURB	EDMF	
Lançon 2005		RSOU	On	On	On
			On	Off	
		ECMWF	On	On	On
			On	Off	
Rondônia 2002	Calm-dry	RSOU	On	On	On
		ECMWF	On	On	
	Windy-wet	RSOU	On	On	On
		ECMWF	On	On	

5.4.2 Comparison of fire forced simulations

Table 5.3 recapitulates the simulations that are reported in the present chapter: RSOU stands for simulations forced by radiosonde data, ECMWF means that the meteorological forcing is taken from the ECMWF re-analyses. For the 1-D PRM model, only results obtained considering the environmental wind drag are shown since the difference between a simulation with the wind effect on/off was already discussed in the work of Freitas et al. (2010). The top of the fire plume as predicted by the PRM is illustrated on all graphics by an horizontal solid line, the horizontal dashed line refers to the plume top when the environmental wind effect is off in the PRM model.

For the 1-D PRM model, the vertical profiles obtained after 10 minutes of simulation are drawn with a dashed-black line, while the solid-black line depicts the attained steady state solution. Results from the 1-D Meso-NH model are presented at the temporal session of the PRM model steady state solution and at the end of the simulation (after 60 minutes).

5.4.2.1 Lançon 2005 wild-fire

Using the radiosounding of Nîmes as meteorological forcing, the 1-D PRM model predicts a plume top near 2.5 km including the environmental wind effect (Fig. 5.4b); looking at the VMD, the main injection layer is localized between 1 and 2.5 km and it maximises near 1.7 km (Fig. 5.4f). This steady state solution is obtained after around 20 minutes. Above 1.5 km of altitude, $r_{v,f}$ records a gain of 1 g kg^{-1} between the first output (after 10 minutes) and the steady state solution (Fig. 5.4a). This increase in $r_{v,f}$ documents the release of humid air masses by a wild-fire with two important contributions: the fuel and the combustion moisture. Within a prescribed grass fire, Clements et al. (2006) measured in situ a net moisture increase of 1-2 g kg^{-1}.

Forcing the 1-D PRM model by the ECMWF re-analyses, the forecast plume top is located at 3 km (wind on) after nearly 20 minutes of simulation. The main injection layer reaches out nearly 1.5 km, from 1.3 to 3 km, with its maximum attained around 2.2 km (Fig. 5.7c). Compared to values obtained using the radiosonde forcing, the plume top is 500 m higher, the injection layer has the same width with an injection height 700 m higher than the RSOU case. Diverse factors may lead to these differences. As observed in Section 5.2.3, the radiosounding has a stronger temperature inversion than the ECMWF atmospheric profile, an atmospheric parameter that may efficiently control the injection height of the fire plume, preventing it from reaching higher altitudes (Trentmann et al., 2003). Moreover, the radiosonde measured a stronger wind velocity at the surface: this results in a quasi-doubled dynamic entrainment ($\epsilon_{f,dyn} = 0.011$ s^{-1} in the RSOU case versus $\epsilon_{f,dyn} = 0.006$ s^{-1} using the ECMWF forcing, not shown), and in a faster decrease of w_f and B_f. In the first kilometres of the atmosphere, in the ECMWF forced simulation, B_f even increases before starting to diminish (Fig. 5.4c versus Fig. 5.7a). The weaker wind drag in the ECMWF simulation has a consequence also on $r_{v,f}$; within the fire plume, the production of water vapour starts higher than the radiosonde case and it is more significant: 3 km above the surface $r_{v,f}$ increases of 3 g kg^{-1} during 10 minutes (not shown).

When forced by the radiosounding of Nîmes, after 60 minutes of simulation, the 1-D Meso-NH/EDMF model simulates an updraft that has its top near 3.8 km (Fig. 5.5b). This altitude is comparable to the plume top predicted by the 1-D PRM model without the wind drag (3.5 km, horizontal dashed line on Fig. 5.5b). The detrainment zone is localized between 2.7 and 3.7 km (Fig. 5.5f), above the turbulent mixing stops to be active (Fig. 5.5d-e), and the detrainment maximises at 3.3 km. The final injection height as predicted by Meso-NH is 1.6 km higher than the value simulated by the 1-D PRM model using the RSOU forcing. This difference is lower than 1 km if we consider the Meso-NH result after 20 minutes (PRM steady state solution). The illustrated difference can be ascribed to the weaker entrainment rate at the surface in the 1-D Meso-NH/EDMF model: $\varepsilon_u = 0.002$ s^{-1} (Fig. 5.5f, positive values) against 0.004 s^{-1} for $\varepsilon_{f,lat}$ in the respective 1-D PRM simulation (Fig. 5.4e). The Meso-NH updraft entrains less environmental air, therefore the cooling of the fire plume due to the mixing with ambient air is weaker, and it determines a more convective updraft than the PRM plume. The same case study is simulated by the 1-D Meso-NH without the EDMF parametrisation. The vertical spread is weaker because only the local mixing due to turbulence is considered: after 60 minutes, the TKE falls to zero at 3.1 km (Fig. 5.6b), as a consequence the fire tracer is not transported higher than this level (Fig. 5.6c). Even if a detrainment zone is not defined for this case, the relative VMD overlays the normalized vertical profile of the tracer mixing ratio just below the level where the diminution of the scalar mixing ratio becomes faster (2.6 km on Fig. 5.6c). The comparison between Figure 5.5 (with EDMF) and Figure 5.6 (without EDMF) shows the contribution of the mass flux approach which transport

efficiently the boundary layer products to the higher altitudes.

Once forced by the ECMWF profile, at the end of the simulation, the updraft in the 1-D Meso-NH/EDMF model stops rising at around 3.2 km, and it detrains between 2.2 and 3.2 km with its maximum at 2.7 km (Fig. 5.8b). In this case, the comparison of the injection layer between the two models is better than for the RSOU forcing with a gap of only 500 m. For both models, the buoyancy acceleration starts reducing around 2 km of altitude (Fig. 5.8c versus Fig. 5.7a); while, using the RSOU forcing, the in-cloud parcels rise higher in the Meso-NH simulation, compared to the PRM model, before inverting its sign (Fig. 5.5c versus 5.4c). The Meso-NH entrainment rate (Fig. 5.7b) is still the half than the PRM lateral entrainment (not shown); considering the total entrainment for the PRM model (Fig. 5.7b), Meso-NH nearly entrains one fourth of the ambient air compared to PRM (Fig. 5.7b). As before, the Meso-NH simulation without the EDMF scheme predicts a lower injection height (2.5 km after 60 minutes of integration time, not shown).

The 1-D PRM model predicts a higher injection height (by nearly 500 m) when it is forced by the ECMWF re-analysis because this meteorological forcing has weaker winds at the surface than the radiosonde. Using the 1-D Meso-NH/EDMF model, the result is opposite with nearly the same variability (600 m): the final injection height is higher for the RSOU case rather than the ECMWF case. The 1-D PRM would prescribe to a host CTM a fire injection height that represents a fire plume escaping the PBL. The measurements recorded downwind of the Lançon fire by the air quality monitoring network gave evidences of a fire plume kept in contact with the surface (Strada et al., 2012). When the EDMF parametrisation is not activated, the 1-D Meso-NH model predicts a lower plume top that is more comparable with the air quality observations reported in the previous chapter for the Lançon fire.

5.4.2.2 Rondonia 2002 wild-fires

Calm-dry case

Once initialised by the radiosonde, the 1-D PRM model predicts a plume top at 6.9 km (wind on) with a maximum of 4% of mass around 5 km and the main injection layer comprised between 3.3 and 6.9 km (Fig. 5.9c). This maximum is substantially lower than the 9% maximum obtained for the Lançon-de-Provence fire but the mass is distributed in a narrower altitude mayer than in the Mediterranean case. The 1-D PRM model steady state solution is obtained after around 30 minutes. At the surface, the buoyancy acceleration is 0.03 m s^{-2} stronger than for the Lançon fire (Fig. 5.9a). In Equation (5.10) the convective energy flux E has diminished and the plume radius R keeps the same, therefore this difference can only be attributed to the lower ambient surface pressure P_e recorded in Rondônia. The dynamic entrainment is critically reduced compared to the Lançon case that leads to a reduction in the total entrainment (Fig. 5.9b) due to the

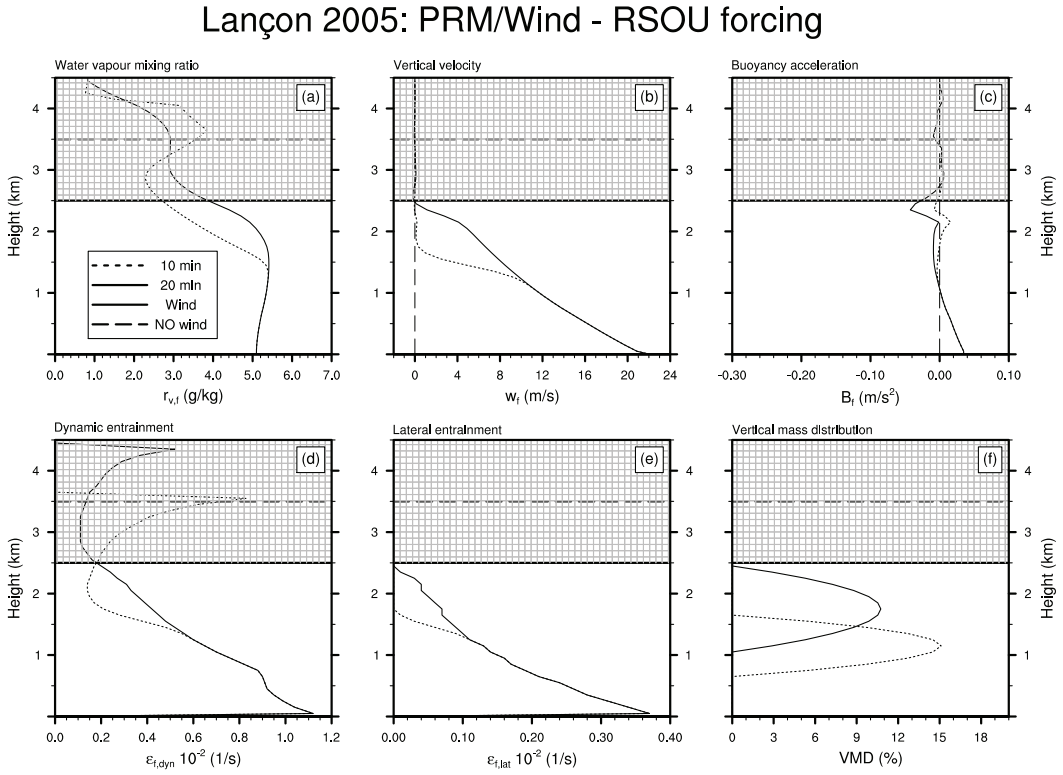

Figure 5.4: 1-D PRM model results for the Lançon fire using the radiosounding of Nîmes as meteorological forcing. The quantities are: (**a**) water vapour mixing ratio (r_v, f, g/kg); (**b**) vertical velocity (w_f, m/s); (**c**) buoyancy acceleration (B_f, m/s^2); (**d**) dynamic entrainment ($\varepsilon_{f,dyn}$, 1/s); (**e**) lateral entrainment ($\varepsilon_{f,lat}$, 1/s); (**f**) vertical mass distribution (VMD, %). The solid line indicates the plume top obtained including the environmental wind effect; the dashed line is the plume top when the wind effect is off.

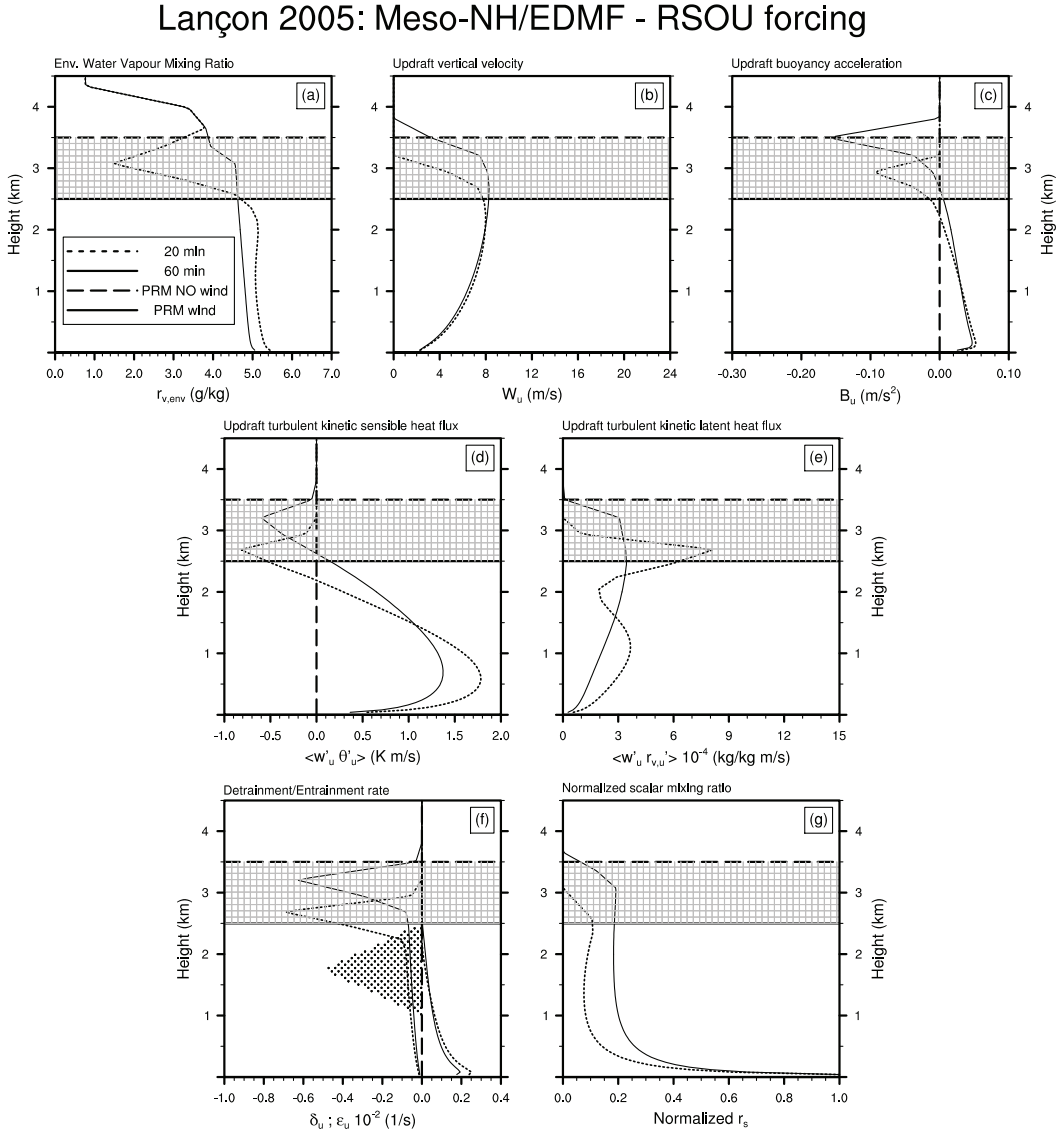

Figure 5.5: 1-D Meso-NH/EDMF results for the Lançon fire using the radiosounding of Nîmes as meteorological forcing. The quantities are: (**a**) environmental water vapour mixing ratio ($r_{v,env}$, g/kg); (**b**) updraft vertical velocity (w_u, m/s); (**c**) updraft buoyancy acceleration (B_u, m/s^2); (**d**) updraft turbulent kinetic sensible heat flux ($< w'_u\theta'_u >$, K m/s); (**e**) updraft turbulent kinetic latent heat flux ($< w'_u r'_{v,u} >$, kg/kg m/s); (**f**) detrainment rate when values are negative (δ_u, 1/s), entrainment rate for positive values (ε_u, 1/s); (**g**) normalized scalar flux. The horizontal solid (dashed) line is the plume top obtained with the environmental wind effect on (off) in the respective 1-D PRM simulation. The dot filled area indicates where the VMD has positive values.

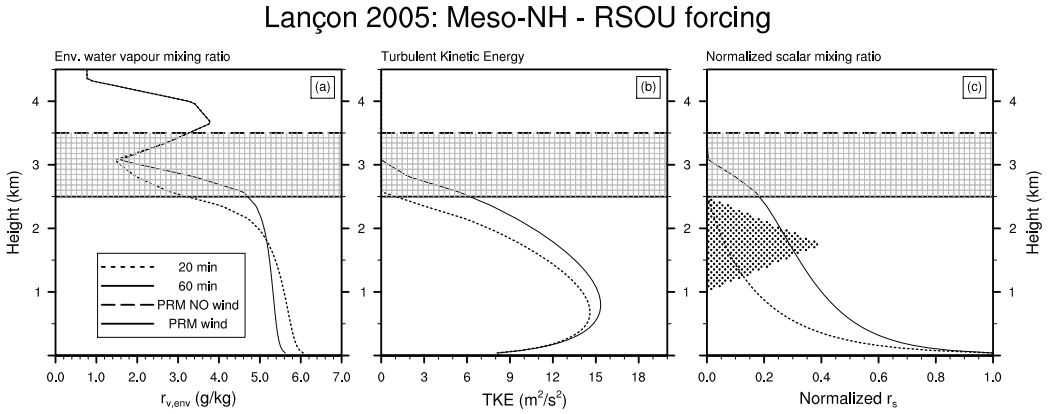

Figure 5.6: 1-D Meso-NH results for the Lançon fire using the radiosounding of Nîmes as meteorological forcing, without activating the EDMF scheme. The quantities are only referred to the environment: (**a**) environmental water vapour mixing ratio ($r_{v,env}$, g/kg); (**b**) turbulent kinetic energy (TKE, m^2 s^2); (**c**) normalized scalar mixing ratio. The horizontal solid (dashed) line is the plume top obtained with the environmental wind effect on (off) in the respective 1-D PRM simulation. The dot filled area indicates where the VMD has positive values.

non negligible difference in the ambient wind speed between the Mediterranean and the Amazonian atmospheric background (Sec. 5.2.3; Fig. 5.1 versus Fig. 5.2).

The 1-D PRM simulation forced with the ECMWF profile has a 700 m lower plume top (6.2 km, when including the wind drag) after around 40 minutes, and a 600 m thinner injection layer (from 3 to 6 km) with a maximum of 5% of mass around 4.8 km (Fig. 5.11c). At 1 km of altitude, the dynamic entrainment maximises using both forcings but with different values: 0.3 10^{-2} s^{-1} for the RSOU case, 0.1 10^{-2} s^{-1} for the ECMWF case. The influence of such a different contribution is still evident on the vertical profile of the total entrainment that decreases quasi monotonically along the vertical (Fig. 5.11b) compared to the more contrasted profile of the RSOU case (Fig. 5.9b).

The 1-D Meso-NH/EDMF simulation forced by the radiosounding reproduces an updraft top at 4.5 km. The detrainment zone is localized between 3 and 4.5 km, just overlaying the lower one third of the PRM injection layer (Fig. 5.10b). The injection height is 1.5 km lower than the value predicted by the 1-D PRM model. Although the well developed daytime mixed layer (Fig. 5.2b-c) and the surface heating associated with the fire, the buoyancy acceleration at the surface is nearly the half of the same parameter in the PRM model (Fig. 5.10a versus Fig. 5.9a). In the Meso-NH model, the influence of the ambient surface pressure seems not to be accounted for as observed for the 1-D PRM.

Using the ECMWF forcing, the convective updraft in the 1-D Meso-NH/EDMF model rises up to around 4.5 km and it detrains between 2.2 and 3.5 km maximising at 2.7 km

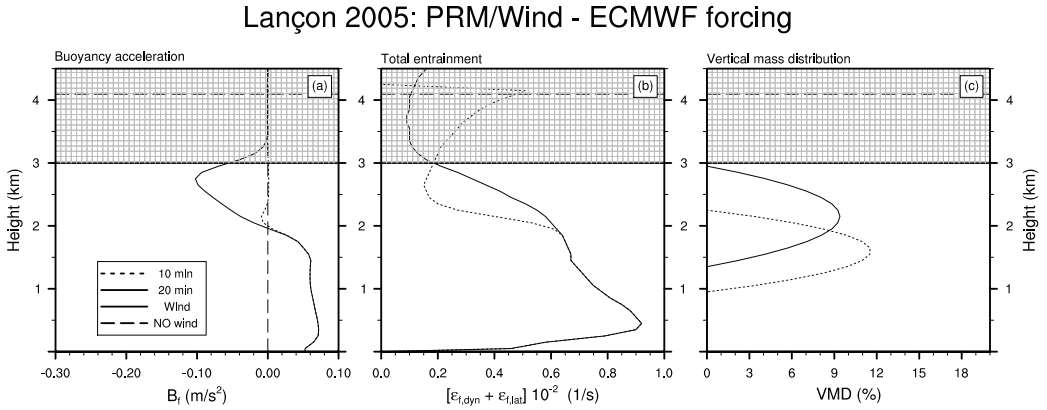

Figure 5.7: 1-D PRM model results for the Lançon fire using the ECMWF re-analyses as meteorological forcing. The quantities are: (**a**) buoyancy acceleration (B_f, m/s^2); (**b**) total entrainment ($\varepsilon_{f,dyn} + \varepsilon_{f,lat}$, 1/s); ; (**c**) vertical mass distribution (VMD, %). The solid line indicates the plume top obtained including the environmental wind effect; the dashed line is the plume top when the wind effect is off.

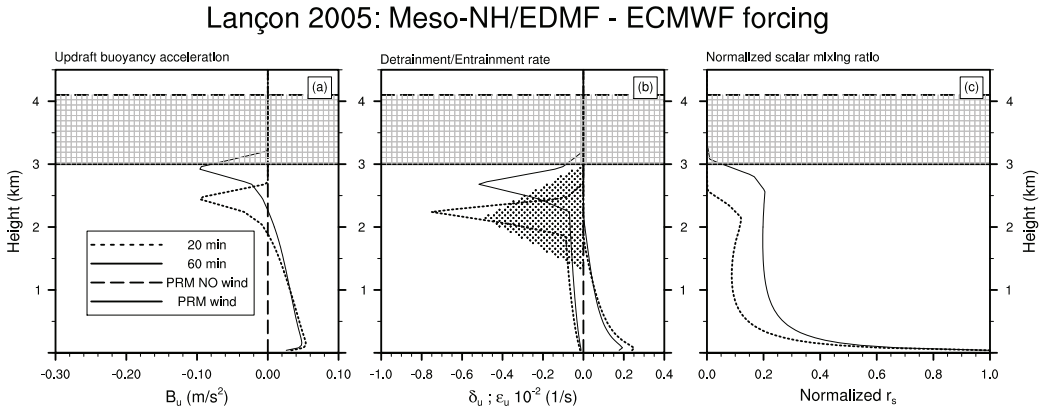

Figure 5.8: 1-D Meso-NH/EDMF results for the Lançon fire using the ECMWF re-analyses as meteorological forcing. The quantities are: (**a**) updraft buoyancy acceleration (B_u, m/s^2); (**b**) detrainment rate when values are negative (δ_u, 1/s), entrainment rate for positive values (ε_u, 1/s); (**c**) normalized scalar mixing ratio. The horizontal solid (dashed) line is the plume top obtained with the environmental wind effect on (off) in the respective 1-D PRM simulation. The dot filled area indicates where the VMD has positive values.

(Fig. 5.12b). Also in this case, the comparison of the injection layer is unsatisfactory with a gap of around 2 km. The less turbulent atmospheric background reproduced by the ECMWF re-analyses (Fig. 5.2b-c) determines weaker turbulent kinetic heat fluxes than the Meso-NH simulation forced by the radiosounding (not shown).

In contrast with general conclusions drawn for the Lançon fire, the 1-D PRM model predicts a higher injection height when forced by the radiosounding: even if the radiosonde recorded a stronger wind speed than the ECMWF re-analyses (hence a stronger dynamic entrainment), a stronger buoyancy acceleration is produced at the surface. Using the 1-D Meso-NH/EDMF model, the updraft stops rising at nearly the same altitude (4.5 km) for both forcings, while the detrainment zone and its maximun are located at different levels: 800 m higher when the environment is more turbulent (RSOU forcing). Concerning the comparison of the fire injection height as predicted by the two numerical models, the result is unsatisfactory: the Meso-NH/EDMF model is between 1.1 and 1.5 km lower than the PRM model. The main injection layers predicted by the two models partly overlay only for the case study initialised by the radiosounding.

Windy-wet case

Forced by the radiosonde, the 1-D PRM model simulates a plume top at 6.7 km (wind on) after around 50 minutes (steady state solution). The main injection layer is localized between 3.2 and 6.7 km and the injection heigth is around 5 km (Fig. 5.13c). The dynamic entrainment is 0.1 10^2 s^{-1} stronger than the calm-dry case implying a similar gap in the total entrainment (Fig. 5.13b versus Fig. 5.9b). At the surface, the buoyancy acceleration is about 0.06 m s^{-2} (Fig. 5.13a), comparable with the Rondônia calm-dry case forced by the radiosounding (5.9a).

In Figure 5.15, the 1-D PRM simulation initialised by the ECMWF profile has a fire plume that rises up to 8.9 km (wind on) after the whole integration time (60 minutes), since the effect of the ambient wind is weaker (lower values for the total entrainment in Fig. 5.15b) and the humidity of the air in the ECMWF profile is remarkably higher than the radiosounding (Fig. 5.3c). The main injection layer reaches out 4.7 km, from 4.2 to 8.9 km, and 3% of mass are injected at 6.5 km (Fig. 5.15c).

When forced by the radiosounding, the 1-D Meso-NH/EDMF model simulates an updraft top at 4.5 km (5.14). Once again, the 1-D Meso-NH/EDMF plume top is notably lower than the one predicted by the 1-D PRM model using the radiosonde. The detrainment zone is localized between 2.5 and 4.5 km and it shows two maxima: at 3 and 4.1 km (Fig. 5.14b). The higher maximum and the associated detrainment overlays the lower half injection layer simulated by the respective 1-D PRM simulation.

Figure 5.15 shows the results of the 1-D Meso-NH/EDMF forced by the ECMWF profile. The updrfat top is located at 5 km. The detrainment process presents two main zones of activity: a stronger one at 2 km, a weaker one at 4 km (Fig. 5.15b). This feature

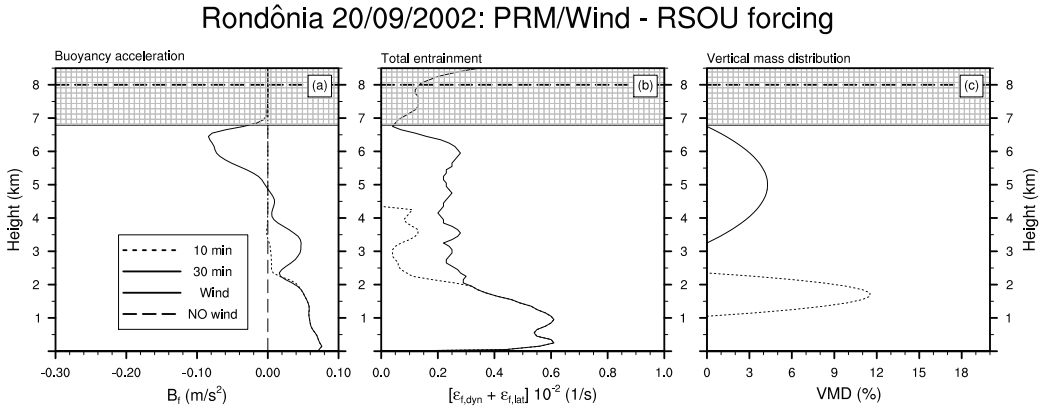

Figure 5.9: The same as Fig. 5.7 but for the calm and dry case of Rondônia (20/09/2002) using the radiosounding as meteorological forcing.

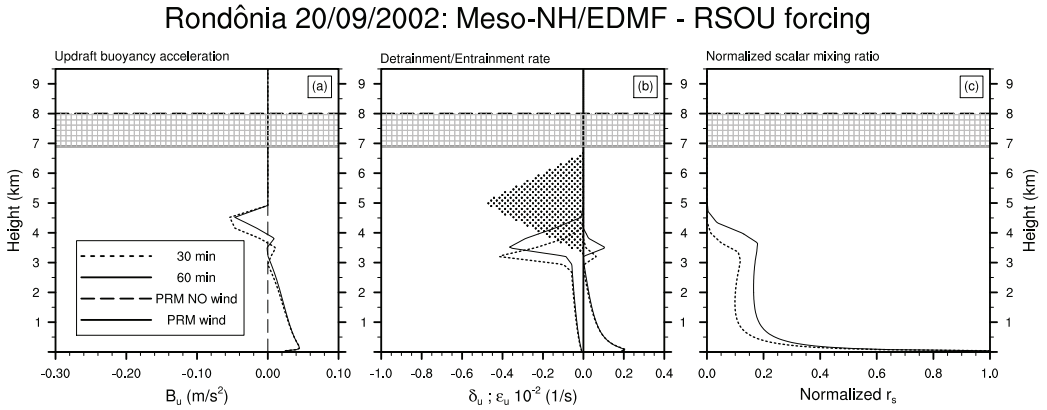

Figure 5.10: The same as Fig. 5.8 but for the calm and dry case of Rondônia (20/09/2002) using the radiosounding as meteorological forcing.

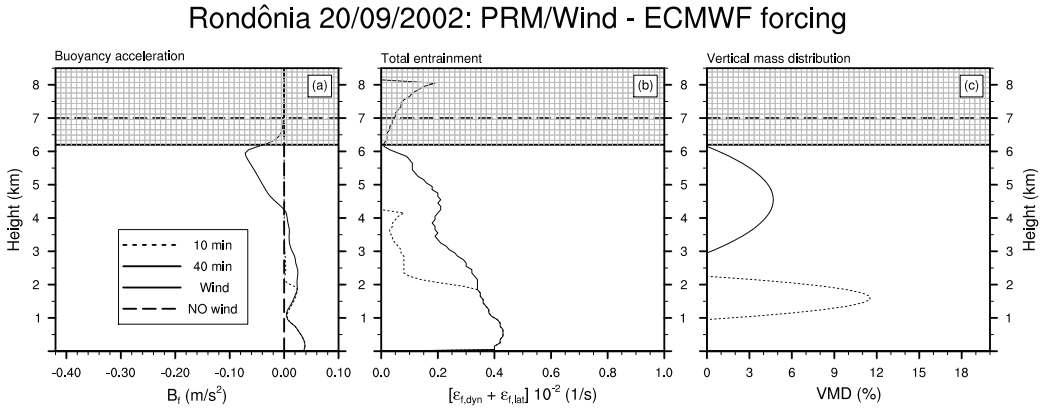

Figure 5.11: The same as Fig. 5.7 but for the calm and dry case of Rondônia (20/09/2002) using the ECMWF re-analyses as meteorological forcing.

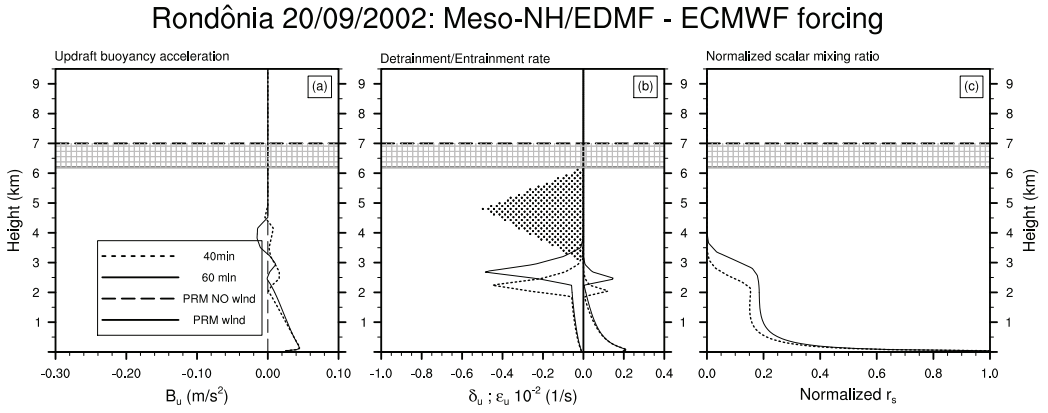

Figure 5.12: The same as Fig. 5.8 but for the calm and dry case of Rondônia fires (20/09/2002) using the ECMWF re-analyses as meteorological forcing.

influences the vertical profile of the scalar mixing ratio: above the first detrainment zone the fire tracer is rapidly transported along the vertical up to 5 km (Fig. 5.15c). Although the extent of the detrainment zone that stretches from 1.6 to 4.8 km, it does not overlay the vertical range of the respective VMD (Fig. 5.15b).

Regarding the PRM model, there is a difference of 1.5 km between the RSOU and the ECMWF case. This gap confirms the sensitivity of the model of Freitas et al. (2010) to the humidity and the wind pattern of the meteorological background: the ECMWF profiles show an atmosphere moister and less windy than the radiosounding (Fig. 5.3c-d). As observed for the calm-dry case, the Meso-NH/EDMF results do not record sensible variations, probably due to intrinsic limitations of the EDMF scheme, as it will be discussed in the following.The 1-D Meso-NH/EDMF model is not able to rise higher than 5 km, therefore the comparison with the 1-D PRM model is less satisfactory than for the calm-dry case. As for the calm-dry case, the comparison between the two numerical model is unsatisfactory, slightly better when using the radiosonde as meteorological forcing rather than the ECMWF re-analyses.

5.4.3 General discussion

Figure 5.17 summarizes the injection heights and layers as predicted by the PRM and the Meso-NH/EDMF models for the three documented fire cases. Looking at this graphic, at first glance an outstanding difference is observed between the Mediterranean (Lançon 2005) and the Amazonian wild-fires (Rondônia 2002): although the fire-induced heat fluxes for the Mediterranean case have higher values than the Amazonian ones (Table 5.1), the windy and dry metorological conditions of the Mediterranean Basin efficiently constrain the vertical development of the fire plume. This sensitivity is evident for the PRM model where the Mediterranean fire has an injection height that is 3-4 km lower than the Amazonian values, and the Mediterranean injection layer is nearly the half of those obtained for the Amazonian cases. The difference Mediterranean/Amazon is less definite for the Meso-NH/EDMF model that predicts fire injection heigths in a range between 2 and 4 km, with a quite similar width of the injection layer (except for the Rondônia windy-wet case where two well distinct detrainment zones are observed).

The kind of meteorological forcing also influences the evolution of the convective updrafts. For the 1-D PRM, the injection height records a variation in a range between 500 m and 1.5 km for the same wild-fire, whereas the extent of the injection layer is quite similar for both meteorological forcings, except for the Rondônia windy-wet where the main injection layer is 1.2 km wider using the ECMWF re-analyses rather than the radiosounding. The identified variabilities for the PRM model are highly influenced by the intensity of the ambient wind speed that determines, in turn, the intensity of the dynamic entrainment that governs the effectiveness of the wind drag; the humidity of the ambient air also plays an important role since, once moist air mixes with the updraft, the net

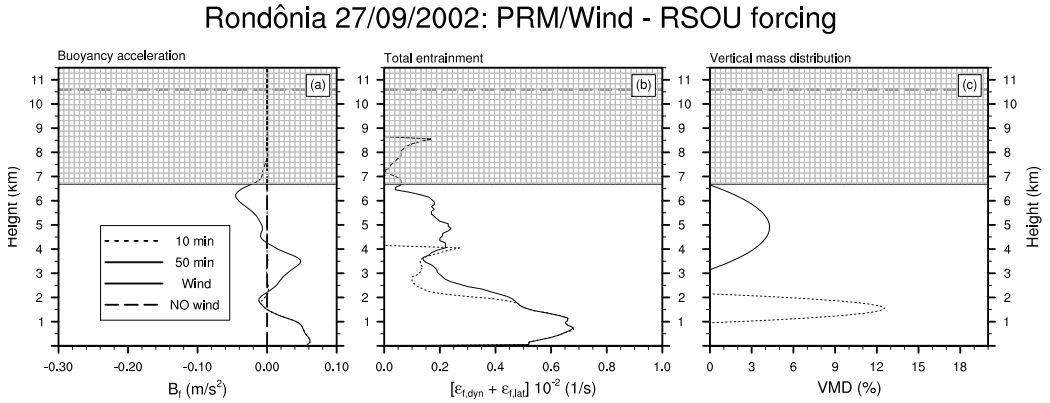

Figure 5.13: The same as Fig. 5.7 but for the windy and humid case of Rondônia fires (27/09/2002) using the radiosounding as meteorological forcing.

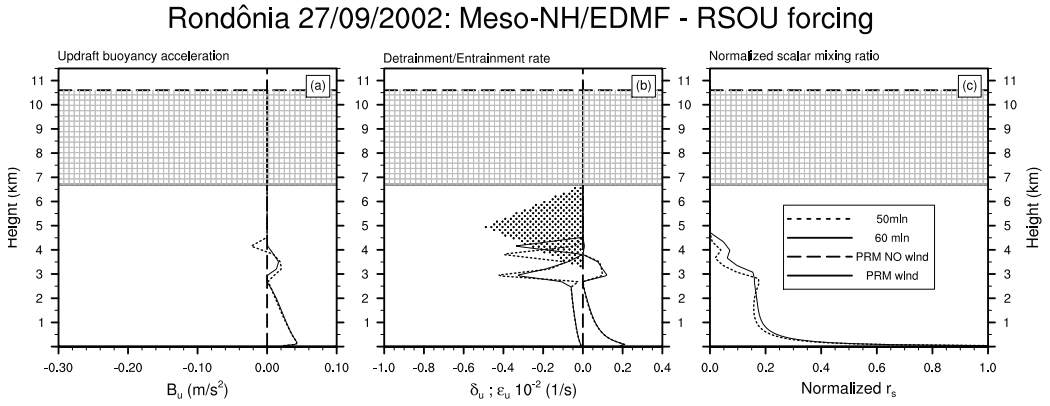

Figure 5.14: The same as Fig. 5.8 but for the windy and humid case of Rondônia fires (27/09/2002) using the radiosounding as meteorological forcing.

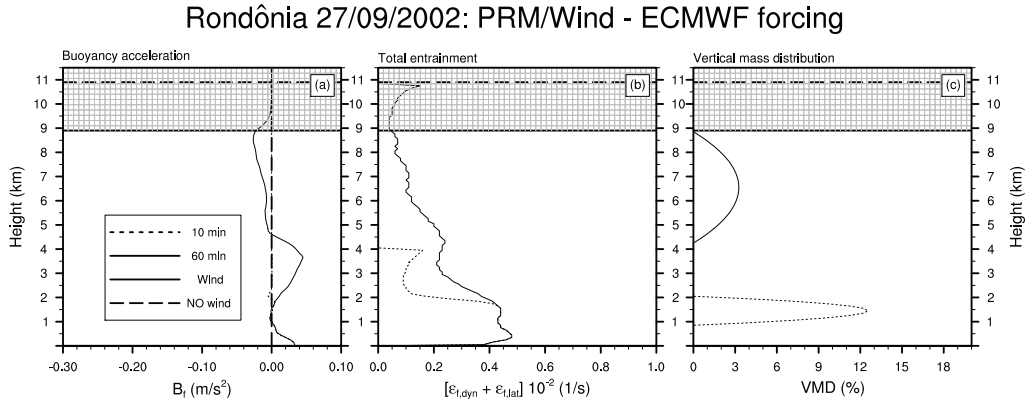

Figure 5.15: The same as Fig. 5.7 but for the windy and humid case of Rondônia fires (27/09/2002) using the ECMWF re-analyses as meteorological forcing.

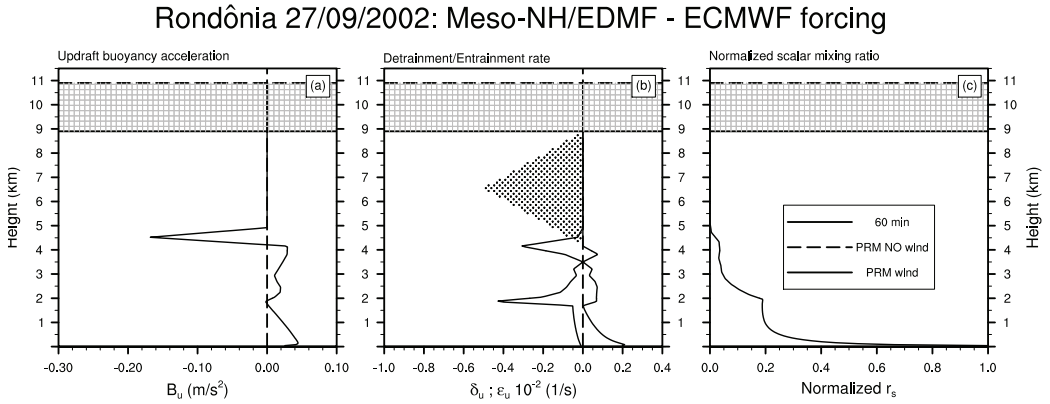

Figure 5.16: The same as Fig. 5.8 but for the windy and humid case of Rondônia fires (27/09/2002) using the ECMWF re-analyses as meteorological forcing.

result is to lighten the rising plume ($\rho_{dry} < \rho_{moist}$, e.g. Fig. 5.13 versus Fig. 5.15). For the 1-D Meso-NH/EDMF model, the level of maximum detrainment can vary between 500 m and 1 km between the two forcings. The 1-D Meso-NH/EDMF model is partly influenced by the atmospheric conditions in terms of turbulence that locally feed the turbulent flux of conservative variables (Chap. 3, Sec. 3.1.2.2, Eq. (3.4)): the less turbulent environment for the Amazonian cases depicted by the ECMWF re-analysed (Fig. 5.2b-c and 5.3b-c) leads to lower injection heights. However, significant values observed for the updraft turbulent kinetic latent heat flux in the Rondônia calm-dry case do not lead to a higher injection height. This model response is coherent with the thesis of Luderer et al. (2009) who state that the fire-released latent heat is of much lesser importance than the fire-released sensible heat.

Comparing the results from the two numerical models, the Meso-NH/EDMF model simulates 0.5-1 km higher injection heights for the Mediterranean wild-fire, and 1.5-3.5 km lower values for the Amazonian cases. These gaps can be ascribed to the different intensity of the entrainment of ambient air in the two approaches. The Meso-NH model takes into account only the lateral entrainment, while the PRM model includes the effect of ambient wind among the environmental factors that may feed the lateral mixing of the rising plume. In the PRM model, this approach results in a total entrainment coefficient at the surface that is always the double of the Meso-NH value. As a consequences, the in-cloud parcels mix more efficiently with the ambient air in the PRM frame; hence, if the surrounding atmosphere is dry and windy (as for the Mediterranean fire), the net result is a drag force, while a humid and less windy atmosphere can feed the rising of the plume (as for the Amazonian fires). For the Lançon fire, the two models simulate a fire injection height above the PBL, in contrast with the existing observations for the Lançon fire (Strada et al., 2012). For the Amazonian fires, there exist considerable differences between the two models. In particular, the 1-D Meso-NH/EDMF model simulates the injection heigths in the lower half of the troposphere, below the zero isothermal (at about 5 km). This is an intrinsic limitation of the current version of EDMF in Meso-NH. The EDMF parametrisation was implemented in the Meso-NH model to reproduce stratocumulus clouds. Its design implies some important features that strongly limit the vertical evolution of the updraft: (1) the altitude of the zero-isothermal is a vertical limit in the rising of the updraft, (2) the ice phase is not yet activated, and (3) the cloud layer can not exceed a fixed 3 km extent. Similarly, Rio et al. (2010) discussed the use of the EDMF scheme in configurations, such as wild-fire episodes, for which this parametrisation has not been initially developed for, possibly leading to deep convection.

In general, it is important to underline the intrinsic limitations of the design that has been chosen for the present study. The choice of a 1 km grid-mesh was justified by the aim to study the vertical evolution of a fire plume in the same configuration of the Lançon-de-Provence 2005 case study (Chap. 4). However, kilometric resolutions are intermediate scales for turbulence movements where these processes are not mainly resolved neither

entirely parametrised. Honnert et al. (2011) investigated the behaviour of atmospheric models at intermediate scales (the so called "Terra Incognita" of the turbulence, Wyngaard, 2004) and they identified some misleading results of atmospheric models due to the presence of too many resolved movements, when the turbulence scheme parametrises the subgrid thermal, or an overestimation of the subgrid part, when a mass-flux scheme is introduced. Concerning the PRM model, a burnt area that measures 100 ha is probably too large leading to a dilution of the entrainment of ambient air (see Eq. (5.21) and (5.22)), hence to a fire plume that rises fastly in the atmosphere and does not mix properly with the surrounding air: utilizing the radiosondes to force the PRM model, a difference of only 200 m is observed between the calm-dry and the windy-wet case. Forcing the PRM model by the radiosoundings, Freitas et al. (2010) observed a difference of nearly 1 km for the injection height between the calm-dry and the windy-wet case considering a burnt area of 10 ha; this difference was not observed when using a burnt area of 10 ha. In addition, at 1 km scale, the hypothesis of the grid size environmental air not impacted by the fire becomes questionable in the PRM model.

5.5 Conclusions and perspectives

When modelling wild-fires, the height of injection of fire products has a crucial importance for determining the distance and the direction the smoke will travel (Guan et al., 2010). The parameter of the fire injection height highlights the tight link that exists between the dynamics and the chemistry of a wild-fire: it depends on fire characteristics and meteorological conditions, and it determines the chemistry that will act on the fire plume. Nowadays, several studies have been carried out to define a database of seasonally and regionally divers plume heights in order to prescribe, or just validate, the fire injection height in CTM model. Another approach is represented by physically-based approachs, as the 1-D PRM model of Freitas et al. (2010) and the EDMF parametrisation implemented in the 1-D Meso-NH model.

In this chapter, sensitivity tests have been realised to compare the fire plume top predicted by the 1-D PRM and the 1-D Meso-NH/EDMF models. Three wild-fires have been chosen: a Mediterranean arson fire and two deforestation Amazonian fires. They distinguish from one another in terms of fire features and meteorological scenarios. Moreover, for each case, two meteorological forcings have been used to initialise each model: a radiosounding and a vertical profile from the ECMWF re-analyses. The predicted injection heights showed considerable differences from one model to the other and, for a given model, between ECMWF and radiosounding forcings. Compared to the 1-D Meso-NH/EDMF model, the 1-D PRM model simulates lower plumes for the Mediterranean case, higher for the Amazonian cases. The difference can attain 3-4 km for the Amazonian fires. The comparison for the Mediterranean fire gives injection heights between 2 and 3 km for both models. For the Lançon case, both models forecast a plume top above the

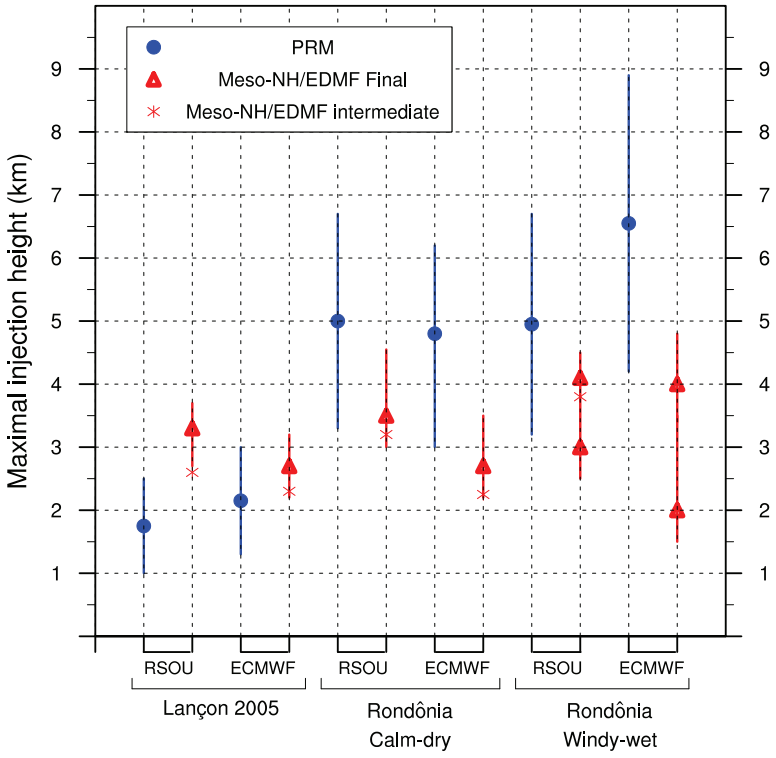

Figure 5.17: Fire injection height and plume base and top as predicted by the two numerical models. For each of the three wild-fires, the two numerical forcings are distinguished: RSOU for the radiosonde, ECMWF for the re-analyses. The blue dots show the steady state solution attained by the PRM model, and they correspond to the level of maximum VMD with the associated width of the injection layer (blue error bar). The red triangles represent the final result given by the Meso-NH/EDMF model (after 60 minutes of simulation): they correspond to the level of maximum detrainment with the associated extent of the injection layer (red error bar). Red crosses are the intermediate results of the Meso-NH/EDMF model at the time of the steady state solution of the PRM model.

BL, although there are evidences that the Lançon fire plume propagated near the surface (Strada et al., 2012). The evolution of the fire plume in the 1-D PRM model seems to be mainly influenced by the ambient wind and humidity. There exists an important difference in the theoretical definitions of the two numerical models: the 1-D PRM model is designed to reach a steady state solution because it does not influence the dynamics and the thermodynamics of the environment; while the 1-D Meso-NH model acts as a single column model where the evolution of the convective updraft perturbs the atmosphere during the whole integration time. Moreover, the PRM model always predicts a fire plume that takes off from the ground. The PRM was designed to feed a 3-D host (CTM) model with the information of the fire injection height; hence, the prescribed elevation of the fire plume may lead to an artificial depletion of the mixing layer in the host (CTM) model in terms of fire products.

Some limits have been identified for both models concerning the chosen configuration: they are forced in the "Terra Incognita" (Wyngaard, 2004; Honnert et al., 2011) of the turbulence, and at a resolution where the fire is supposed to impact the environmental air. Actually, some developments are in progress concerning the activation of the ice phase in the EDMF frame (S. Riette, personal communication) to properly induce the transition from shallow to deep convection. These developments are expected to significantly improve the accuracy of Meso-NH. Moreover, sensitivity tests have to be run on more documented fire episodes (e.g. the Quinault fire; Trentmann et al., 2003; Freitas et al., 2007), and at resolutions higher than kilometric scales in order to study the behaviour of Meso-NH when the atmospheric dynamics is fully resolved, as it is shown in the next chapter.

Chapter 6

A coupled fire/atmosphere model at the fire scale

Contents

The major source of uncertainty in wildfire behaviour prediction is the transient behaviour of fires due to changes in flows in the fire's environment (Sun et al., 2009). Coupled fire/atmosphere models incorporate the ability of the fire to affect its own local weather (Clark et al., 1996; Filippi et al., 2009; Mandel et al., 2011). These interactions however cover multiscale processes (see Chapter 2). Since it is not possible to consider all these scales in the same model, compromises in the choice of processes to be modeled and parametrisation are critical (Mandel et al., 2011). The previous chapters presented modelling exercises at kilometric resolution and pointed out the dilution of the fire effect on the atmosphere due to the burning area smaller than the atmospheric grid mesh (Trentmann et al., 2003). The underestimation of the fire impacts in terms of emissions and heat flux to the atmosphere is a current limitation to better assess the impact on atmospheric chemistry and dynamics. To overcome this limitation, a novel approach is described in this chapter based on a two-way fire/atmosphere coupling at high LES resolutions. Since Clark et al. (1996) it has been shown that an important range of wildland fire behaviour could be captured by the coupling of a mesoscale weather model with a simple fire spread model. In Filippi et al. (2009) the MesoNH-ForeFire coupled model was applied on idealized experimental configurations. The authors found that the coupled model was able to reproduce the convective effects of the heat produced by the fire on the atmosphere. Mandel et al. (2011) presented the coupled WRF/SFIRE model which could run on a cluster faster than real time and at fine resolution in dekameters.

The present chapter presents the fully coupled fire/atmosphere model MesoNH-ForeFire with important numerical improvements coded since the version in Filippi et al. (2009) (Chap. 3, Sec. 3.3.2). For the first time, the coupled model was applied to real cases and the impact of the two-way coupling between the fire and the atmosphere was discussed.

6.1 Resume of the research article

The brand-new version of the coupled model MesoNH-ForeFire has undergone a two-step validation process: first, 5 idealized cases have been run in order to compare the semi-physical coupled model MesoNH-ForeFire with the fully-physical one HIGRAD/FIRETEC (Linn et al., 2002); then, the potential of the MesoNH-ForeFire model has been tested on two real-case scenarios and qualitatively compared with observations.

The theoretical base of the semi-physical ForeFire model, the front tracking method and the coupling method were described in Filippi et al. (2009) and in Chapter 3. The coupled model version used in this study was significantly improved by the collaborators at the SPE laboratory with regards to the parallelization of the code that has significantly reduced the simulation time. The ForeFire model itself has been improved and is now able to estimate if a fire can or cannot pass through a non-burnable area (i.e. at each time step, fuel parameters are checked ahead of all fire markers along its normal at a distance equal to the fire front thickness). In addition, ForeFire can take the fire fighting

into account, if information are available.

In order to test the realism of the coupled simulations, the MesoNH-ForeFire model was compared to a sophisticated 3-D computational fluid dynamics and combustion simulator: the HIGRAD/FIRETEC model. In their study, Linn et al. (2002) proposed and solved a partial set of idealized configurations that reproduce five different topographies (flat, canyon, hill ridge, and upcan terrains), without using actual field observations. They used the fully-resolving Navier-Stokes simulator, HIGRAD/FIRETEC, explicitly designed to be applied at very fine scales (some meters, Chap. 3, Sec. 3.3.1). The MesoNH-ForeFire model was run at rougher scales (some tens of meters), taken the Linn et al. (2002) test cases as a reference. The simulated results clearly show that taking into account fire/atmosphere coupling always improves the simulated MesoNH-ForeFire Rate of Spread (RoS): there is a better agreement with the reference simulation of HIGRAD/FIRETEC, even if there exists an underestimation in all cases. Running the same tests without the fire/atmosphere coupling (i.e. the feedback of the fire on the atmospheric wind is not considered), the uncoupled RoS is even lower than the coupled RoS and the depth of the fire front is smaller in the uncoupled case than in the coupled one.

The coupled model MesoNH-ForeFire was applied to simulate two typical Mediterranean large wildfires that occurred in the Corsican region in 2007 (the Vazzio fire) and in 2009 (the Favone fire). Both fires were favoured by stable, dry and windy meteorological conditions. Simulations were run at the typical resolution of LES; an equally high-resolution database was used for topography and vegetation, with non-burnable areas now taken into account by the coupled model. Atmospheric conditions were initialized with radiosoundings taken from the Ajaccio station (1 km away from Vazzio; 51 km away from Favone). For the selected fires, model's behaviour is qualitatively similar to the real fire in simulating the fire propagation. The smoke plumes contours and evolution showed interesting similarities with pictures taken during the fire episodes.

The results from the simulations obtained using the MesoNH-ForeFire coupled model are promising in terms of plume behaviour and fire wind effect. The improvement in terms of simulation time thanks to the parallelization is tangible (few hours for a medium size fire on a small cluster) and make it suitable for operational forecasting and simulations including gas and aerosols for the survey of air pollution and health effect.

6.2 Simulation of Coupled Fire/Atmosphere Interaction with the MesoNH-ForeFire Models

Hindawi Publishing Corporation
Journal of Combustion
Volume 2011, Article ID 540390, 13 pages
doi:10.1155/2011/540390

Research Article

Simulation of Coupled Fire/Atmosphere Interaction with the MesoNH-ForeFire Models

Jean-Baptiste Filippi,[1] Frédéric Bosseur,[1] Xavier Pialat,[1] Paul-Antoine Santoni,[1] Susanna Strada,[2] and Céline Mari[2]

[1] *SPE-CNRS UMR 6134, Campus Grossetti, BP 52, 20250 Corte, France*
[2] *LA-CNRS UMR 5560, OMP, 14 Avenue Edouard Belin, 31400 Toulouse, France*

Correspondence should be addressed to Jean-Baptiste Filippi, filippi@univ-corse.fr

Received 15 January 2011; Accepted 16 May 2011

Academic Editor: William E. Mell

Simulating interaction between forest fire and atmospheric processes requires a highly detailed and computationally intensive model. Processing this type of simulations in wildland fires forbids combustion-based models due to the large amount of fuels to be simulated in terms of quantity and diversity. In this paper, we propose an approach that couples a fire area simulator to a mesoscale weather numerical model in order to simulate local fire/atmosphere interaction. Five idealized simulation cases are analysed showing strong interaction between topography and the fire front induced wind, interactions that could not be simulated in noncoupled simulations. The same approach applied to a real-case scenario also shows results that are qualitatively comparable to the observed case. All these results were obtained in less than a day of calculation on a dual processor computer, leaving room for improvement in grid resolution that is currently limited to fifty meter.

1. Introduction

Wildland fires are influenced by many physical processes, from which several of them directly stem from the atmosphere behaviour such as wind or humidity, showing a direct influence of the atmosphere on the fire. Feedback from the fire to the atmosphere has been studied and observed since the fifties [1], and several attempts to model and simulate fire-atmosphere interaction have been successful since then.

Among the most recent numerical studies of fire/atmosphere interaction, Mell et al. [2] have obtained with the wildland-urban interface fire dynamics simulator (WFDS) model a good correspondence between numerical results and real prescribed burning experiment of Australian grassland Cheney and Gould [3]. Similar numerical results were obtained by Linn et al. [4] using the HIGRAD/FIRETEC model performing several numerical investigations with different topography and wind conditions, but, unlike Mell et al. [2], no comparison to actual burns were made in these academic cases. These models focus on the processes of solid fuel pyrolysis, heat transfer, gas phase combustion, and *local* fire-atmosphere interaction that are essential to the physical mechanisms involves in fire spread. Nevertheless simulating these interactions at the scale of their appearance (i.e., the combustion scale) requires a highly detailed and computationally intensive model that is nowadays not reachable for actual wildland fires. Moreover, it is rarely possible to gather sufficient data to initiate a simulation at the level of detail required for such simulations.

On other hand, less physically detailed models based on the fire area simulator, such as FARSITE, are of a prime interest to the people who fight wildfires, and taking into account more of these coupled physical effects may permit to enhance the accuracy of such models.

The proposed approach has been developed to enable numerical fire/atmosphere coupling between available mesoscale atmospheric models (WRF, Meso-NH, etc.) with the family of fire area simulators. Numerical fire/atmosphere coupling has already undergone numerous studies, starting from the static fire simulations of [5] to more recent works where a simplified model of Rothermel type [6] fire spread is coupled with the so-called Clark-Hall atmospheric model [7]

or the WRF mesoscale model [8]. While efforts at simulating coupled effects were fruitful even at the scale of large fires (several square kilometres), the use of Rothermel model may be subject to caution as effects of wind and slope on the rate of spread are expressed through coefficients that are experimentally fitted to wind values and usually uncorrelated. Moreover, the wind input into a fire area simulator, such as the Rothermel model, when used in a current operational setting, is almost always a near-surface single (temporal and spatial) mean wind provided by either a weather observing station (often hundreds of kms away from the fire) or predicted by a weather forecast model with resolution on the tens-of-kilometer scale at best. The operational forecast for surface fire propagation is, therefore, based on an input wind *as if the fire was not here*, that is, no local heterogeneous change in the wind field and fire behaviour due to the fire/atmosphere coupling can be taken into account.

In an effort to tackle these problems, a fire area simulator, named ForeFire, based on the propagation speed model of Balbi et al. [9] has been developed. In order to investigate fire/atmosphere coupling while aiming for operational ForeFire simulation code, it has been coupled with the Meso-NH model [10]. In an approach similar to Clark et al. [7], the mesoscale atmospheric model is coupled to a reduced front tracking wildfire model. This setup allows investigations on the differences induced by the atmospheric feedback in terms of propagation speed and behaviour. The main originalities of this combination resides in the fact that Meso-NH is run in a Large Eddy Simulation (LES) configuration and that the rate of spread model used in ForeFire provides a physical formulation to take into account effect of wind and slope.

2. Numerical Models and Coupling Method

In order to numerically couple the atmospheric and fire models, one has first to determine the physical phenomena responsible for the actual coupling.

Modelling the effects of the atmosphere on the fire (influence of the wind, humidity, etc.) represents a complex topic and has undergone a lot of studies. Modelling such a strong nonlinear dependence (moreover when slope is taken into account) has forced operational fire simulators such as Farsite to consider really simple models (usually, it is assumed that propagation velocity is linear with respect to the wind velocity normal to the front). This influence was also a challenge even for nonoperational research-oriented fire simulators fire simulators like FIRETEC or WFDS. In our case, these phenomena are embodied in the theoretical (and physicallybased) model of Balbi et al. [9] for the propagation speed that is presented hereafter.

Concerning the feedback from the fire on the atmosphere, one should take into account several phenomena such as heat transfer by means of convective heating and radiation and modification of the roughness of the canopy. In this first attempt to investigate the numerical coupling of both models solely energy fluxes from the fire front are taken into account as atmospheric model boundary conditions. Still, the fire spatial scales are usually much lowers than the scale of resolution of the atmospheric (typically the order of hundreds-of-meter in our simulations). Thus, the front tracking method used to simulate the fire front needs a higher resolution than the atmospheric model.

2.1. Fire Propagation Model and Simulator. The rate of spread (ROS) model for the fire front (see, [9]) is based on the assumption that the flame is acting lake a tilted radiant panel heating the vegetation in front of it. It provides an analytical formulation of the propagation speed accounting for slope, wind speed, and fuel parameters effects. It belongs to the family of Rothermel-like models in the sense that the fire behaviour is only described by the mean of the propagation velocity of the fire front. Although more complete than the Rothermel formulation, several physical assumptions on the flow are made in order to derive the rate of spread R in order to provide a computationally reachable for operational-use fire area simulator (unlike models solving the full Navier-Stokes equations like WFDS or FIRETEC).

Readers are referred to Balbi et al. [9] for full derivation of the model. For self-consistency, we will review here the major assumptions.

(i) Shape of the flame is assumed triangle with the base size on the ground given by the depth of the front in the normal direction.

(ii) Velocity in the flame is the geometric sum of the wind at the flame location and the buoyancy velocity.

(iii) Pre-heating is only induced by radiation (no heat convection).

(iv) Input air flow in the flame is supposed stoichiometric.

(v) Degradation kinetic is constant over time; that is, heat release from a flaming fuel is constant over the burning time R_T.

(vi) Propagation is normal to the existing front.

In the end, the model for the propagation speed of the front R can be summarized in

$$R = R_0 + A\frac{R}{1 + (R/r_0)\cos\gamma}(1 + \sin\gamma - \cos\gamma), \quad (1)$$

with R_0 the propagation speed in case of null wind and no slope (to be measured) and a the radiant coefficient.

The flame tilt angle relative to the ground normal γ (which includes wind U, buoyancy effect u_0 and slope α) is given by

$$\tan\gamma = \tan\alpha + \frac{U}{u_0}. \quad (2)$$

Model parameters are either fitted, or can be deduced from fuel properties (see, Balbi et al. [9]). Given this velocity in supposedly each point of the fire front, a Lagrangian front tracking method is used for simulating the evolution of the fire front and, by the means of historical fronts, also the evolution of the burning area.

ForeFire [11] simulation code uses the velocity model in order to integrate the front surface over time using a front tracking method. In this Lagrangian method, the fire front line is decomposed into a set of connected points or markers. According to the configuration of the two neighbouring markers, each marker is affected with a normal vector to the front pointing to the unburned material, as shown in Figure 1. As the front shape is represented as a polygon, the normal vector is approximated as the bisector angle. The front is propagating towards the outside of the polygon (in white in Figure 1), while markers are linked in the clockwise direction.

The velocity of each marker is given by the rate of spread model of Balbi et al. [9] and the direction that coincides with the normal to the fire front. This method has been selected due to its computational efficiency, and the ability to simulate the propagation of an interface at high resolution (less than one meter) needed to take into account different vegetations, roads, houses, and fire breaks over a large area typical of a wildfire accident (hundreds of square kilometres). Indeed, by advecting the markers by less than one meter at each step, the fuels seen by the markers can be spatially fine-grained so as to have nonburnable areas such as roads or fire breaks. To estimate if a fire can or cannot pass a nonburnable area, fuel parameters are checked ahead of all fire marker along its normal at a distance equal to the front thickness.

The fire front thickness is constructed by looking into the history of the fronts. Each marker has a "parent" marker, and each parent keep in memory the time of ignition. With a simple tracing back of the parents till one is found to be completely burned (the current time is superior to the sum of the ignition time and the burning time τ), one can find the rear of the fire area and thus the thickness of the fire front. It should be noted that this calculation of the front thickness is only an approximation of the theoretical front thickness in the direction of the normal needed in Balbi et al. [9], but allows for highly nonstationary effects when the fire front crosses discontinuities (in fuels, humidity, or topography, for example).

2.2. Meso-NH Atmospheric Model. Meso-NH is an anelastic nonhydrostatic mesoscale model [10] intended to be applicable to all scales ranging from large (synoptic) scales to small (large eddy) scales and can be coupled with an online atmospheric chemistry module. For the fire coupling application, Meso-NH is run in large eddy simulation configuration ($\Delta x \leq 50$ m) mode without chemistry. Turbulence parameterization is based on a 1.5-order closure [12], with a prognostic equation for turbulent kinetic energy in 3D. We selected open boundary condition for all tests. Momentum variables are advected with a centered 4th order scheme, while scalar and other meteorological variables are advected with a so-called monotonic piecewise parabolic method [13]. The externalised surface module SURFEX (aimed at providing physicallybased boundary conditions to Meso-NH at ground level) is used for the fire feedback in the simulation.

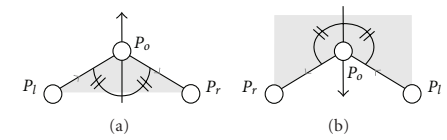

Figure 1: Front tracking and markers. Circles represent markers along the firefront line. Arrows show the propagation vector (bisector of the local angle at the marker P_0 between the point at left, P_l, and point at right, P_r). Grey area represents the burned fuel.

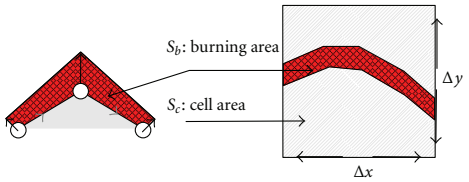

Figure 2: Integration of burning area. Red shape represents the fire front. Integration is performed on each atmospheric cell to compute the ratio of the burning area over the cell area.

2.3. Coupling Atmospheric and Wildfire Model. Finally, a specifically designed coupling component performs the simulation synchronisation, the data transformation, and interpolation.

The wildfire model acts in the atmospheric model as a new boundary condition, that is, injecting a heat flux Q_e ($\mathrm{W\cdot m^{-2}}$), a water vapour flux Wv_e ($\mathrm{kg\cdot m^{-2}}$), and a radiant temperature T_e (K). Polygon clipping is used to derive the burning surface of an atmospheric cell (noted S_b) over the total cell area noted S_c ($\Delta x \Delta y$) (Figure 2). The burning ratio for each atmospheric grid cell is noted $Rb = S_b/S_c$.

As only a portion of the cell is burning, an equivalent radiant temperature for the whole cell is averaged from a nominal flame temperature (T_n) and the soil temperature from the atmospheric model (T_s). T_e is given by

$$T_e = \sqrt[4]{(1 - R_b)T_s^4 + R_b T_n^4}. \tag{3}$$

Equivalent heat fluxes corresponding to the energy of the hot gaseous column over an atmospheric cell is approximated from a nominal convective heat flux (Q_n) with $Q_e = R_b Q_n$. Finally, equivalent water vapour fluxes, representing the amount of water vapour evaporated from the vegetation is interpolated over an atmospheric cell from nominal water vapour content (Wv_n) with $Wv_e = R_b Wv_n$.

T_n is a fuel model parameter between 950 and 1100 K experimentally measured and different for oil/resin/lignin rich vegetation, and for all experiments, it has been set to 1000 K. T_s is the day temperature at the ground level. Wv_n, is taken as the water content of the fuel per unit area.

The operation is performed for all atmospheric grid cells at ground level, that is, constructing three matrices that are passed to the atmospheric model as additional boundary conditions at the beginning of each time step of the atmospheric model.

Table 1: Experimental parameters, with A: Radiant factor, R_0: rate of spread without wind and slope, r_0 flame thickness speed factor, u_0: flame gas velocity, R_T: fire residence time, Q_n: nominal heat flux, Wv_n: nominal water vapor flux, and T_n: nominal radiant temperature.

A	R_0	r_0	u_0	R_T	Q_n	Wv_n	T_n
1.5	$0.1\,\mathrm{m\cdot s^{-1}}$	$0.01\,\mathrm{m\cdot s^{-1}}$	$5\,\mathrm{m\cdot s^{-1}}$	30 s	$250\,\mathrm{kW\cdot m^{-2}}$	$0.1\,\mathrm{kg\cdot m^{-2}\cdot s^{-1}}$	1000 K

Concerning the effect of the atmosphere on the fire propagation, wind is interpolated in space using a bicubic method at the very location of the markers and in time by assuming the values of the wind, humidity, and all atmospheric variables to be constant throughout the atmospheric time step. All atmospheric model values are approximated from the first atmospheric level. Slope angle in the fire propagation direction is estimated from the elevation difference between the elevation at the fire marker and the elevation at the location projected after the estimated burning time R_T. Each elevation is also obtained a bicubic interpolation method.

3. Idealised Experimental Setup

In order to evaluate the ability of the proposed coupling approach and estimate the coupled influences of topography and wind on fire spread, five tests were run corresponding to a partial set of configurations proposed by Linn et al. [14] and solved by the same authors using fire spread model designed for smaller scales than the one presented here, thus making these simulations a reference for models designed for large wildfires. It should be pointed out that the configurations of Linn et al. [14] are idealized and were not compared to actual field observations. Given the paucity of observations in real-case scenario, the only available method of evaluation of models like MNH/ForeFire is the direct comparison with "reference" simulations such as the ones carried by Linn et al. [14].

The domain size is set to $640*320*500$ m for all cases and discretized for the atmospheric model with a Cartesian grid whose parameters are a horizontal spacing of 16 m (in both direction of the ground) and an average vertical spacing of 20 m. Boundary conditions were taken as open boundary conditions.

Base functions used to create the different topographies are taken from Linn et al. [14], which functions are used to create an idealized flat, canyon, hill ridge, and upcan terrains. In these simulations, the vegetation was modelled as a grass fuel bed with an inhomogeneous canopy with details as fine as discrete trees. As this level of refinement is not directly relevant to our propagation, model vegetation in our simulations is assumed homogeneous in the domain for all simulations. These values are based on mean values deduced from experimental studies [15] which exhibited rate of spread at flanks (relatively unaffected by wind or slope) close to the ones simulated by Linn et al. [14]. This resulted in an average dry fuel load of $7\,\mathrm{kg\cdot m^{-2}}$ and parameters given in Table 1.

Atmospheric model background wind field is exactly the same for each case, with values of $6\,\mathrm{m\cdot s^{-1}}$ constant in height. Ignition line in all cases is set to a 60 by 8 meters fire line located at the centre of the domain. A passive scalar tracer with a distribution set to the burning ratio of each grid point and for each atmospheric time step is used as a marker for smoke injection.

Figures 3, 4, 5, 6, and 7 present the simulation results for the flat, canyon, hill, ridge, and upcan cases 120 s after ignition. In all the figures, the red indicates the fire burning at the time of the snapshot, whereas the grey area represents the same front in an "uncoupled" simulation. The terms uncoupled stands for simulations without the two-way coupling of the fire and atmosphere considered here; that is, the atmospheric simulation is still performed, and winds at the Lagrangian marker location are still given by the interpolation of the atmospheric data. Slope is computed equally in each case, and thus, the only difference between the red and grey plots is taking into account the feedback of the fire on the atmosphere (influence of the atmosphere on the fire is modelled equally in both cases).

In the flat case (Figure 3(a)), the flow remains largely unaffected behind the fire. The simulation reveals an area of confluence ahead of the front with some recirculation that is located at the base of the fire plume (Figure 3(b)). The plume is relatively weak, affecting the flow to an altitude of 60 m over ground. Overall flow speed does not greatly differ from the original flow speed of $6\,\mathrm{m\cdot s^{-1}}$. However, local enhancement of the surface velocity due to the coupling between the fire and the atmosphere leads to a greater ROS at the head of the fire compared to the noncoupling case. This effect can be attributed to the induced wind being taken into account in the coupled simulation.

The canyon case (Figure 4) clearly enlightens the strong influence of taking into account the coupling between fire and atmosphere in the simulation of the fire dynamics. In that case, the surface wind is strongly decreased in the canyon by topographic effects. These effects are not fully compensated by the increased slope, and we observe weaker ROS than in the flat case. In such scenario, the induced wind plays a major role in the dynamics of the fire spread, and the use of a coupled model results in increased ROS and better accounting of the physics.

With the same slope and same wind speed, the Hill case (Figure 5) presents a slightly different behaviour. The area of confluence is located here ahead of the fire front, so the maximum wind speed are just over the fire head. The resulting tilt angle results in a stronger ROS and a larger burning injection area. The effects of considering a coupling between the atmosphere and the fire are also of prime importance in the prediction of the rate of spread. In the hill case, the predictions issued by noncoupled simulations can be as low as half the rate of spread predicted during coupled simulations.

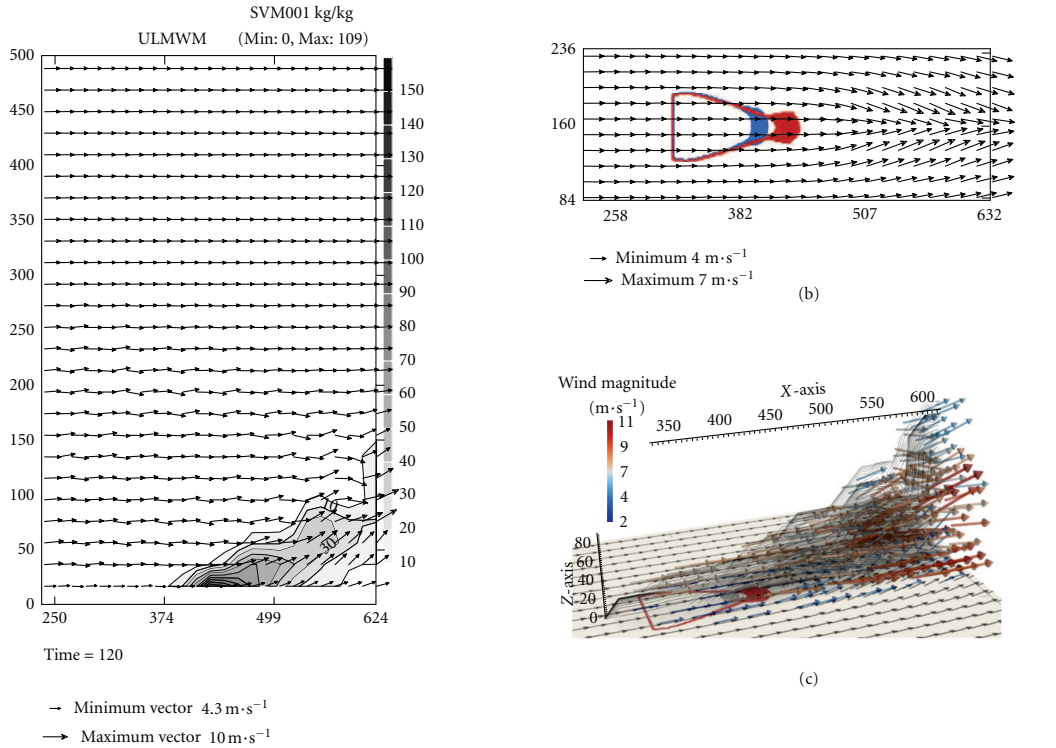

FIGURE 3: FLAT (a) Horizontal section (x/y) at $Z = 10$ m, fire lines after 120 seconds for the coupled (red) and noncoupled (grey) simulations. Arrows denote the wind vectors at ground level for the coupled case. (b) Cross-section (x/z) of the coupled case at $Y = 160$ m, shading represents concentration of the injected passive tracer. (c) 3d wind field and passive tracer concentration isocontours.

Results for the ridge test case are presented in Figure 6. The topographic effects results in a widening of the burning area in the transverse direction of the wind due to slope gradient in that direction. In this case, the effect of taking into account the feedback from the fire on the atmosphere has less drastically changed the propagation speed of the front but still has a major influence on the depth of the fire front.

Results for the upcan test are shown in Figure 7. The narrowing of the fire head compared to the ridge case is of factor 3 in our case, whereas Linn et al. [14] results show a factor around 2. But in this case, simulating with a coupled approach provides much higher rates of spread than in the noncoupled simulation, accounting for the strong induced wind in the upcan.

Finally, Figure 8 presents for all cases the propagation distance of the fire front in the wind direction for three different types of simulations:

(i) results of Linn et al. [14] using FIRETEC, that is, where the fire propagation is resolved using a fully-resolving Navier-Stokes simulator,

(ii) results of ForeFire for uncoupled simulations, that is, Rothermel-like propagation model with no feedback from the fire on the atmosphere is accounted for,

(iii) results of ForeFire for coupled simulations, that is, Rothermel-like propagation model with injection of heat, vapour, and passive scalar.

One can relate directly relate the rate of spread to the derivative of the propagation distance plotted in Figure 8, and thus make comparison on the behaviour of each model. As the FIRETEC simulations account for more physical phenomena than our simulation, it is assumed that the results of Linn et al. [14] represent the reference simulations.

Compared to FIRETEC results, uncoupled and coupled simulations both show an underestimation of the rate of spread in all cases. This is especially the case at the beginning of the simulations when the propagation model used in ForeFire is not able to capture the unsteady effects taking place in the transition regime. Though the underestimation can be partly imputed to the fuel properties which are different in our simulations and those of Linn et al. [14],

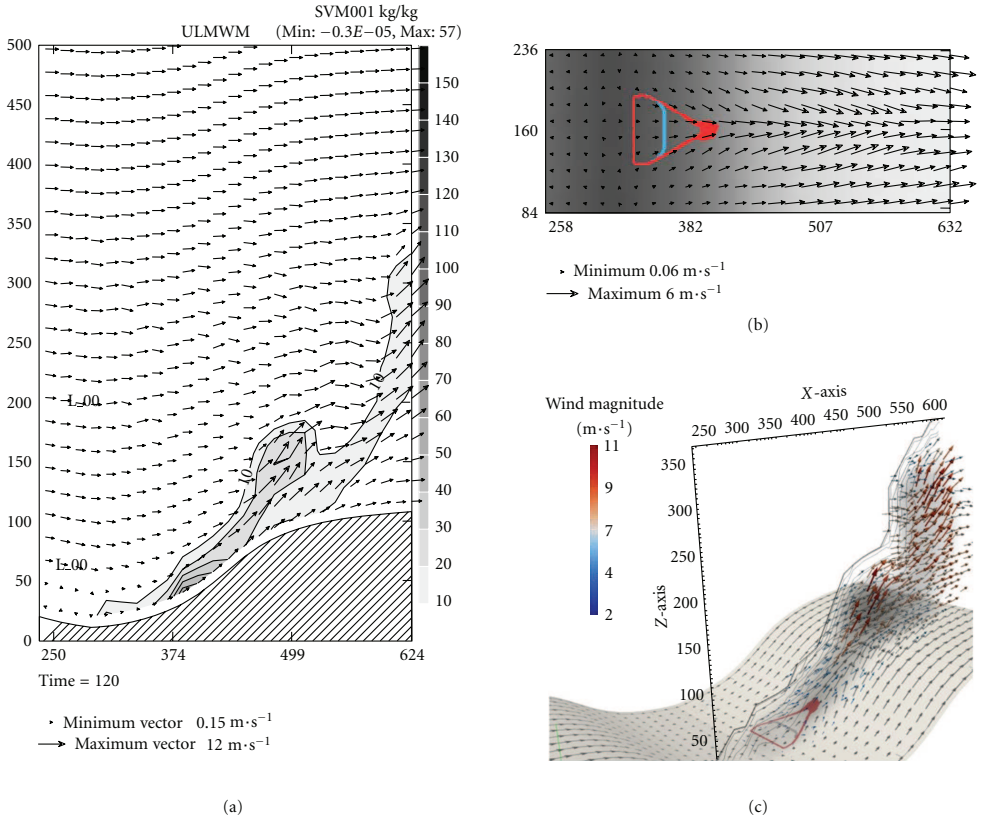

Figure 4: CANYON (a) Horizontal section (x/y) at $Z = 10$ m, fire lines after 120 seconds for the coupled (red) and noncoupled (grey) simulations. Arrows denote the wind vectors at ground level for the coupledcase. (b) Cross-section (x/z) of the coupled case at $Y = 160$ m, shading represents concentration of the injected passive tracer. (c) 3d wind field and passive tracer concentration isocontours.

we decided not to change the parameters of the propagation model in order to assess only the effect of considering a full fire/atmosphere coupling.

Figure 8 shows that taking into account fire/atmosphere coupling always improve the results in terms of propagation distance. The term "improve" should be taken as "results are in better agreement with the reference simulation of FIRETEC". These improvements are of two types.

On one hand, the flat ridge and canyon cases exhibit only a quantitative improvement in the prediction of the propagation distance. Indeed, no change in the behaviour of the fire front is observed between uncoupled and coupled simulations. This is best seen in the canyon and flat cases where the propagation velocity tends to very low values whereas FIRETEC simulations do not show that kind of behaviour. These low values of rates of spread in our simulations are the consequences of a narrowing of the head front in our homogeneous ground-level vegetation, whereas in FIRETEC simulations, it is supposed that the fire propagates mainly in the crown.

On the other hand, in the hill and upcan cases, one definitely needs a coupled simulation in order to obtain subtle effects such as velocity enhancement by the fire and be able to predict plausible rate of spread. In these cases, simulations without fire/atmosphere coupling exhibit a different behaviour from the coupled ones as the rate of spread tends to very low values if uncoupled, whereas coupled simulations show rates of spread similar to the ones observed in Linn et al. [14].

While only comparing model to model, the level of accuracy (and computational cost) of both models are different and comparing results from a fire area simulator coupled to an atmospheric model such as ForeFire/MNH to a Navier-Stokes solver such as FIRETEC is once again a good way of assessing our model's results. As a consequence results show that taking into account fire/atmosphere coupling seems mandatory even in fire area simulator such as ForeFire. The authors believe this is a promising way of improvement of such simulators that should not be overlooked while fitting a Rothermel-like propagation model.

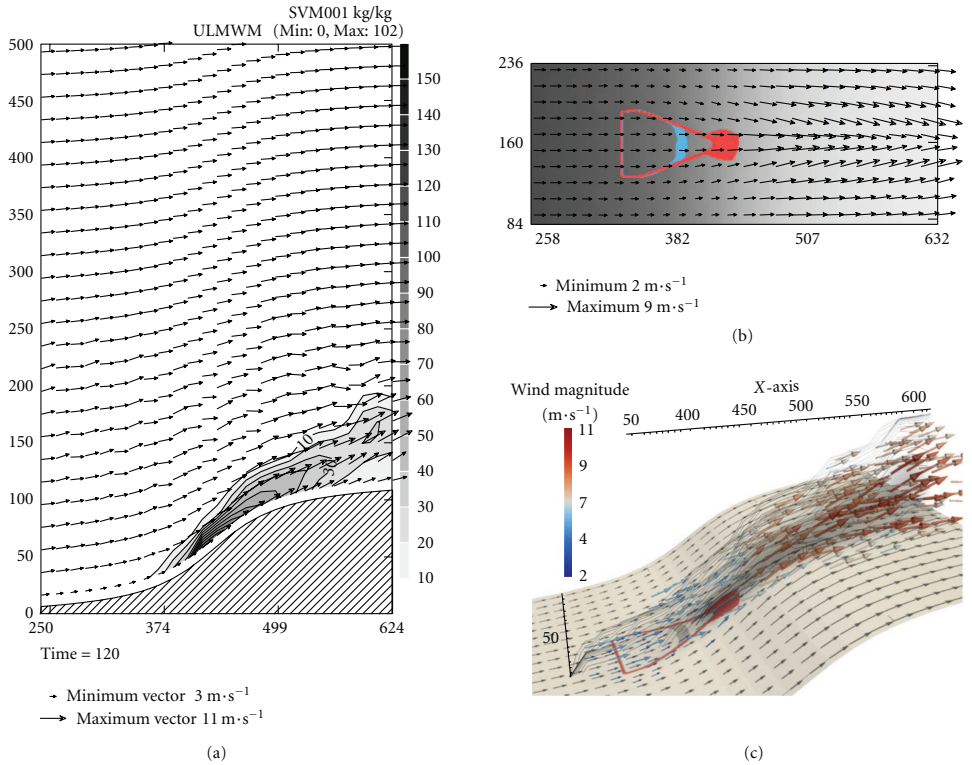

FIGURE 5: HILL (a) Horizontal section (x/y) at $Z = 10$ m, fire lines after 120 seconds for the coupled (red) and noncoupled (grey) simulations. Arrows denote the wind vectors at ground level for the coupledcase. (b) Cross-section (x/z) of the coupled case at $Y = 160$ m, shading represents concentration of the injected passive tracer. (c) 3d wind field and passive tracer concentration isocontours.

4. Real-Case Simulations

The aim of coupling a fire area simulator (with underlying Rothermel-like model) to an atmospheric is to build a computationally affordable numerical tool for operational use while providing a frame for later improvements based upon physics. We then performed simulations of the coupled approach in two real-case scenarios (relatively well-documented fires). These two fires occurred in the Corsican region, thus facilitating access to fuel data available.

4.1. Simulations Setup. The coupled simulations were run on a 2.5 km × 2.5 km × 1.5 km domain discretized on a 50 × 50 × 30 mesh for the atmospheric model simulation ($\Delta x = \Delta y = \Delta z = 50$ m). Topography is given by the BDTOPO (IGN database) with a precision of 50 m. Vegetation is extracted from the IFN database and classified between a homogeneous Mediterranean Maquis where fuel is present and nonburnable areas representing roads and buildings.

Both atmospheric conditions were initialized with radio soundings taken from the Ajaccio station at mid-day on the day of the fire (Figure 9).

Simulations were run on a Xeon 3.0 Ghz processor (4 cores) for which it approximately takes 4 hours of simulation to obtain one hour of spreading in the real physical space. In those simulations, the fire propagation accounts for less than 5% of the total CPU time, and exact timing is difficult to point because the front tracking algorithm consumption depends of the number of markers in the simulation.

Vegetation in both simulations consisted of shrubs, similar to the fuel model described in [15]. The only differences with model parameters of Table 1 is the vegetation water content, that is reflected by a larger R_0, water vapor emission, and a lower u_0. For both cases, vegetation water content was assumed to be similar, as it corresponds to three consecutive days without rain, reaching ambient humidity (60% relative air humidity in both cases) (Table 2).

Case 1 (Vazzio). The Vazzio fire occurred on the 16th of October 2007 near. The fire ignited around 14:30 on a day with stable and dry meteorological conditions, with a ground temperature of 20 degrees. The radiosounding made at the airport about three kilometers away at 12:00 gives a sustained westerly wind of about 4 to 5 m·s^{-1} with gusts of about the

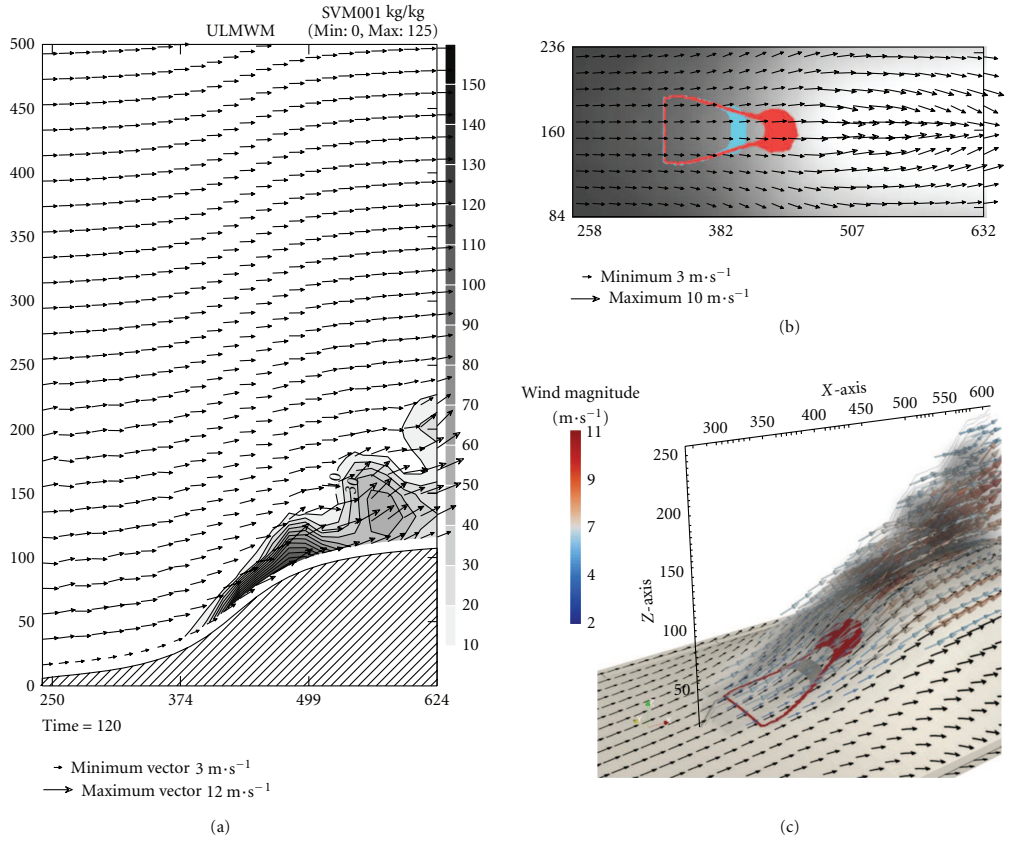

Figure 6: RIDGE (a) Horizontal section (x/y) at $Z = 10$ m, fire lines after 120 seconds for the coupled (red) and noncoupled (grey) simulations. Arrows denote the wind vectors at ground level for the coupledcase. (b) Cross-section (x/z) of the coupled case at $Y = 160$ m, shading represents concentration of the injected passive tracer. (c) 3d wind field and passive tracer concentration isocontours.

Table 2: Experimental parameters, with A: Radiant factor, R_0: rate of spread without wind and slope, r_0 flame thickness speed factor, u_0: flame gas velocity, R_T: fire residence time, Q_n: nominal heat flux, Wv_n: nominal water vapour, flux and T_n: nominal radiant temperature.

A	R_0	r_0	u_0	R_T	Q_n	Wv_n	T_n
1.5	0.12 m·s^{-1}	0.01 m·s^{-1}	4 m·s^{-1}	30 s	250 kW·m^{-2}	0.03 kg·m^{-2}.s^{-1}	1000 K

same magnitude. The wind changed direction during the event, but as no radiosounding are available to account for wind changes, the simulation was run with only the westerly forcing wind. The fire experienced almost free propagation till 15:40 and was finally stopped around 18:30 and was fought mainly over the head of the front by air attack. It burned up to 0.60 km^2 of land with the burned area contour reported in Figure 10.

Case 2 (Favone). The Favone fire occurred on the 8th of July 2009 near the village of Favone (south east Cosica). The fire was detected at 15:00 and experienced almost free propagation till 16:30 under a sustained and whirling wind of about 4 to 5 m·s^{-1}. The fire was fought for protection along its flanks, passed the road at 16:00 and arrived to the sea at 16:15. Total extinction of the fire was declared at 19:00, with a total burning area of 25 ha. As in the Vazzio case, direct comparison between simulations and observations are to be handled with care as no fire fighting is taken into account in simulations (taking the fire fighting into account is possible, but information about fire fighting is scarce).

As for the first case, atmospheric conditions were stable and dry with a ground temperature of about 27 degrees and a west westerly wind of about 5 m·s^{-1}.

4.2. Results and Discussion. For the selected fires, it was not possible to gather specific quantitative measures over the fire plume (such as plume height or smoke concentration at

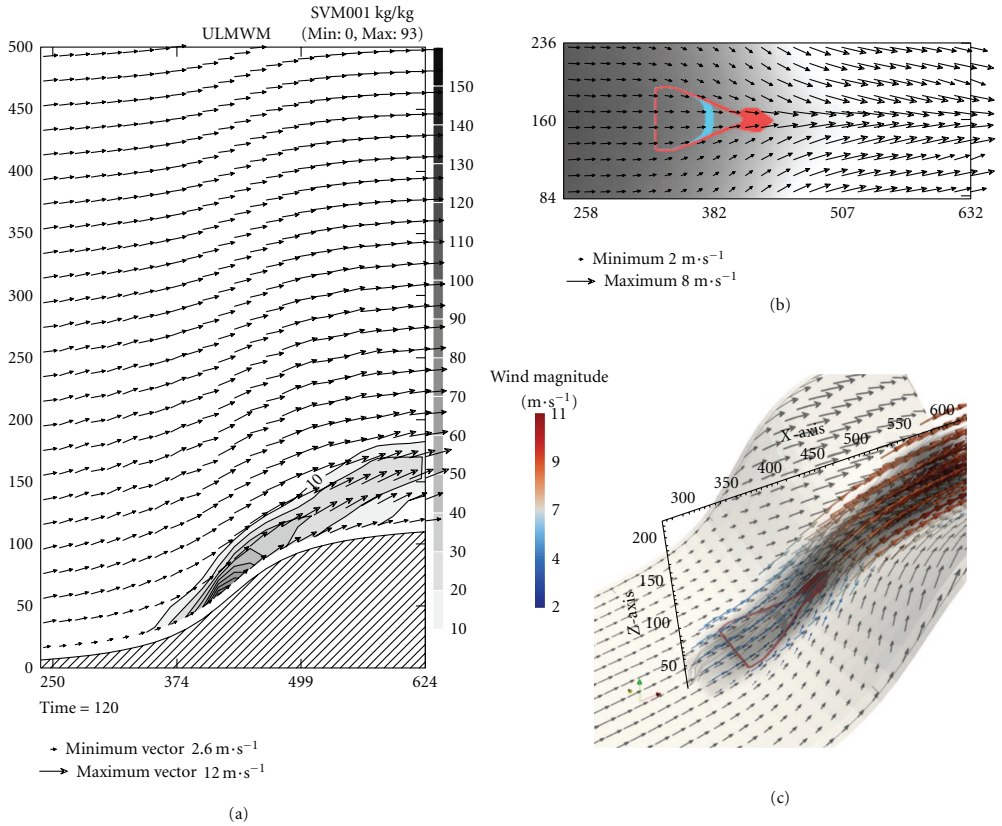

Figure 7: UPCAN (a) Horizontal section (x/y) at $Z = 10$ m, fire lines after 120 seconds for the coupled (red) and noncoupled (grey) simulations. Arrows denote the wind vectors at ground level for the coupledcase. (b) Cross-section (x/z) of the coupled case at $Y = 160$ m, shading represents concentration of the injected passive tracer.

specific points); nevertheless, a qualitative analysis is possible since some pictures were taken during those fires, thus enabling some qualitative verification. As the goal of the simulation is to be used as a decision support system, a satisfying verification would be to compare the general aspect of the plume as well as the modification of the wind field that affects the front. For all simulations, smoke concentration is given in unit$\cdot$m^{-3} and corresponds to the passive scalar tracer, with one unit being injected every second per mater square. Wind is provided in m$\cdot$s^{-1}.

A general behavior observed in both cases is the separation of the plume in two distinct area, the first one (from the front to about 500 meters) is the strong convective column and a second one, more diffuse, where the atmospheric flow is transporting the smoke into the atmosphere.

Results are in qualitative agreement with this behavior in both cases (Figures 10 and 11). In Case 1, the first part of the fire plume appears as a concentrated, opaque, and thick area of smoke that becomes suddenly diffuse. In Case 2 (Figure 11), both parts are separated, with the upper part changing direction while catching higher atmospheric winds. Both changes in direction and shape are in accordance with the tephigrams (Figure 9), where a ground atmospheric layer of about 100 meters high can be observed as a faster drop in temperature.

Another observation that can be made on Figure 11 (Case 2) is the initial separation of the plume into two parts, one on each flank of the fire. From the picture, we can note that the two flanks are generating two plumes that are later rejoined just over the most active front of the fire. Simulation well reproduced this behavior with the same initial separation of the plume that are merging while on top of the most active part of the front. While these two convective columns appears to be clearly separated, it is difficult to analyze and draw a picture of the flow along the columns and distinguish clear contrarotative behavior as simulation outputs at discrete time steps mainly represent eddies moving along these columns.

Figure 12 shows a thick plume that is transported over the sea with very little smoke reaching the shore. Similar

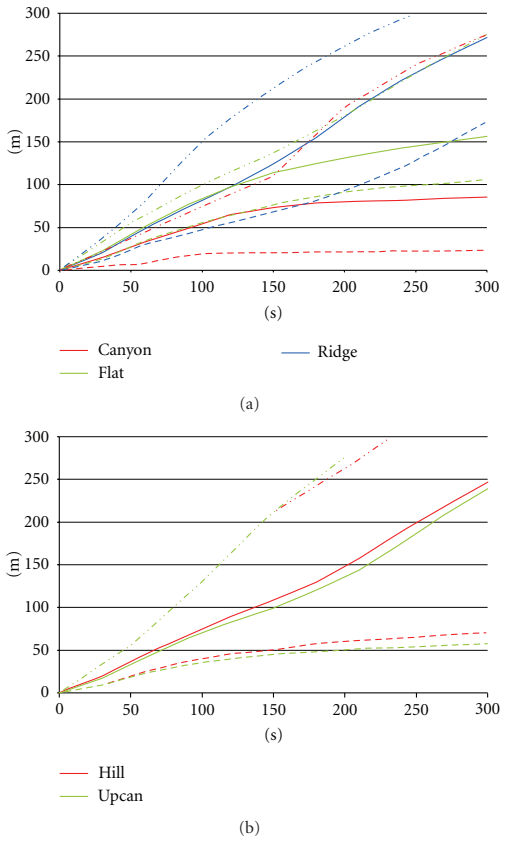

Figure 8: Propagation distance of the fire front function of time for the Canyon, Flat, Ridge cases (a) and Upcan, Hill cases (b). Firetec results are represented in dashed-dotted lines, while uncoupled results are shown by dashed lines and coupled results in plain lines.

behavior is observed in the simulation, with the front arriving approximately at the same time over the road as a thick, well-formed plume. Nevertheless, it appears that the angle between the plume plane and the sea plane is not well represented, but without knowing the exact time of the picture or the time of ignition, it is not possible yet to use this observation as a qualitative measure for the validation.

For all simulations, the structures of the simulated plume are not as refined as in the real one, but this is mainly due to the relatively low refinement of the grid for the atmospheric simulation (50 m). Simulated direction and height of the plume are similar to the observed ones. Nevertheless, dispersion seems to be underestimated in our simulation as the plume expansion is slightly lower in the simulation. This drawback supposedly mainly stems from the coupling fluxes injected by the fire simulation. As explained earlier in this paper the forcing fluxes from the fire are the heat flux, the flux of water vapor and the radiant temperature. Thus, no turbulent kinetic energy is directly injected in the atmospheric simulation, and thus, the fine structures of characteristic length less than 50 m (observed in the fire and assumed to contribute to the agitation of the atmosphere) are not taken into account in the present coupling.

Figures 13 and 14 present the intermediate and final front shape for Cases 1 and 2. One major feature of the proposed model is the ability to simulate topographic effects such as fire confinement by crests. In Figure 12 (Case 1), we can observe that the simulated contours reported in Figure 12 are in better agreement with the observations concerning the north side of the fire front, where changing slope effects have maintained the fire on one side of the hill. With a constant, noncoupled wind field, the simulated front is passing over the hill, which is less in accordance with the observed fire.

A major effect of the coupled wind field for Case 2 (Figure 14) is the acceleration near the ignition point. A direct consequence of this wind acceleration is that the backfire is propagating much slower, with a better accordance with observation.

Nevertheless, a side effect of the wind acceleration near the front in coupled simulation is to constrain the front on the flanks. For both cases, it appears that coupled simulation does underestimate the side propagation of the fire; it is particularly true in the Favona fire (Case 2), as this fire was fought on its flanks and is still underestimated by the simulation.

Plotting the general surface wind field for both simulations is not possible due to the fact that fields from the coupled simulation are dynamic and constantly changing during the simulation.

5. Conclusions

In order to be able to simulate subtle but nonetheless important physical phenomena such as induced wind or smoke dispersion, a coupled model has been developed synchronising the MesoNH atmospheric model with the physically based Lagrangian front tracking ForeFire wildfire simulator. With a straightforward coupling method, the atmospheric model is able to simulate the atmosphere dynamic induced by the fire and the subsequent effects on the RoS with meaningful results.

The five idealized scenarios allowed simulating induced flow patterns similar to those observed from simulations done by Linn et al. [14] with HIGRAD/FIRETEC. Transverse topological effects seem to be of more importance in our model as the widening/narrowing of the head fire is significantly greater in our simulations. The main feature of these simulations still remains that the fire head spread rate in the wind direction exhibits similar behaviours to those found by Linn et al. [14] in coupled simulations. The use of such fire/atmosphere coupling is mandatory in two of the five cases to retrieve behaviours similar to those simulated with FIRETEC. Results show large improvements in the prediction of the propagation distance along the wind direction for all cases when using coupled models. Rates of spread are still underestimated but show a much stronger qualitative

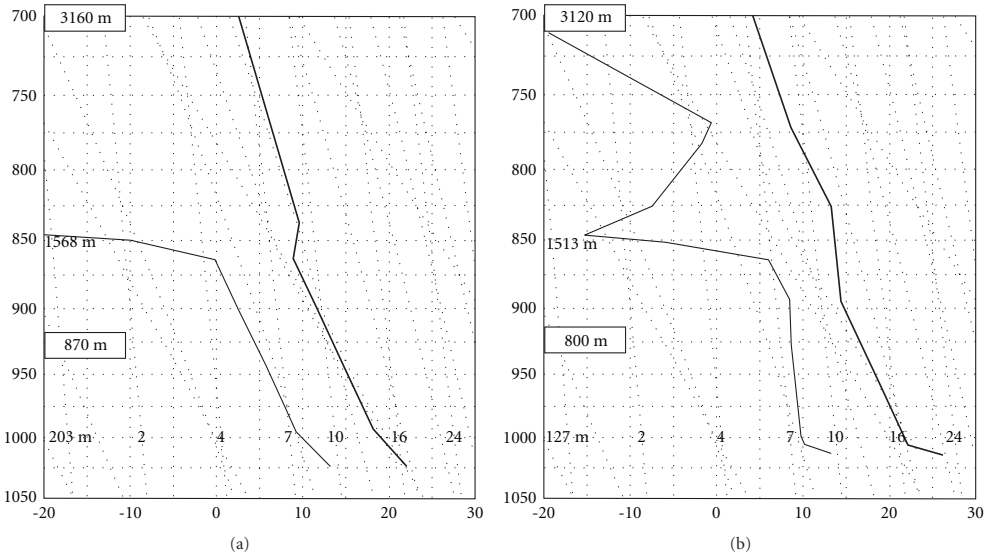

Figure 9: Tephigrams to 700 mb for Case 1 (a) and 2 (b). Thicker line represent Temperature and thinner line the dew-point temperature. Wind profile for each case is represented by wind arrows on the right side of each graph.

Figure 10: Case 1: Simulated and observed plume. Simulated plume is given 1 h after the fire ignition (the blue contour represents the fire front at that time) as the observation was taken approximately at the same time.

agreement with the reference simulations. This behaviour is of particular interest, as performing HIGRAD/FIRETEC simulations of the flow and fire patterns over a complex vegetation distribution with high resolution is nowadays computationally unreachable for large-scale wildland fires.

The proposed coupled model was then applied to two real-case scenarios and compared with observations. Model's behaviour is qualitatively similar to the real fire in simulating the fire propagation in terms of plume behaviour, with apparent plume similarities based on pictures taken the day of the actual fire. Nevertheless, while the front velocity formulation used in this study was not built to use input wind "as the fire was not there", it is still remains a rather parametric model that must be enhanced.

The objective in this paper was to move from fire area model with forced wind fields to coupled wind field that could represent the local perturbations affecting fire behaviour. As such, and considering the relatively small computational time (few hours for a medium size fire on a small cluster), these simulations seem to provide yet a good insight in terms of plume behaviour and fire wind effect.

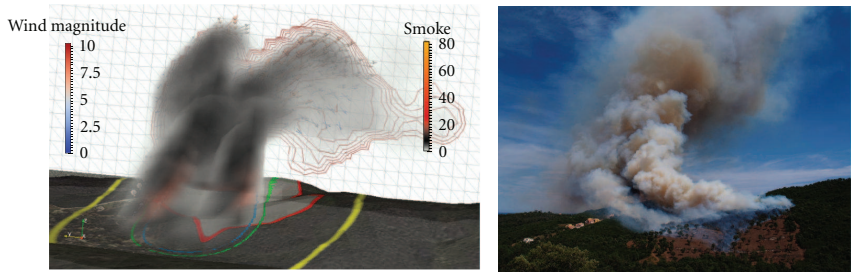

Figure 11: Case 2: Simulated and observed plume. Simulated plume is given 50 minutes after ignition (the blue contour represents the fire front at that time) with observation taken approximately at the same time.

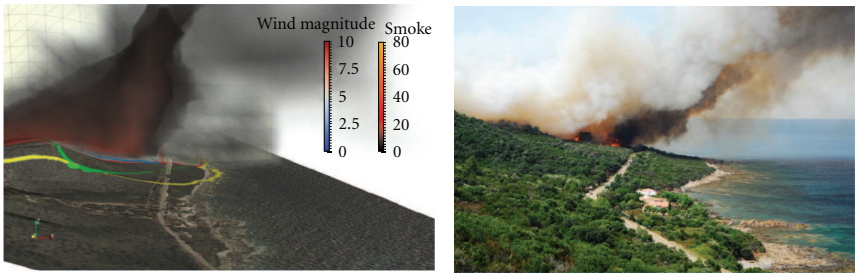

Figure 12: Case 2: Simulated and observed plume. Simulated plume is given 50 minutes after ignition (the blue contour represents the fire front at that time) with observation taken approximately at the same time.

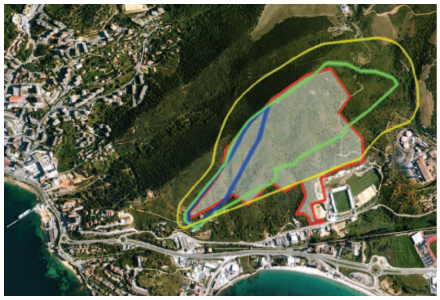

Figure 13: Case 1: Simulations results and observations for the Vazzio fire. Blue: simulated fire contour at 15:30 (after 1 h), Green: simulated contour at 18:30, Yellow: Simulated contour at 18:30 (non coupled); Red: final observed contour of the fire.

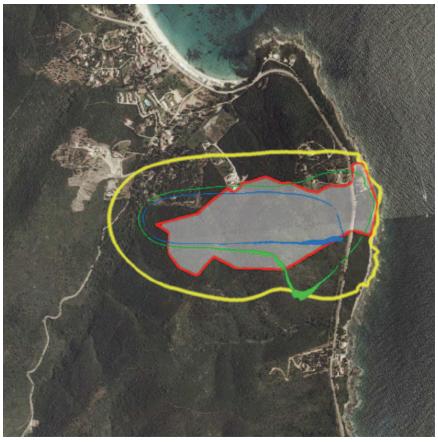

Figure 14: Case 2: Simulations results and observations for the Favone fire. Blue: simulated fire contour at 15:50 (after 50′′), Green: simulated contour at 19:00, yellow: simulated contour at 19:00 (non coupled); Red: final observed contour of the fire.

As a decision support tool, coupled simulation may help to forecast plume size, transport dispersion and smoke concentration at the ground, information of prime importance to protect the population, and anticipate the visibility loss for the fire fighters and civil transport in general.

More work is now carried out on the forest fire propagation code in order to use a better, nonparametric, description of fire fuels. Further enhancements are also planned to perform simulation of large past fire and simulation with the online chemistry module of Meso-NH to investigate fire smoke and particle transport and validation with LIDAR measurements.

Acknowledgments

Authors wish to thank the MesoNH team that helped developed the coupling. This research is developed within the IDEA project ANR-09-COSI-006-01. Field data was compiled in the scope of project PROTERINA-C supported by the EU under the Thematic 3 of the Operational Program Italia/France Maritime 2007–2013, Contract no. G25I08000120007.

References

[1] H. E. Graham, "Fire whirlwinds," *Bulletin of the American Meteorological Society*, vol. 36, no. 3, pp. 99–103, 1955.

[2] W. Mell, M. A. Jenkins, J. Gould, and P. Cheney, "A physics-based approach to modelling grassland fires," *International Journal of Wildland Fire*, vol. 16, no. 1, pp. 1–22, 2007.

[3] N. P. Cheney and J. S. Gould, "Fire growth in grassland fuels," *International Journal of Wildland Fire*, vol. 5, no. 4, pp. 237–347, 1995.

[4] R. Linn, J. Reisner, J. J. Colman, and J. Winterkamp, "Studying wildfire behavior using FIRETEC," *International Journal of Wildland Fire*, vol. 11, no. 3-4, pp. 233–246, 2002.

[5] W. E. Heilman and J. D. Fast, "Simulations of horizontal roll vortex development above lines of extreme surface heating," *International Journal of Wildland Fire*, vol. 2, pp. 55–68, 1992.

[6] R. Rothermel, "A mathematical model for predicting fire spread in wildland fuels," Research Paper INT-115, USDA Forest Service, 1972.

[7] T. L. Clark, J. Coen, and D. Latham, "Description of a coupled atmosphere-fire model," *International Journal of Wildland Fire*, vol. 13, no. 1, pp. 49–63, 2004.

[8] W. C. Skamarock and J. B. Klemp, "A time-split nonhydrostatic atmospheric model for weather research and forecasting applications," *Journal of Computational Physics*, vol. 227, no. 7, pp. 3465–3485, 2008.

[9] J. H. Balbi, F. Morandini, X. Silvani, J. B. Filippi, and F. Rinieri, "A physical model for wildland fires," *Combustion and Flame*, vol. 156, no. 12, pp. 2217–2230, 2009.

[10] J. P. Lafore, J. Stein, N. Asencio et al., "The Meso-NH Atmospheric Simulation System. Part I: adiabatic formulation and control simulations," *Annales Geophysicae*, vol. 16, no. 1, pp. 90–109, 1998.

[11] J. B. Filippi, F. Morandini, J. H. Balbi, and D. R. Hill, "Discrete event front-tracking simulation of a physical fire-spread model," *Simulation*, vol. 86, no. 10, pp. 629–644, 2010.

[12] J. Cuxart, P. Bougeault, and J. L. Redelsperger, "A turbulence scheme allowing for mesoscale and large-eddy simulations," *Quarterly Journal of the Royal Meteorological Society*, vol. 126, no. 562, pp. 1–30, 2000.

[13] P. Colella and P. R. Woodward, "The Piecewise Parabolic Method (PPM) for gas-dynamical simulations," *Journal of Computational Physics*, vol. 54, no. 1, pp. 174–201, 1984.

[14] R. Linn, J. Winterkamp, C. Edminster, J. J. Colman, and W. S. Smith, "Coupled influences of topography and wind on wildland fire behaviour," *International Journal of Wildland Fire*, vol. 16, no. 2, pp. 183–195, 2007.

[15] P. A. Santoni, A. Simeoni, J. L. Rossi et al., "Instrumentation of wildland fire: characterisation of a fire spreading through a Mediterranean shrub," *Fire Safety Journal*, vol. 41, no. 3, pp. 171–184, 2006.

Chapter 7

Conclusions and perspectives

In the last ten years, the Mediterranean Basin region has been the scene of unprecedented heat waves and extreme droughts that have triggered several fires in the largest European Mediterranean countries (Portugal, Spain, France, Italy and Greece) (EFFIS, 2008). Future scenarios seem even to be worse since extreme meteorological situations (increased temperatures and reduced rainfalls) are likely to allow forested areas to become ignited, strengthening fire intensity, fire extent and fire frequency (IPCC, 2007). The increasing vulnerability of the Mediterranean Basin region, and the environmental and human risks associated with wild-fires motivated the present study that, as primary goal, investigated the chemical and physical behaviour of Mediterranean wild-fires. A deepened knowledge of both chemical and physical aspects could offer an important support to diverse stakeholders that usually face up to these natural hazards (e.g. firefighters, forest service agents), helping them to reduce the dramatic consequences of wild-fire episodes.

Experimental studies contributed to point out the tight interaction that exists between the fire and the atmosphere in terms of dynamics (e.g. Santoni et al., 2006; Clements et al., 2007), an aspect of wild-fires that firefighters know and fear. Other experimental field fires explored more deeply the interplay fire/atmosphere in terms of chemistry in the Mediterranean region (e.g. Miranda et al., 2005; Barboni et al., 2010; Alves et al., 2011). Other works tried to reproduce this complex and multiscale interaction by means of coupled models that combined a fire spread model, which describes the fire propagation, with an atmospheric model, which simulates the atmospheric movements (e.g. Linn et al., 2002; Mell et al., 2007; Mandel et al., 2011). Miranda (2004) explored the non-negligible impact of fire pollutant emissions on the composition of the air at the meso-scale by using a one-way (or off-line) coupled fire/atmosphere/chemistry model. In the present work, we presented the first effort to explore both chemical and dynamical interactions between the fire and the atmosphere at different scales (from meso to micro scale) focusing on typical Mediterranean wild-fires.

The scientific scope was addressed within a coupled fire/atmosphere modelling framework, making use of the coupling between the atmospheric model Meso-NH (Lafore et al.,

1998) and the fire spread model ForeFire (Balbi et al., 2007) in combination with a chemical reactive scheme: the MesoNH-ForeFire model. This model was configured and run from meso to high Large Eddy Simulation (LES) resolution in its standard 3-D form and even in the most simple 1-D form. Concerning chemical interactions, we mostly concentrated our study on the gaseous phase, while the aerosol phase was only explored by means of passive tracers released from the ignition point. The present study addressed three main objectives (Chapter 1) that are reported in the following list with the relative discussion of achieved results and perspectives:

1. **Wild-fire impacts on the atmosphere at meso scale**

   The simulation of the Lançon-de-Provence 2005 forest fire (Strada et al., 2012) pointed out the ability of the coupled MesoNH-ForeFire model to fairly represent the impact of a typical Mediterranean wild-fire on the atmospheric dynamics at meso scale, and to reproduce the fire impacts on the chemical composition of air downwind of the burning area.

   The Lançon fire was simulated using the MesoNH-ForeFire model in its one-way configuration (Chapter 4) with no feedback from the perturbed atmosphere to the fire propagation. With this design, the coupled fire/atmosphere model highlighted the dominant role of the sensible heat released by the fire in the vertical plume development rather than the fire-released moisture, supporting the hypothesis of Luderer et al. (2009). Although the fire-induced sensible heat flux altered the atmospheric turbulence and influenced the convective transport and turbulent mixing over and downwind of the ignition point (over some tens of kilometres), the presence of strong horizontal winds and a dry atmosphere during the fire efficiently constrained the plume in the Planet Boundary Layer (PBL), a common feature of Mediterranean wild-fires (Langmann et al., 2009; Labonne and Chevallier, 2007). The simulated Lançon smoke plume spread for several tens of kilometres downwind of the fire ignition, matching the horizontal extension of the real plume as captured by the MODIS-AQUA instrument. The comparison of the fire pollutants simulated by the coupled model and the ground-based measurements of air quality provided by the regional network (AtmoPACA) showed the ability of the coupled model to reproduce well the advection of the smoke plume within the PBL at the right timing downwind of the burning area. In particular, the peculiar chemical signatures (two-fold PM_{10} levels and O_3 depletion) registered on the day of the fire in some monitoring stations located along the trajectory of the Lançon fire plume could not be explained by changes in meteorological conditions (strong northwesterly winds, no clouds and high temperatures remained during several days) or by traffic emissions. Therefore, the Lançon fire seemed to be the most probable cause of the unusual behaviour in the measured O_3 and PM_{10} concentrations at the surface. The coupled model with simplified hypothesis on emissions and initialization

simulated a sharp increase of O_3 precursors and a consequent O_3 depletion in the fire plume and a strong increase of a fire aerosol-like tracer at the right timing compared to the observations. Production of O_3 was simulated several kilometres downwind of the fire as already observed in field campaigns (Sanhueza et al., 1999; Jost et al., 2003; Yokelson et al., 2003) and other modelling studies (Lin et al., 1988; Trentmann et al., 2003).

The qualitative comparison between measured and observed values was limited by the chosen design of the model exercise. In particular, a complete aerosol model and the interaction between the photolysis rates and the smoke plume were not accounted in the study of the Lançon fire. Anthropogenic emissions were not considered either. These missing processes could explain part of the bias between the modelled and observed pollutants levels at the surface. In order to better explore the potential of the MesoNH-ForeFire model, a dramatic and well documented episode of the Lisbon 2003 wild-fires was identified as a case study with a full constrain on the anthropogenic emissions and a complete set of ground-based measurements. The modelling of the Lisbon 2003 case study is currently under way in the framework of a bilateral project PESSOA (France-Portugal). This work also includes an inter-comparison exercise with the coupled fire/atmosphere/chemistry model, Farsite/Lotos-Euros, that is used by our partners from the University of Aveiro in Portugal.

The study of the Lançon-de-Provence wild-fire also revealed the need for further work on fire emissions released by the Mediterranean vegetation, including a better characterisation of emissions factors and burning efficiency which are currently incomplete (Miranda et al., 2005; Alves et al., 2010a). In the framework of a national ANR project (IDEA project), the collaboration between the University of Corte (SPE) and the University of Toulouse (LA) has been established with the aim to improve the emission database for the Mediterranean vegetation. Within this collaborative project, some controlled fires have been already carried out at the combustion facility of the Laboratoire d'Aérologie in Lannemezan (France). Specific emission information for the Mediterranean biome will have a fundamental importance for chemical modelling of wild-fire episodes in the considered region. To pursue further this effort, it is necessary to continue performing ground based measurements during prescribed and, when possible, even real fires with the intent to document emissions and heat fluxes that are associated with wild-fires. Another support may come from numerical combustion models that reproduce the pyrolysis chemistry at very fine resolutions (e.g. some centimetres). Within the IDEA project, a collaboration has been launched with the European Centre for Research and Advanced Training in Scientific Computation (CERFACS) aiming to set up an adaptative chemistry. This work consists in building a chemical reactive scheme

that could directly link the different scales of the wild-fire chemistry, from the flame to the fire landscape scale, without passing through emission factors.

Ultimately, the bibliographic study accomplished during this thesis about biomass burning markers highlighted trace gases that are primarily emitted by wild-fires. These trace gases could be easily included in the chemical reactive scheme of Meso-NH (e.g. HCN and CH_3CN).

2. **Wild-fire injection height**

The fire injection height plays a key role in chemical and aerosol transport modelling. However, this parameter is still highly uncertain. Sensitivity tests, carried out within an inter-comparison exercise, assessed the capacities and limits of the Meso-NH model to properly determine the fire injection height when the fire is a sub-grid process.

The Meso-NH model was used in a one-dimensional configuration with a static fire to study the strong updrafts associated with one Mediterranean and two tropical Amazonian fires (Chapter 5). The fires burnt under contrasted meteorological scenarios and have different fire characteristics in terms of burnt area and heat fluxes. The Eddy-Diffusivity/Mass-flux (EDMF) scheme, recently implemented in Meso-NH (Pergaud et al., 2009), was activated to parametrise the shallow convective processes in the PBL that are triggered by surface heating. Results from the Meso-NH 1-D version model were compared to the 1-D physically-based model PRM (Plume Rise Model) specifically designed to provide a diagnostic value for the fire injection height (Freitas et al., 2010). The inter-comparison highlighted the different design of the two models: the 1-D PRM model does not influence the dynamics and the thermodynamics of the environment; whereas, the 1-D Meso-NH model acts as a single column model where the evolution of the convective updraft perturbs the atmosphere during the whole integration time. Both models simulated similar injection heights for the Mediterranean fire under 3 km. The comparison was less satisfactory for tropical fires with higher injection heights simulated by the 1-D PRM model. The lower injection heights in the Meso-NH model can be explained by the actual hypothesis in the EDMF parametrisation which restrict the simulated cloud thickness to 3 km and do not account for ice formation. It is interesting to note that in the case of the Mediterranean fire, both models predicted a plume top above the PBL and a plume base deconnected from the surface for the 1-D PRM model. This result is in contradiction with the Lançon-de-Provence study for which fire plume propagation near the surface was both simulated and observed (Strada et al., 2012). Hence, the 1-D-PRM and EDMF approaches can artificially isolate the smoke plume from the surface. The vertical evolution of the fire plume in the 1-D PRM model was mainly influenced by the ambient wind, while the evolution of

the convective updraft in the 1-D Meso-NH model was mainly constrained by the intrinsic limitations of the EDMF parametrisation.

Current research on the EDMF parametrisation in the Meso-NH model including the ice phase and the transition to the deep convective scheme are in progress. To better constrain fire injection heights in Meso-NH and to improve the physically-based scheme EDMF, complementary information will be taken from lidar measurements of smoke plumes accomplished during prescribed fires, such as those that are scheduled for Summer 2012 in the framework of the IDEA project. Moreover, a complementary approach is the use of high resolution simulations (at fire scale, Chap. 6) where convective updrafts are fully resolved. Furthermore, high resolution simulations and the EDMF scheme should be tested on a better documented wild-fire such as the Quinault 1994 case study that has been already simulated by other models (Trentmann et al., 2003; Freitas et al., 2007).

3. **Wild-fire impacts on the atmosphere at fire scale**

Through a two-step validation process (academic and real case studies), the two-way coupled MesoNH-ForeFire model (Filippi et al., 2011) demonstrated its high potential in reproducing the fire propagation in a more realistic way.

The two-way (or on-line) coupled MesoNH-ForeFire model was configured to fully simulate fire/atmosphere interaction at high LES resolution (fire scale) in order to better explore the multiscale and complex behaviour of wild-fires (e.g. Pyne et al., 1949; Mell et al., 2007; Mandel et al., 2011) and to avoid the dilution of the fire effect on the atmosphere due to the burning area smaller than the atmospheric grid mesh (e.g. Trentmann et al., 2003; Freitas et al., 2007) (Chap. 6). Since the original work of Filippi et al. (2009), the coupled model was improved by reducing the computational cost and making the representation of the fire propagation more realistic by taking into account non-burnable areas and fire-fighting operations. Through the set of idealized configurations proposed by Linn et al. (2002), the MesoNH-ForeFire model was compared with the fully-resolving Navier-Stokes simulator HIGRAD/FIRETEC (Linn et al., 2002) in five different topographies (flat, canyon, hill, ridge, and upcan terrains). The MesoNH-ForeFire model was run at rougher scales (some tens of meters) than those used by Linn et al. (2002) (some meters). The simulated results clearly showed the improvement in the Rate of Spread (RoS) determination and the depth of the fire front due to the full fire/atmosphere coupling: there was always a better agreement with the reference simulation of HIGRAD/FIRETEC, even if the RoS was underestimated in all cases. Thereafter, the coupled model MesoNH-ForeFire was applied to simulate two typical Mediterranean large wild-fires observed in Corsica (the Vazzio 2007 and the Favone 2009 fire) at the typical resolution of LES. A passive tracer was released to follow the 3-D evolution of the smoke plume. Both fires were favoured by stable, dry and windy meteorolog-

ical conditions. For the selected wild-fires, the model's results presented interesting similarities in terms of plume behaviour and fire wind effect with pictures taken during these fire episodes. The simulated front envelope was compared successfully to the fire perimeter recorded by fire fighters.

Recently, using the on-line coupled MesoNH-ForeFire model presented in this study, some tests were performed at LES resolution to simulate the gaseous composition of the smoke plume. Thanks to these validation tests, the feasibility of such fire/atmosphere/chemistry coupled approach has been demonstrated and the model is now ready to be used for detailed studies of smoke plume composition and aging. In particular, LES permits to simulate the evolution of the chemistry of a wild-fire by separating the flaming from the smouldering phase in terms of fire emissions. Furthermore, at high LES resolution, the impact of aerosols on O_3 production can be further explored. As stated in the previous point, LES are also useful means for delving into wild-fire dynamics, with a special attention for convective processes that controlled the wild-fire injection heights; once validated by lidar experiments, LES may be the starting point for the improvement of physical parametrisations that are used to predict the fire injection height.

The study of the impact of Mediterranean fires on the dynamics and chemistry of the atmosphere is still in its infancy. The development of the coupled MesoNH-ForeFire model provides an unique opportunity to reconcile the observations made during prescribed and natural fires and to integrate the fire dynamics and chemical emissions. Here mentioned future works with the coupled model will serve to improve the parametrisation for regional and global models and help to reduce the uncertainties of the impact of wild-fires on air pollution and climate.

Conclusions et perspectives[1]

Au cours des dix dernières années, le bassin méditerranéen a été touché par des vagues de chaleur intenses accompagnées par de fortes périodes de sécheresse, deux conditions idéales pour le déclenchement des feux de végétation dans la zone euro-méditerranéenne (Portugal, Espagne, France, Italie et Grèce) (EFFIS, 2008). Les projections climatiques indiquent d'une augmentation des évènements météorologiques extrêmes (hautes températures et réduction des précipitations) qui pourraient faciliter le déclenchement des feux de végétation et accroître leur intensité, leur extension et leur fréquence (IPCC, 2007). La vulnérabilité croissante du bassin méditerranéen et les risques humains et environnementaux qui sont associés aux feux de végétation ont motivé cette étude. En particulier, ce travail s'est centré sur le comportement dynamique et la pollution atmosphériques induites par les feux méditerranéens. Une connaissance plus approfondie des feux de végétation est aujourd'hui indispensable pour la protection des acteurs de terrains (pompiers, sécurité civile) et des populations sous le vent des incendies.

La recherche sur les feux en méditerranée a pris un essor important ces dernières années. Pourtant, les études scientifiques réalisées sont souvent cloisonnées à un aspect du feu (combustion, propagation, ...) et rarement dédiées à l'impact atmosphérique. La forte interaction qui existe entre le feu et l'atmosphère du point de vue de la propagation du front de feu a été mise en évidence par des travaux récents (e.g. Santoni et al., 2006; Clements et al., 2007). Ce couplage bien connu empiriquement par les pompiers mérite d'être approfondi et formalisé. D'autres expériences pilotes ont exploré plus spécifiquement les espèces chimiques émises par des feux méditerranéens (e.g. Miranda et al., 2005; Barboni et al., 2010; Alves et al., 2011) mais ces études restent encore trop rares. Le développement de modèles couplés feu-atmosphère a ouvert la recherche vers l'intégration des interactions multi-échelles entre un modèle de propagation de feu en surface, qui décrit l'avancement du feu, et un modèle atmosphérique, qui simule les mouvements atmosphériques (e.g. Filippi et al., 2009; Linn et al., 2002; Miranda, 2004; Mell et al., 2007; Mandel et al., 2011). C'est cette approche qui a été privilégiée pour les trois études présentées dans ce manuscrit avec des degrés de couplage feu-atmosphère différents en fonction de l'échelle spatiale considérée. Le modèle couplé intègre le modèle atmosphérique Méso-NH (Lafore et al., 1998) incluant un module de chimie atmosphérique et le modèle de propagation

[1]Ceci est une version condensée du Chapitre 7 qui est rédigé en anglais. This chapter is a condensed version of Chapter 7.

de feu en surface ForeFire (Balbi et al., 2007) : le modèle MésoNH-ForeFire. Ce modèle couplé a été utilisé depuis la méso-échelle jusqu'à des configuration dites *Large Eddy Simulation* (LES), dans des configurations 3-D et 1-D et en interaction simple (one-way) et bi-directionnelle (two-way). Les travaux exposés concernent essentiellement la chimie dans la phase gazeuse. L'impact des aérosols a été exploré uniquement par émissions de traceurs passifs à partir du point d'éclosion. Les trois objectives principaux de cette thèse (Chapitre 1) ainsi que les principaux résultats et perspectives sont résumés ci-après :

1. **Impacts des feux de végétation sur la dynamique et la chimie de l'atmosphère**

   La simulation du feu de végétation de Lançon-de-Provence 2005 (Strada et al., 2012) a permis de mettre en évidence les perturbations induites par le feu sur la colonne atmosphérique située à la verticale de l'incendie, mais aussi plusieurs dizaines de kilomètres sous le vent du feu.

   Le feu de Lançon-de-Provence a été simulé avec le modèle MésoNH-ForeFire utilisé dans sa configuration uni-directionnelle, Chapitre 4) sans rétroaction de l'atmosphère perturbée sur la propagation du feu. Cette étude a établi le rôle prépondérant du flux de chaleur sensible sur le développement vertical du panache par rapport au flux de chaleur latente, ce qui confirme l'hypothèse de Luderer et al. (2009). Le flux de chaleur sensible induit par le feu altère sensiblement la turbulence de l'atmosphère et influence le transport convectif et turbulent sous le vent du feu (sur une distance de quelques dizaines de kilomètres). La présence de vents horizontaux forts (Mistral) et d'une atmosphère sèche ont efficacement limité l'extension verticale du panache qui est resté confiné dans la couche limite, une caractéristique commune aux feux méditerranéens (Langmann et al., 2009; Labonne and Chevallier, 2007). Le panache de fumée simulé s'est déplacé sur plusieurs dizaines de kilomètres, en accord avec l'estimation issue de l'image satellite de MODIS-AQUA. La comparaison des polluants simulés par le modèle couplé sous le vent du feu avec les mesures en surface du réseau régional de la qualité de l'air (AtmoPACA) a montré le bon accord temporel des signatures du feu simulé avec les observations. Cet accord renforce l'hypothèse d'un panache de feu restant en contact avec la surface pendant son advection vers le sud-est par le Mistral. En particulier, la signature chimique exceptionnelle (niveaux doublés de PM_{10} et destruction de O_3) enregistrée le jour du feu dans certaines stations de mesure de la qualité de l'air localisées le long de la trajectoire du feu de Lançon ne pourrait pas être expliquée par un changement des conditions météorologiques (forts vents nord-occidentaux permanents, absence de nuages et températures élevées pendant plusieurs jours) ou par des émissions urbaines différentes le jour de l'incendie. Le feu de Lançon est donc la cause la plus probable du comportement atypique des concentrations mesurées en surface pour le O_3 et le PM_{10}. Le modèle couplé avec des hypothèses simplificatrices sur les

émissions et l'initialisation des espèces chimiques a simulé effectivement une augmentation forte des précurseurs de O_3 et, par conséquence, une destruction de O_3 dans le panache du feu. En outre, une forte augmentation d'un traceur passif, qui représente les aérosols du feu, a été reproduite en phase avec les observations. La production d'O_3 a été simulée plusieurs kilomètres sous le feu lorsque le panache atteint la côte. Ce comportement est similaire a celui observé pendant des campagnes de mesures (Sanhueza et al., 1999; Jost et al., 2003; Yokelson et al., 2003) ou des exercices de modélisation dédiés (Lin et al., 1988; Trentmann et al., 2003).

La comparaison qualitative entre les valeurs mesurées et observées était par ailleurs limitée par la configuration choisie pour cet exercice de modélisation. En particulier, le schéma complet des aérosols et l'interaction entre les taux de photolyse et le panache de fumée n'ont pas été pris en compte dans l'étude du feu de Lançon-de-Provence. Les émissions anthropiques n'étaient pas non plus considérées. Ces processus manquants pourraient expliquer en partie le biais entre les niveaux des polluants observés et simulés à la surface. Pour mieux explorer les potentialités du modèle MésoNH-ForeFire, un épisode dramatique et bien documenté de l'été 2003 dans la région de Lisbonne a été identifié comme cas d'étude avec intégration d'un inventaire approprié des émissions anthropiques et une série complète de mesures en surface sous le vent des incendies. Á l'heure actuelle, la modélisation du cas d'étude de Lisbonne 2003 est en cours dans le cadre d'un projet bilateral PESSOA (France-Portugal). Ce travail comprend aussi un exercice d'inter-comparaison avec le modèle couplé feu/atmosphère/chimie, Farsite/Lotos-Euros, qui est utilisé par nos partenaires de l'Université d'Aveiro au Portugal.

Cette étude a aussi révélé la nécessité de poursuivre les travaux pour la détermination des émissions des feux issues par la végétation méditerranéenne, en incluant une meilleure caractérisation des facteurs d'émission et de l'efficacité de la combustion qui sont, à l'état actuel, incomplets (Miranda et al., 2005; Alves et al., 2010a). Dans le contexte d'un projet national financé par l'ANR (projet IDEA), une collaboration entre l'Université de Corte (SPE) et l'Université de Toulouse a été mise en place avec le but d'améliorer la base de données pour la végétation méditerranéenne. Dans le cadre de ce projet, des premières expériences de brûlage de végétaux ont été réalisées dans la chambre de combustion du Laboratoire d'Aérologie à Lannemezan (France). Ces informations spécifiques pour les émissions de la flore méditerranéenne auront une importance fondamentale pour la modélisation de la chimie associée à des épisodes de feu dans cette région. Elles manquent cruellement à l'heure actuelle. Pour pousser plus loin cet effort, il est nécessaire de poursuivre les campagnes expérimentales qui effectuent des mesures au sol pendant des brûlages dirigés et, si possible, des feux réels pour pouvoir documenter les émissions et les flux de chaleur qui sont associés aux feux de végétation. Un autre support pourrait venir des

modèles numériques pour la combustion qui décrit la chimie de la pyrolyse à des résolutions très fines (de l'ordre du centimètre). Dans le contexte du projet IDEA, une collaboration a débutée avec le Centre Européen de Recherche et de Formation Avancée en Calcul Scientifique (CERFACS) en ayant pour enjeu celui de mettre un place une chimie adaptative. Ce travail consiste à développer un schéma chimique réactionnel capable de faire le lien direct entre les différentes échelles de la chimie de feux de végétation, de la flamme à l'échelle du feu dans l'environnement, sans passer par la définition de facteurs d'émissions.

Enfin, l'étude bibliographique menée au cours de cette thèse sur la thématique des marqueurs de feu de biomasse a mis en évidence des gaz trace qui sont émis essentiellement par les feux de végétation. Certains entre ces gaz trace pourraient être facilement inclus dans le schéma réactionnel de Méso-NH (e.g. HCN and CH_3CN).

2. **Hauteur d'injection des feux de végétation**

   La hauteur d'injection joue un rôle clé dans la modélisation du transport chimique et des aérosols. Pourtant, une forte incertitude est encore associée à ce paramètre difficile à mesurer. Des tests de sensibilités, réalisés dans le cadre d'un exercice d'inter-comparaison, ont attesté les capacités et les limites du modèle MésoNH-ForeFire à prévoir correctement la hauteur d'injection des feux de végétation quand ces épisodes sont des processus sous-maille.

   Le modèle Méso-NH a été utilisé dans sa configuration unidimensionnelle (1-D) avec un feu statique pour étudier les mouvements verticaux convectifs (les thermiques) induits par un feu méditerranéen et deux feux tropicaux d'Amazonie (Chapitre 5). Les feux ont brûlés dans des conditions météorologiques contrastées. Les feux différaient aussi par leurs caractéristiques en terme d'aire brûlée et flux de chaleur. Le schéma *Eddy-Diffusivity/Mass-flux* (EDMF), récemment inclus dans Méso-NH (Pergaud et al., 2009), a été activé pour paramétrer la convection associée au réchauffement à la surface. Les résultats de la version 1-D de Méso-NH ont été comparés avec le modèle physique 1-D PRM (Plume Rise Model) spécifiquement conçu pour fournir une diagnostique de la hauteur d'injection des feux (Freitas et al., 2010). Les deux modèles suivent une philosophie différente : le modèle 1-D PRM, développé pour être introduit dans des modèles à faible résolution, n'influence pas la dynamique et de la thermodynamique de l'environnement. A contrario, le modèle 1-D Méso-NH fonctionne comme un *single column model* où l'évolution convective du panache perturbe l'atmosphère pendant la totalité du temps d'intégration. Les deux modèles ont simulé des hauteurs d'injection comparables pour le feu méditerranéen, c'est à dire en dessous de 3 km. La comparaison a été moins satisfaisante pour les feux tropicaux avec des hauteurs d'injection simulées par 1-D PRM systématiquement plus hautes de plusieurs kilomètres. Les hauteurs d'injection plus basses simulées par le modèle Méso-NH peuvent être expliquées par les hypothèses

inhérentes à sa construction : l'épaisseur du nuage est limitée à 3 km et la formation de la glace n'est pas prise en compte. Il est intéressant de noter que dans le cas des feux méditerranéens, les deux modèles prévoient une hauteur du panache au dessus de la couche limite et un panache détaché de la surface pour le modèle 1-D PRM. Ce résultat est en contradiction avec l'étude du feu de Lançon-de-Provence pour lequel les observations suggèrent que le panache de fumée s'est propagé prés de la surface (Strada et al., 2012). Les approches 1-D-PRM et EDMF peuvent donc artificiellement isoler le panache de fumée de la surface. La variable la plus sensible dans le modèle 1-D PRM pour l'évolution verticale du panache de fumée était le vent ambiant. L'évolution convective du panache dans le modèle 1-D Méso-NH était fortement contrainte par les limitations intrinsèques de la paramétrisation EDMF.

Des recherches sont actuellement en cours en ce qui concerne la paramétrisation EDMF dans le modèle Méso-NH avec l'introduction de la phase glace et la transition vers le schéma de convection profonde. Pour mieux contraindre la hauteur d'injection dans les modèles et améliorer le schéma physique EDMF, des informations complémentaires seront obtenues par des mesures lidar qui seront effectuées pendant l'été 2012 au cours des brûlages dirigés prévus dans le cadre du projet IDEA. En outre, une approche complémentaire est celui d'utiliser des simulations à haute résolution (LES, à l'échelle du feu, Chap. 6) où la convection n'est plus paramétrée mais entièrement résolue.

3. **Impacts des feux de végétation sur l'atmosphère à l'échelle du feu**

   Le modèle couplé MésoNH-ForeFire a été utilisé pour cette étude dans sa configuration bi-directionnelle à des échelles hectométriques. Le modèle couplé en bi-directionnel MésoNH-ForeFire a été configuré pour simuler dans son intégralité l'interaction feu/atmosphère à haute résolution (LES, à l'échelle du feu) pour mieux explorer le comportement complexe et multi-échelle des feux de végétation (e.g. Pyne et al., 1949; Mell et al., 2007; Mandel et al., 2011). Dans cette approche, la dilution de l'effet du feu sur l'atmosphère n'est plus un verrou alors que le feu était un processus sous-maille dans les deux études précédentes (e.g. Trentmann et al., 2003; Freitas et al., 2007) (Chapitre 6). A partir du travail original de Filippi et al. (2009), le modèle couplé a été amélioré avec une réduction du coût de calcul et une représentation plus réaliste de la propagation du feu qui prend désormais en compte les surfaces non brûlables et l'intervention des pompiers. A travers une série des cas idéalisés proposés par Linn et al. (2002), le modèle MésoNH-ForeFire a été comparé avec le simulateur physique (*fully-resolving Navier-Stokes*) HIGRAD/FIRETEC (Linn et al., 2002) dans cinq différentes topographies (plaine, canyon, colline et terrains pentus). Le modèle MésoNH-ForeFire a été utilisé à une résolution plus grossière (quelques dizaines de mètres) par rapport à celle utilisée par Linn et al. (2002) (quelques mètres). Les résultats simulés ont montré clairement

des améliorations de la vitesse de propagation du feu et de la profondeur du front du feu du fait du couplage complet feu/atmosphère. Cette amélioration par rapport au modèle de propagation non couplé a été systématique pour tous les cas simulés même si MésoNH-ForeFire sous-estimait la vitesse de propagation du feu par rapport au modèle de référence HIGRAD/FIRETEC. Le modèle couplé MésoNH-ForeFire a ensuite été utilisé pour reproduire deux grands feux représentatifs des épisodes méditerranéens qui ont été observés en Corse (Vazzio 2007 et Favone 2009) toujours dans une configuration LES. Un traceur passif a été émis pour suivre l'évolution en 3-D du panache de fumée. Le déclenchement des deux feux avaient été favorisés par une météorologie stable, sèche et venteuse. Pour les cas sélectionnés, les résultats de la modélisation ont montré des similarités intéressantes avec le comportement du panache et l'effet du vent documentés par des photos prises pendant le feu même. L'enveloppe simulée du feu a été comparée avec succès avec les périmètres du feu relevés par les pompiers.

Le modèle couplé MésoNH-ForeFire comme présenté dans cette étude a été récemment testé en simulant la composition gazeuse du panache de fumée. Grâce à ces tests, la faisabilité du couplage feu/atmosphère/chimie a été démontrée. Le modèle couplé est maintenant prêt à être utilisé pour des études détaillées de la composition de panache de fumée et leur vieillissement. En particulier, les simulations à haute résolution vont permettre de simuler l'évolution de la chimie d'un feu de végétation en pouvant séparer la phase flamme de la phase feu couvant en terme des émissions chimiques. En outre, à fine échelle (LES), l'impact des aérosols sur la production d'O_3 pourrait être approfondie. Enfin, comme il a été expliqué au point précèdent, les simulations LES représentent un moyen utile pour comprendre la dynamique des feux de végétation, avec une attention spéciale pour les processus convectifs qui contrôlent les hauteurs d'injection des feux ; une fois validées par des mesures lidar, les simulations LES pourraient être le point de départ pour l'amélioration des paramétrisations physiques qui sont actuellement appliquées pour prédire la hauteur d'injection des feux.

L'étude de l'impact des feux méditerranéens sur la dynamique et la chimie de l'atmosphère progresse aux différentes échelles du feu. Le développement du modèle couplé MésoNH-ForeFire offre une opportunité unique de réconcilier les observations faites pendant des feux prescrits ou naturels à l'échelle locale et de considérer dans un même outil intégrateur la dynamique du feu et les émissions chimiques. Les travaux envisagés avec le modèle couplé, qui ont été ici évoqués, serviront à l'amélioration des paramétrisations dans les modèles régionaux ou globaux et à réduire les incertitudes de l'impact de feux de végétation sur la pollution de l'air et le climat.

Bibliography

Aber, J. D., Melillo, J. M., 2001. Terrestrial Ecosystems, 2nd Edition. Saunders College Publishing.

Achard, F., Eva, H. D., Stibig, H. J., Mayaux, P., Gallego, J., Richards, T., Malingreau, J. P., 2002. Determination of deforestation rates of the World's humid tropical forests. Science 297, 999–1002.

Adetona, O., Hall, D. B., Naeher, L. P., 2011. Lung function changes in wildland firefighters working at prescribed burns. Inhal. Toxicol. 23 (13), 835–841.

Albini, F. A., 1993. Dynamics and Modeling of Vegetation Fires: Observations. John Wiley & Sons, Inc., Berlin, Ch. 3, pp. 39–52.

Albuquerque, L. M. M., Longo, K. M., Freitas, S. R., Tarasova, T., Fattori, A. P., Nobre, C., Gatti, L. V., 2005. Sensitivity studies on the photolysis rates calculation in the Amazonian atmospheric chemistry Part i: The impact of the direct radiative effect of biomass burning aerosol particles. Atm. Chem. Phys. Discussions 5, 9325–9353.

Alessio, G. A., Lillis, M. D., Fanelli, M., Pinelli, P., Loreto, F., 2004. Direct and indirect impacts of fire on isoprenoid emissions from Mediterranean vegetation. Funct. Ecol. 18 (3), 357–364.

Alexandrian, D., Esnault, F., Calabri, G., 1999. Forest fires in the Mediterranean area. Unasylva 197 (50), 35–41.

Alves, C., Gonçalves, C., Evtyugina, M., Pio, C., Mirante, F., Puxbaum, H., 2010a. Particulate organic compounds emitted from experimental wildland fires in a Mediterranean ecosystem. Atm. Env. 44 (23), 2750–2759.

Alves, C., Vicente, A., Nunes, T., Gonçalves, C., Fernandes, A. P., Mirante, F., Tarelho, L., de la Campa, A. M. S., Querol, X., Caseiro, A., Monteiro, C., Evtyugina, M., Pio, C., 2011. Summer 2009 wildfires in portugal: Emission of trace gases and aerosol composition. Atm. Env. 45 (3), 641–649.

Alves, C. A., Goncalves, C., Pio, C. A., Mirante, F., Caseiro, A., Tarelho, L., Freitas, M. C., Viegas, D. X., 2010b. Smoke emissions from biomass burning in a Mediterranean shrubland. Atm. Env. 44 (25), 3024–3033.

Amiridis, V., Giannakaki, E., Balis, D., Pytharoulis, I., Zanis, P., Melas, D., Zerefos, C., 2009. Injection height of smoke from biomass burning in Eastern Europe by the synergy of satellite active and passive remote sensing. In: Apituley, A., Russchenberg, H. W. J., Monna, W. A. A. (Eds.), Proc. 8th International Symposium on Tropospheric Profiling. Delft, Netherlands.

Andreae, M. O., 1991. Biomass Burning: Its History, Use, and Distribution and Its Impact on Environmental Quality and Global Climate. J. S. Levine, Cambridge, MA, Ch. 1, pp. 1–21.

Andreae, M. O., Atlas, E., Harris, G. W., Helas, G., deKock, A., Koppmann, R., Maenhaut, W., Mano, S., Pollock, W. H., Rudolph, J., Scharffe, D., Schebeske, G., Welling, M., 1996a. Methyl halide emissions from savanna fires in southern Africa. J. Geophys. Res. 101 (D19), 23603–23613.

Andreae, M. O., Fishman, J., Lindesay, J., 1996b. The Southern Tropical Atlantic Region Experiment (STARE): Transport and Atmospheric Chemistry near the Equator-Atlantic (TRACE A) and Southern African Fire-Atmosphere Research Initiative (SAFARI): An introduction. J. Geophys. Res. 101 (D19), 23519–23520.

Andreae, M. O., Merlet, P., 2001. Emission of trace gases and aerosols from biomass burning. Global Biogeochem. Cycles 15, 955–966.

Andreae, M. O., Rosenfeld, D., Artaxo, P., Costa, A. A., Frank, G. P., Longo, K. M., Silva-Dias, M. A. F., 2004. Smoking rain clouds over the Amazon. Science 303, 1337–1342.

Artaxo, P., Gatti, V. G., Leal, A. M. C., Longo, K. M., de Freitas, S. R., Lara, L. L., Pauliquevis, T. M., Procópio, A. S., Rizzo, L. V., 2005. Química atmosférica na amazônia: A floresta e as emissões de queimadas controlando a composição da atmosfera amazônica. Acta Amazonica 35 (2), 191–208.

Artaxo, P., Martins, J. V., Yamasoe, M. A., Procópio, A. S., Pauliquevis, T. M., Andreae, M. O., Guyon, P., Gatti, L. V., Leal, A. M. C., 2002. Physical and chemical properties of aerosols in the wet and dry season in Rondônia, Amazonia. J. Geophys. Res. 107 (D20).

Auzillon, P., Fiorina, B., Vicquelin, R., Darabiha, N., Gicquel, O., Veynante, D., 2011. Modeling chemical flame structure and combustion dynamics in LES. P. Combust. Inst. 33 (1), 1331–1338.

Balbi, J. H., Morandini, F., Silvani, X., Filippi, J. B., Rinieri, F., 2009. A physical model for wildland fires. Combust. Flame 156, 2217–2230.

Balbi, J. H., Rossi, J. L., Marcelli, T., Santoni, P. A., 2007. A 3D physical real time model of surface fires across fuel beds. Combust. Sci. Technol. 179, 2511–2537.

Barboni, T., Cannac, M., Pasqualini, V., Simeoni, A., Leoni, E., Chiaramonti, N., 2010. Volatile and semi-volatile organic compounds in smoke exposure of firefighters during prescribed burning in the Mediterranean region. Int. J. of Wildland Fire 19, 606–612.

Barbosa, P., Camia, A., Kucera, J., Libertà, G., San-Miguel-Ayanz, G., Schmuck, G., 2009. Assessment of Forest Fire Impact and Emissions in the European Union Based on the European Forest Fire Information System. Vol. 8. Elsevier, Cambridge, UK, Ch. 8, pp. 197–208.

Barbosa, P. M., Grégoire, J.-M., Pereira, J. M. C., 1999. An algorithm for extracting burned areas from time series of AVHRR GAC data applied at a continental scale. Remote Sens. Environ. 69, 253–263.

Barnaba, F., Angelini, F., Curci, G., Gobbi, G. P., 2011. An important fingerprint of wildfires on the European aerosol load. Atm. Chem. Phys. 11, 10487–10501.

Battle, J., Golladay, S. W., 2003. Prescribed fire's impact on water quality of depressional wetlands in southwestern Georgia. Am. Midl. Nat. 150 (1), 15–25.

Bechtold, P., Bazile, E., Guichard, F., Mascart, P., Richard, E., 2001. A mass flux convection scheme for regional and global models. Quart. J. Roy. Meteor. Soc. 127, 869–886.

Bell, T., Adams, M., 2009. Smoke from Wildfires and Prescribed Burning in Australia: Effects on Human Health and Ecosystems. Vol. 8. Elsevier, Cambridge, UK, Ch. 14, pp. 289–316.

Benson, R. P., Roads, J. O., Weise, D. R., 2009. Climatic and Weather Factors Affecting Fire Occurence and Behaviour. Vol. 8. Elsevier, Cambridge, UK, Ch. 2, pp. 37–59.

Beverly, J. L., Martell, D. L., 2005. Characterizing extreme fire and weather events in the boreal shield ecozone of Ontario. Agric. For. Meteorol. 133 (1-4), 5–16.

Bougeault, P., Lacarrère, P., 1989. Parameterization of orography-induced turbulence in a meso-beta-scale model. Mon. Rea. Rev. 117, 1872–1890.

Brasseur, G. P., Orlando, J. J., Tyndal, G. S., 1999. Atmospheric Chemistry and Global Change. Oxford Univesrity Press.

Bravo, A. H., Sosa, E. R., Sanchez, A. P., Jaimes, P. M., Saavedra, R. M. I., 2002. Impact of wildfires on the air quality of Mexico City, 1992-1999. Environ. Pollut. 117 (2), 243–253.

Bremer, H., , Kar, J., Drummond, J. R., Nichitu, F., Zou, J., Liu, J., Gille, J. C., Deeter, M. N., Francis, G., Ziskin, D., Warner, J., 2004. Spatial and temporal variation of MOPITT CO in Africa and South America: A comparison with SHADOZ ozone and MODIS aerosol. J. Geophys. Res. 109.

Burgan, R. E., Rothermel, R. C., 1984. Characterizing Sources of Emissions from Wildland Fires. BEHAVE: fire behavior prediction and fuel modeling system - FUEL subsystem. General Technical Report, Ogden, UT.

Bursik, M., 2001. Effect of wind on the rise height of volcanic plumes. Geophys. Res. Lett. 28 (18).

Butler, B. W., Cohen, J., Latham, D. J., D.Schuette, R., Sopko, P., Shannon, K. S., Jimenez, D., Bradshaw, L. S., 2004. Measurements of radiant emissive power and temperatures in crown fires. Can. J. For. Res. 34 (8), 1577–1587.

Bytnerowicz, A., Cayan, D., Riggan, P., Schilling, S., Dawson, P., Tyree, M., Wolden, L., Tissell, R., Preisler, H., 2010. Analysis of the effects of combustion emissions and Santa Ana winds on ambient ozone during the October 2007 southern California wildfires. Atm. Env. 44 (5), 678–687.

Caballero, D., 2003. Synthetic report of some fires that affected WUI in Spain. International report of warm project.

Cardoso, M. F., 2004. Fire Dynamics in Amazonia. Ph.D. thesis, University of New Hampshire.

Carmona-Moreno, C., Belward, A., Malingreau, J.-P., Hartley, A., Garcia-Alegre, M., Antonovskiy, M., Buchshtaber, V., Pivovarov, V., 2005. Characterizing interannual variations in global fire calendar using data from Earth observing satellites. Global Change Biol. 11, 1537–1555.

Chatfield, R., Delany, A., 1990. Convection Links Biomass Burning to Increased Tropical Ozone: However, Models Will Tend to Overpredict O_3. J. Geophys. Res. 95 (D11).

Chen, W.-T., Kahn, R. A., Nelson, D., Yau, K., Seinfeld, J. H., 2008. Sensitivity of multiangle imaging to the optical and microphysical properties of biomass burning aerosols. J. Geophys. Res. 113 (D10).

Cheng, L., McDonald, K. M., Angle, R. P., Sandhu, H. S., 1998. Forest fire enhanced photochemical air pollution. A case study. Atm. Env. 32 (4), 673–681.

Chou, S. C., Marengo, J., Dereczynski, C. P., Waldheim, P. V., Manzi, A. O., 2007. Comparison of CPTEC GCM and Eta Model Results with Observational Data from the Rondonia LBA Reference Site, Brazil. J. Meteor. Soc. Japan 85A, 25–42.

Christian, T. J., Kleiss, B., Yokelson, R. J., Holzinger, R., Crutzen, P. J., Hao, W. M., Saharjo, B. H., Ward, D. E., 2003. Comprehensive laboratory measurements of biomass-burning emissions: 1. Emission from Indonesian, African, and other fuels. J. Geophys. Res. 107, 4719.

Chubarova, N. Y., Prilepsky, N. G., Rublev, A., Riebau, A. R., 2009. A Mega-Fire Event in Central Russia: Fire weather, Radiative and Optical Properties of the Atmosphere, and Consequences for Subboreal Forest Plants. Vol. 8. Elsevier, Cambridge, UK, Ch. 11, pp. 247–264.

Chuvieco, E., 2009. Global Impacts of Fire. E. Chuvieco, Berlin Heidelberg, Ch. 1, pp. 1–10.

Chuvieco, E., Giglio, L., Justice, C., 2008. Global characterization of fire activity: toward defining fire regimes from Earth observation data. Glob. Change Biol. 14 (7), 1488–1502.

Cinnirella, S., Pirrone, N., Allegrini, A., Guglietta, D., 2008. Modeling mercury emissions from forest fires in the Mediterranean region. Environ. Fluid Mech. 8 (2), 129–145.

Clark, T. L., Coen, J., Latham, D., 2004. Description of a coupled atmosphere-fire model. Int. J. Wildland Fire 13, 49–63.

Clark, T. L., Jenkins, M. A., Coen, J. L., Packham, D. R., 1996. A Coupled Atmosphere-Fire Model: Role of the Convective Froude Number and Dynamic Fingering at the Fireline. Int. J. Wildland Fire 6, 177 – 190.

Clements, C. B., Potter, B. E., Zhong, S., 2006. In situ measurements of water vapor, heat, and co2 fluxes within a prescribed grass fire. Int. J. Wildland Fire 15 (299-306), 1369–1382.

Clements, C. B., Zhong, S., Goodrick, S., Li, J., Potter, B. E., Bian, X., Heilman, W. E., Charney, J. J., Perna, R., Jang, M., Lee, D., Patel, M., Street, S., Aumann, G., 2007. Observing the Dynamics of Wildland Grass Fires: FireFlux - A Field Validation Experiment. Bull. Amer. Meteor. Soc. 88 (9), 1369–1382.

Coheur, P.-F., Clarisse, L., Turquety, S., Hurtmans, D., Clerbaux, C., 2009. IASI measurements of reactive trace species in biomass burning plumes. Atm. Chem. Phys. 9 (15), 5655–5667.

Colella, P., Woodward, P. R., 1984. The piecewise parabolic method (PPM) for gas-dynamical simulations. J. Comput. Phys. 54, 174–201.

Conard, S. G., Solomon, A. M., 2009. Effects of Wildland Fire on Regional and Global Carbon Stocks in a Changing Environment. Vol. 8. Elsevier, Cambridge, UK, Ch. 5, pp. 109–138.

Crassier, V., Suhre, K., Tulet, P., Rosset, R., 2000. Development of a reduced chemical scheme for use in mesoscale meteorological models. Atmos. Env. 34, 2633–2644.

Crutzen, P. J., Andreae, M. O., 1990. Biomass Burning in the Tropics - impact on Atmospheric Chemistry and Biogeochemical Cycles. Science 250 (4988), 1669–1678.

Crutzen, P. J., Lelieveld, J., 2001. Human impacts on atmospheric chemistry. Ann. Rev. of Earth and Planetary Sciences 29, 17–45.

Cuxart, J., Bougeault, P., Redelsperger, J. L., 2000. A turbulence scheme allowing for mesoscale and large-eddy simulations. Q. J. R. Meteorol. Soc. 126, 1–30.

Damoah, R., Spichtinger, N., Servranckx, R., Fromm, M., Eloranta, E. W., Razenkov, I. A., James, P., Shulski, M., Forster, C., Stohl, A., 2006. A case study of pyro-convection using transport model and remote sensing data. Atm. Chem. and Phys. 6 (1), 173–185.

Darley, E. F., Burleson, F. R., Mateer, E. H., Middleton, J. T., Osterli, V. P., 1976. Contribution Of Burning Of Agricultural Wastes To Photochemical Air Pollution. J. Air Pollut. Control. Assoc. 16, 685–690.

Dasch, J. M., 1982. Particulate and gaseous emissions from wood-burning fireplaces. Environ. Sci. Technol. 16 (10), 639–649.

de Barros Ferraz, S. F., Vettorazzi, C. A., Theobald, D. M., Ballester, M. V. R., 2005. Landscape dynamics of amazonian deforestation between 1984 and 2002 in central rondônia, brazil: assessment and future scenarios. Forest Ecol. Manag. 204 (1), 69 – 85.

Delmas, E. A., Loudjani, P., Podaire, A., Menaut, J.-C., 1991. Biomass Burning in Africa: An Assessment of Annually Burned Biomass. J. S. Levine, Cambridge, MA, Ch. 16, pp. 126–132.

Dirksen, R. J., Boersma, B. K. F., de Laat, J., Stammes, P., van der Werf, G. R., Martin, M. V., Kelder, H. M., 2009. An aerosol boomerang: Rapid around-the-world transport of smoke from the December 2006 Australian forest fires observed from space. J. Geophys. Res. 114, 148–227.

Dokas, I., Statheropoulos, M., Karma, S., 2007. Integration of field chemical data in initial risk assessment of forest fire smoke. Sci. Total Environ. 376 (1-3), 72–85.

Dufour, G., Boone, C. D., Rinsland, C. P., Bernath, P. F., 2006. First space-borne measurements of methanol inside aged southern tropical to mid-latitude biomass burning plumes using the ACE-FTS instrument. Atm. Chem. Phys. 6 (11), 3463–3470.

Dwyer, E., Pinnock, S., Grégoire, J.-M., 2000. Global spatial and temporal distribution of vegetation fire as determined from satellite observations. Int. J. Remote. Sens. 21, 1289–1302.

Edwards, D. P., Emmons, L. K., Gille, J. C., Chu, A., Attié, J.-L., Giglio, L., Wood, S. W., Haywood, J., Deeter, M. N., Massie, S. T., Ziskin, D. C., Drummond, J. R., 2006.

Satellite-observed pollution from Southern Hemisphere biomass burning. J. Geophys. Res. 111.

EFFIS, 2008. Forest Fires in Europe 2008 report.
URL `http://effis.jrc.ec.europa.eu/`

Elguindi, N., Clark, H., Ordóñez, C., Thouret, V., Flemming, J., Stein, O., Huijnen, V., Moinat, P., Inness, A., Peuch, V.-H., Stohl, A., Turquety, S., Athier, G., Cammas, J.-P., Schultz, M., 2010. Current status of the ability of the GEMS/MACC models to reproduce the tropospheric co vertical distribution as measured by MOZAIC. Geosci. Model Dev. 3 (2), 501–518.

Erisman, J. W., Baldocchi, D., 1994. Modelling dry deposition of SO_2. Tellus B 46, 159–171.

Evans, L. F., King, N. K., Packham, D. R., Stephens, E. T., 1974. Ozone measurements in smoke from forest fires. Environ. Sci. Tech. 8 (1), 75–76.

Falke, S. R., Husar, R. B., Schichtel, B. A., 2001. Fusion of SeaWiFS and TOMS satellite data with surface observations and topographic data during extreme aerosol events. J. Air Waste Manage. Assoc. 51 (11), 1579–1585.

Fendell, F. E., Wolf, M. F., 2001. Wind-aided fire spread. pp. 171–223.

Filippi, J. B., Bosseur, F., Mari, C., 2011. Simulation of Coupled Fire/Atmosphere Interaction with the MesoNH-ForeFire Models. J. Combust. 1D.

Filippi, J. B., Bosseur, F., Mari, C., Lac, C., Lemoigne, P., Cuenot, B., Veynante, D., Cariolle, D., Balbi, J. H., 2009. Coupled atmosphere-wildland fire modelling. J. Advances in Modeling Earth Systems 1 (11).

Finney, M. A., 2004. FARSITE: Fire Area Simulator-model development and evaluation. Ogden, UT.

Fishman, J., Hoell, J. M. J., Bendura, R. D., McNeal, R. J., Kirchhoff, V. W. J. H., 1996. NASA GTE TRACE A Experiment (September-October 1992): Overview. J. Geophys. Res. 101 (D19), 865–879.

Fishman, J., Watson, C., Larsen, J., Logan, J., 1990. Distribution of Tropospheric Ozone Determined From Satellite Data. J. Geophys. Res. 95 (D4), 3599–3617.

Fox, D. G., Riebau, A. R., 2009. Effects of Forest Fires on Visibiity and Air Quality. Vol. 8. Elsevier, Cambridge, UK, Ch. 7, pp. 171–195.

Freitas, S. R., Longo, K. M., Andreae, M. O., 2006. Impact of including the plume rise of vegetation fires in numerical simulations of associated atmospheric pollutants. Geophys. Res. Lett. 33.

Freitas, S. R., Longo, K. M., Chatfield, R., Latham, D., Dias, M. A. F. S., Andreae, M. O., Prins, E., Santos, J. C., Gielow, R., Jr., J. A. C., 2007. Including the sub-grid scale plume rise of vegetation fires in low resolution atmospheric transport models. Atm. Chem. Phys. 7, 3385–3398.

Freitas, S. R., Longo, K. M., Silva Dias, M. A. F., Chatfield, R., Silva Dias, P., Artaxo, P., Andreae, M. O., Grell, G., Rodrigues, L. F., Fazenda, A., Panetta, J., 2009. The Coupled Aerosol and Tracer Transport model to the Brazilian developments on the Regional Atmospheric Modeling System (CATT-BRAMS) - Part 1: Model description and evaluation. Atm. Chem. Phys. 9 (8), 2843–2861.

Freitas, S. R., Longo, K. M., Trentmann, J., Latham, D., 2010. Technical note: Sensitivity of 1-d smoke plume rise models to the inclusion of environmental wind drag. Atm. Chem. Phys. 10 (2), 585–594.

Fromm, M., Bevilacqua, R., Servranckx, R., Rosen, J., Thayer, J. P., Herman, J., Larko, D., 2005. Pyro-cumulonimbus injection of smoke to the stratosphere: Observations and impact of a super blowup in northwestern Canada on 3-4 August 1998. J. Geophys. Res. 110 (D08205).

Fromm, M., Shettle, E. P., Fricke, K. H., Ritter, C., Trickl, T., Giehl, H., Gerding, M., Barnes, J. E., O'Neill, M., Massie, S. T., Blum, U., McDermid, I. S., Leblanc, T., Deshler, T., 2008. Stratospheric impact of the Chisholm pyrocumulonimbus eruption: 2. Vertical profile perspective. J. Geophys. Res. 113 (D8).

Giglio, L., Descloitres, J., Justice, C. O., Kaufman, Y., 2003. An enhanced contextual fire detection algorithm for MODIS. Remote Sens. Environ. 87, 273–282.

Goldammer, J. G., 1991. Tropical Wild-land Fires and Global Changes: Prehistoric Evidence, Present Fire Regimes, and Future Trends. J. S. Levine, Cambridge, MA, Ch. 10, pp. 83–91.

Goldammer, J. G., 1996. Fire in ecosystems of boreal Eurasia: The Bor Forest Island Fire Experiment, Fire Research Campaign Asia-North (FIRESCAN). Vol. II. J. S. Levine, Cambridge, MA, Ch. 3, pp. 848–873.

Goldammer, J. G., Price, C., 1998. Potential impacts of climate change on fire regimes in the Tropics based on MAGICC and a GISS GCM-derived lightning model. Clim. Change 39, 273–296.

Goldammer, J. G., Statheropoulos, M., Andreae, M. O., 2009. Impacts of Vegetation Fire Emissions on the Environment, Human Health, and Security: A Global Perspective. Vol. 8. Elsevier, Cambridge, UK, Ch. 1, pp. 3–36.

Gonzi, S., Palmer, P. I., 2010. Vertical transport of surface fire emissions observed from space. J. Geophys. Res. 115, 148–227.

Goode, J. G., Yokelson, R. J., , Susott, R. A., Ward, D. E., 1999. Trace gas emissions from laboratory biomass fires measured by open-path Fourier transform infrared spectroscopy: Fires in grass and surface fuels. J. Geophys. Res. 104, 21237–21245.

Govaerts, Y. M., Pereira, J. M., Pinty, B., Mota, B., 2002. Impact of fires on surface albedo dynamics over the African continent. J. Geophys. Res. 107 (D22).

Graf, H., Herzog, M., Oberhuber, J., Textor, C., 1999. Effect of environmental conditions on volcanic plume rise. J. Geophys. Res. 104 (D20).

Granier, C., Müller, J.-F., Brasseur, G. P., 2000. The impact of biomass burning on the global budget of ozone and ozone precursors. Innes, Beniston, and Verstraete, Advances in Global Change Research, The Netherlands.

Greenberg, J. P., Friedli, H., Guenther, A. B., Hanson, D., Harley, P., Karl, T., 2006. Volatile organic emissions from the distillation and pyrolysis of vegetation. Atmos. Chem. Phys. 6, 81–91.

Grell, G., Freitas, S. R., Stuefer, M., Fast, J., 2011. Inclusion of biomass burning in WRF-Chem: impact of wildfires on weather forecasts. Atm. Chem. Phys. 11 (11), 5289–5303.

Grulke, N. E., Minnich, R. A., Paine, T., Dunn, A., Chavez, D., 2009. Air Pollution Increases Forest Susceptibility to Wildfires:a case Study in the San Bernardino Mountains in Southern California. Vol. 8. Elsevier, Cambridge, UK, Ch. 17, pp. 365–403.

Guan, H., Esswein, R., Lopez, J., Bergstrom, R., Warnock, A., Follette-Cook, M., Fromm, M., Iraci, L. T., 2010. A multi-decadal history of biomass burning plume heights identified using aerosol index measurements. Atmospheric Chemistry and Physics 10 (14), 6461–6469.

Hansen, J., Nazarenko, L., 2004. Soot climate forcing via snow and ice albedos. Vol. 101. pp. 423–428.

Hanson, H. P., Bradley, M. M., Bossert, J., Linn, R. R., Younker, L. W., 2000. The potential and promise of physics-based wildfire simulation. Environ. Sci. Policy 3 (4), 161 – 172.

Hao, W. M., Lui, M.-H., 1994. Spatial and temporal distribution of tropical biomass burning. Global Biogeochem. Cycles 8.

Heilman, W. E., Fast, J. D., 1992. Simulation of Horizontal Roll Vortex Development Above Lines of Extreme Surface Heating. Int. J. Wildland Fire 2, 55–68.

Helas, G., Andreae, M. O., Fontan, J., Cros, B., Delmas, R., 1989. Ozone measurements in equatorial Africa during DECAFE 88. In: Bojkov, R. D., Fabian, P. (Eds.), Proc. of the Quadrennial Ozone Symposium 1988. A. Deepak Publishing, Hampton, VA, pp. 430–432.

Helas, G., Lobert, J., Scharfee, D., Schafer, L., Goldammer, J., Baudet, J., Ahoua, B., Ajavon, A. L., Lacaux, J. P., Delmas, R., Andreae, M. O., 1995. Ozone Production Due to Emissions from Vegetation Burning. J. Atmos. Chem. 22 (1-2), 163–174.

Hobbs, P. V., Radke, L. F., 1969. Cloud condensation nuclei from a simulated forest fire. Science 163, 279–280.

Hobbs, P. V., Sinha, P., Yokelson, R. J., Christian, T. J., Blake, D. R., Gao, S., Kirchstetter, T. W., Novakov, T., Pilewskie, P., 2003. Evolution of gases and particles from a savanna fire in South Africa. J. Geophys. Res. 108, 8485.

Hodzic, A., Madronich, S., Bohn, B., Massie, S., Menut, L., Wiedinmyer, C., 2007. Wildfire particulate matter in Europe during summer 2003: meso-scale modeling of smoke emissions, transport and radiative effects. Atm. Chem. Phys. 7, 4043–4064.

Hoelzemann, J. J., 2006. Global Wildland Fire Emission Modeling for Atmospheric Chemistry Studies. Ph.D. thesis, International Max Planck Research School on Earth System Modelling.

Hoelzemann, J. J., Schultz, M. G., Brasseur, G. P., Granier, C., Simon, M., 2004. Global wildland fire emission model (GWEM): Evaluating the use of global area burnt satellite data. J. Geophys. Res. 109.

Hoff, R. M., Palm, S. P., Engel-Cox, J. A., Spinhirne, J., 2005. GLAS long-range transport observation of the 2003 California forest fire plumes to the northeastern US. Geophys. Res. Lett. 32 (22).

Holzinger, R., Warneke, C., Hansel, A., Jordan, A., Lindinger, W., Scharffe, D. H., Schade, G., Crutzen, P. J., 1999. Biomass burning as a source of formaldehyde, acetaldehyde, methanol, acetone, acetonitrile, and hydrogen cyanide. Geophys. Res. Lett. 26, 1161–1164.

Honnert, R., Masson, V., Couvreux, F., 2011. A Diagnostic for evaluating the Representation of Turbulence in Atmospheric Models at the Kilometric Scale. J. Atmos. Sci.In press.

Hourdin, F., Couvreux, F., Menut, L., 2002. Parameterization of the Dry Convective Boundary Layer Based on a Mass Flux Representation of Thermals. J. Atmos. Sci. 59 (6), 1105–1123.

Hu, Y., Odman, M. T., Chang, M. E., Jackson, W., Lee, S., Edgerton, E. S., Baumann, K., Russell, A. G., 2008. Simulation of Air Quality Impacts from Prescribed Fires on an Urban Area. Environ. Sci. Technol. 42, 3676–3682.

Hurst, D. F., Griffith, D. W. T., Cook, G. D., 1994. Trace gas emissions from biomass burning in tropical Australian savannas. J. Geophys. Res. 99, 16441–16456.

IPCC, 2001. Climate Change 2001: The Scientific Basis. Contribution of Working Group I to the Third Assessment Report of the Intergovernmental Panel on Climate Change. Cambridge University Press, Cambridge, UK.

IPCC, 2007. Climate Change 2007: Impacts, Adaptation and Vulnerability. Contribution of Working Group II to the Fourth Assessment Report of the Intergovernmental Panel on Climate Change. Cambridge University Press, Cambridge, UK.

Ito, A., Penner, J. E., 2004. Global estimates of biomass burning emissions based on satellite imagery for the year 2000. J. Geophys. Res. 109.

Jacobson, M. Z., 2001. Strong radiative heating due to the mixing state of black carbon in atmospheric aerosols. Nature 409, 695–697.

James, S. R., 1989. Hominid Use of Fire in the Lower and Middle Pleistocene: A Review of the Evidence. Current Antro. 30, 1 – 26.

Jin, Y., Roy, D. P., 2005. Fire-induced albedo change and its radiative forcing at the surface in northern Australia. Geophys. Res. Lett. 32 (13).

Johnson, D. W., Murphy, J. D., Miller, W. W., Walker, R. F., 2009. Wildfire Effects on Forest Carbon and Nutrient Budgets and Water Quality in Sierran Forests. Vol. 8. Elsevier, Cambridge, UK, Ch. 18, pp. 405–424.

Jost, C., Trentmann, J., Sprung, D., Andreae, M. O., McQuaid, J. B., Barjat, H., 2003. Trace gas chemistry in a young biomass burning plume over Namibia: Observations and model simulations. J. Geophys. Res. 108 (D13), 3676–3682.

Justice, S. K. C. O., Scholes, R. J., 2003. Influence of timing and spatial extent of savanna fires in southern Africa on atmospheric emissions. J. Arid. Environ. 54, 395–404.

Kahn, R. A., Chen, Y., Nelson, D. L., Leung, F.-Y., Li, Q., Diner, D. J., Logan, J. A., 2008. Wildfire smoke injection heights: Two perspectives from space. Geophys. Res. Lett. 35.

Kahn, R. A., Li, W. H., Moroney, C., Diner, D. J., Martonchik, J. V., Fishbein, E., 2007. Aerosol source plume physical characteristics from space-based multiangle imaging. J. Geophys. Res. 112.

Kain, J., Fritsch, J., 1990. A One-Dimensional Entraining/Detraining Plume Model and Its Application in Convective Parameterization. J. Atmos. Sci. 47, 2784–2802.

Kain, J., Fritsch, J., 1993. Convective parameterization for mesoscale models: The Kain-Fritsch scheme. Meteorol. Monogr. 46, 165–170.

Kaiser, J. W., Boucher, O., Doutriaux-Boucher, M., Flemming, J., Govaerts, Y. M., Gulliver, J., Heil, A., Jones, L., Lattanzio, A., Morcrette, J.-J., Perrone, M. R., Razinger, M., Roberts, G., Schultz, M. G., Simmons, A. J., Suttie, M., Wooster, M. J., 2009. Smoke in the Air. ECMWF Newsletter 119, 9–15.

Kasischke, E. S., Hyer, E. J., c Novelli, P., Bruhwiler, L. P., French, N. H. F., Sukhinin, A. I., Hewson, J. H., Stocks, B. J. M., 2005. Influences of boreal fire emissions on Northern Hemisphere atmospheric carbon and carbon monoxide. Global Biogeochem. Cycles 19.

Kaufman, Y., 1995. Remote sensing of direct and indirect aerosol forcing. R. J. Charlson and J. Heintzenberg, New York, pp. 297–332.

Kaufman, Y. J., Fraser, R. S., 1997. The effects of smoke particles on clouds and climate forcing. Science 277, 1636–1639.

Kee, R. J., Yang, H., Yan, R., Liang, D. T., 1989. Sandia Report SAND89-8009B, Sandia National Laboratories, Livermore, CA.

Konovalov, I. B., Beekmann, M., Kuznetsova, I. N., Yurova, A., Zvyagintsev, A. M., 2011. Atmospheric impacts of the 2010 Russian wildfires: integrating modelling and measurements of an extreme air pollution episode in the Moscow region. Atmos. Chem. Phys. 11 (19), 10031–10056.

Labonne, M., Chevallier, F.-M. B. F., 2007. Injection height of biomass burning aerosols as seen from a spaceborne. Geophys. Res. Letters 34, 11806–11811.

Lafore, J. P., Stein, J., Ascencio, N., Bougeault, P., Ducrocq, V., Duron, J., Fisher, C., Hereil, P., Mascart, P., Pinty, J. P., Redelsperger, J. L., Richard, E., de Arellano, J. V.-G., 1998. The Meso-NH atmospheric simulation system. Part I: adiabatic formulation and control simulations. Ann. Geophys. 16, 90–109.

Langmann, B., Duncan, B., Textor, C., Trentmann, J., van der Werf, G. R., 2009. Vegetation fire emissions and their impact on air pollution and climate. Atm. Env. 43, 107–116.

Latham, D., 1994. A one-dimensional plume predictor and cloud model for fire and smoke managers. In: General Technical Report INT-GTR-314. USDA Forest Service, pp. 305–312.

Lavorel, S., 1999. Ecological diversity and resilience of Mediterranean vegetation to disturbance. Divers. Distrib. 5 (1-2), 3–13.

Lavoue, D., Liousse, C., Cachier, H., Stocks, B. J., Goldammer, J. G., 2000. Modeling of carbonaceous particles emitted by boreal and temperate wildfires at northern latitudes. J. Geophys. Res. 105 (D22), 26871–26890.

Lee, S., Kim, H. K., Yan, B., Cobb, C. E., Hennigan, C., Nichols, S., Chamber, M., Edgerton, E. S., Jansen, J. J., Hu, Y., Zheng, M., Weber, R. J., Russell, A. G., 2008. Diagnosis of aged prescribed burning plumes impacting an urban area. Environ. Sci. Technol. 42 (5), 1438–1444.

Leone, V., Lovreglio, R., Martín, M. P., Martínez, J., Vilar, L., 2009. Human Factors of Fire Occurrence in the Mediterranean. E. Chuvieco, Berlin Heidelberg, Ch. 11, pp. 149–170.

Leroy, V., Cancellieri, D., Leoni, E., 2009. Relation between forest fuels composition and energy emitted during their thermal degradation. J. Therm. Anal. Cal. 96, 293–300.

Leroy, V., Leoni, E., Santoni, P.-A., 2007. Combustion of Pyrolysis Gases Involved in Wildland Fire: Experimental Study. Turkish J. Eng. Env. Sci. 31, 365–370.

Leroy, V., Leoni, E., Santoni, P.-A., 2008. Reduced mechanism for the combustion of evolved gases in forest fires. Combust. Flame 154 (3), 410–433.

Levine, J. S., Bobbe, T., Ray, N., Singh, A., Witt, R. G., 1999. Wildland Fires and the Environment: a Global Synthesis. Tech. rep., United Nations Environment Programme (UNEP), Nairobi, Kenya.

Lin, X., Trainer, M., Liu, S., 1988. On the Nonlinearity of the Tropospheric Ozone Production. J. Geophys. Res. 193, 15879–15888.

Linn, R., Reisner, J., Colman, J. J., Winterkamp, J., 2002. Studying wildfire behavior using firetec. Int. J. Wildland Fire 11, 233–246.

Linn, R. R., 1997. A transport model for prediction of wildfire behavior. Ph.D. thesis, New Mexico State University.

Liousse, C., Penner, J. E., Chuang, C., Walton, J. J., Eddleman, H., Cachier, H., 1996. A global three-dimensional model study of carbonaceous aerosols. J. Geophys. Res. 101 (D14), 19411–19432.

Lipps, F., Hemler, R. S., 1982. A scale analysis of deep moist convection and some related numerical calculations. J. Atmos. Sci. 39, 2192–2210.

Lobert, L. M., Warnatz, J., 1993. Emission from the Combustion Process in Vegetation. John Wiley & Sons, Inc., Berlin, Ch. 2, pp. 15–37.

Lovejoy, T. E., 1991. Biomass Burning and the Disappearing Tropical Rainforest. J. S. Levine, Cambridge, MA, Ch. 9, pp. 77–82.

Luderer, G., Trentmann, J., Andreae, M. O., 2009. A new look at the role of fire-released moisture on the dynamics of atmospheric pyro-convection. Int. J. Wildland Fire 18, 554–562.

Luderer, G., Trentmann, J., Winterrath, T., Textor, C., Herzog, M., Graf, H. F., Andreae, M. O., 2006. Modeling of biomass smoke injection into the lower stratosphere by a large forest fire (Part II): sensitivity studies. Atm. Chem. Phys. 6 (12), 5261–5277.

Lupu, A., Kaminski, J. W., Neary, L., McConnell, J. C., Toyota, K., Rinsland, C. P., Bernath, P. F., Walker, K. A., Boone, C. D., Nagahama, Y., Suzuki, K., 2009. Hydrogen cyanide in the upper troposphere: GEM-AQ simulation and comparison with ACE-FTS observations. Atm. Chem. Phys. 9 (13), 4301–4313.

Madronich, S., 1987. Photodissociation in the Atmosphere 1. Actinic Flux and the Effects of Ground Reflections and Clouds. J. Geophys. Res. 92, 9740–9752.

Mallet, V., Keyes, D., Fendell, F., 2009. Modeling wildland fire propagation with level set methods. Comput. Mat. Appl. 57 (7), 1089 – 1101.

Mandel, J., Beezley, J. D., Kochanski, A. K., 2011. Coupled atmosphere-wildland fire modeling with WRF 3.3 and SFIRE 2011. Geosci. Model Devel. 4 (3), 591–610.

Marenco, A., Thouret, V., Nédélec, P., Smit, H., Helten, M., Kley, D., Karcher, F., Simon, P., Law, K., Pyle, J., Poschmann, G., Wrede, R. V., Hume, C., Cook, T., 1998. Measurement of ozone and water vapor by Airbus in-service aircraft: The MOZAIC airborne program, An overview. J. Geophys. Res. 103 (D19), 631–642.

Mari, C., Jacob, D. J., Bechtold, P., 2000. Transport and scavenging of soluble gases in a deep convective cloud. J. Geophys. Res. 105 (D17), 22255–22267.

Martin, M. V., Logan, J. A., Kahn, R. A., Leung, F.-Y., Nelson, D. L., Diner, D. J., 2010. Smoke injection heights from fires in North America: analysis of 5 years of satellite observations. Atm. Chem. Phys. 10 (4), 1491–1510.

Mason, S., Trentmann, J., Winterrath, T., Yokelson, R., Christian, T., Carlson, L., Warner, T., Wolfe, L., Andreae, M., 2006. Intercomparison of two box models of the chemical evolution in biomass-burning smoke plumes. J. Atm. Chem. 55, 273–297.

Mason, S. A., Field, R. J., Yokelson, R. J., Kochivar, M. A., Tinsley, M. R., Ward, D. E., Hao, W. M., 2001. Complex effects arising in smoke plume simulations due to inclusion of direct emissions of oxygenated organic species from biomass combustion. J. Geophys. Res. 106, 12527–12539.

Masson, V., Champeaux, J. L., Chauvin, F., Meriguet, C., Lacaze, R., 2003. A Global Database of Land Surface Parameters at 1-km Resolution in Meteorological and Climate Models. J. Climate 16 (9), 1261–1282.

Mauzerall, D. L., Jacob, D. J., Fan, S. M., Bradshaw, J. D., Gregory, G. L., Sachse, G. W., Blake, D. R., 1996. Origin of tropospheric ozone at remote high northern latitudes in summer. J. OF Geophys. Res. 101 (D2), 4175–4188.

Mazzoni, D., Logan, J. A., D., D., Kahn, R., Tong, L., Li, Q., 2007. A data-mining approach to associating MISR smoke plume heights with MODIS fire measurements. Remote Sens. Environ. 107 (1-2), 138–148.

McMahon, C. K., Ryan, P. W., 1976. Some chemical and physical characteristics of emissions from forest fires. In: Proc. 69th APCA Annual Meeting. Air Pollut. Control. Assoc., Portland, OR.

Mebust, A. K., Russell, A. R., Hudman, R. C., Valin, L. C., Cohen, R. C., 2011. Characterization of wildfire NO_x emissions using MODIS fire radiative power and OMI tropospheric NO_2 columns. Atm. Chem. Phys. 11 (12), 5839–5851.

Mell, W., Gould, M. A. J. J., Cheney, P., 2007. A physics based approach to modeling grassland fires. Int. J. Wildland Fire 16, 1–22.

Menaut, J.-C., Abbadie, L., Lavenu, F., Loudjani, P., Podaire, A., 1991. Biomass Burning in West Africa Savannas. J. S. Levine, Cambridge, MA, Ch. 17, pp. 133–146.

Miranda, A. I., 2004. An integrated numerical system to estimate air quality effects of forest fires. Int. J. of Wildland Fire 13, 217–226.

Miranda, A. I., Borrego, C., Martin, H., Martins, V., Amorim, J. H., Valente, J., Carvalho, A., 2009a. Forest Fire Emissions and Air Pollution in Southern Europe. E. Chuvieco, Berlin Heidelberg, Ch. 12, pp. 171–187.

Miranda, A. I., Ferreira, J., Valente, J., Santos, P., Amorim, J. H., Borrego, C., 2005. Smoke measurements during Gestosa-2002 experimental field fires. Int. J. of Wildland Fire 14, 107–116.

Miranda, A. I., Marchi, E., Ferretti, M., Millán, M. M., 2009b. Forest Fires and Air Quality Issues in Southern Europe. Vol. 8. Elsevier, Cambridge, UK, Ch. 9, pp. 209–231.

Miranda, A. I., Monteiro, A., Martins, V., Carvalho, A., Schaap, M., Builtjes, P., Borrego, C., 2008. Forest Fire Impact on Air Quality over Portugal. In: Borrego, C., Miranda, A. I. (Eds.), Air Pollution Modeling and Its Application XIX. NATO Science for Peace and Security Series C: Environmental Security. Springer Netherlands, pp. 190–198.

Mobley, H. E., 1990. Summary of smoke-related accidents in the south from prescribed frie (1979-1988). Technical release 90-R-11, Forest Resources Association, Rockville, MD.

Moigne, P. L., 2009. SURFEX SCIENTIFIC DOCUMENTATION. `http://www.cnrm.meteo.fr/surfex/`.

Molion, L. C. B., 1991. Amazonia Burning and Global Climate Impacts. J. S. Levine, Cambridge, MA, Ch. 56, pp. 457–462.

Moriondo, M., Good, P., Durao, R., Bindi, M., Giannakopoulos, C., Corte-Real, J., 2006. Potential impact of climate change on fire risk in the Mediterranean area. Clim. Res. 31 (1), 85–95.

Muraleedharan, T. R., Radojevic, M., Waugh, A., Caruana, A., 2000. Chemical characterisation of the haze in Brunei Darussalam during the 1998 episode. Atm. Env. 34 (17), 2725–2731.

Nepstad, D. C., Verissimo, A., Alencar, A., Nobre, C., Lima, E., Lefebvre, P., Schlesinger, P., Potter, C., Moutinho, P., Mendonza, E., Cochrane, M., Brooks, V., 1999. Large-scale impoverishment of Amazonian forests by logging and fire. Nature 398, 505–508.

Noilhan, J., Planton, S., 1989. A simple parameterization of land surface processes for meteorological models. Mon. Wea. Rev. 117, 536–549.

Ottmar, R. D., Miranda, A. I., Sandberg, D. V., 2009. Characterizing Sources of Emissions from Wildland Fires. Vol. 8. Elsevier, Cambridge, UK, Ch. 3, pp. 61–78.

Pace, G., Meloni, D., di Sarra, A., 2005. Forest fire aerosol over the Mediterranean basin during summer 2003. J. Geophys. Res. 110.

Parmar, R. S., Welling, M., Andreae, M. O., Helas, G., 2008. Water vapor release from biomass combustion. Atm. Chem. Phys. 8 (20), 6147–6153.

Pausas, J. G., 2004. Changes in fire and climate in the eastern iberian peninsula (Mediterranean basin). Climatic Change 63, 337–350.

Penkett, S. A., Law, K. S., Cox, T., Kasibhatla, P., 2003. Atmospheric Photo-oxidants. IGBP Series. G. P. Brasseur and R. G. Prinn and A. P. Pszenny.

Pergaud, J., Masson, V., Malardel, S., Couvreux, F., 2009. A Parameterization of Dry Thermals and Shallow Cumuli for Mesoscale Numerical Weather Prediction. Boundary-Layer Met. 132, 83–106.

Pfister, G., Hess, P. G., Emmons, L. K., Lamarque, J.-F., Wiedinmyer, C., Edwards, D. P., Pétron, G., Gille, J. C., Sachse, G. W., 2005. Quantifying CO emissions from the 2004 Alaskan wildfires using MOPITT CO data. Geophys. Res. Lett. 32.

Pfister, G. G., Wiedinmyer, C., Emmons, L. K., 2008. Impacts of the fall 2007 California wildfires on surface ozone: Integrating local observations with global model simulations. Geophys. Res. Lett. 35 (19).

Phuleria, H. C., Fine, P. M., Zhu, Y., Sioutas, C., 2005. Air quality impacts of the October 2003 Southern California wildfires. J. Geophys. Res. 110 (D7), 148–227.

Pinty, J. P., Jabouille, P., 1999. A mixed-phase cloud parameterization for use in mesoscale non-hydrostatic model: simulations of a squall line and of orographic precipitations. In: Proc. Conf. of Cloud Physics. Amer. Met. Soc., Everett, WA, USA, pp. 217–220.

Pommier, M., Law, K. S., Clerbaux, C., Turquety, S., Hurtmans, D., Hadji-Lazaro, J., Coheur, P.-F., Schlager, H., Ancellet, G., Paris, J.-D., Nedelec, P., Diskin, G.-S., Podolske, J. R., Holloway, J. S., Bernath, P., 2010. IASI carbon monoxide validation over the Arctic during POLARCAT spring and summer campaigns. Atmos. Chem. Phys. 10 (21), 10655–10678.

Poppe, D., Koppmann, R., Rudolph, J., 1998. Ozone formation in biomass burning plumes: Influence of atmospheric dilution. Geophys. Res. Lett. 25, 3823–3826.

Prins, E. M., Menzel, W. P., 1992. Geostationary satellite detection of biomass burning in South-America. J. Remote. Sens. 13, 2783–2799.

Pyne, S. J., 1995. World Fire. The Culture of fire on Earth. University of Washington Press, Seattle and London.

Pyne, S. J., Andrews, P. L., Laven, R. D., 1949. Introduction to wildland fire. John Wiley & Sons, Inc.

Pyne, S. J., Goldammer, J. G., 1997. The Culture of Fire: An Introduction to Anthropogenic Fire History. In: Clark, J. S., Cachier, H., Goldammer, J. G., Stocks, B. (Eds.), Sediment Records of Biomass Burning and Global Change. Vol. 151 of NATO ASI Series. Springer-Verlag.

Pérez-Cabello, F., Echeverría, M. T., Ibarra, P., de la Riva, J., 2009. Effects of Fire on Vegetation, Soil and Hydrogeomorphological Behavior in Mediterranean Ecosystems. E. Chuvieco, Berlin Heidelberg, Ch. 9, pp. 111–128.

Radke, L. F., Hegg, D. A., Hobbs, P. V., Nance, J. D., Lyons, J. H., Laursen, K. K., Weiss, R. E., Riggan, P. J., Ward, D. E., 1991. Particulate and Trace Gas Emissions from Large Biomass Fires in North America. J. S. Levine, Cambridge, MA, Ch. 28, pp. 209–224.

Ramanathan, V., Cicerone, R. J., Singh, H. B., Kiehl, J. T., 1985. Trace Gas Trends and Their Potential Role in Climat Change. J. Geophys. Res. 90 (ND3), 5547–5566.

Ramanathan, V., Crutzen, P. J., Kiehl, J. T., Rosenfeld, D., 2001. Aerosols, climate, and the hydrological cycle. Science 294, 2119–2124.

Randall, D. A., Albrechtb, B., Coxa, S., Johnsonc, D., Minnisd, P., Rossowe, W., Starrf, D. O., 1996. On fire at ten. Adv. Geophys. 38, 37–128.

Reid, J. S., Koppmann, R., Eck, T. F., Eleuterio, D. P., 2005. A review of biomass burning emissions part II: intensive physical properties of biomass burning particles. Atmos. Chem. Phys. 5, 799–825.

Rein, G., Cleaver, N., Ashton, C., Pironi, P., Torero, J. L., 2008. The severity of smouldering peat fires and damage to the forest soil. CATENA 74 (3), 304–309.

Reisner, J., Bossert, J., Winterkamp, J., 1998. Numerical Simulations of Two Wildfire Events Using a Combined Modeling System (HIGRAD/BEHAVE). In: Proc. 2nd Symposium on Fire and Forest Meteorology. Amer. Met. Soc., Phoenix, AZ.

Rio, C., Hourdin, F., Chédin, A., 2010. Numerical simulation of tropospheric injection of biomass burning products by pyro-thermal plumes. Atm. Chem. Phys. 10 (8), 3463–3478.

Rolph, G. D., Draxler, R. R., Stein, A. F., Taylor, A., Ruminski, M. G., Kondragunta, S., Zeng, J., Huang, H.-C., Manikin, G., Mcqueen, J. T., Davidson, P. M., 2009. Description and Verification of the NOAA Smoke Forecasting System: The 2007 Fire Season. Weather Forecast. 24 (2), 361–378.

Rosenfeld, D., 1999. TRMM observed first direct evidence of smoke from forest fires inhibiting rainfall. Geophys. Res. Lett. 26 (20).

Roy, D. P., Boschetti, L., Justice, C. O., Ju, J., 2005. The Collection 5 MODIS Burned Area Product - Global Evaluation by Comparison with the MODIS Active Fire product. Remote Sens. Environ. 112, 3690–3707.

Saarikoski, S., Sillanp$\acute{a}\acute{a}$, M., Sofiev, M., Timonen, H., Saarnio, K., Teinil$\acute{a}$, K., Karppinen, A., Kukkonen, J., Hillamo, R., 2007. Chemical composition of aerosols during a major biomass burning episode over northern europe in spring 2006: Experimental and modelling assessments. Atm. Env. 41 (17), 3577 – 3589.

San-Miguel-Ayanz, J., Pereira, J. M. C., Boca, R., Strobl, P., Kucera, J., Pekkarinen, A., 2009. Forest Fires in the European Mediterranean Region: Mapping and Analysis of Burned Areas. E. Chuvieco, Berlin Heidelberg, Ch. 13, pp. 189–203.

Sandstrom, T., Nowak, D., van Bree, L., 2005. Health effects of coarse particles in ambient air: messages for research and decision-making. Eur. Resp. J. 26 (2), 187–188.

Sanhueza, E., Crutzen, P. J., Fernandez, E., 1999. Production of boundary layer ozone from tropical American Savannah biomass burning emissions. Atm. Env. 33 (30), 4969–4975.

Santis, A. D., Asner, G. P., Vaughan, P. J., Knapp, D. E., 2010. Mapping burn severity and burning efficiency in California using simulation models and Landsat imagery. Remote Sensing Env. 114 (7), 1535–1545.

Santoni, P. A., Simeoni, A., Rossi, J. L., Bosseur, F., Morandini, F., Silvani, X., Balbi, J. H., Cancellieri, D., Rossi, L., 2006. Instrumentation of wildland fire: Characterisation of a fire spreading through a Mediterranean shrub. Fire Saf. J. 41 (3), 171–184.

Schaap, M., van der Gon Denier, H. A. C., 2007. On the variability of black smoke and carbonaceous aerosols in the Netherlands. Atmos. Environ. 41 (28), 5908–5920.

Scholes, M. C., Matrai, P. A., Andreae, M. O., Smith, K. A., et al., M. R. M., 2003. Biosphere-Atmosphere Interactions. IGBP Series. G. P. Brasseur and R. G. Prinn and A. P. Pszenny.

Schule, W., 1990. Landscape and Climate in Prehistory: Interaction of Wildlife, Man and Fire. J. Goldammer, Berlin, pp. 273–318.

Seiler, W., Crutzen, P. J., 1980. Estimates of gross and net fluxes of carbon between the biosphere and the atmosphere from biomass burning. Clim. Change 2, 207–247.

Sessions, W. R., Fuelberg, H. E., Kahn, R. A., Winker, D. M., 2011. An investigation of methods for injecting emissions from boreal wildfires using WRF-Chem during ARCTAS. Atm. Chem. Phys. 11 (12), 5719–5744.

Siebesma, A. P., Soares, P. M. M., Teixeira, J., 2007. A combined eddy-diffusivity mass-flux approach for the convective boundary layer. J. Atmos. Sci. 64 (4), 1230–1248.

Siebesma, A. P., Teixeira, J., 2000. An advection-diffusion scheme for the convective boundary layer: description and 1d-results. In: Proc. 14th Symposium on Boundary Layers and Turbulence. Amer. Met. Soc., Aspen, CO, USA, pp. 133–136.

Silvani, X., Morandini, F., 2009. Fire spread experiments in the field: Temperature and heat fluxes measurements. Fire Safety J. 44, 279–285.

Simpson, D., Winiwarter, W., Borjesson, G., Cinderby, S., Ferreiro, A., Guenther, A., Hewitt, C. N., Janson, R., Khalil, M. A. K., Owen, S., Pierce, T. E., Puxbaum, H., Shearer, M., Steinebrecher, U. S. R., Tarasson, L., Oquist, M. G., 1999. Inventorying emissions from nature in Europe. J. Geophys. Res. 104, 8113–8152.

Simpson, J., Wiggert, V., 1969. Models of precipitating cumulus towers. Mon. Wea. Rev. 97, 471–489.

Singh, H. B., Anderson, B. E., Brune, W. H., Cai, C., Cohen, R. C., Crawford, J. H., Cubison, M. J., Czech, E. P., Emmons, L., Fuelberg, H. E., Huey, G., Jacob, D. J., Jimenez, J. L., Kaduwela, A., Kondo, Y., Mao, J., Olson, J. R., Sachse, G. W., Vay, S. A., Weinheimer, A., Wennberg, P. O., Wisthaler, A., the ARCTAS Sci Team, 2010. Pollution influences on atmospheric composition and chemistry at high northern latitudes: Boreal and California forest fire emissions. Atm. Env. 44 (36), 4553–4564.

Singh, H. B., Herlth, D., Kolyer, R., Chatfield, R., Viezee, W., Salas, L. J., Chen, Y., Bradshaw, J. D., Sandholm, S. T., Talbot, R., Gregory, G. L., Anderson, B., Sachse, G. W., Browell, E., Bachmeier, A. S., Blake, D. R., Heikes, B., Jacob, D., Fuelberg, H. E., 1996. Impact of biomass burning emissions on the composition of the South Atlantic troposphere: Reactive nitrogen and ozone. J. Geophys. Res. 101 (D19), 24203–24219.

Smith, G. P., Golden, D. M., Frenklach, M., Moriarty, N. W., Eiteneer, B., Goldenberg, M., Bowman, C. T., R. K. Hanson, S. S., Gardiner, W. C., Lissianski, J. V. V., Qin, Z., 2000. Gri-mech 3.0 home page. `http://www.me.berkeley.edu/gri-mech/`.

Soares, P. M. M., Miranda, P. M. A., Siebesma, A. P., Teixeira, J., 2004. An eddy-diffusivity/mass-flux parametrization for dry and shallow cumulus convection. Q. J. R. Meteorol. Soc. 130 (604, Part c), 3365–3383.

Sofiev, M., Siljamo, P., , Karppinen, A., Kukkonen, J., 2008. Air Quality Forecasting During Summer 2006: Forest Fires as One of Major Pollution Sources in Europe. In: Borrego, C., Miranda, A. I. (Eds.), Air Pollution Modeling and Its Application XIX. NATO Science for Peace and Security Series C: Environmental Security. Springer Netherlands, pp. 305–312.

Stein, A. F., Rolph, G. D., Draxler, R. R., Stunder, B., Ruminski, M., 2009. Verification of the NOAA Smoke Forecasting System: Model Sensitivity to the Injection Height. Wea. Forecasting 24, 379–394.

Stocks, B. J., 1991. The extent and impact of forest fires in northern circumpolar countries. J. S. Levine, Cambridge, MA, Ch. 26, pp. 196–202.

Stocks, B. J., Fosberg, M. A., Wottom, B. M., Lynham, T. J., Ryan, K. C., 2000. Climate Change and forest fire activity in North American boreal forests. E. S. Kasischke and B. J. Stocks, Berlin, Ch. 26, pp. 368–376.

Stockwell, W. R., Kirchner, F., Kuhn, M., Seefeld, S., 1997. A new mechanism for regional atmospheric chemistry modeling. J. Geophys. Res. 102, 25847–25879.

Stohl, A., Forster, S. E. C., James, P., Spichtinger, N., 2006. On the pathways and timescales of intercontinental air pollution transport. J. Geophys. Res. 107 (D23).

Strada, S., Mari, C., Filippi, J. B., Bosseur, F., 2012. Forest Fire and Atmosphere: the Lançon-de-Provence 2005 Case Study, in press.

Sullivan, A. L., 2007a. A review of wildland fire spread modelling 1990-2007. 1: Physical and quasi-physical models. Int. J. Wildland Fire 18, 349–368.

Sullivan, A. L., 2007b. A review of wildland fire spread modelling 1990-2007. 2: Empirical and quasi-empirical models. Int. J. Wildland Fire 18, 369–386.

Sullivan, A. L., 2007c. A review of wildland fire spread modelling 1990-2007. 3: Simulation and mathematical analogue models. Int. J. Wildland Fire 18, 387–403.

Sun, R., Krueger, S. K., Jenkins, M. A., Zulauf, M. A., Charney, J. J., 2009. The importance of fire/atmosphere coupling and boundary-layer turbulence to wildfire spread. Int. J. Wildland Fire 18, 50–60.

Szczygieł, R., Ubysz, B., a Niedźwiecki, T. Z., 2009. Spatial and Temporal Trends in Distribution of Forest Fires in Central and Eastern Europe. Vol. 8. Elsevier, Cambridge, UK, Ch. 10, pp. 233–245.

Takegawa, N., Kondo, Y., Ko, M., Koike, M., Kita, K., Blake, D. R., Hu, W., Scott, C., Kawakami, S., Miyazaki, Y., Russel-Smith, J., Ogawa, T., 2003. Photochemical production of O_3 in biomass burning plumes in the boundary layer over northern Australia. Geophys. Res. Letters 30 (10).

Tansey, K., Gregoire, J. M., Defourny, P., Leigh, R., Pekel, J.-F., van Bogaert, E., Bartholome, E., 2008. A new, global, multi-annual (2000-2007) burnt area product at 1 km resolution. Geophys. Res. Lett. 35 (1).

Tansey, K., Gregoire, J. M., Stroppiana, D., Sousa, A., Silva, J., Pereira, J. M. C., Boschetti, L., Maggi, M., Brivio, P. A., Fraser, R., Flasse, S., Ershov, D., Binaghi, E., Graetz, D., Peduzzi, P., 2004. Vegetation burning in the year 2000: Global burned area estimates from SPOT VEGETATION data. J. Geophys. Res. 109 (D14).

Thomas, W., Hegels, E., S., Slijkhuis, Spurr, R., Chance, K., 1998. Detection of biomass burning combustion products in Southeast Asia from backscatter data taken by the GOME Spectrometer. Geophys. Res. Lett. 25 (9), 1317–1320.

Thompson, A. M., Diab, R. D., Bodeker, G. E., Zunckel, M., Coetzee, G. J. R., Archer, C. B., McNamara, D. P., Pickering, K. E., Combrink, J., Fishman, D., Nganga, D., 1996. Ozone over southern africa during SAFARI-92/TRACE A. J. Geophys. Res. 101, 293–300.

Tosca, M. G., Randerson, J. T., Zender, C. S., Nelson, D. L., J.Diner, D., Logan, J. A., 2011. Dynamics of fire plumes and smoke clouds associated with peat and deforestation fires in Indonesia. J. Geophys. Res. 116.

Trelles, J., Mcgrattan, K., Baum, H., 1999. Smoke transport by sheared winds. Combust. Theory and Modelling 3, 323–341.

Trentmann, J., Andreae, M. O., Graf, H.-F., 2003. Chemical processes in a young biomass-burning plume. J. Geophys. Res. 108 (D22).

Tressol, M., Ordonez, C., Zbinden, R., Brioude, J., Thouret, V., Mari, C., Nedelec, P., Cammas, J. P., Smit, H., Patz, H.-W., Volz-Thomas, A., 2008. Air pollution during the 2003 European heat wave as seen by MOZAIC airliners. Atm. Chem. and Phys. 8 (8), 2133–2150.

Turquety, S., Hurtmans, D., Hadji-Lazaro, J., Coheur, P.-F., Clerbaux, C., Josset, D., Tsamalis, C., 2009. Tracking the emission and transport of pollution from wildfires using the IASI CO retrievals: analysis of the summer 2007 Greek fires. Atm. Chem. Phys. 9 (14), 4897–4913.

Turquety, S., Logan, J. A., Jacob, D. J., Hudman, R. C., Leung, F. Y., Heald, C. L., Yantosca, R. M., Wu, S., Emmons, L. K., Edwards, D. P., Sachse, G. W., 2007. Inventory of boreal fire emissions for North America in 2004: Importance of peat burning and pyroconvective injection. J. Geophys. Res. 112 (D12).

Urbanski, S. P., Hao, W. M., Baker, S., 2009. Chemical Composition of Wildland Fire Emissions. Vol. 8. Elsevier, Cambridge, UK, Ch. 4, pp. 79–107.

Urbanski, S. P., Hao, W. M., Nordgren, B., 2011. The Wildland Fire Emission Inventory: emission estimates and an evaluation of uncertainty. Atm. Chem. Phys. 11 (8), 23349–23419.

USGS/EROS, 1996. GTOPO30 Homepage. `http://eros.usgs.gov/#/Find_Data/Products_and_Data_Available/gtopo30_info`.

Valente, J., Miranda, A. I., Lopes, A. G., Borrego, C., Viegas, D. X., Lopes, M., 2007. Local-scale modelling system to simulate smoke dispersion. Int. J. Wildland Fire 16 (2), 196–203.

van der Werf, G. R., Randerson, J. T., Collatz, G. J., Giglio, L., Kasibhatla, P. S., Arellano, A. F., Olsen, S. C., Kasischke, E. S., 2004. Continental-scale partitioning of fire emissions during the 1997 to 2001 El Nino/La Nina period. Science 303 (5654), 73–76.

van der Werf, G. R., Randerson, J. T., Giglio, L., Collatz, G. J., Kasibhatla, P. S., Arellano, J. A. F., 2006. Interannual variability in global biomass burning emissions from 1997 to 2004. Atm. Chem. Phys. 6 (11), 3423–3441.

Warner, J., Twomey, S., 1967. Comparison of measurements of cloud droplets and cloud nuclei. J. Atmos. Sci. 24, 702–703.

Wesely, M., 1989. Parameterization of surface resistances to gaseous dry deposition in regional-scale numerical models. Atmos. Env. 23 (6), 1293–1304.

Whitcomb, M. A., Decker, C., Fendell, F., the staff at the Oxnard, C. W. F. O., 2008. Fire Weather Research: A Burning Agenda for NOAA. Noaa final report, NOAA.

WHO/UNEP/WMO, 2000. Health Guidelines for Vegetation Fire Events. IFFN 22.

Witek, M. L., Teixeira, J., Matheou, G., 2011. An eddy-diffusivity/mass-flux approach to the vertical transport of turbulent kinetic energy in convective boundary layers. J. Atmos. Sci.In press.

Woods, D. C., Chaun, R. L., III, W. R. C., Levine, J. S., 1991. Aerosol Characterization in Smoke Plumes from a Wetland Fire. J. S. Levine, Cambridge, MA, Ch. 31, pp. 240–244.

Wuebbles, D. J., Brasseur, G. P., et al., H. R., 2003. Changes in the Chemical Composition of the Atmosphere and Potential Impacts. IGBP Series. G. P. Brasseur and R. G. Prinn and A. P. Pszenny.

Wyngaard, J. C., 2004. Toward Numerical Modeling in the "Terra Incognita". J. Atmos. Sci. 61, 1816–1826.

Xu, L., Raman, S., Madala, R. V., 1992. A review of non-hydrostatic numerical models for the atmosphere. In: 1st World Congress of Nonlinear Analysis Fire and Forest Meteorology. Nonlinear World, Walter de Gruyter, New York, Tampa, FL.

Yokelson, R. J., Bertschi, I. T., Christian, T. J., Hobbs, P. V., Ward, D. E., Hao, W. M., 2003. Trace gas measurements in nascent, aged, and cloud-processed smoke from african

savanna fires by airborne fourier transform infrared spectroscopy (AFTIR). J. Geophys. Res. 108, 8478.

Yokelson, R. J., Goode, J. G., Ward, D. E., Susott, R. A., Babbitt, R. E., Wade, D. D., Bertschi, I. T., Griffith, D. W. T., Hao, W. M., 1999. Emissions of formaldehyde, acetic acid, methanol, and other trace gases from biomass fires in North Carolina measured by airborne Fourier transform infrared spectroscopy. J. Geophys. Res. 104, 30109–30125.

Yokelson, R. J., Griffith, D. W. T., Ward, D. E., 1996. Open-path Fourier transform infrared studies of large-scale laboratory biomass fires. J. Geophys. Res. 101, 21067–21080.

Yokelson, R. J., Karl, T., Artaxo, P., Blake, D. R., Christian, T. J., Griffith, D. W. T., Guenther, A., Hao, W. M., 2007. The Tropical Forest and Fire Emission Experiment: overview and airborne fire emission factor measurements. Atm. Chem. Phys. 7, 5175–5196.

Yokelson, R. J., Susott, R., Ward, D. E., Reardon, J., Griffith, D. W. T., 1997. Emissions from smoldering combustion of biomass measured by open-path Fourier transform infrared spectroscopy. J. Geophys. Res. 102, 18865–18877.